



**HAL**  
open science

## Design of protective structures against rock impacts

Stéphane Lambert

► **To cite this version:**

Stéphane Lambert. Design of protective structures against rock impacts. 3rd Euro-mediterranean symposium on advances in geomaterials and structures (AGS10), May 2010, Djerba, Tunisia. pp.146, 2010. hal-02593650

**HAL Id: hal-02593650**

**<https://hal.inrae.fr/hal-02593650>**

Submitted on 15 May 2020

**HAL** is a multi-disciplinary open access archive for the deposit and dissemination of scientific research documents, whether they are published or not. The documents may come from teaching and research institutions in France or abroad, or from public or private research centers.

L'archive ouverte pluridisciplinaire **HAL**, est destinée au dépôt et à la diffusion de documents scientifiques de niveau recherche, publiés ou non, émanant des établissements d'enseignement et de recherche français ou étrangers, des laboratoires publics ou privés.

*Advances*  
*in*  
*Geomaterials and Structures*

*Third edition*

2010



Euromediterranean Symposium on  
Advances in Geomaterials and Structures

Third edition  
Djerba, 2010

Edited by

**F. Darve**

*Institut National Polytechnique de Grenoble, France*

**I. Doghri**

*Université Catholique de Louvain, Belgium*

**R. El Fatmi, H. Hassis and H. Zenzri**

*Ecole Nationale d'Ingénieurs de Tunis, Tunisia*

with the support of

**LGC-ENIT, Tunisia**

*Laboratoire de Génie Civil  
de l'Ecole Nationale d'Ingénieurs de Tunis*

## Scientific Committee

### Chairman

Félix Darve Institut National Polytechnique de Grenoble France

### Vice Chairman

Issam Doghri Université Catholique de Louvain Belgium

### Members

Abriak N. Ecole des mines de Douai France  
Ben Oueddou M. Ecole Nationale d'Ingénieurs de Tunis Tunisia  
Binda L. Politecnico di Milano Italy  
Bouassida M. Ecole Nationale d'Ingénieurs de Tunis Tunisia  
Darve F. Institut National Polytechnique de Grenoble France  
De Buhan P. Ecole Nationale des Ponts et Chaussées France  
Del Piero G. Ferrara University Italy  
Doghri I. Université Catholique de Louvain Belgium  
El Fatmi R. Ecole Nationale d'Ingénieurs de Tunis Tunisia  
Fremont M. Laboratoire Central des Ponts et Chaussées France  
Friâa A. Ecole Nationale d'Ingénieurs de Tunis Tunisia  
Guerlement G. Faculté Polytechnique de Mons Belgium  
Hassis H. Ecole Nationale d'Ingénieurs de Tunis Tunisia  
Hicher P. Y. Ecole Centrale de Nantes France  
Ibrahimbegovic A. Ecole Normale Supérieure de Cachan France  
Laloui L. Ecole Polytechnique Fédérale de Lausanne Switzerland  
Lambert S. CEMEGREF Grenoble France  
Léné F. Université Pierre et Marie Curie, Paris 6 France  
Mazars J. Institut National Polytechnique de Grenoble France  
Nicot F. CEMEGREF Grenoble France  
Nova R. Politecnico di Milano Italy  
Pastor M. ETSICCP Spain  
Radjai F. Université de Montpellier II France  
Raphael W. Ecole supérieure d'ingénieurs de Beyrouth (USJ) Liban  
Sab K. Ecole Nationale des Ponts et Chaussées France  
Vermeer P. Stuttgart University Germany  
Wood D. M. University of Bristol United Kingdom  
Zenzri H. Ecole Nationale d'Ingénieurs de Tunis Tunisia

## PREFACE

*The strong development of phenomenological visco-elasto-plastic relations in the seventies and, in parallel, the fabulous increase of the computational power have given rise to a deep revolution in mechanical and civil engineering particularly by unifying elastic analyses in small strain and plastic failure in large deformations in a unique modelling framework. Today phenomenological constitutive relations are more and more based on material microstructures, where the basic interaction laws between the elemental constituents can properly be defined and be expressed often in a simple way from a mechanical point of view. The third Euro-mediterranean Symposium on Advances in Geomaterials and Structures is offering several examples of such micromechanical models developed in the line of that new avenue for formulating constitutive relations based on proper microscopic descriptions.*

*The finite element method is a tremendous engineering tool for modelling geomaterials and structures subjected to complex loading programs. However some limitations have been reached recently when the discontinuous aspects of matter have to be taken into account as for granular materials ( sands, ... ) , fractured media ( rocks, ... ) or discontinuous failure modes ( fragmentation, ... ). In these situations discrete element methods, which are essentially particular applications of molecular dynamics methods to geomaterials, are today a fascinating tool to describe these discontinuities and the induced global behaviour in a natural way. Several examples of such discrete computations in AGS10 are illustrating the capacities of this numerical method.*

*Finally the question of failure is also revisited today by considering it as a bifurcation problem. It appears in the experiments, but also in the elasto-plastic theory through the second order work criterion, that failure defined by a limit state is linked to a burst of kinetic energy. This change of regime from static to dynamic conditions is a good indicator of a bifurcation state. Thus the existence of a bifurcation domain in the stress space (and not only of a plastic limit surface), where different failure modes can develop, represents probably a great breakthrough in this crucial domain from an engineering point of view. These new analyses are also well represented in AGS10 !*

*This third event in AGS series, considering the number and the scientific quality of the contributions, will be assuredly a success under Djerba sun !*

*Editors*



# Table of Contents

- **Volume 1**  
**Applications of Nonlinear Continuum Mechanics in Civil and in Materials Engineering**  
**Composite Materials and Reinforcements**
  - Variational approach to fracture and delamination of thin films bonded on an elastic substrate** ..... 17  
*B. Bourdin, C. Maurini, K. Pham, J. J. Marigo*
  - Numerical variational models for fracture mechanics** ..... 23  
*G. Lancioni*
  - Decomposed-strain smeared fixed-crack models: a variational approach** 29  
*F. Freddi, G. Royer-Carfagni*
  - Cohesive zone model and bipotential formulation: application to a pile/soil interface** ..... 45  
*T. Terfaya, M. Raous, A. Berga*
  - Wrinkling and pull-in instabilities of electro-active polymeric films** ..... 51  
*D. De Tommasi, S. Marzano, G. Puglisi, G. Saccomandi, G. Zurlo*
  - Folded states of thin walled tubes as energy minimizers** ..... 57  
*E. Babilio, A. Fortunato*
  - Phase change with the possibility of voids and bubbles** ..... 63  
*F. Ascione, M. Frémond, E. Rocca*
  - Field-Induced Phase Transitions in Nematic Liquid Crystals: A Numerical Study - Paper 9/AGS10/NL** ..... 71  
*A. Pandolfi, G. Napoli*
  - On the emergence of periodic bifurcating modes for a compressible hollow cylinder** ..... 77  
*P. Foti, A. Fraddosio, S. Marzano, M. D. Piccioni*
  - On the Mechanical Behavior of Carbon Nanotube Foams** ..... 83  
*F. Fraternali, A. Amendola, R. Del Regno, T. Blesgen, C. Daraio*

|  |     |
|--|-----|
| <b>On the rate-dependent behavior of open-cell polymeric foams in uniaxial compression</b> .....   | 89  |
| <i>G. Delpiero, G. Pampolini</i>   |     |
| <b>Design of a polymeric prototype with variable geometry controlled by shape-memory strips</b> .....  | 95  |
| <i>M. Merlin, R. Rizzoni</i>   |     |
| <b>A decoupled approach to the investigation of the equilibrium and stability of a spherical aneurysm, in the presence of local changes in the blood flow dynamics</b> ..... | 103 |
| <i>M. Buonsanti, P. F. Filianoti, A. Pontari</i>   |     |
| <b>Singular stress fields in masonry walls</b> .....   | 109 |
| <i>M. Angelillo, C. Ceraldi, A. Fortunato</i>  |     |
| <b>On the limit analysis of masonry beams</b> .....  | 115 |
| <i>M. Lucchesi, M. Silhavy, N. Zani</i>  |     |
| <b>An asymptotic finite plane deformation analysis of the elastostatic fields at a notch vertex of an incompressible Mooney-Rivlin material</b> .....                        | 123 |
| <i>K. Mansouri, M. Arfaoui, M. Trifa</i>   |     |
| <b>Influence of temperature variations on the mechanical behavior of stay cables using a catenary-based approach</b> .....   | 129 |
| <i>M. Montassar, O. Ben Mekki, G. Vairo, H. Ben Salah, F. Aloulou</i>  |     |
| <b>Damping stay-cable transverse vibration using shape memory alloys and magneto rheological dampers</b> .....   | 135 |
| <i>S. Soltane, O. Ben Mekki, M. Montassar, F. Auricchio</i>  |     |
| <b>Monitoring of creeping tunnel shells: influence of shotcrete mixture characteristics</b> .....  | 141 |
| <i>C. Hellmich, S. Ullah, B. Pichler, S. Scheiner</i>  |     |
| <b>Settlement and stability analysis of stone column-reinforced soils by means of a homogenization method</b> .....  | 151 |
| <i>G. Hassen, P. De Buhan, M. Abdelkrim</i>  |     |
| <b>Theoretical study of a foldable Wood-Dry carbon fibers sheets-Composite-Beam</b> .....  | 157 |
| <i>O. Benjeddou, O. Limam, M. Ben Ouezdou</i>  |     |
| <b>Three-dimensional analysis of piled-raft foundations using a multiphase approach</b> .....  | 163 |
| <i>E. Bourgeois, G. Hassen, P. De Buhan</i>  |     |
| <b>Experimental study to improve the bond between CFRP bars and UH-PFRC: optimization of lug geometries of machined CFRP bars</b> .....                                      | 169 |
| <i>F. Sayed-Ahmed, G. Foret, R. Leroy</i>  |     |

|   |     |
|---|-----|
| <b>Macroscopic behaviour of fibre-reinforced materials using a multiphase approach</b> .....                                    | 175 |
| <i>G. Hassen, V. T. Nguyen</i>  |     |
| <b>Influence of the connection stiffness on the mechanical behavior of old timber frames</b> .....                              | 181 |
| <i>T. Descamps, G. Guerlement, J. Noel</i>  |     |
| <b>A numerical homogenization method of rate-dependent composite materials with viscoelastic-viscoplastic behavior</b> .....    | 187 |
| <i>B. Miled, I. Doghri, L. Delannay</i>   |     |
| <b>Crack pattern in heritage buildings: a practical toolbox</b> .....   | 195 |
| <i>J. Noel, S. Datoussaid</i>   |     |
| <b>Investigation of GFRP-concrete bond: experimental and numerical studies</b> .....  | 203 |
| <i>M. Masmoudi, D. Daoud, M. Ben Ouezdou, R. Masmoudi</i>   |     |
| <b>On pollutant transport in soil</b> .....   | 209 |
| <i>P. Giovine</i>   |     |
| <b>Numerical Simulations on Eddy Currents Evaluation at High Speed in CFRP</b> .....  | 217 |
| <i>M. Cacciola, G. Megali, D. Pellicano, S. Calcagno, M. Versaci, F. C. Morabito</i>  |     |
| <b>Towards a standard pull-out test specimen</b> .....  | 229 |
| <i>M. Makni, D. Daoud, M. A. Karray, M. Lorrain</i>   |     |
| <b>Micromechanical model of viscoelastic behavior for glass fiber reinforced polymers</b> .....                                 | 239 |
| <i>S. Barboura, J. F. Caron, K. Sab</i>   |     |
| <b>Calculation of the limit load for pile by theory of limited analysis</b> .....   | 245 |
| <i>G. Boukhatem, S. Messast, D. Mendjel</i>   |     |
| <b>Micromechanical simulations of biaxial yield, hardening and plastic flow in short Glass fiber reinforced Polyamide</b> ..... | 251 |
| <i>A. Selmi, I. Doghri, L. Adam</i>   |     |
| <b>The use of Algerian phosphogypsum in the manufacture of sulphoaluminates cement</b> .....                                    | 257 |
| <i>L. Kacimi, A. Merouane, A. Simon-Masseron, Z. Derriche</i>   |     |
| <b>Substitution of regular cement by reactive cement of fly ash sulfates</b> ..   | 261 |
| <i>L. Kacimi, M. Cyr, P. Clastres</i>   |     |

• **Volume 2**

**Design of protective structures against rock impacts  
Risk, earthquake and dynamic analysis (Materials and Structures)**

**Numerical modeling of ground reinforced embankments used for rockfall protection** .....269  
*C. Ronco, C. Oggeri, P. Bertolo, P. Ferraiolo, G. Giacchetti*

**An innovative design process for rockfall embankments: Application in the protection of a building at Val d'Isère**.....277  
*J. Lorentz, J. P. Plassiard, L. Muquet*

**Finite element analysis of Geo-grid-reinforced protective wall against snow avalanche**.....283  
*K. Sawada, A. Yashima, S. Moriguchi, S. Inoue, N. Nishida, E. Sung*

**Modelling of block impacts with a combined discrete-continuum approach** ..... 289  
*A. Breugnot, P. Gotteland, P. Villard, P. Garcin*

**CE marking of rockfall protection kits - The new European approach** ..... 297  
*G. Kohlmaier*

**Comparative analysis between the Swiss Standard (FOEN) and the Recommendation ETAG-027 (EOTA) for rockfall protection kits approval**.....303  
*A. Roth, R. Luis Fonseca, C. R. Qunitana, J. T. Barrat, J. A. Planes, J. A. Mitjana*

**Test site Erzberg Full scale tests of rockfall protection kits up to 5000 kJ according ETAG 27: Experiences and outlook from the point of view of a system supplier** .....311  
*G. Stelzer, M. Hamberger, A. Bichler*

**A new site in the French Alps for full-scale tests on rockfall protection works: project and realization** ..... 317  
*F. Rocher-Lacoste, L. Dubois, M. Feregotto, M. Bost*

**Design of rockfall net fence interventions**.....323  
*D. Peila, C. Ronco, L. Borio, S. Pelizza*

**Impact load transmission within a half-scale sandwich rockfall protection wall** ..... 331  
*A. Heymann, P. Gotteland, S. Lambert*

|   |     |
|---|-----|
| <b>Impact loads of falling rocks on granular material</b> .....   | 337 |
| <i>W. Gerber, A. Volkwein</i>   |     |
| <b>Use of the ultrasound to predicting the collapsible soils</b> .....  | 343 |
| <i>M. S. Laouar, K. Abbeche, F. Messaoud</i>  |     |
| <b>Genetic algorithm search for critical slip surface in slope stability analysis</b> .....                                     | 349 |
| <i>M. Djenatte, M. Salah</i>  |     |
| <b>Falling-weight impact test for 2/5 scale model of rockfall protection gallery with/without sand cushion</b> .....            | 355 |
| <i>H. Kon-no, S. Yamaguchi, H. Nishi, N. Kishi, Y. Kurihashi</i>  |     |
| <b>Weight impact test for rockfall protection wall jointed to steel-pile foundation with H-section steel</b> .....              | 361 |
| <i>S. Yamaguchi, H. Nishi, H. Kon-no, N. Kishi, Y. Ushiwatari</i>   |     |
| <b>Numerical analysis method for prototype reinforced concrete girders under consecutive impact loading</b> .....               | 367 |
| <i>N. Kishi, S. G. Krasraghy, H. Kon-No</i>   |     |
| <b>Reinforced concrete structures for rockfall protection</b> .....   | 373 |
| <i>T. Tonello, J. L. Palle</i>  |     |
| <b>Hydration Rockfall attenuator and hybrid drape systems - design and testing considerations</b> .....                         | 379 |
| <i>J. Glover, A. Volkwein, F. Dufour, M. Denk, A. Roth</i>  |     |
| <b>New energy dissipating device for rockfall protection barriers</b> .....   | 385 |
| <i>A. Trad, A. Limam, P. Robit</i>  |     |
| <b>Dissipating devices for rockfall protection kits</b> .....   | 393 |
| <i>B. Boutillier, A. Marzouk</i>  |     |
| <b>Discrete element simulation of an innovative metallic net dedicated to rockfall protection: a multi-scale approach</b> ..... | 399 |
| <i>D. Bertrand, A. Trad, R. Chauvel, A. Limam</i>   |     |
| <b>A numerical model for the design of low energy rockfall protection nets</b> .....  | 407 |
| <i>F. Bourrier, C. Bigot, D. Bertrand, S. Lambert, F. Berger</i>  |     |
| <b>Hydration induced meso-stresses in concrete and their consequences on the cyclic behavior</b> .....                          | 413 |
| <i>C. La Borderie, M. Matallah, M. Briffaut, F. Benboudjema, J. M. Torrenti</i>   |     |
| <b>Impact characterization on a concrete slab using the inverse method</b> .  | 421 |
| <i>P. Perrotin, Z. Boukria, A. Bennani, A. Limam</i>  |     |

|   |     |
|---|-----|
| <b>A new device to simulate explosion blast on reduced-scale structures</b> .....   | 429 |
| <i>P. Berthet-Rambaud, A. Limam</i>   |     |
| <b>Dynamic behavior of a tensegrity ring</b> .....  | 435 |
| <i>J. F. Dubé, A. Averseng, B. Crosnier</i>   |     |
| <b>Damage mechanics applied on the seismic behavior of concrete structures</b> .....                                      | 445 |
| <i>S. Ghavamian, L. Jason, J. Bonenfant</i>   |     |
| <b>ISS modelling and its contribution to the seismic response of RC structures</b> .....                                  | 453 |
| <i>S. Grange, P. Kotronis, J. Mazars</i>  |     |
| <b>Seismic vulnerability reduction: numerical modeling of FRP reinforcement using multifiber beams elements</b> .....     | 459 |
| <i>C.Desprez, S. El Arem, P. Kotronis, J. Mazars</i>  |     |
| <b>Seismic vulnerability of quasi-symmetric structures with reinforced concrete shear walls</b> .....                     | 465 |
| <i>M. Hemsas, S. M. Elachachi, cD. Breysse</i>  |     |
| <b>Towards Implicit Performance Based Seismic Design Rules</b> .....  | 473 |
| <i>F. Legeron, M. N. Sheikh</i>   |     |
| <b>From concrete modeling to infrastructure risk management, what can be learned from experience?</b> .....               | 479 |
| <i>B. Gerard, S. Crouigneau</i>   |     |
| <b>An experimental analysis of the bond-slip cracking in corroded reinforced concrete structures</b> .....                | 487 |
| <i>Y. Berthaud, F. Ragueneau, T. B. Hop</i>   |     |
| <b>Risk-based design of reinforced concrete structures: uncertainties maximization related to corrosion process</b> ..... | 493 |
| <i>B. Capra, C. Descellier, vC. Soize</i>   |     |
| <b>Learning from experiences: forensic engineering and collapse databases</b> .....                                       | 499 |
| <i>D. Breysse</i>   |     |
| <br>  |     |
| • <b>Volume 3</b>   |     |
| <b>Assessment and preservation of historic masonry structures</b>   |     |
| <b>Valorization of Wastes in construction</b>   |     |
| <br>  |     |
| <b>L'Aquila earthquake: emergency actions for the preservation of Cultural Heritage buildings</b> .....                   | 509 |
| <i>C. Modena, F. da Porto, F. Casarin, M. Munari, G. Bettiol, E. Simonato</i>   |     |

|  |     |
|--|-----|
| <b>The effects of floods on masonry walls: ND techniques to evaluate the drying rate</b> .....   | 523 |
| <i>G. Cardani, L. Cantini, S. Munda, C. Tiraboschi, L. Binda</i>   |     |
| <b>Monumental heritage in the L'Aquila, Italy, earthquake: considerations on a case-study</b> .....  | 529 |
| <i>L. Binda, C. Chesi, M. Parisi, J. Magi, C. Marsili</i>  |     |
| <b>Structural monitoring of damaged cultural heritage buildings after the April 2009 Abruzzi earthquake</b> .....  | 535 |
| <i>F. Casarin, C. Modena, M. R. Valluzzi, F. Da Porto</i>  |     |
| <b>Use of scratching techniques to characterize the strength of materials in historic masonry structures</b> .....   | 541 |
| <i>F. Dagrain</i>  |     |
| <b>Large masonry models study implementing shaking table tests: Hagia Irene case study. Part I: model design, material design, not reinforced and reinforced model results</b> ..... | 551 |
| <i>G. Croci, A. Viskovic, A. Herzalla, L. Antonelli</i>  |     |
| <b>Large masonry models study implementing shaking table tests: Hagia Irene case study. Part II: actions, energy evaluations, dynamic behavior</b> .....                             | 559 |
| <i>G. Croci, A. Viskovic, A. Herzalla, G. De Canio, M. Mongelli, I. Roselli</i>  |     |
| <b>Studies on historical mortars Application of <sup>27</sup>Al MAS-NMR</b> .....  | 567 |
| <i>T. Hanzlicek, Y. Perna, Z. Ertl</i>   |     |
| <b>Cultural Heritage Protection Against Flooding (CHEF) - A European Research Project</b> .....  | 573 |
| <i>C. Kopp, R. Helmericha</i>  |     |
| <b>Experimental study of lime pouzzolanic renders for conservation of historical buildings</b> .....   | 579 |
| <i>M. R. Labiadh, M. Ben Ouezdou, B. Abderahmane</i>   |     |
| <b>Implementation of a new method of formulation for road base layer by the use of packing density model</b> .....   | 587 |
| <i>A. Zri, N. Abriak, M. Benzerzour</i>  |     |
| <b>Implementation of a new method of formulation for road base layer by the use of packing density model</b> .....   | 595 |
| <i>M. Miraoui, R. Zentar, N. Abriak</i>  |     |
| <b>Recovery of material used tires in concrete</b> .....   | 601 |
| <i>M. Benzerzour, N. Abriak, C. Deboffe, L. Verbrugge</i>  |     |

|   |     |
|---|-----|
| <b>Valorisation by crushing of thermoset composites (polyester/glass fiber) in Ultra High Performance Concrete (UHPC)</b> .....             | 607 |
| <i>N. Sebaibi, M. Benzerzour, N. Abriak, C. Binetruy</i>  |     |
| <b>Agglomeration processes and pozzolanic reactivity of metakaolins</b> ....  | 617 |
| <i>E. Garcia-Diaz, A. Benhassaine</i>   |     |
| <b>Waste materials, their radioactivity and their use as building materials</b>   | 623 |
| <i>M. Zucchetti, L. Bonavigo</i>  |     |
| <b>Soils treatments as model of waste passivation process: mechanism of soils treatment with quicklime and hydraulic Binders</b> .....      | 631 |
| <i>N. Cabane, D. Nectoux, P. Gaudon, M. Fouletier</i>   |     |
| <b>Valorization of two wastes of food industry in manufacturing of lightweight building materials</b> .....                                 | 647 |
| <i>A. Remadnia, R. Dheilily, A. Goullieux, M. Quéneudec</i>   |     |
| <b>The study of behavior of bottom ash under homogeneous stresses. Determination of parameters for Nova behavior models</b> .....           | 653 |
| <i>H. Le Ngoc, N. Abriak, C. Binetruy, M. Benzerzour, S. Chaki</i>  |     |
| <b>Utilization of biomass ashes for construction purposes</b> .....   | 661 |
| <i>I. Perna , T. Hanzlicek, Z. Ertl</i>   |     |
| <b>The influence of filler content on the compactness of the bituminous mixture</b> .....   | 667 |
| <i>S. Yaich, K. Machta</i>  |     |
| <b>Genetic algorithm search for critical slip surface in slope stability analysis</b> .....   | 673 |
| <i>D. Mendjel , S. Messast</i>  |     |
| <b>Caractérisation de deux composites à matrice minérale et fibres végétales en vue d'utilisation dans le domaine de construction</b> ..... | 679 |
| <i>M. Bentchikou, S. Hanini, K. Silhadi, F. Debieb</i>  |     |
| <b>Contribution of the marine sediments of Bizerte harbor in the RCC formulation for pavement</b> .....                                     | 685 |
| <i>M. Zdiri, N. Abriak, J. Neji</i>   |     |
| <b>Development of integrated bioenergy devices for improvement of quality of life of poor people</b> .....                                  | 691 |
| <i>A. Omer</i>  |     |
| <b>The effect of the Fly-ashes and the Fillers limestones on performances of the superplastified mortars</b> .....                          | 701 |
| <i>C. Amouri, H. Houari</i>   |     |

|  |     |
|--|-----|
| <b>Study of properties of a self-compacting concrete base of local materials</b> ..... | 707 |
| <i>G. Benkechkeche, H. Houari, S. E. Bensebti, A. H. Chabane</i>                       |     |
| <b>Crack dynamics and water flow in cracking soils</b> .....                           | 713 |
| <i>H. Trabelsi, M. Jamei, H. Zenzri, S. Olivella, E. Romero</i>                        |     |

● **Volume 4**  
**Geomaterials and structures**

|  |     |
|--|-----|
| <b>Discontinuum mechanics</b> .....  | 723 |
| <i>M. Frémond</i>  |     |
| <b>Effective elastic properties of porous materials: comparison between theoretical averaging predictions and experimental results</b> ..... | 733 |
| <i>K. Miled, K. Sab, R. Le Roy</i>   |     |
| <b>Modeling of tire-road contact "Development of a tire crushing model"</b>  | 741 |
| <i>A. Bouabid, H. Hassis</i>   |     |
| <b>Solving parallel Markov Decision Processes under capital rationing constraints</b> .....  | 747 |
| <i>W. Raphael, R. Faddoul, A. H. Soubra, A. Chateauneuf</i>  |     |
| <b>Clay Concrete: Application for the stabilized earth blocks</b> .....  | 757 |
| <i>H. Ben Ayed, A. Kallel, O. Limam</i>  |     |
| <b>Contribution to the experimental study of the effect of adding Tunisian clay in the mortar</b> .....                                      | 763 |
| <i>N. Salem, M. Ltifi, H. Hassis</i>   |     |
| <b>Effects of elevated temperature on the bond between steel reinforcement and concrete</b> .....  | 769 |
| <i>C. Fatnassi, A. Kallel, O. Ben Mekki</i>  |     |
| <b>Chemical, physical and mineralogical characterization of basic oxygen furnace slag (BOF slag)</b> .....                                   | 775 |
| <i>E. Belhadj, C. Diliberto, A. Lecomte</i>  |     |
| <b>A fuzzy approach for optimizing the feasibility of underground gas-storage caverns</b> .....  | 781 |
| <i>D. Boumezerane, B. Zlender</i>  |     |
| <b>Comparison of different probabilistic methods for shallow foundation analysis</b> .....   | 787 |
| <i>K. Farah, M. Ltifi</i>  |     |

|   |     |
|---|-----|
| <b>Development of a reliability analysis of slopes stability</b> .....  | 793 |
| <i>M. Selmi, M. Ltifi, H. Hassis</i>  |     |
| <b>Finite element analysis on the factor of bearing capacity, <math>N_\gamma</math> of a strip footing resting on top surface of a slope adjacent to another foundation</b> ..... | 801 |
| <i>K. Abbeche, T. Ayadat, L. Demagh</i>   |     |
| <b>Contribution to the study of the influence of the geometrical factors, geotechnics and hydraulics on the stability of the homogeneous earth dams</b> .....                     | 809 |
| <i>M. Meksaouine, H. Chabbi</i>   |     |
| <b>Migration of heavy metals in saturated reconstituted kaolinite and its impact on the permeability</b> .....  | 815 |
| <i>X. Liu, N. Saiyouri, P. Y. Hicher</i>  |     |
| <b>The macroscopic behaviour of the granular medium with soft particles</b> .....   | 823 |
| <i>L. El Ghezal, M. Jamei</i>   |     |
| <b>Modelling of water flow in deformable unsaturated porous media</b> .....   | 829 |
| <i>S. Rafrat , L. Guellouz</i>  |     |
| <b>The singular elastostatic fields at the plane notch vertex of a compressible hyperelastic Blatz Ko Material</b> .....  | 835 |
| <i>A. Karoui, M.Trifa, M. Arfaoui, R. Abdelmoula</i>  |     |
| <b>Rheology and grouting of colloidal silica in soil</b> .....  | 841 |
| <i>A. Guefrech, N. Saiyouri, P. Y. Hicher</i>   |     |
| <b>The contribution of the clinker microstructure to cement quality control</b> .....   | 847 |
| <i>N. Ben Jamaa, M. Bagané</i>  |     |
| <b>A coupled Finite Elements/Discrete Elements approach for the simulation of impacts on reinforced concrete structures</b> .....   | 855 |
| <i>J. Rousseau, S. Gavaille, M. Marin , L. Daudeville, S. Potapov</i>   |     |
| <b>Numerical simulation of concrete under high confining pressure using discrete element modeling</b> .....   | 861 |
| <i>V. T. Tran, F. V. Donze , F. Marin</i>   |     |
| <b>Interfacial erosion: a three-dimensional numerical model</b> .....   | 867 |
| <i>F. Golay, D. Lachouette, S. Bonelli, C. Galusinski, P. Seppecher</i>   |     |
| <b>Micromechanical modeling of geomaterials: from the material point scale to boundary value problems</b> .....   | 873 |
| <i>F. Nicot, F. Darve</i>   |     |

|   |     |
|---|-----|
| <b>Periodic homogenization of ionic transfer in porous materials</b> .....  | 879 |
| <i>O. Millet, K. Boubartache, A. Ait-Mokhtar</i>  |     |
| <b>Soilmicrostructure changes induced by internal fluid flow: investigations with coupled DE/LB methods</b> .....       | 885 |
| <i>F. Lominè, L. Scholtès, P. Poullain, L. Sibille</i>  |     |
| <b>Experimental analysis on real and analogical granular media materials</b> .....                                      | 893 |
| <i>K. Ait Mokhtar, J. Fortin, N. E. Abriak</i>  |     |
| <b>Theoretical study of the behaviour of anchors in homogeneous soil</b> ..   | 905 |
| <i>F. Mekki, M. Meksaouine, M. Guenfoud</i>   |     |
| <b>Evaluation of corrosion resistance of an Algerian pozzolanic concrete under accelerated testing conditions</b> ..... | 913 |
| <i>N. Kaid, M. Cyr, H. Khelafi, S. Julien, R. Idir</i>  |     |
| <b>• Author Index</b> .....   | 921 |



**Advances in Geomaterials and Structures**  
**Volume 2**

---

*Design of protective structures against rock impacts*

*Guest editor: S. Lambert*

*Risk, earthquake and dynamic analysis (Materials and Structures)*

*Guest editor: J. Mazars*

---



## Numerical modeling of ground reinforced embankments used for rockfall protection

Chiara Ronco<sup>1</sup>, Claudio Oggeri<sup>1</sup>, Daniele Peila<sup>1</sup>, Paola Bertolo<sup>2</sup>, Francesco Ferraiolo<sup>2</sup>, Giorgio Giacchetti<sup>2</sup>

<sup>1</sup> Dept. of Land, Environment and Geo-technology, Politecnico di Torino, Italy  
chiara.ronco@polito.it, claudio.oggeri@polito.it, daniele.peila@polito.it

<sup>2</sup> Officine Maccaferri S.p.A., Zola Predosa, Italy  
paola.bertolo@maccaferri.com, francesco.ferraiolo@maccaferri.com,  
giorgio.giacchetti@maccaferri.com

---

**Abstract.** Rockfall protection embankments are widely used to stop high kinetic energy rolling, bouncing and sliding blocks, in order to protect roads, inhabited areas, quarry plants or yards. Different embankment types have been used, but actually the most frequently installed devices are reinforced ones with geotextiles, geogrids or metallic wire mesh. Nevertheless a design procedure has not been set up because the prediction of rockfall effects on passive protection structures, such as reinforced ground embankments, is a very complex task. In order to develop a design scheme for reinforced ground embankments, a systematic set of finite element method (FEM) numerical models has been implemented to evaluate effects of block impacts on the mountain-side and valley-side faces of embankments. Different impact characteristics and embankment sizes have been evaluated. The series of impact analyses permitted design charts to be obtained. These charts could be used to help engineers choose embankment characteristics.

**Keywords:** reinforced soil, rockfall phenomena, finite element method, design procedure.

---

### 1 Introduction

Rockfall protection embankments are widely used to stop high kinetic energy rockfall events in order to protect roads, inhabited areas, quarry plants or yards (figure 1). Different embankment types made of natural compacted soil, huge rock blocks, gabions or reinforced ground have been used (Nomura et al., 2002; Peila et al., 2007). Actually the most frequently used devices are reinforced ones with geotextiles, geogrids or metallic wire mesh.

Despite the large number of installations, a design procedure has not been set up yet, because of problems related to the non linear stress-strain behaviour of the soil, the large deformations that occur during impact and uncertainties regarding the dynamic behaviour of the soil and the soil-reinforcement interaction. In order to understand the behaviour of

ground reinforced embankments during impact, some full-scale tests have been carried out by various authors (Barrett and White, 1991; Burroughs et al., 1993; Peila et al., 2007; Tissieres, 1999; Yoshida, 1999). These experiments only permitted a limited number of variations in geometries and impact energies to be studied, due to their complexity. Furthermore, there are different examples of numerical modelling application (Prisco and Vecchiotti, 2006; Bertrand et al., 2005; Lambert et al., 2008; Peila et al., 2007; Plassiard et al., 2008), but these researches have not provided a general design procedure for this type of protection work.

Engineers, instead, need a simple design procedure that can provide a feasible and robust evaluation of the type and size of the structure that has to be used to withstand the impact energy of the forecasted rockfall and to quantify its safety factor. In order to develop a general design scheme, based on evidence already acquired and reported in literature from full-scale tests, a systematic series of numerical models, based on Maccaferri Rockfall Embankment System, has been carried out to provide design charts that can help engineers choose of embankment characteristics. This note is based on some of the original results provided by the PhD dissertation by Chiara Ronco (2010, unpublished) in the frame of a research contract supported by Officine Maccaferri S.p.A.



**Figure 1.** Example of reinforced soil embankment used for rockfall protection in Cogne (Italy)

## 2 The numerical model calibration

The commercial code utilized for numerical modelling of reinforced embankments subjected to rockfall is ABAQUS/Explicit, which uses Finite Element Method (FEM). The numerical algorithm on which the software is based is an explicit time integration known as “central difference method”. It is able to take into account the dynamic aspects of the problems, considering also consequent large displacements in the modelled structures. The computation is divided into several small time steps and numerous parameters, like displacement, speed and acceleration of each node of the mesh, are evaluated and registered at each time step.

Tamping tests, available in technical literature, were modelled to define contact characteristics between impacting block and soil during impulsive phenomenon. Mayne et al. (1984) tamping results highlight a linear relation in two-logarithmic chart between impact kinetic energy for surface unit and block penetration in the compacted soil. The numerical model is a soil mattress with fixed joints constrains at the structure base. A rigid spherical body, with defined mass and vertical speed, impacts it in the middle of the top surface (figure 2). The mattress soil is modelled with eight-node brick elements and is considered a perfectly elasto-plastic material, with characteristic parameters of a compacted sand with heterogeneous grains: density  $2100 \text{ kg/m}^3$ , Young modulus 150

MPa, Poisson ratio 0.25, yield stress 1 MPa and corresponding plastic strain 0.1. The soil-block contact was defined like only frictional one using a frictional coefficient equal to 0.40.

Two tamping events were modelled:

- the impact of a 2080 kg block (radius equal to 0.58 m) with impact speed 40 m/s (impact kinetic energy equal to 800 kJ/m<sup>2</sup>);
- the impact of a 520 kg block (radius equal to 0.36 m) with impact speed 40 m/s (impact kinetic energy equal to 500 kJ/m<sup>2</sup>).

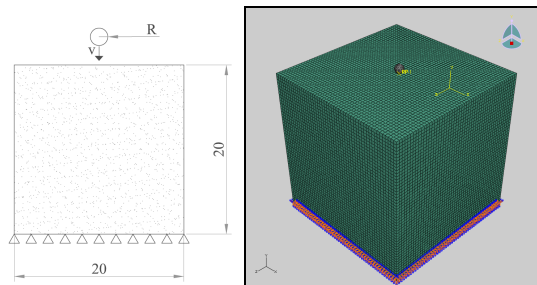


**Figure 2.** Model sizes (quotes in m) with highlighted constraints and speed vector

The obtained penetrations are comparable with results reported in literature: 0.35 m in the first model and 0.23 m in the second one. Observing stresses behaviour during block impact, the mid stress can be seen with a semi-spherical geometry, bigger than area directly interested by the impact. Instead shear stresses create sliding surfaces like Terzaghi and Brich-Hansen foundation criteria (figure 3). These simple models were useful to evaluate code behaviour in modelling dynamic phenomena and permit to define block-soil contact with tangential friction characteristic.

After that, numerical modelling of full-scale tests executed in Meano (Italy) by Politecnico di Torino on reinforced soil embankments used like rockfall protection (Oggeri et al., 2004) were developed to calibrate completely the model itself and to define soil yield criterion. The embankments soil was modelled with eight-node linear bricks using a Drucker-Prager yield criterion and a plastic hardening law. The soil was considered a homogeneous and mono-phase material and the presence of water was neglected. The geotechnical parameters were the usual ones of a granular soil used for embankment construction (Lancellotta, 1995; Bourrier et al., 2008): density 2100 kg/m<sup>3</sup>, Young modulus 110 MPa, Poisson ratio 0.25, drained friction angle 34°, drained cohesion 0 kPa, flow stress ratio 0.78, dilatation angle 0 and yield stress 540 kPa. These were also derived from in situ tests carried out during the construction of the rockfall protections. Due to numerical calculation problems linked to the management of the impact surfaces, the steel net used on upslope and downslope embankments faces was not modelled. The contact between the soil layers, which is obtained with the reinforcement elements, was modelled using a “master-slave weighted penalty method”, assuming a friction angle of 24° between the various layers. This is an average value which has been obtained from shear tests on reinforcing elements (Del Greco and Oggeri, 1999). The adopted connection definition method checks for possible mesh collisions between the given surfaces or nodes during each time step and calculates the surface reaction force that will be applied in the next time step. The reinforcing elements were not directly modelled: they were taken into account considering reinforced soil embankments divided into soil layers connected only

with specific friction ties. The impacting block was modelled as a perfectly rigid body, with a friction angle of 22° between the block and the soil. This friction value was defined on the basis of the tamping tests back analysis (Mayne et al., 1984).

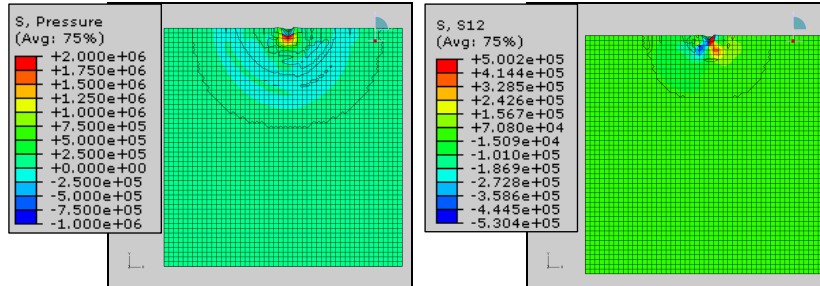


Figure 3. Stresses contours plot (mid pressure and shear stress) after block impact sized 0.58 m (legend in Pascal)

Two full-scale tests on rockfall embankments were modelled:

- the impact of a 5000 kg block (edge equal to 1.25 m) with impact speed 31 m/s, perpendicular to mountain-side face (impact kinetic energy equal to 2400 kJ);
- the impact of a 8700 kg block (edge equal to 1.50 m) with impact speed 31 m/s, perpendicular to mountain-side face (impact kinetic energy equal to 4200 kJ).

The back analyses results showed good agreement with the measured data:

- in the first model, mountain-side penetration results equal to 0.60 m e valley-side deformation 0.20 m;
- in the second one, mountain-side penetration results equal to 1.00 m e valley-side deformation 0.80 m (figure 4).

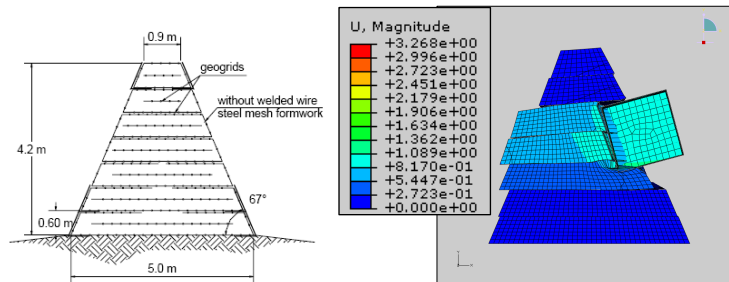


Figure 4. Geometrical features of modelled reinforced embankment and contour plot of total displacement at the end of embankment deformation after 4200 kJ impact (legend in metres)

### 3 The rockfall protection embankments design charts

Reinforced embankments subjected to impact have therefore been studied using a systematic set of three-dimensional models developed with the ABAQUS/Explicit Finite Element Method code. The aim was to create summary charts useful to design these rockfall protection structures when characteristics of rockfall events are known.

Four different sizes of Green Terramesh embankment (figure 5) were modelled to obtain results concerning rockfall protection behaviour. Green Terramesh embankments are assembled with units made of double twisted wire mesh, heavily galvanized with Galfan (Zn - Al 5% - MM mischmetal alloy) and polymer (self extinguish modified polyethylene) coating steel wire. In order to verify the reaction of embankments at different energy levels and to obtain design charts for the modelled structures, the speed of the impacting block was raised till the collapse energy was reached (constant block mass) for the different sizes of the embankments. The block speed was always assumed horizontally directed, which is the worst impact scenarios. The model features (elements type, soil parameters, contacts characteristics) are the same used for calibration embankments model (table 2) and are typical for the specific reinforcement type. The developed series of models were:

- impact of cubic block (mass 8700 kg, edge size 1.50 m) at 2.25 m height, increasing impact speed until embankments collapse with all illustrated embankments sizes (figure 5);
- impact of cubic block (mass 20000 kg, edge size 2.00 m) at 2.25 m height, increasing impact speed until embankments collapse with all illustrated embankments sizes.

The developed models permit to define charts reporting mountain and valley sides displacements corresponding to defined impact energy levels (Figure 6). They highlight the linear correlation between impact kinetic energy and mountain and valley-side displacements. Increasing the block mass, embankment deformations increase and the collapse impact energy decreases. This behaviour is more evident for little sizes embankments and derives from the involvement of narrowest layers with bigger masses. Moreover it is evident that mountain-side penetration increases more quickly than valley-side sliding, that is penetration importance increases with impact kinetic energy increase. The limit impact kinetic values defined in the charts (the last points in the curves) are bigger than usual values of full-scale tests because they consider the ultimate limit state with the block arrest. The limit displacements for maintenance have to be defined to evaluate a serviceability limit state.

Other series of models were developed by increasing the impacting block mass, considering a constant impact velocity equal to 30 m/s, varying the block shape and impact height. Particularly, they regarded:

- impact of cubic block with constant speed (horizontal and equal to 30 m/s) at 2.25 m height, increasing block mass until embankment collapses (only embankments size 3);
- impact of spherical block (mass 8700 kg, radius size 0.94 m) at 2.25 m height, increasing impact speed until embankment collapses (only embankment size 3);
- impact of spherical block (mass 8700 kg, radius size 0.94 m) at 3.40 m height, increasing impact speed until embankment collapses (only embankment size 3);
- impact of spherical block (mass 20000 kg, radius size 1.24 m) at 2.90 m height, increasing impact speed until embankment collapses (only embankment size 3);
- impact of cubic block (mass 8700 kg, edge size 1.50 m) at 3.75 m height, increasing impact speed until embankment collapses (only embankment size 3);
- impact of cubic block (mass 20000 kg, edge size 2.00 m) at 3.35 m height, increasing impact speed until embankment collapses (only embankment size 3);
- impact of cubic block (mass 8700 kg, edge size 1.50 m) at 3.00 m height, increasing impact speed until embankment collapses (only embankment size 3);

- impact of cubic block (mass 20000 kg, edge size 2.00 m) at 2.70 m height, increasing impact speed until embankment collapses (only embankment size 3);
- impact of cubic block (mass 40000 kg, edge size 2.50 m) at 2.25 m height, increasing impact speed until embankment collapses (only embankment size 3).

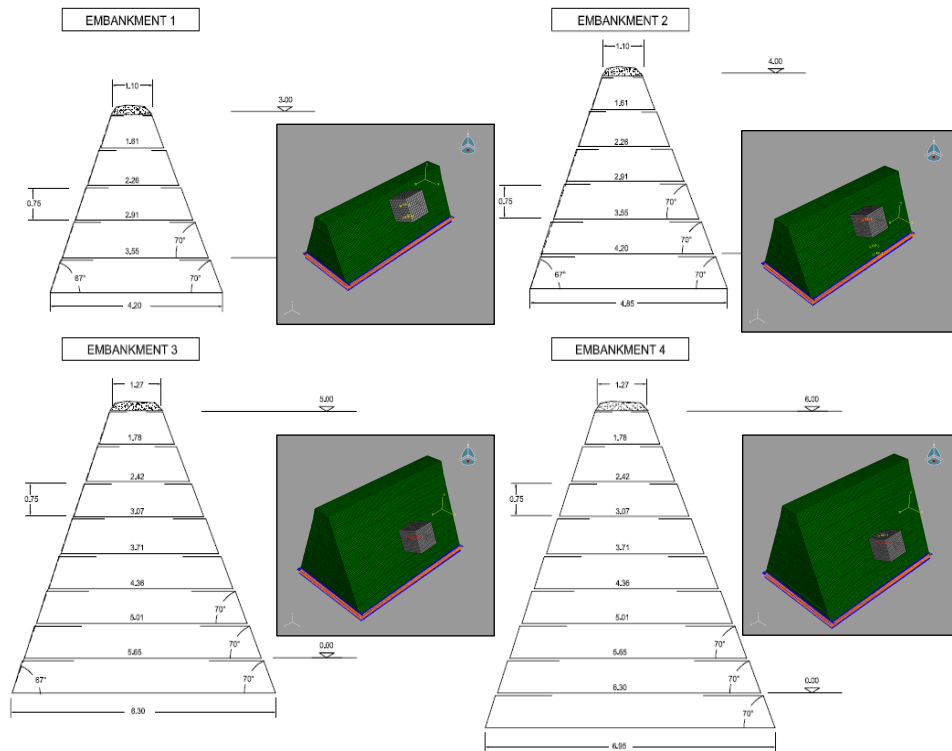


**Figure 5.** Geometrical features of modelled reinforced embankments (Maccaferri Rockfall Protection Embankment - MAC.RO. System) and developed models of the four embankments sizes with impacting block mass equal to 8700 kg. The fixed joints constraints can be seen at the structures base

All the obtained results can be charted in displacement vs impact kinetic energy chart with variation of dimensionless  $sp/h$ , where  $sp$  is embankment thickness at the impact height (the major value) and  $h$  is the impact height, measured between the embankment crown and the impacting block in its lower point. In these charts variability brackets were created by deformation ranges of developed models corresponding the same impact kinetic energy and  $sp/h$  ratio.

These charts, that were obtained for the specific Maccaferri Rockfall Embankment, highlight that limit impact kinetic energy and limit displacements decrease when  $sp/h$  increases. They could be a useful design instrument. In fact, if impact kinetic energy and impact height are known, it is possible to define the embankment sizes when the admissible displacements and deformations are established. They only regards the minimum thickness of embankments. The safety factor of the protection structure could be increased if the embankment thickness is increased.

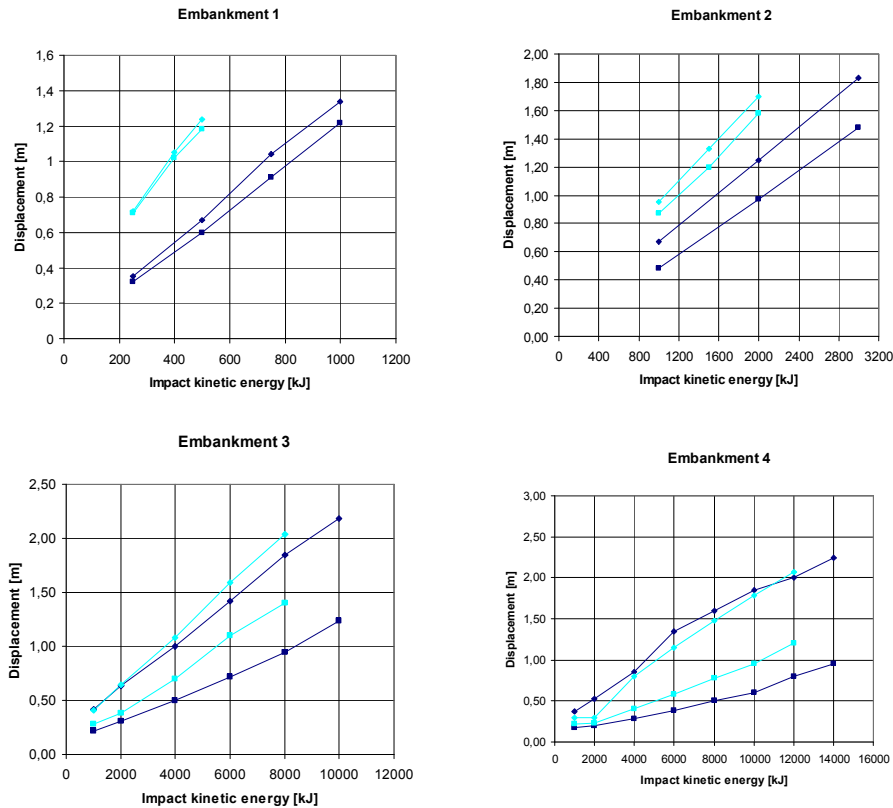


**Figure 6.** Charts reporting mountain and valley-sides displacements (mountain-side penetration and valley-side sliding) vs impact energy levels for the four modelled embankment sizes (♦ mountain-side penetration mass 8700 kg ■ valley-side sliding mass 8700 kg ◆ mountain-side penetration mass 20000 kg ■ valley-side sliding mass 20000 kg)

## 4 Conclusion and perspectives

This paper dealt with the FEM numerical modelling of impacting blocks against reinforced soil embankments. The analyses were developed in dynamic way, using elasto-plastic parameters for soil. The used FEM code manages warping mesh, updating nodes co-ordinates at every time increment. Contacts between block and soil and soil layers were defined with friction behaviour, without meshes overlapping. Reinforcing elements were only defined with specific contact characteristics definition between soil layers. Developed models varied for block shape and mass, impact speed and height, embankment sizes. The model validation derived from back-analysis of full-scale tests of rockfall against reinforced soil embankments and tamping tests.

Models permitted to define mountain-side penetration and valley-side sliding values for every modelled impacts. They highlight the limit kinetic energy, corresponding to embankment collapse, for every impact type and allowed to define classes of embankment behaviour using resume charts, that obviously have to be carefully tuned for different

materials and products, that could be used in design stage of the Green Terramesh rockfall embankment. Of course, they have to be supported by an adequate static and quasi-static analysis, considering equivalent load for impacting phenomena.

New perspectives could interest the dynamic effects in soil layers after block impact, to understand the effective behaviour of reinforcing elements and to define the design criteria. For example, soil accelerations could be obtained from dynamic modelling, analysing behaviour and effectiveness of every reinforcing elements in detail during dynamic phenomena, with the aim of improving interaction behaviour. Further and more detailed original results will be presented after the discussion of the PhD dissertation by the first author, Chiara Ronco, foreseen in 2010.

## References

- Barrett, R. K. and White, J. L. (1991) Rock fall prediction and control. *In Proc. National Symposium on Highway and Railway Slope Maintenance*, pp. 23–40.
- Bertrand, D., Nicot, F., Gotteland, P., and Lambert, S. (2005) Modelling a geo-composite cell using discrete analysis, *Comput. Geotech.*, Vol. 32(8), pp. 564–577.
- Bourrier, F., Nicot, F., and Darve, F. (2008) Physical processes within a 2-D granular layer during an impact, *Granul. Matter*, Vol. 10(6), pp. 415–437.
- Burroughs, D. K., Henson, H. H., and Jiang, S. S. (1993) Full scale geotextile rock barrier wall testing, analysis and prediction. *In Proc. Geosynthetics 1993*, pp. 959–970.
- Del Greco, O. and Oggeri, C. (1999) Caratteristiche di resistenza a taglio di geosintetici. *In Proc. XX Convegno Nazionale di Geotecnica*, pp. 79–86.
- Di Prisco, C. and Vecchiotti, M. (2006) A rheological model for the description of boulder impacts on granular strata, *Geotechnique*, Vol. 56(7), pp. 469–482.
- Lambert, S., Nicot, F., and Gotteland, P. (2008) Experimental study of the impact response of geocells as components of rockfall protections ditches. *In Proc. Interdisciplinary Workshop on Rockfall Protection*, pp. 52–54.
- Lancellotta, R. (1995) *Geotechnical Engineering*, Balkema, Rotterdam.
- Mayne, P.W., Jones, J.S., Dumas, J.C. (1984) Ground response to dynamic compaction, *Journal of geotechnical engineering*, Vol. 110 (6).
- Nomura, T., Inoue, S., Fuchigami, M., Yokota, Y., Kubo, T., Tatta, N., and Arai, K. (2002) Experimental research of reinforced soil wall for rock-fall protection. *In Proc. 7th International conference on geosynthetics*, pp. 303–308.
- Oggeri, C., Peila, D., and Recalcati, P. (2004) Rilevati paramassi. *In Proc. Convegno Bonifica di versanti rocciosi per la protezione del territorio*, pp. 191–232.
- Peila, D., Oggeri, C., and Castiglia, C. (2007) Ground reinforced embankments for rockfall protection: design and evaluation of full scale tests, *Landslides Investigations and Mitigation*, Vol. 4(3), pp. 255–265.
- Plassiard, J. P., Donzé, F. V., and Lorentz, J. (2008) Simulations of rockfall impacts on embankments using a discrete element method. *In Proc. of Interdisciplinary Workshop on Rockfall Protection*, pp. 84–86.
- Ronco, C. (2010) *Soil reinforced embankments used for slope protection: numerical and analytical methods for design support*, unpublished.
- Tissieres, P. (1999) Ditches and reinforced ditches against falling rocks. *In Proc. of the Joint Japan-Swiss Scientific Seminar on Impact load by rock fall and design of protection structures*, pp. 65–68.
- Yoshida, H. (1999) Recent experimental studies on rockfall control in Japan. *In Proc. Joint Japan-Swiss Scientific Seminar on Impact load by rock fall and design of protection structures*, pp. 69–78.

## **An innovative design process for rockfall embankments: Application in the protection of a building at Val d'Isère**

Julien Lorentz<sup>1</sup>, Jean-Patrick Plassiard<sup>2</sup>, Laurent Muquet<sup>2</sup>

<sup>1</sup> Bureau d'étude IMS RN, Parc Pré Millet, 38330 Montbonnot, France  
[julien.lorentz@imsrn.com](mailto:julien.lorentz@imsrn.com), [laurent.muquet@imsrn.com](mailto:laurent.muquet@imsrn.com)

<sup>2</sup> IUT Lyon 1, Département de Génie Civil, 43 Bd du 11 Novembre 1918,  
69622 Villeurbanne  
[jeanpatrick.plassiard@gmail.com](mailto:jeanpatrick.plassiard@gmail.com)

---

**Abstract.** A rockfall embankment has been designed by IMSRN during the summer 2008 at the ski resort of Val d'Isère (France). This embankment has the specificity of being built in an urban area under strong space constraints. The design of the project has been carried out with the discrete element method. Dynamical numerical simulations allowed verifying the internal stability of the structure during the impact. By the way, this model allows computing the force transmitted to the base of the structure during the impact. Finally, this force has been taken into account in the study of the global stability.

**Keywords:** Rockfall embankment, dynamical simulations, discrete element method.

---

### **1 Introduction**

In order to protect new buildings the construction of a rockfall embankment has been required in 2008 at the ski resort of Val d'Isère (France). This embankment has the specificity of being built in an urban area and under strong space constraints (Figure 1). The project has been carried out by the civil engineering consultancy IMSRN. The innovative design process used to optimize the profile of the construction is presented hereafter.

First, the geotechnical context and the resulting choice of a protection structure are introduced. Then, the numerical model dedicated to impact simulations is exposed, as well as the optimization of the embankment profile. Finally, the global stability of the embankment during the impact is presented.

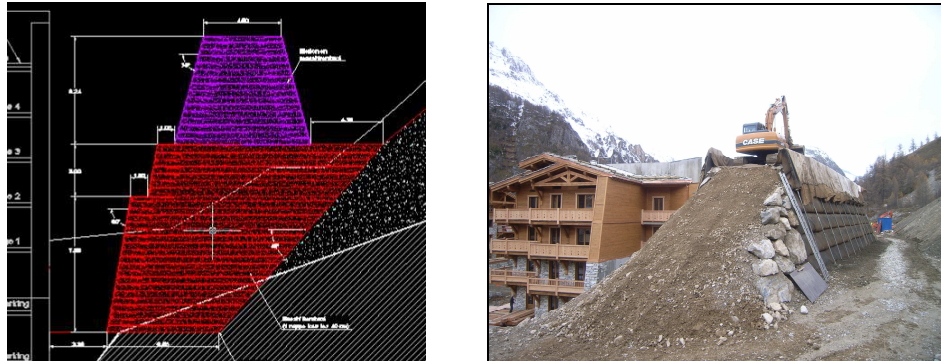


Figure.1. The embankment construction, Val d'Isère, summer 2008

## 2 Geotechnical context

Initially, the implantation of the embankment was planned along the slope that overlooks the building. But the slope inclination as well as the instable fallen debris that composed the soil foundation did not allow this implementation. Geotechnical investigations have shown that the stability of such structure could not be ensured.

Thus, the embankment has to be built on a secure moraine directly located behind the building in the direction of the slope. Because of the lack of space, an embankment with inclined sides to 75°, reinforced with geotextiles, has been planned (Figure 1).

## 3 Embankment design

### 3.1 Reference phenomenon

#### 3.1.1 Diagnosis of the instable rocks on the cliff

A detailed study of the cliff located at the top of the slope has been carried out. Several instable hazard areas of various volumes have been identified (Figure 2).



Figure.2. Cliffs on the top of the slope

Example of an instable block

The huge amount of instable blocks and their spread locations did not allow consolidating them directly on the cliff by active means. Hence, a passive protection such like an embankment was required, the only protection well adapted to the characteristics of the site. The reference phenomenon taken into account is a rockfall of several blocks able to reach the project location with a maximum volume of 30 m<sup>3</sup>.

### 3.1.2 Trajectory path of the blocks

First the blocks fall down from a cliff of 100 m high. Then they go down on a grassy mountainside inclined between 30 and 40° on a length of more than 600 m. The trajectory study has been carried out with 2D numerical simulations. The passing height and the energy of each block at the location of embankment project have been estimated. Simulations showed that the protection structure has to resist against a block having a passing height of 4 m and an impact energy of almost 10 000 kJ (Figure 3).

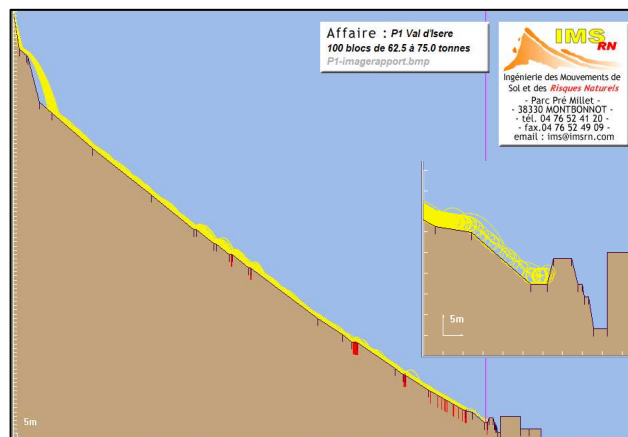


Figure 3. Presentation of the trajectory simulations

## 3.2 Verification of the impact resistance

In order to ensure the resistance of the embankment during an impact, numerical simulations have been undertaken with a discrete element code. By the way, the force transmission to the base of the embankment could be computed and used hereafter for the verification of the global stability.

### 3.2.1 The choice of a discrete element approach

Numerical simulations have been carried out in three dimensions with the software SDEC (Spherical Discrete Element Code). This code has been developed in collaboration with the university Joseph Fourier from Grenoble (3SR laboratory, Donze, 2001). The discrete element method is quite suitable for dynamical phenomena such like impact loadings. Furthermore, the discrete nature of the elements is analogous to that of the granular media. Hence, large strains and damage that occurs during an impact of a block on an embankment can be represented reliably.

### 3.2.2 Numerical model of the reference configuration

A simplified model of the real embankment has been considered for the numerical simulations. The structure is represented by a homogeneous embankment (Figure 4). In order to represent the reinforcement's effect the media's cohesion is enhanced. Here, a cohesion of 30 kPa has been applied, as proposed by the CETE (Subrin, 2006). The geometrical properties of the model are presented in table I.

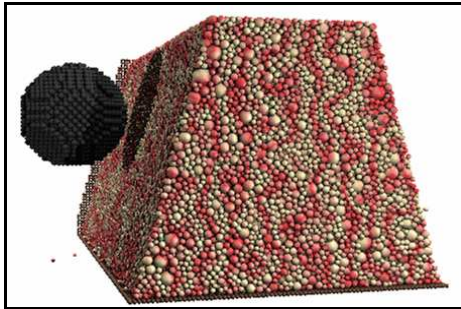


**Figure.4.** The numerical model

|                    |                              |
|--------------------|------------------------------|
| Embankment height  | 6,5 m                        |
| Crest thickness    | 5 m                          |
| Sides orientations | 75°                          |
| Embankment length  | 16 m                         |
| Number of elements | 150 000                      |
| Impact height      | 2/3 of the embankment height |

**Table I.** Main properties of the reference configuration.

The embankment which has been planned is roughly 100 m long, but an impact induces irreversible deformations in a more restricted zone. According to Montani (1998), the force transmission in a horizontal section is delimited by two straight lines oriented at 45°, compared to the impact direction (Montani, 1998). By taking into account the height of impact and the block diameter, a numerical model with a length of 16 m is required to prevent any influence of the boundary conditions. The quasi static properties of the constitutive material of the embankment are presented in Table II. The step by step calibration of the local parameters allows reaching a reliable reproduction of these properties with the numerical model (Plassiard, 2007). They are introduced in the table II.

|                         |                       |
|-------------------------|-----------------------|
| Density                 | 18 kN.m <sup>-3</sup> |
| Young modulus           | 100 MPa               |
| Poisson's ratio         | 0,2                   |
| Internal friction angle | 43°                   |
| Residual friction angle | 32°                   |
| Dilatancy angle         | 15 °                  |
| Cohesion                | 30 kPa                |

**Table II.** Mechanical properties of the numerical embankment

### 3.2.3 Impact simulations

From the reference configuration introduced in the previous part, several numerical simulations were carried out exceeding the initial aim of the initial project. The influence of the impact inclination has been studied to understand the embankment behavior during the impact. Compaction has been also studied to optimize the capacity of the embankment to dissipate the kinetic energy of the block. Also, the combined influence of the impact orientation and of the rotation velocity has been examined.

In this article, we focus on the influence of the impact orientation and on the optimization of the crest thickness. To study the influence of the impact orientation, two numerical simulations have been carried out (Figure 5). First, a horizontal impact as been considered (which corresponds to the most disadvantageous scenario for the construction stability). Then, an inclined impact at  $30^\circ$  has been simulated, according to the results of the trajectory study.

Both simulations show that the reference numerical embankment is efficient in stopping the block. The penetration depth is twice as much important for a horizontal impact than for the inclined impact.

Then, the optimization of the embankment has been undertaken by reducing the crest thickness of the numerical configuration from 5 to 4m, whereas other parameters remain unchanged. Again, a horizontal impact and an inclined impact at  $30^\circ$  have been also studied. The simulation results indicate that an embankment with a 4 m crest thickness still stops the block.

Before building the embankment, raising the height of the reinforced foundation soil to several meters is required by the geotechnical context. The force transmission to the base of the embankment during the impact has been deduced from the previous simulations. The horizontal and vertical components of this force are presented for the 4 scenarios in figure 6 (crest thickness of 4 and 5 m and inclined impacts from 0 to  $30^\circ$ ).

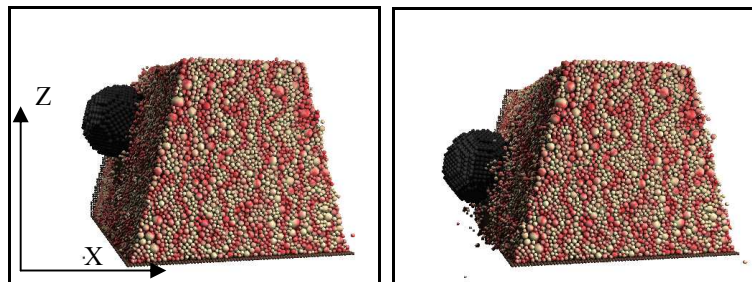


**Figure 5.** The reference configuration: Horizontal impact and impact inclined at  $30^\circ$

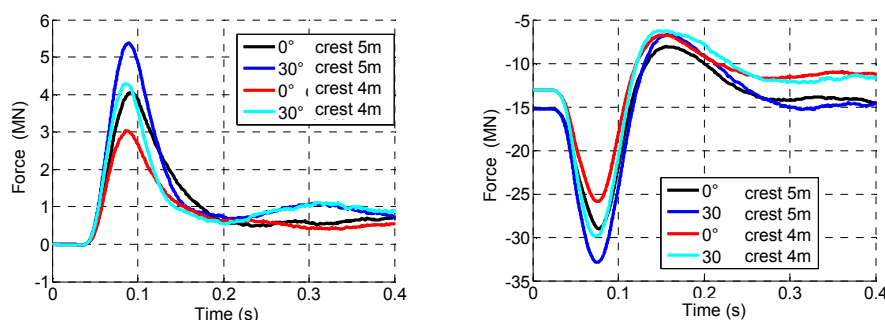


**Figure 6.** Evolution of horizontal and vertical forces transmitted to the base of the embankment

The transmission of the horizontal and vertical forces is more important for an impact orientation inclined at  $30^\circ$  than for a horizontal one. Moreover, the horizontal component increases for the structure involving a larger crest thickness.

### 3.3 Verification of the general stability

Finally, the general stability of the project has been carried out with the software Talren©. Here, the static load of the embankment and the maximal force transmitted to the base during the impact have been considered. The calculation shows that the global stability is ensured by a soil reinforced by geotextiles HS300/50 inserted vertically every 40 cm.

## 4 Conclusions

An innovative method for the design of a rockfall embankment built at Val d'Isère has been undertaken by the civil engineering consultancy IMSRN. The design process has been carried out in 3 dimensions for the dynamics part, with the discrete elements code SDEC. These simulations show that an embankment with a height of 6 m,  $75^\circ$  inclined sides and a 4 m thickness crest was sufficient to resist to an impact energy of almost 10 000 kJ. Moreover, the force transmitted to the base of the embankment during an impact has been taken into account in the verification of the general stability of the construction.

## References

- Donzé, F. V (2001) SDEC (Spherical Discret Element Code) Version 2.00, isrn geonum-nst-2001-03-fr edn. [www.geonum.com](http://www.geonum.com), France,
- Montani, S. (1998) Sollicitation dynamique de la couverture des galeries de protection lors de chute de blocs, Thèse EPFL, Lausanne, Suisse,
- Plassiard, J.P (2007) Modélisation par la méthode des éléments discrets d'impacts de blocs rocheux sur structure de protection type merlon, Thèse, Grenoble.
- Subrin, D. (2006) Modélisation analytique et numérique pseudo-statique des merlons de protection contre les chutes de blocs rocheux, JNGG 2006, Lyon.

## Finite element analysis of Geo-grid-reinforced protective wall against snow avalanche

Kazuhide Sawada<sup>1</sup>, Atsuh Yashima<sup>2</sup>, Shuji Moriguchi<sup>2</sup>, Shoichi Inoue<sup>3</sup>, Yoichi Nishida<sup>3</sup> and Eunsu Sung<sup>4</sup>

<sup>1</sup> River basine research center, Gifu University, Yanagido1-1, Gifu, Japan  
sawada@gifu-u.ac.jp

<sup>2</sup> Department of civil engineering, Gifu University, Yanagido1-1, Gifu, Japan  
[yashima@gifu-u.ac.jp](mailto:yashima@gifu-u.ac.jp)

<sup>3</sup> Protec Engineering, co. Ltd., 5322-26, Hasugata, Seirocho, Niigata, Japan  
[inoue@proteng.co.jp](mailto:inoue@proteng.co.jp), [nishida@proteng.co.jp](mailto:nishida@proteng.co.jp)

<sup>4</sup> Sambo Engineering, co. Ltd., 138-834, 200-2, Bang i-1dong, Songpa-gu, Seoul, Korea  
geoeunsu@hotmail.com

---

**Abstract.** In order to protect the infrastructures and citizens life from snow avalanche, a new type protective wall using geo-material and geo-synthetics has been proposed. For understanding what is taking place inside the protective wall by the impact of snow avalanche, two kinds of numerical simulations are applied to predict the behavior of protective wall during and after impact of snow in this study. Features of geo-grid reinforced protective wall are expressed by the results of a series of real scale rock fall tests to protective wall are introduced.

**Keywords:** reinforced soil, snow avalanche, finite element method

---

### 1 Introduction

A new type protective wall using geo-material and geo-synthetics has been proposed for snow avalanche. In order to understanding what is taking place inside the protective wall made with geo-material and geo-grid by the impact of snow avalanche, two different kind of numerical schemes are used. Firstly, a numerical technique based on fluid dynamics based numerical method (Moriguchi et al.2005) is introduced to simulate an impact force caused by snow avalanche. The calculated impact force and influenced area are used for input data for next step simulation as an example. Secondary, a dynamic finite element analysis of geo-grid reinforced soil protective wall is conducted to predict the behavior of wall. Finally, the stability of reinforced protective wall with geo-grid and geo-material against snow avalanche is discussed based on the numerical results.

## 2 Sand-flow experiment and its simulation

In order to obtain detail information of impact force generated by the flowing sediment, a laboratory experiment was carried out using dry sand and a model slope. A photo and a schematic view of the model slope are shown in Figure 1 and 2. A box-type instrument was installed at the lower end of the flume to measure the impact force. A load cell was placed inside the instrument. A sand-box was set at top of the slope and flow of the sand was initiated by opening side door of the box. The available length of the flume is 1.8 m, and its width is 0.3 m. Different slope angles, 45, 50, 55, 60 and 65 degrees, were used to investigate the effect of slope angle on impact force. The weight of the sand was fixed at 50 kg and the density calculated from the volume of the box and the weight of the sand is  $1,379 \text{ kg/m}^3$ . The surface of the slope was coated with the same sand to provide surface friction.

A series of two-dimensional numerical simulations of the laboratory experiments was also conducted. The fluid dynamics based numerical method (Moriguchi et al.2005) was used in this simulation.

Fig. 3 shows a numerical model used in the simulations. The Eulerian grid included an additional domain to the left of the wall to allow the simulation of sand overtopping the wall. In the numerical simulations the slope was placed in a horizontal position and the



Figure.1. Photograph of slope model

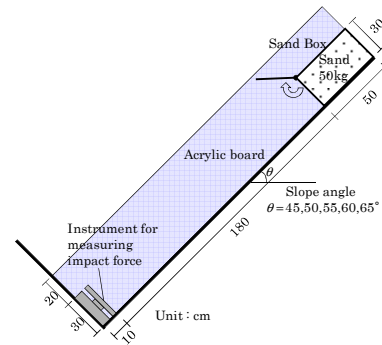


Figure.2. Schematic illustration of slope model

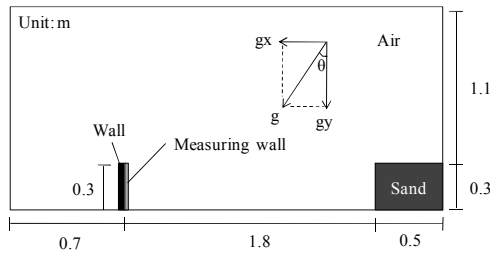


Figure.3. Numerical model

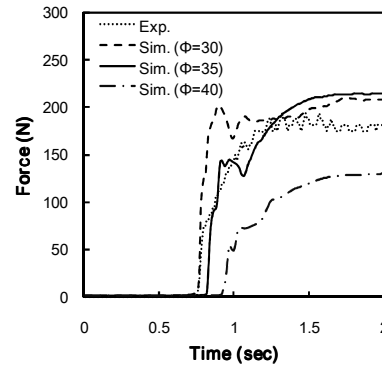


Figure.4. Simulated time histories of impact force for a slope inclination 45 degree

slope inclination was specified in the form of a horizontal component of gravity force. For the record, the distance from the front face of the sand box to the fixed wall was 1.8 m, and the height of the wall was 0.3 m. The base of the flume was coated with sand, so a no-slip boundary condition was specified for the bottom of the slope. The impact force was obtained by integrating the hydrodynamic pressure calculated in front of the measuring wall. To simulate the initial conditions of the laboratory experiment, the sand was placed initially inside a box 30 cm high and 50 cm long on the right side of the Eulerian grid. A uniform Cartesian mesh of dimension 2 cm was used for the simulations. The density of the sand was assumed to be  $1,379 \text{ kg/m}^3$ , in accord with that obtained from the experiment. Because the sand was dry, we specified zero cohesion.

As a first phase of the simulation, Effect of internal friction angle was investigated. While it may be possible to specify the static value of the internal friction angle for the sand, the granular flow experiment is really a dynamic process and the value of the friction angle should reflect this process. Therefore, we conducted a parametric study to determine a value of the dynamic friction angle that is suitable for the mechanical model. To this end, we conducted preliminary simulations for a flume inclination of  $\theta=45$  degrees. Three different values of friction angle,  $\phi=30, 35,$  and  $40$  degrees were considered in the simulations. Figure 4 shows comparison between the simulated time histories of impact force and that measured from the experiment. From the result of the simulation with  $\phi=40$ , it is confirmed that the impact force is much smaller than the experimental result. On the other hand, the simulation with  $\phi=30$  degrees predicted the peak impact force sooner than that observed from the experiment. It appears that the simulation with  $\phi=35$  degrees generally captured the observed flow behavior and time-history of the impact force most accurately, and therefore is henceforth selected as the dynamic internal friction angle for the sand.

In all the remaining numerical simulations we have fixed the internal friction angle for the sand at  $\phi=35$  degrees and used this calibrated parameter to simulate the variation of impact force with flume inclination. Time histories obtained from the experiment and the simulations at different slope angle  $\theta=45, 50, 55, 60, 65$  degrees are shown in Figs. 5 and

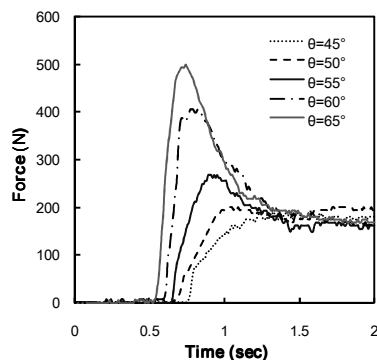


Figure 5. Time history of impact force (Exp.)

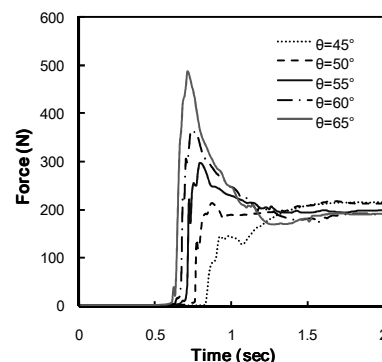


Figure 6. Time history of impact force (Sim.)

6 respectively. It is confirmed the peak impact force increases with steeper slope angles, with the exception of the two flatter slopes of  $\theta=45$  and 50 degrees. In case of these two flatter slope angles the peak value of the impact force is nearly the same as the 'post-peak' value, and for  $\theta=45$  degree there is no peak value. These tendencies can be seen in both experimental and simulated results. In addition, the figures suggest that the peak impact force and residual post-peak value of the wall reactions at each different slope angles were well captured by the numerical model.

### 3. Geo-material and Geo-grid composed protective wall

A protective countermeasure is required a certain performance of absorption of falling rock, soil/snow avalanche energy and reasonable cost for design and construction. Because of this situation, an interest of protecting wall using ground materials such as soil or boulders is increasing due to their energy absorption.

However, the effect of protection affected by rockfall to a measurement has not been fully understood. Recently, several studies on the interaction problem between falling rock and protective barrier have been published. Prisco & Vecchiotti(2006) presented the study about a rheological model for the description of rockfall on homogeneous ground and discussed impact load against vertical falling rock. Wu & Thomson(2007) also presents the interaction between a guardrail post and soil during quasi-static and dynamic loading by field tests and numerical analyses using LS-DYNA(2003). Kawahara and Muro(2006) are investigated the effects of the dry density and thickness of sand cushion on response by a falling rock. In the former study, in order to investigate the interaction problem between rockfall and protecting wall using ground materials, constitutive models of geo-materials and shape of protecting wall should have considered. Therefore, to investigate the mechanical behaviors of protecting wall with ground material against rockfall, full-scale model tests and numerical analyses are presented (Aminata et. al 2008). For the request of protection from snow avalanche in this paper, a protective wall composed by geo-materials and geo-grid which has modified for snow is introduced and the effect of a protective wall for snow is discussed based numerical results.

### 4. Numerical model and simulation

Figure 7a shows the typical model of protective wall for snow avalanche for numerical simulation. The wall is composed with geo-material, geo-grid and concrete wall for simplify in numerically. The most significant feature that deferent from against for rockfall is a concrete wall. In the point of view from design for snow, a concrete wall is installed in front face to absorb on wide area.

For design a protective wall in reasonable performance, it is necessary to predict an impact force of snow avalanche. However, it is difficult to obtain a real value of impact by real snow avalanche. Therefore, an impact force of snow avalanche should be determined by numerical simulation aforementioned based on CFD (Moriguchi et. al. 2005). In order to simulate a behavior of protective wall by snow avalanche in simply in this paper, an impact force is determined artificially.

In this study, a dynamic finite element program 'LIQCA (Oka et. al 1994)' is modified for a snow avalanche problem. By modification of the program, it is possible to input a random load as a snow flow. Figure 7a and 7b are the numerical models respectively, figure 7a shows a model with concrete face in front and figure 7b shows without concrete face. The bodies of both models are composed with geo-material and geo-grid. Material parameters used in models are indicated in table 1. In this study, geo-material is expressed with elastic solid material, geo-grid is a beam element and a joint element is used for interaction between geo-grid and geo-material. The time history of impact force input in the face is shown in Fig. 8 and the boundary condition is in Fig. 9. A snow avalanche is assumed full depth avalanche and the bottom boundary of the wall is fixed.

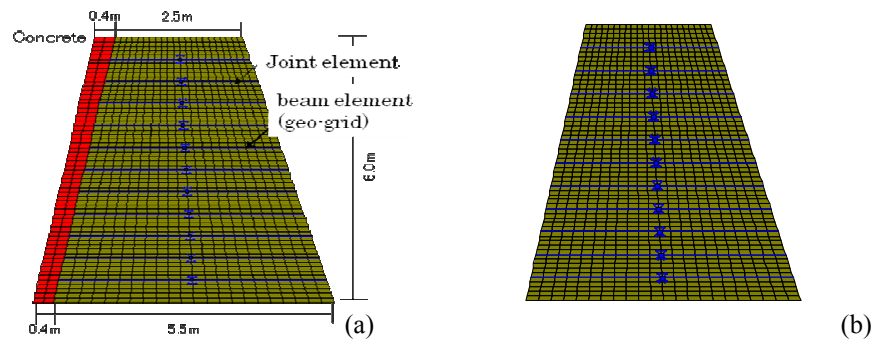


Figure 7. Protective wall (a) with concrete face and (b) without concrete

Table 1. Material parameters

|               | wet density        | Elastic modulus  | Poisson's ratio | elastic modulus (shear dir.) | elastic modulus (normal dir.) | friction      | tensile strength | section force | 2nd momen of section | axial yield force | depression coefficient of axis after yield |
|---------------|--------------------|------------------|-----------------|------------------------------|-------------------------------|---------------|------------------|---------------|----------------------|-------------------|--|
|               | $\rho$ ( $t/m^3$ ) | $E$ ( $kN/m^2$ ) | $\nu$           | $k_s$ ( $kN/m^2$ )           | $k_n$ ( $kN/m^2$ )            | $\tan \phi_s$ | ( $kN/m^2$ )     | $A$ ( $m^2$ ) | $I$ ( $m^4$ )        | ( $kN/m$ )        | $a_3$                                      |
| wall(e:astic) | 1.90               | 1.00E+04         | 0.33            | -                            | -                             | -             | -                | -             | -                    | -                 | -  |
| concrete      | 2.45               | 1.00E+09         | 0.33            | -                            | -                             | -             | -                | -             | -                    | -                 | -  |
| geo-grid      | 1.00               | 2.50E+06         | 0.33            | -                            | -                             | -             | -                | 0.005         | 1.00E-06             | 50                | 0.200                                      |
| joint element | -                  | -                | -               | 3.38E+04                     | 1.00E+08                      | 4.36E-01      | -1.00E+08        | -             | -                    | -                 | -  |

## 5. Results and discussions

Figure 10 shows the distribution of results in shear strain after 1.5 second of impact. Figure 10a is the result with concrete face and 10b without. From Figure 10b, it is found that, the distribution of shear strain is concentrated at the both corner at bottom boundary. On the other hand, the shear strain is concentrated just behind of the concrete face in the case with concrete face. The most important matter is the magnitude of shear strain. The value without concrete face indicates almost double compare with the case with concrete face. It means that the concrete face behave rigid with its stiffness and transmit the impact force to the body which is distributed by the concrete body. From these results, there is a possibility to make an appropriate design of the reinforced protective wall for a snow avalanche. More reasonable investigation will be discussed in near future.

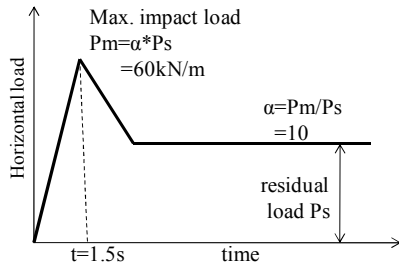


Figure 8. Time history of input loading

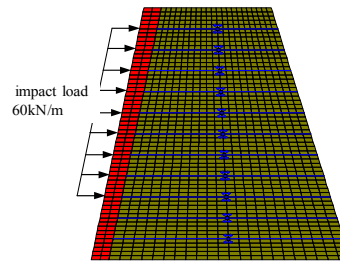


Figure 9. Section of impact loading

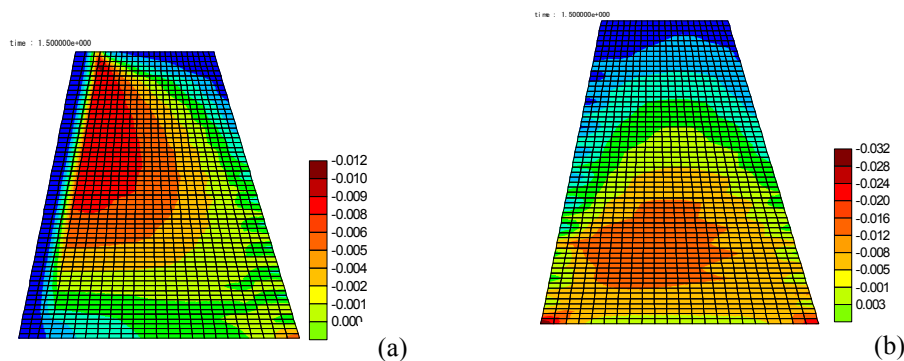


Figure 10. Distribution of shear strain (a) with concrete face and (b) without concrete face

## References

- Aminata, D., Yashima, A., Sawada, K., Sung, E., New Protection Wall Against Rockfall Using a Ductile Cast Iron Panel, *Journal of Natural Disaster Science*, Vol.30, No.1, pp.25-33, 2008.
- Compilation by Japan Road Association. "Handbook for rockfall measures," 2000.
- Hallquist, J. O. 2003. "LS-DYNA Theoretical Manual V.970," Livermore, CA: Livermore Software Technology Corporation
- Kawahara, S and Muro, T. 2006. "Effects of dry density and thickness of sandy soil on impact response due to rockfall," *Int. Jour. Impact engineering* **43**: 329-340.
- Moriguchi S., Yashima A., Sawada K., Uzuoka R., Ito M., 2005, Numerical simulation of flow failure of geomaterials based on fluid dynamics. *Soils Found.*, 45:155-166.
- Oka, F., Yashima, A., Shibata, T., Kato, M., and Uzuoka, R.: FEM-FDM coupled liquefaction analysis for a porous soil using an elasto-plastic model, *Applied Scientific Research*, Vol.52, pp.209-245. 1994.
- Prisco, C. DI. And Vecchiotti, M. 2006. "A rheological model for the description of boulder impacts on granular strata," *Geotechnique* **56**(7): 469-482.
- Wu, W. and Thomson, R. 2007. "A study of the interaction between a guardrail post and soil during quasi-static and dynamic loading," *Int. Jour. Impact engineering* **34**: 883-898.

## Modelling of block impacts with a combined discrete-continuum approach

Antonin Breugnot<sup>1,2</sup>, Philippe Gotteland<sup>2</sup>, Pascal Villard<sup>2</sup>, Patrick Garcin<sup>1</sup>

<sup>1</sup> Egis Géotechnique, Seyssins, France.

[antonin.breugnot@egis.fr](mailto:antonin.breugnot@egis.fr), [antonin.breugnot@hmg.inpg.fr](mailto:antonin.breugnot@hmg.inpg.fr), [patrick.garcin@egis.fr](mailto:patrick.garcin@egis.fr)

<sup>2</sup> L3S-R, UJF-INPG-CNRS UMR 5521, Grenoble Universités, Grenoble, France.

[philippe.gotteland@ujf-grenoble.fr](mailto:philippe.gotteland@ujf-grenoble.fr), [pascal.villard@ujf-grenoble.fr](mailto:pascal.villard@ujf-grenoble.fr)

---

**Abstract.** In mountainous areas, infrastructures and inhabitants need to be safe from risk of rockfall. In order to improve the prediction of structures' behaviour under impact, this paper investigates modelling of granular material layer submitted to high energy impact. An original combined discrete-continuum method is proposed which permits to use discrete element method to model precisely the complex behaviour of granular material in the vicinity of the impacted zone while a continuum approach is used in farther areas. In this contribution, coupled methods are faced on a simulating of an experimental test of a cubic boulder impact on granular material. Finally, this paper draws the prospects of the used of coupled method to model large impacted structures as embankments.

**Keywords:** impact, rockfall, protection structures, combined method, discrete element method.

---

### 1 Introduction

The behaviour of ground structures submitted to local impact due to rockfall is quite complex to characterize precisely. Indeed, high energy loading induces large and irreversible deformations, high strain rates and stresses in geomaterials which make difficult the prediction of mechanical behaviour of rockfall protection structures.

Considering the granular nature of geomaterials, the Distinct Element Method (DEM) (Cundall & Strack, 1979) seems to be particularly adapted to model local mechanical behaviours in geomaterials under dynamical impact. However, the use of this approach, to model large scale works, requires a large number of particles, which increases both the times of modelling and computation.

In order to improve the design of large structures, modelling needs to maintain accuracy in highly stressed areas while representing the mechanical behaviour of the global structure. Consequently, an innovative and original multi-scale approach is developed (Xiao & Belytschko, 2004) to improve the computational efficiency: a discrete element method is coupled with a continuum mechanical model, which resolution can be far

coarser than in DEM. Thereby, continuum domain, adapted to materials with non significant discontinuities, is used as a boundary condition. The first part of the paper is devoted to the procedure of the combined discrete-continuum method and its validation through simple numerical test. In the second part, simulation of an impact with a cubic impactant on a soil layer is led to show the prospects of this approach to model large structure as embankments.

### 2 Combined discrete-continuum method

The researches concerning combined discrete-continuum approaches began in the early eighties, and were led in physical domain in order to study material's behaviour at molecular scale. Since then, the coupling methods and domains application were widely developed (Munjiza, 2004; Itasca 2006; Onate, 2003...). Xiao & Belytschko (2004) and Xiao & Hou (2007) proposed two different domain decompositions which permitted to link continuum and discrete domains, either with an "edge-to-edge" method or a "bridging" domain method, to study dynamical wave propagation or crack propagation in micromechanical structures.

In the latter case, discrete and continuum domains are overlapped in a bridging sub-domain, where Hamiltonian  $H$  is taken to be a linear combination of the discrete and continuum total energies (figure 1), respectively  $H_{Discrete}$  and  $H_{Continuum}$  (1).

$$H = \alpha H_{Discrete} + \beta H_{Continuum} \tag{1}$$

$$\vec{d}_j = \sum_{i=a}^g \overline{k_{ji}} \vec{u}_i \tag{2}$$

$$\vec{g} = \vec{d}_j - \sum_{i=a}^g \overline{k_{ji}} \vec{u}_i = \vec{0} \tag{3}$$

To ensure displacement continuities in bridging zone, displacement  $\vec{d}_j$  of each discrete particle  $j$  is linked to displacements  $\vec{u}_i$  of surrounding continuum nodes  $i$  (figure 2) by the mean of kinematic relations  $\overline{k_{ji}}$  (2). The two domains are finally constrained via (3).

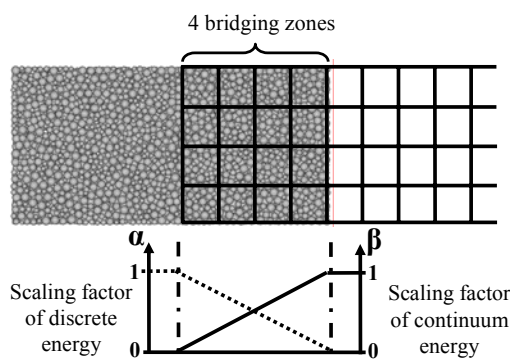


Figure.1. Discrete and continuum scaling factors in overlapping domain

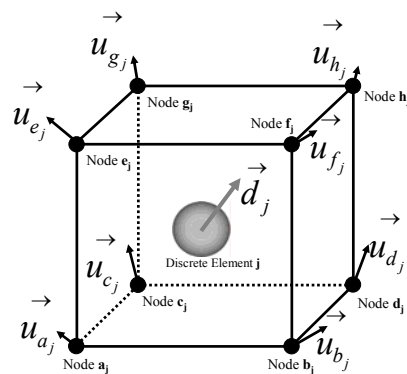


Figure.2. Discrete element position in a continuum volume belonging to bridging domain

Originally formulated for ordered particles, the formulation of the method proposed by Xiao and Belytschko (2004) remains applicable for amorphous sample used for modelling geomaterials. For the simpler “edge-to-edge” model, the Hamiltonian is defined as the sum of discrete and continuum ones (no scaling) because domains are disjoint. Aiming at adapting seamless method for non ordered discrete element sample, the kinematics constraints are calculating using displacement of fictive nodes obtained by orthogonal projection of the DE in the vicinity of the junction, on the continuum plane border. Combined problem is solved by minimizing modified Hamiltonian  $H_L$  for the complete model, using the Lagrangian multiplier  $\lambda$  method to ensure continuity in bridging domain (4). An explicit algorithm is used for dynamical application and the scheme of resolution is detailed in Xiao and Belytschko 2004 and Frangin *et al.* 2006.

$$H_L = \alpha H_{Discrete} + \beta H_{Continuum} + \lambda \cdot \vec{g} \quad (4)$$

In our approach, distinct element method (DEM) (PFC<sup>3D</sup> code, Itasca) is employed in the discrete domain while finite difference method (FLAC<sup>3D</sup> code, Itasca) is employed in the continuum domain. The implementation of these combined methods has been tested and validated by comparing “edge-to-edge” and “bridging” coupled methods to discrete and continuum models, for static and dynamic tests. So, a numerical quasi-static test and a dynamical compression (wave propagation) have been performed on an elastic medium (Breugnot *et al.*, 2010). And the good accordance between responses of different approaches proved that material continuity was ensured at the transition areas. These validation tests provided interesting results regarding the capability of combined model to describe static and dynamical behaviours in elastic domains.

### 3 Impact block simulation

#### 3.1 Model description

The coupling method is used to investigate modelling possibilities of a rock impact on geomaterial layer or later on a global structure. The model presented thereafter is adapted from experimental research, described by Pichler *et al.* (2005), concerning the loading of layers of gravel subjected to rockfall. The experimental approach is based on measurements or estimations of penetration depth, impact force and impact duration when a cubic rock impacts onto the ground with a tip.

The following model is composed by a trench of 4 m width and 2 m depth, dug in natural soil, and filled by well-graded gravel (figure 3a). Bloc impact on gravel is simulated with the “edge-to-edge” and “bridging” combined model, and entirely discrete one in order to validate the numerical processes.

In the different approaches, mechanical behaviour of gravel is described by elasto-plastic behaviour to take into account the absorbing energy capacity of gravel. Elastic parameters of the gravel cushion were estimated by the mean of tests on the embankment (E=198 MPa,  $\nu=0.32$ ), but no significant information was available to estimate plasticity’s parameters. However, the well-graded gravel cushion can be considered as a high frictional material and we assumed that plasticity’s limit can be characterized by a friction angle of 45° without cohesion. The natural soil is not submitted to high load, and is modelled by elastic behaviour. It can be viewed as a boundary condition. Micro-mechanical parameters of the natural soil insure an elastic behaviour characterized by

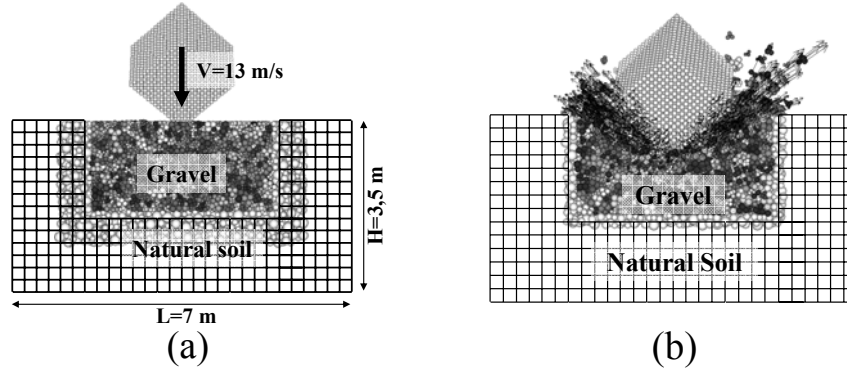


**Figure.3.** (a) Cross section scheme of the bridging coupled model, defined by two overlapping zones, before impact (b) Cross section scheme of the “edge-to-edge” coupled model after impact.

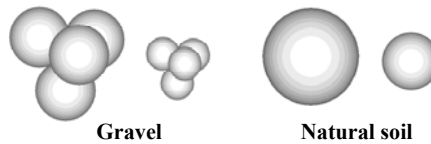


**Figure.4.** Elementary particles used in gravel (clumps) and natural soil (spherical ED) models

$E=500$  MPa and  $\nu=0.32$ ). In the discrete part of the models, clumps, composed by four spherical discrete elements, are used to simulate angularity and thus upper friction angle in gravel cushion particles (Bertrand *et al.*, 2005; Salot *et al.*, 2009), while simple bonded spherical discrete elements are utilized for natural soil (figure 4).

The constitution of the different approaches is summarized in table 1, and highlights that coupled methods permit to reduce drastically the number of discrete elements, which generates long-time of both modelling and computation. The shape of the impactant block is quite cubic, has a masse of around  $m=10\ 000$  kg, and is supposed very stiffer compared to the impacted soil. The cubic shape is a model, so the tip which impacts soil is truncated to avoid a very localized contact. Fall isn't calculated but consequently, the velocity of the boulder was initialized to  $v=13$  m/s, which corresponds to a 8.5 m high fall. The kinetic energy of the impact is almost  $E=850$  kJ which corresponds to the experimental work of Pichler *et al.* (2005).

| Models          | Gravel                 | Natural Soil             |                        | Coupling Zone            |                        |      |
|-----------------|------------------------|--------------------------|------------------------|--------------------------|------------------------|------|
|                 | <i>Discrete Clumps</i> | <i>Discrete Elements</i> | <i>Continuum Nodes</i> | <i>Discrete Elements</i> | <i>Continuum Nodes</i> |      |
| <b>Discrete</b> | 7620                   | 42992                    | -                      | -                        | -                      |      |
| <b>Coupling</b> | <b>Edge-to-edge</b>    | 7620                     | 7701                   | 10815                    | 1962                   | 801  |
|                 | <b>Bridging</b>        | 7620                     | 15138                  | 10815                    | 8983                   | 3051 |

**Table.1.**Repartition between discrete particles and continuum nodes used in gravel, natural soil and coupling zones

### 3.2 Calculation results and comments

During impact, penetration and resulting force on the cubic impactant are recorded to be compared to experimental measures (Pichler et al., 2005). The response of models based on coupling methods is close to the entirely discrete one (figure 5) and the slight differences can be partially affected to material characterization in natural soil for both discrete and continuum approaches. This study draws the prospects of this approach to large geometry of structure which needs locally accurate description.

However, due to simplifying assumptions made to model the gravel soil, the comparison with experimental and analytical results given by Pichler *et al.* (2005) shows that dynamical resistance of the gravel layer is under-estimated. Indeed, experimental penetration  $P_{exp}$  ( $P_{exp} = 0,51$  m) and analytical impact force  $F_{exp}$  ( $F_{exp} = 3,5$  MN) are respectively 15% and 12 % lower (Table 3).

These differences can be partially explained by both static characterisation of the mechanical parameters and no consideration of dynamical effect during impact (energy dissipation, local plasticity, braking of grains, etc.).

Furthermore, the influence of boulder's shape has been tested through a cubic, a cubic with truncated tip, and a spherical impactants which all have the same mass (figure 6). It was obvious that the spherical one was the less perforating, but we didn't expect that the boulder could bounce on the gravel cushion (figure 7). This finding corroborates the phenomenon of particles ejection observed numerically around impact (figure 3b). The

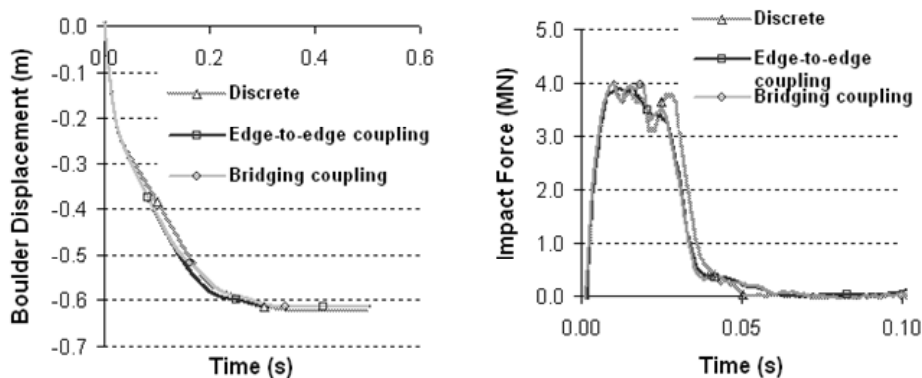


Figure.5. Penetration and impact force calculated by coupled and discrete approaches

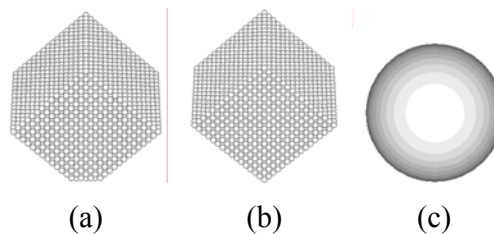
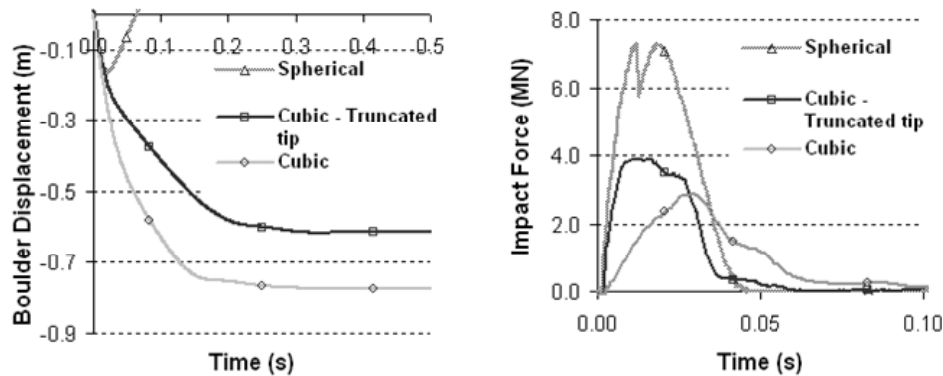


Figure.6. Boulder's shapes: (a) cubic with truncated tip (b) cubic (c) spherical



**Figure.7.** Penetration and impact force calculated by "edge-to-edge" coupled method for different boulder's shapes

model seems not to dissipate enough energy, and the elastic restitution is over-estimated, for shallow discrete element, compared to experimental observations.

The actual constitutive law, calibrated from quasi-static triaxial tests, can't model phenomenon as viscosity, compaction and local breaking in high loaded areas. Dissipations due to interparticle sliding (friction) are not sufficient to represent all sources of dissipation during impact. Aiming at improving the response of the granular material, and in the same time the validity of this model, additional dissipative laws need to be implemented.

#### 4 Perspectives and conclusions

In this paper, an innovative combined discrete-continuum method has been adapted to study mechanical behaviour of a soil layer impacted by a boulder. In this case, the good accordance between discrete and combined discrete-continuum methods shows the interest of such method to describe locally impact phenomenon. Generally, even if constitutive laws, used to describe behaviour of granular material under high loading, were rather simple, penetration and impact force numerically calculated were close to those measured experimentally. At this step, the limits of the numerical model are based on the description of the dissipative behaviour of high loading granular material. Local constitutive laws needs to be further developed to take into account dynamical behaviour of granular under high energy impact.

In the framework of REMPARE research project ([www.rempare.fr](http://www.rempare.fr)), high energy impact experiments (2000 kJ) have been performed to test protection dams at real scale. The aim of our research is to benefit from numerical development (combined approach) to model large civil and geotechnical engineering structures as rockfall protection embankments (figure 8) and experimental data should permit us to feat our model in order to optimize and improve protection structure design.

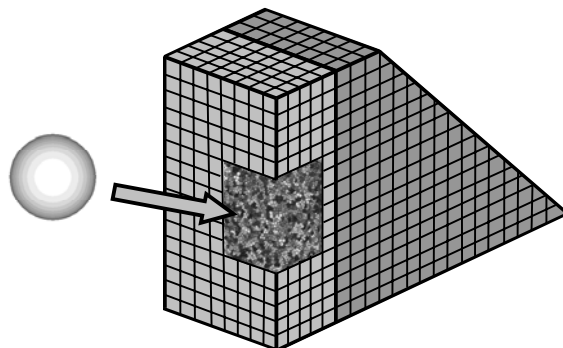


**Figure.8.** Model of a rockfall protection embankment, using combined discrete-continuum method

## References

- Bertrand, D. Nicot, F. Gotteland, P. & Lambert, S. (2005) Modelling a geo-composite cell using discrete analysis. *Computers and Geotechnics* Vol 32: pp 564–577.
- Breugnot, A. Gotteland, P. Villard, P. (2010) Numerical modelling of impacts on granular materials with combined discrete-continuum approach, *Proc. Numge 2010*, to be published June 2010, 6 pp, Trondheim, Norway.
- Cundall, P.A. & Strack, O.D.L. (1979) A discrete numerical model for granular assemblies. *Géotechnique* Vol 29(1): pp 47-65.
- Frangin, E. Marin, P. & Daudeville, L. (2006) On the use of combined finite/discrete element method for impacted concrete structures. *Journal de Physique IV* 134: pp 461–466.
- Itasca Consulting Group. (2006) Fish in PFC3D, AC/DC (Adaptive Continuum/Discontinuum) logic.
- Munjiza, A. (2004) The Combined Finite-Discrete Element Method. John Wiley (eds).
- Oñate, E. (2003) Multiscale computational analysis in mechanics using finite calculus: an introduction. *Multiscale Computational Mechanics for Materials and Structures. Computer Methods in Applied Mechanics and Engineering* Vol 192 (28-30): pp 3043-3059.
- Pichler, B. Hellmich, Ch. & Mang, H.A. (2005) Impacts of rocks onto gravel. Design and Evaluation of experiments. *International Journal of Impact Engineering* Vol 31: pp 559-578.
- Salot, C. Gotteland, Ph. & Villard P. (2009) Influence of relative density on granular materials behavior: DEM simulations of triaxial tests. *Granular Matter* Vol 11: pp 221-236.
- Xiao, S.P. & Belytschko, T. (2004) A bridging domain method for coupling continua with molecular dynamics. *Computer methods in applied mechanics and engineering* Vol 193: pp 1645-1669.
- Xiao, S. Hou, W. (2007) Studies of nanotube-based aluminium composites using the bridge domain coupling method. *International journal for multiscale computational engineering* Vol 5.



## CE marking of rockfall protection kits – The new European approach

Georg Kohlmaier<sup>1</sup>

<sup>1</sup> Austrian Institute of Construction Engineering (OIB), Approval Body for European Technical Approvals, Vienna, Austria  
[kohlmaier@oib.or.at](mailto:kohlmaier@oib.or.at)

---

**Abstract.** This contribution presents the concept of the European Technical Approval Guideline 027 “Falling rock protection kits”, adopted on the level of Member States of the European Union in 2008. It serves as reference document for issuing European Technical Approvals (ETA) and has been elaborated on European level under the responsibility of the European Organisation for Technical Approvals (EOTA). ETAG 027 defines the test procedures and boundary conditions for the assessment of rockfall protection kits. The ETA is the harmonized European technical specification for the certification procedure. Having passed the certification procedure, the manufacturer is allowed to affix the CE marking on the product according to the concerned rules. The CE marking is the only legally binding marking of construction products in the European Union. Designers, executors and administrative people are confronted in their “daily business” with CE marked rockfall protection kits. In this contribution information on how ETAs and CE marking are acting is given.

**Keywords:** Construction Products Directive 89/106/EEC, European Technical Approval Guideline, European Technical Approval, Content of ETA, Favorable assessment of the intended use, Technical classes for energy level, Evaluation of the attestation of conformity, CE marking.

---

### 1 Introduction

Since February 2008 in the European Union manufacturers have the opportunity for getting European Technical Approvals (ETA) for rockfall protection kits. The European Technical Approval Guideline 027 (hereafter: ETAG 027) of “Falling Rock Protection Kits”, elaborated and published by the European Organization for Technical Approvals (EOTA), is forming the basis for issuing ETAs. The approval procedures are ongoing in Europe. Thereto, designers and authorities are confronted in their “daily business” with CE marked rockfall protection kits.

The Construction Products Directive 89/106/EEC (thereafter: CPD) is offering two types of harmonized technical specifications: Harmonized European standards (e.g. EN 10025-1:2004) and European technical approvals. Both form the basis for the CE marking of the covered product(s).

## 2 European Technical Approval as harmonized technical specification

### 2.1 Concept of the European technical approval

The structure of the ETA is following the rules laid down in the European Commission decision 97/571/EC. The ETA comprises the interception structure (principal net and additional layer, if any), the support structure (posts, including its base plate) and the connection components (ropes, energy dissipating devices, clamps, etc.). The anchorage system (anchor loops, bolts, piles, etc.) is not covered by ETAG 027 and not part of the ETA. For the use of additional layers the following applies: The kit can be provided on site with an additional layer, although this layer has not been subject to approval testing. Thereto, the additional layer is not part of the CE marked kit. If the layer has been included in the approval testing, it is part of the kit and of the factory production control.

The ETA comprises:

- ◇ product description, intended use and information about intended working life;
- ◇ performance of the assembled kit in respect to energy absorption, deformation characteristics and actions on the foundations, information about durability of the components by means of addressing their corrosion protection;
- ◇ results of identification tests for the components and system of attestation of conformity, including tasks and responsibilities of the bodies involved in the certification procedure;
- ◇ guidance about the CE marking and information accompanying the CE marking, information about packaging, transport and storage of the kit as well as correct maintenance/repair of installed CE marked kits or at least reference to an obligatory set of information to be attached to the delivered kit;
- ◇ sketches regarding the assembly of the kit, geometry and dimensions of its components (net, posts, energy dissipating devices, clamps etc. – as far as not standardized) and position of load cells for measurement of forces.

### 2.2 Intended use of falling rock protection kit according to ETAG 027

The intended use is referred to the verified energy level (see clause 2.4 in this report) and related to an ambient temperature range ( $-40^{\circ}\text{C}$  to  $+50^{\circ}\text{C}$ ) in general. In respect to the verification of the applicable range of ambient temperature, the following approach applies: Due to the material characteristics of metallic products in general, for the kit a temperature down to  $-20^{\circ}\text{C}$  is considered as normal case without detailed assessment. In case of intended use lower than  $-20^{\circ}\text{C}$  (down to  $-40^{\circ}\text{C}$  or beyond  $-40^{\circ}\text{C}$ ), specific consideration (e.g. check of behavior based on relevant tests for sensitive components) is requested in order to evaluate this intended use. This is considered as individual case-by-case procedure and needs detailed evaluation by the approval body. The result of such assessment will be declared in the ETA.

### 2.3 Assumed working life of falling rock protection kit according to ETAG 027

The ETA addresses an intended working life (provided the installed product is subject to appropriate maintenance) of 25 years, except if the product is to be used in environmental aggressive conditions. In the latter case the intended working life may be reduced to at least 10 years. The definition of normal environmental conditions and environmental aggressive conditions is linked to standards in which such terms are specified. In general, which means without further detailing, an assumed working life of 25 years is covered for corrosivity category C2 (definition of category C2 - see ISO 9223:1992, EN ISO

14713:1999, ISO 12944-2:1998); the same applies for an assumed working life of 10 years for C3 and C4. In ISO 12944-2:1998 and EN ISO 14713:1999 the corrosivity category C1 is referred to indoor use and therefore not of relevance. If one of these standards will cover in future outdoor use in category C1 as well, further consideration, eventually in conjunction with related ambient temperature conditions, is needed. For evaluation of the fulfillment of an assumed working life of 25 years in relation to corrosivity category C3 or higher, e.g. reliable verification of the amount of mass loss rate of the corrosion protection over the 25 years could be subject of consideration. The term “assumed working life” in the ETA cannot be interpreted as a guarantee given by the manufacturer or any other involved body. It should be regarded as a means for choosing the appropriate product in relation to the expected economically reasonable working life of the works under the assumption of no rock impact. This kind of “warning” is accompanying each individual ETA and should be noted by administrative people and designer! The term “assumed working life” is used similar to the term “design working life” in EN 1990:2002, but EN 1990 is using a more detailed categorization.

#### 2.4 Performance characteristics in the ETA

The falling rock protection kit, subject to tests, is consisting of a sequence of three functional modules. The distance between the posts of the modules is not defined in ETAG 027, for practical reasons a distance of 10 meters is in use. ETAG 027 defines two energy levels (SEL “Service Energy Level” and MEL “Maximum Energy Level”) and their verification by means of full-scale tests. MEL and SEL and their relationship (see table 1) are used for classification of the falling rock protection kit according to table 1. The trade name and the description of the generic type of the product, addressed on the cover page of the ETA, normally refer to the MEL. The maximum size of the test block, made of (reinforced) concrete with a certain degree of density and defined shape, shall be three times smaller than the nominal height of the kit. In the last meter of the trajectory of the kit the average speed of the block must be not less than 25 m/s.

SEL is defined as kinetic energy of a block that impacts the central functional module with a defined impact point, including a certain tolerance, twice without repair between the two impacts. The two SEL impacts can be evaluated in a positive way if:

- ◇ the block is stopped by the kit;
- ◇ the block has not touched the ground until the kit has reached its maximum elongation during the test;
- ◇ after first SEL impact damages of the kit do not exceed the amount as defined in ETAG 027;
- ◇ after first SEL impact the residual height of the kit, defined as minimum distance between the lower and the upper rope (figure 1) and measured before removing the block, shall be declared on basis of a threshold value of 70 % of the height of the kit before the test (nominal height; figure 2); consequently, if one of these ropes breaks the product fails in the approval testing.

MEL is defined as the kinetic energy of the block that impacts the central functional module with a defined impact point, including a certain tolerance, and can be evaluated in a positive way if:

- ◇ the block is stopped by the kit;
- ◇ the block has not touched the ground until the kit has reached its maximum elongation during the test.

The residual height of the kit after MEL is declared in the ETA according to the categories in table 2. In case of break of upper or lower rope it can only be classified as category C. The maximum elongation (definition see figure 3) during SEL and MEL is declared in the ETA. The plastic deformation resulting from SEL 1 test is taken into account for SEL 2.

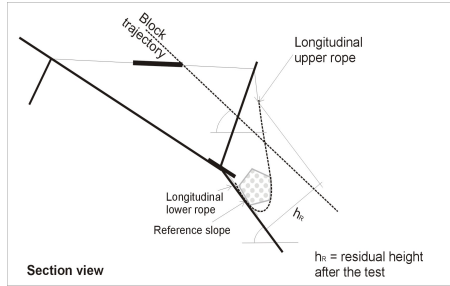


Figure.1. Residual height according to ETAG 027

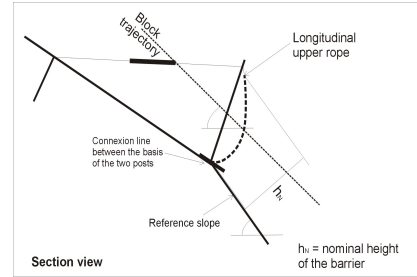


Figure.2. Nominal height according to ETAG 027

In case of SEL 1 and MEL impact the ETA shall comprise a detailed description of occurred damages, including information about break of mechanical fuses designed to break under impact. It is task of approval body to state in the ETA in a transparent way all these information in order to give clear guidance about the behavior of the kit under impact to the potential user of the product.

| Energy level classification | 0   | 1   | 2   | 3    | 4    | 5    | 6    | 7    | 8     |
|-----------------------------|-----|-----|-----|------|------|------|------|------|-------|
| SEL                         | -   | 85  | 170 | 330  | 500  | 660  | 1000 | 1500 | >1500 |
| MEL $\geq$                  | 100 | 250 | 500 | 1000 | 1500 | 2000 | 3000 | 4500 | >4500 |

Table.1. Technical classes for energy level

| Category | Residual height for MEL                                    |
|----------|--|
| A        | Residual Height $\geq$ 50 % nominal height                 |
| B        | 30% nominal height < Residual Height < 50 % nominal height |
| C        | Residual Height $\leq$ 30 % nominal height                 |

Table.2. Technical classes for residual height for MEL

Figures 1-3 show that the ETAG 027 does not promote any type of test site. The conditions for full-scale tests are applicable to inclined and vertical test sites. According to the knowledge of the author, an inclined test site is in use in Austria, vertical test sites so far in France, Italy and Switzerland.

For the designer and contractor installing the kit in the field the actions and their respective forces on foundation are of essential interest. This is mainly related to the number and position of the load cells in the approval testing. The ETA is a favorable assessment of the performance of the kit. Therefore, the load cells should be positioned such that the performance of the kit can be evaluated properly. ETAG 027 is offering a certain degree of flexibility for case-by-case verification. It depends on the individual design of the kit and its behavior how the position of the load cells should be. For kits with upstream cables measurement of forces at the posts is normally not considered as

necessary (although it may be included in the ETA, when measured). The approval body decides, whether measurements at the posts are necessary. The ETA provides measured values of peak forces and related time-force diagrams. Verification based on calculation is outside of the ETA and the responsibility of the involved approval body.

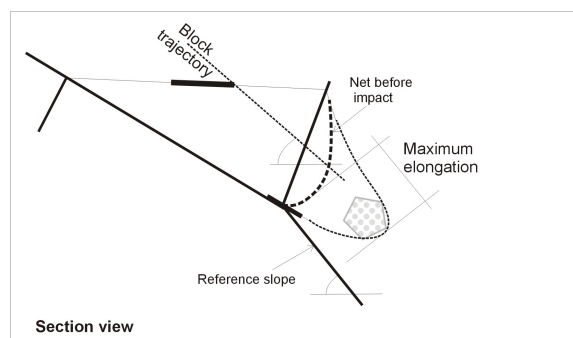


Figure.3. Maximum elongation according to ETAG 027

Due to regulations in the Member States the release and/or content of dangerous substances is considered in the ETA in a general way.

### 2.5 Identification of components for the assembled falling rock protection kit

ETAG 027 provides a set of verification methods for identification of components, either by reference to concerned test standards (e.g. EN 12385-1:2008 for ropes) or by providing specific test methods due to the individual design of the component. In particular and due to the diversity of their design, for energy dissipating devices identification tests are mainly subject to individual procedure, taking into account the conditions given in ETAG 027. Components are crucial for the proper functioning and the durability of the falling rock protection kit and they are subjected to dynamic loads. Verification of components by means of identification tests and by internal factory production control tests can be considered as an improvement of quality control for proper functioning of the kit.

### 2.6 European Technical Approval and evaluation of attestation of conformity

The elements for initial type testing, factory production control and continuous surveillance of the factory production control are included in the ETA. A detailed control plan for the factory production control (e.g. including frequencies of internal controls, types of requested certificates according to EN 10204:2004 for incoming materials) is deposited at the approval body and used in the certification procedure. This control plan is not part of the public available ETA. The ETA completed by the individual control plan allows to tailor the latter to the specificity of each product and production process.

## 3 CE marking on basis of European technical approval

The compliance of a product, put on the market, with the ETA is demonstrated by attaching the CE mark. The basic documents for attaching the CE mark are the EC certificate and the EC declaration of the manufacturer. On request, these documents have

to be provided to the authorities in the official language of the Member State(s) of destination. The number of the EC certificate (nnnn-CPD-zzzz in figure 4) is in line with that on the CE marking label and shall be repeated in the EC declaration. Figure 4 shows the information in the CE marking label for rockfall protection kits. But this does not supersede the need to consider the technical specification in detail and carefully.

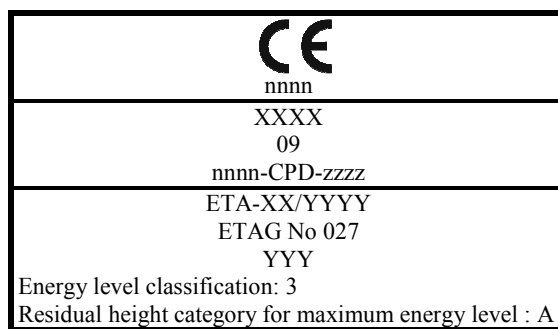


**Figure.4.** Example of CE Marking affixed on post of the rockfall protection kit

Full legend is given in cl. 3.3 in ETAG 027. ETA-XX/YYYY indicates the number of the ETA; XXXX the name of the producer, YYY the definition of the product. Additional information to the symbols CE specifies the key points for the use of CE marked products.

#### 4 Conclusion and perspectives

The ETA is operating as technical specification for the certification procedure for rockfall protection kits. Due to the fact that the concept for the verification of the energy levels in the approval procedure is rather new, it will be interesting to compare the results with those based on already existing national guidelines. The approach for the energy level classification may lead to a new orientation in the public procurement and consequently in the availability of the range of products in the future.

#### References

- Construction Products Directive 89/106/EEC (CPD): Council Directive of 21 December 1988 on the approximation of laws, regulations and administrative provisions of the Member States relating to construction products (Incl. Amendment 93/68/EEC).
- Commission Decision of 22 July 1997 on the general format of European Technical Approval for construction products (Text with EEA relevance) (97/571/EC).
- ETAG 027 Guideline for European Technical Approval of Falling Rock Protection Kits. Edition February 2008. <http://www.eota.be/>.
- Gerber, W., Baumann, R., and Volkwein, A.: Swiss guidelines for the approval of rockfall protection kits – 7 years of experience, in: Proceedings of Interdisciplinary Workshop on rockfall protection, Morschach, Switzerland, 23-25 June 2008, 34-36, 2008.
- Kohlmaier G.: European Technical Approvals. The way for CE marking of rockfall protection kits, in: Proceedings of Interdisciplinary Workshop on rockfall protection, Morschach, Switzerland, 23-25 June 2008, 43-45, 2008.
- Peila D. and Ronco C.: Design of rockfall net fences and the new ETAG 027 European guideline. Nat.Hazards Earth Syst.Sci., 9, 1291-1298, 2009.

## Comparative analysis between the Swiss Standard (FOEN) and the Recommendation ETAG-027 (EOTA) for rockfall protection kits approval

Andrea Roth<sup>1</sup>, Roberto Luis Fonseca<sup>1</sup>, Carles Raïmat Qunitana<sup>1</sup>, Joan Torreadella Barrat<sup>2</sup>, Joan Altimir Planes<sup>2</sup>, Jordi Amigó Mitjana<sup>3</sup> and Javier Gonzalez-Gallego<sup>4</sup>

<sup>1</sup> Geobrugg [info@es.geobrugg.com](mailto:info@es.geobrugg.com)

<sup>2</sup> EuroConsult-Andorra [qualitat@euroconsult.ad](mailto:qualitat@euroconsult.ad)

<sup>3</sup> EuroGeotecnica, S.A. [eurogeo@europroject.es](mailto:eurogeo@europroject.es)

<sup>4</sup> Cedex. Spain [javier.gonzalez@cedex.es](mailto:javier.gonzalez@cedex.es)

---

**Abstract.** Since June 2001 the Federal Office of Environment, Switzerland, developed a Guideline for the approval of rockfall protection kits. This standard provides a rigorous methodology for testing dynamic barrier systems, with the aim of ensuring that it works correctly. This standard have been well received in countries where very serious problems about landslides and rockfalls. For this reason it has spread and it is now also mandatory for use, in Switzerland, Andorra, in some regions of the United States, in Australia, Japan and other countries. Some years ago, the European Organization for Standardization based in Brussels (EOTA), has worked on legislation and development of the European Technical Guideline for the approval of falling rock protection kits to standardize this activity in Europe. The standard (ETAG-27), was published on February 1, 2008 and its introduction in each European Union country, will depend on the particular administrative procedure. The purpose of this communication, is primarily a brief description of both standard procedures and finally establishes some methodological differences that set them apart in ways that are clear on the standards of each procedure, ie. which standard is more restrictive and secure.

**Keywords:** rockfall, standard, protection kits, EOTA, ETAG-27, Technical Guideline,

---

### 1 Swiss standard (FOEN)

The Rockfall Protection Kits are divided into 9 categories for energies between 100kJ and 5.000kJ. These energies are also called test energies. The structures have to overcome the partial tests from *a*) to *d*) depending on the energy category, for which different requirements apply. In the case of the tests *a*) to *c*) the structure is subjected to single tests with test bodies, while the test *d*) is a qualitative assessment of the kit and documentation provided. The test description is as follow:

**Preliminary tests a) with small energies: (lateral section)**

This preliminary test is used to check the mesh deformation behaviour and also to smaller blocks. The blocks are thrown together by size categories in a section of a lateral impact velocity of 25 m/s.

- 5 small blocks 10 x 10 x 10cm, total mass 12kg energy 3.8kJ
- 3 small blocks 20 x 20 x 20cm, total mass 59kg energy 18kJ
- 1 body test<sup>1</sup> de 50 x 50 x 50cm, mass ≈300kg energy 94kJ

<sup>1</sup> the kits of the energy categories 1 and 2 are not tested with this block.

The deformations in the net and the affected net components are measured and described by size categories of rocks. Will be recorded the rope or single wire damage. No strength measurements are made. The test bodies must be stopped by the kit. Not allowed to occur holes in the net. No repairs are allowed between releases.

**Preliminary test b) with 50% power (mid section)**

This test can help determine the repair effort, ease of use of the kit and the braking distance with half the energy. The block referred to this energy (Table 1) is launched to the center of the middle section with an impact speed of 25m/s. Prior to the test are measured and recorded the positions of the single bearing elements. During the test measure and record the tensile forces on the ropes in about 10 anchor points. The test is recorded from two directions. After the test, the following values are recorded: rope deformation, braking elements, posts and nets, the height (altitude) of the test block, damage to single bearing elements. It records the time and equipment necessary for the repair kit. Since video images determines the braking time  $t_s$  and  $b_s$  maximum braking distance based on the point of investment below the block. The block has to be stopped by the kit. Not allowed to occur holes in the net. It requires the least effort possible repair.

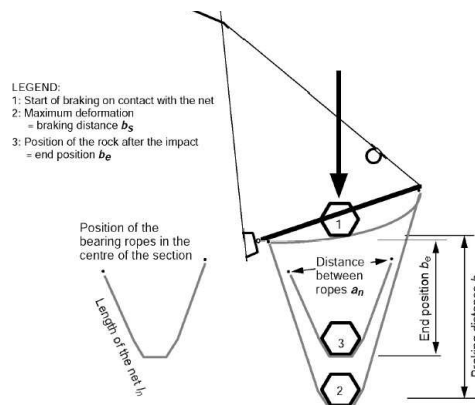


**Figure.1.** Positions of the block during tests b) and c). The net length is measured at position 3

**Full test c) with 100% power (mid section)**

In this test the maximum kinetic energy of the block is transformed into deformation work of the kit. So, it tests both the structural bearing and deformability. The block referred to this energy (Table 1) is launched to the centre of the middle section at an impact speed of 25m/s. Prior to the test, are measured and recorded the positions of the single bearing

elements. During the test, are measured and recorded the tensile forces on the ropes in about 10 anchor points. The test is recorded from two directions. After the test, it's recorded the following values: rope deformation, braking elements, posts and nets, the height (altitude) of the body of the test, damage in to single bearing elements. Since a video image determines the braking time  $t_s$  and  $b_s$  maximum braking distance based on the point of investment below the block (Fig.1) The block has to be stopped by the kit. Not allowed to occur holes in the net. The maximum braking distance  $b_s$  must be less than the value specified in Table 1. After impact, the net height  $h_n$  at the middle section must be at least the value specified in Table 1 (measured before removal of the block).

#### Evaluation d) kit following special criteria

This test is concerned with the non-measurable and practical suitability evaluation criteria. Evaluation of documentation: Comparison of the dimensions in the planes with the kit. Should be ensured that was installed in correspondence with the documentation provided for the kit. Manufacturers should indicate that meets applicable standards the product (including standards for protection against corrosion, steel wire and clips). Structure Evaluation: Installation is observed and compared with installation instructions, taking into account the special circumstances prevailing. Assesses the simplicity of the structure and estimated its adaptability to the terrain. The lifetime of the kit is evaluated based on the life of the individual components, corroborated by the supplier. The plans and the actual structure must correspond in every detail. The installation instructions should be practical and should correspond with reality. Unsophisticated designs should have a positive impact on price. The aim should be to ensure long life. In 2006 the Swiss authorities was made a revision of the criteria and found that the residual height in 2001, had been set too high. Therefore, the requirements were reduced and now agree with EU standards in 2006 was in preparation. The post heights given in the directive now refer to the net height and the height useful. The certificates for protective barriers that had stood the test of approval in 2001-2004 were revised in 2006 and changed to the values calculated using the new methods (Table 1). The current revised licenses are available at the following web site: [www.umwelt-schweiz.ch/typenpruefung](http://www.umwelt-schweiz.ch/typenpruefung)

**Table 1.** Test parameters in type b) and c) (update 2006)

| Category | Post height (m) | Test b) (50%) |                            |                             | Test c) (100%) |                            |                             |                                |                             |
|----------|-----------------|---------------|----------------------------|-----------------------------|----------------|----------------------------|-----------------------------|--------------------------------|-----------------------------|
|          |                 | Energy (kJ)   | Mass of the test body (kg) | Edge of the test body S (m) | Energy (kJ)    | Mass of the test body (kg) | Edge of the test body S (m) | Max braking distance $b_s$ (m) | Min height of net $h_n$ (m) |
| 1        | 1.5             | 50            | 160                        | 0.41                        | 100            | 320                        | 0.52                        | 4.0                            | 0.75                        |
| 2        | 2.0             | 125           | 400                        | 0.56                        | 250            | 800                        | 0.70                        | 5.0                            | 1.00                        |
| 3        | 3.0             | 250           | 800                        | 0.70                        | 500            | 1600                       | 0.88                        | 6.0                            | 1.50                        |
| 4        | 3.0             | 375           | 1200                       | 0.80                        | 750            | 2400                       | 1.01                        | 7.0                            | 1.50                        |
| 5        | 4.0             | 500           | 1600                       | 0.88                        | 1000           | 3200                       | 1.11                        | 8.0                            | 2.00                        |
| 6        | 4.0             | 750           | 2400                       | 1.01                        | 1500           | 4800                       | 1.27                        | 9.0                            | 2.00                        |
| 7        | 5.0             | 1000          | 3200                       | 1.11                        | 2000           | 6400                       | 1.40                        | 10.0                           | 2.50                        |
| 8        | 5.0             | 1500          | 4800                       | 1.27                        | 3000           | 9600                       | 1.60                        | 12.0                           | 2.50                        |
| 9        | 6.0             | 2500          | 8000                       | 1.51                        | 5000           | 16000                      | 1.90                        | 15.0                           | 3.00                        |

## 2 European standard ETAG-27 (EOTA)

There must be a structure to release a concrete block, with speed and precision needed. The slope of the slope in the direction of impact shall be parallel to the block trajectory; it allows a deviation of +/- 20 degrees. The installation contains three functional modules (4 posts). The installation is performed by the manufacturer according to the requirements of the installation manual; this process will be supervised by the inspection body, which also will be responsible of measuring and recording equipment. The foundations and anchors are the responsibility of the manufacturer and must be formally accepted before testing begins. The block will be built of mass concrete or concrete reinforced, will form the polyhedron. Its density varies between 25kN/m<sup>3</sup> to 30kN/m<sup>3</sup>. If steel is used, it must be placed symmetrically so that does not change the centre of gravity.  $L_{\text{exter}}$  size should be 3 times less than the nominal height of the barrier. The block path will enter in a vertical plane perpendicular to the connecting line between the posts of the kit. It may be steep or vertical. The speed of the block in the last meter before contact with the net is greater than or equal to 25m/s. The test consists of dropping the block on the kit described above, measuring the speed and determining the impact energy. The value of this energy is given by the expression:

$$E_k = \frac{1}{2} \cdot m \cdot V^2 \qquad E_k = E_p = m \cdot g \cdot \Delta H$$

The  $h_N$  nominal height is measured perpendicular to the slope of reference and is the shortest distance between the upper support cable and the connecting line between posts. Be rounded to the centimetre. The  $h_R$  residual height is measured perpendicular to the reference slope is measured after the test without removing the block and is the shortest distance between the support wire top and bottom (be rounded to centimeter). The maximum elongation is measured in parallel to the slope of reference, taking into account the maximum deflection of the network during the test, using video camera (be rounded to centimeter).

**Test procedure for the SEL:** This test is carried out with two releases of a block with the same kinetic energy. The objective of this test is to see if the kit is capable of accepting the successive impacts and reducing the useful height of the barrier, remains within an acceptable value. First impact position for the SEL: centre and middle functional module ( $h_N / 2$ ). Second impact position for the SEL: centre and middle functional module ( $h_R / 2$ ). At the middle of the high residual functional module  $h_R$ , this was reached after the first test SEL. The kinetic parameters (mass and velocity of the block) are the same as for the first launch, within the limits of tolerance, due to the deformation of the network after the first pitch.

### Test procedure for the MEL.

The test is carried out with a single block release. The aim of this study is to characterize the full potential of the kit. The MEL will also test the residual height and maximum elongation of the grid in the impact direction; therefore, allow the safe location of the kit (minimum distance between the kit and protected objects). The MEL test may be in the same kit used for the SEL test after being repaired or a new kit. The manufacturer will be chosen the option. Impact position for the MEL: centre and middle functional module ( $h_N$

/2). Will be measured and will be declared, height and maximum residual elongation of the net during the test. It is mandatory to make a detailed description of the damage (including the aforementioned residual height).

### 3 Comparative analysis between the standards

Below are some important differences between both standards to take into account when establishing an assessment and try to compare and select products. After verification of the products it showed that are not equivalent.

Table.2. Energy level in each standard

#### ETAG-27 (EU)

| Energy level | 0   | 1   | 2   | 3    | 4    | 5    | 6    | 7    | 8     |
|--------------|-----|-----|-----|------|------|------|------|------|-------|
| SEL          | -   | 85  | 170 | 330  | 500  | 660  | 1000 | 1500 | >1500 |
| MEL $\geq$   | 100 | 250 | 500 | 1000 | 1500 | 2000 | 3000 | 4500 | >4500 |

#### FOEN (Switzerland)

| Energy level | 1   | 2   | 3   | 4   | 5    | 6    | 7    | 8    | 9    |
|--------------|-----|-----|-----|-----|------|------|------|------|------|
| SEL          | 50  | 125 | 250 | 375 | 500  | 750  | 1000 | 1500 | 2500 |
| MEL $\geq$   | 100 | 250 | 500 | 750 | 1000 | 1500 | 2000 | 3000 | 5000 |

ETAG-27 (EU)

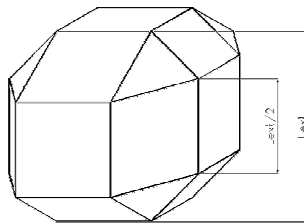


Figure.3. Test body 25 y 30kN/m<sup>3</sup>

The SEL energy values of service are 1 / 3 of the maximum energy

The angle of the cable car and the height difference between the starting and ending points, can limit the speed and thus the test. For example, in the former test site of Beckenried the  $V_{max} = 27\text{m/s}$ , while in the field of Trento was  $V_{max} = 30\text{m/s}$

- speeds up to 25m/s (90km/h) can generate energy up 2000kJ
- speeds up to 29m/s (104km/h) can generate energy up 3000kJ
- depending on the type of cable car and slope problems are increased by increasing the size of the blocks, to test high energies. (ie. in Trento only reaches 10000kg)
- handling heavy blocks, for more than 2000kJ on slopes, is complex and dangerous.

FOEN (Swiss)

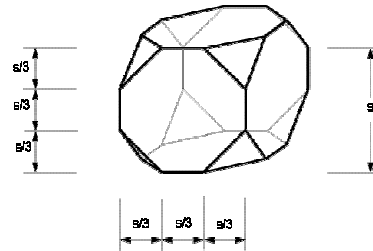


Figure.4. Test body 24,5kN/m<sup>3</sup>

The SEL energy values of service are 1/2 of the maximum energy

Only the height is crucial. It could reach speeds of up to generate 34m/s. What happens is that it has been shown that events in nature move in a range between 10 and 20m/s, an extraordinary 25m/s, so this value is set high in Walenstadt 32m.

- for speeds of 25m/s (90km/h) can generate up energy 5000kJ
- to increase energy only depends on the crane. (ie. in Walenstadt can get to overcome 16000kg)
- safely handling heavy blocks up to 5000kJ and 16000kg without danger of damage to personnel, or infrastructure.

ETAG-27 (EU)

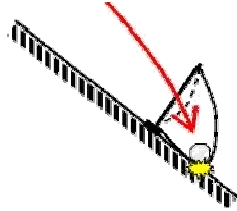


**Figure.5.** Test with inclined slope, contact with the ground, a part of the energy is absorbed by the ground surface.  
 $E_k = 0,5 \cdot m \cdot v^2$

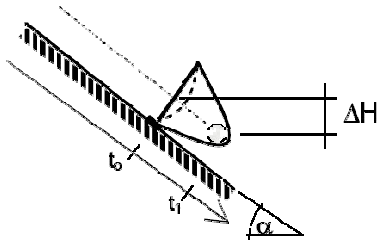


**Figure.7.** If the barrier is used on slopes steeper than the test site, it can't be guaranteed to function properly.

There are categories according to the residual height

- Category A:  $h_R \geq 50\% h_N$
- Category B:  $30\% h_N < h_R < 50\% h_N$
- Category C:  $h_R \leq 30\% h_N$

approximate accuracy:  
 horizontal  $\pm 30-50\text{cm}$  vertical  $\pm 50-100\text{cm}$

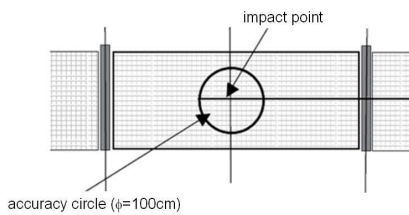


**Figure.9.** According to the experience, using inclined cable cars, the acceleration of the block on the guide rope creates vibrations and oscillations, which causes uncertainty in the trajectory of the block (to the extent that the block is bigger increasing these adverse effects). This isn't possible to predict the impact point.

FOEN (Swiss)

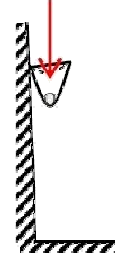


**Figure.6.** Vertical test, freefall, all the energy absorbed by the net.  
 $E_k = E_p = m \cdot g \cdot h$

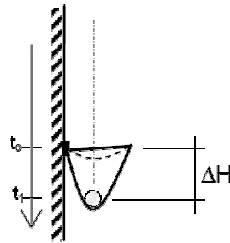


**Figure.8.** As the barrier tested in the worst conditions, whatever the job side slope will meet the needs

No categorization, from 2001 to 2006, the  $h_R \geq 60\% h_N$  to make a comparative analogy could be called A'.  
 From 2006 corrections  $h_R \geq 50\% h_N$ , the equivalent with the category A of the European standard.

accuracy  $\pm 5-10\text{cm}$

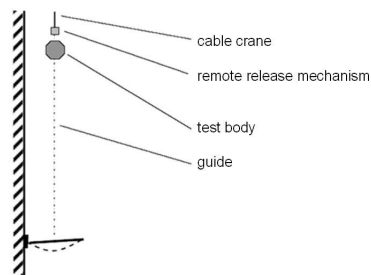


**Figure.10.** As the path is vertical; it's easy to determine the exact point where you want to make an impact.

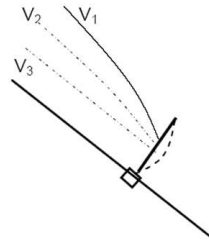


**Figure.11.** The speed depends on the path, it's impossible to play two tests the same, even to do a preliminary test to "point target".

Only central module is tested therefore there is no guarantee that modules extreme exercise their protective function (not functional). As we know there is always a negative effect on the ends, because there are fewer share options tensions. Despite the modules would need to extremes, in the total length of barriers evaluated by this method.

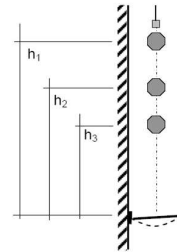


**Figure.12.** The speed can be varied by changing the drop height of the block, without variation in the trajectory.

It's possible to make tests in the same conditions. It is the preliminary test *a*) low energy in the end sections to an impact velocity of 25m/s.

## 4 Conclusions

The publication of an ETAG-27 directive (Standard) is a step forward, while there was no European directive for the control and/or regulation of these important security measures. This ETAG, at least set minimum parameters that must meet the rockfall protection systems, avoiding some improvised solutions, lacking in quality, which are in practice and are extremely dangerous, because as we know, what the stakes are generally human lives, whose economic value is difficult to quantify. Despite the above-mentioned step forward, we believe that European legislation is less stringent than the Swiss, and therefore provides less security because the test conditions and measurement, which allegedly require, give rise to interpretations especially with regard tolerances. Others are completely theoretical, difficult to achieve in the time test site, with inclined cable car is almost impossible to repeat two tests equivalent. During the 90s were made in Switzerland several tests under the supervision of the WSL (Swiss Federal Institute of Snow Research, Forests and Landscape). The tests were done at sites like the one located in Beckenried (fig.13) which was inclined cable car and some of the tests that were run were unsuccessful. On several occasions it was necessary to repeat tests to achieve the goals set by the vagueness of the installation.

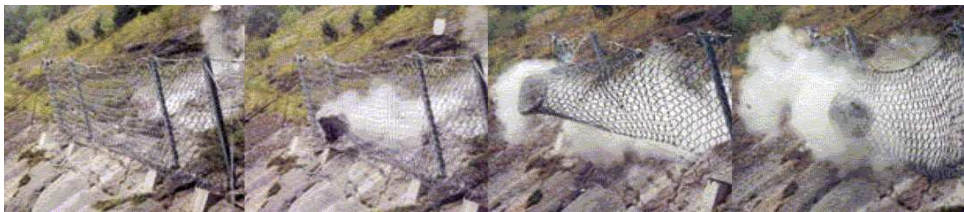


**Figure.13.** Sequence impact 5600kg block to 27m/s inclined cable car tested in Beckenried during 1997. Barrier type RX-200 (2000kJ)

Since 2001, Switzerland began testing free fall in the field tests Walenstadt (fig.14). Experience shows that how best chance of ensuring the proper use of further rockfall protection systems, is to follow a somewhat restrictive procedure, ie. free fall test.



**Figure.14.** Sequence impact 16000kg block to 25m/s h=32m vertical test tested in Walenstadt during 2006. Barrier type RXI-500 (5000kJ)

Although the Swiss standard not set this detail, is considered positive in the sense of giving greater guarantees, additional to the test performs c) 100%, it makes an additional test in the extremes to ensure functionality modules in the area. It's also advisable to make punching test (freefall) with tree trunks, to ensure functionality to high punching loads. Taking into account the considerations detailed in this paper, is desirable and advisable to know when selecting a dynamic barrier to protect a particular infrastructure advantages and disadvantages of the products certified and approved by the recommendation ETAG-27 (EOTA) and the guarantees offered by products that meet the Swiss (FOEN), which allows test conditions in general more restrictive.

## References

- EOTA (2008). *Guideline for European Technical approval of falling rock protection kits*. ETAG-027. Brussels.
- Geobrugg. (2008). *Rockfall protection systems*. <http://www.geobrugg.com>
- Gerber, Werner. (2001). *Guideline for the approval of rockfall protection kits*. Swiss Agency for the Environment, Forests and Landscape (SAEFL) and the Swiss Federal Research Institute. WSL. Berne.
- Gerber, Werner. (2006). *Guideline for the approval of rockfall protection kits. Amendment 2006*. Swiss Agency for the Environment, Forests and Landscape (SAEFL) and the Swiss Federal Research Institute. WSL. Berne.
- Gerber W., Böll A. & Ammann W. (2001). *Filed testing of rockfall protection barriers. A comparison between inclined ropeway and vertical crane testing*. WSL. Birmensdorf.
- González Gallego, J. & Luis Fonseca, R. (2007) *Optimization criteria for using of rockfall protection*. Congreso ISMR. Lisboa.
- Luis Fonseca, R. & González Gallego, J. (2008) *Protección contra desprendimiento de rocas. Barreras dinámicas*. Ingeoter 10. Madrid.
- Luis Fonseca, R. & Torreadella, J. (2008) *Análisis comparativo entre la norma Suiza y la ETAG-27*. Andorra.
- Roth, A. (2006) *Remarks to the report for the EOTA EXCOM, ETAG for falling rock protection kits, WG 01-06/02*

## Test site Erzberg – Full scale tests of rockfall protection kits up to 5000 kJ according ETAG 27: Experiences and outlook from the point of view of a system supplier

Gernot Stelzer<sup>1</sup>, Maik Hamberger<sup>2</sup>, Ahren Bichler<sup>3</sup>

<sup>1</sup> Trumer Schutzbauten GmbH, Kuchl, Austria  
[g.stelzer@trumerschutzbauten.com](mailto:g.stelzer@trumerschutzbauten.com)

<sup>2</sup> Trumer Schutzbauten GmbH, Kuchl, Austria  
[m.hamberger@trumerschutzbauten.com](mailto:m.hamberger@trumerschutzbauten.com)

<sup>3</sup> Trumer Schutzbauten Canada Ltd., Vancouver, Canada  
[a.bichler@trumerschutzbauten.com](mailto:a.bichler@trumerschutzbauten.com)

---

**Abstract.** At the Styrian "Erzberg" near Eisenerz, Austria a test site for full scale testing of rockfall protection kits using a cable car system has existed since 2000. Due to necessary adaptations in accordance with the new EOTA guideline ETAG 27, extensive rebuilding of the site was undertaken in 2005 and 2006. The site now operates in full compliance of these guidelines. In this presentation, experiences with tests according to the new European guideline ETAG 27 will be reported. Innovation and challenges due to a common European guideline, as well as the advantages for the clients will be discussed. Furthermore, parallels and differences to other (older) guidelines will be highlighted. Finally, an outlook of the future of rockfall protection systems concerning bearing capacity, installation and maintenance will be given.

**Keywords:** ETAG 27, full scale testing, rockfall protection kits, geohazard mitigation

---

### 1 Introduction

Rockfall protection is a costly and often resource intense undertaking for authorities or institutions in regions where people and their goods as well as infrastructure are endangered by such processes. The number of elements at risk increases mainly in densely populated areas, as do the consequences. As such, it becomes imperative that mitigative measures are reliable and cost effective.

For more than 50 years, rockfall protection systems that absorb the dynamic energy of an event have become common place. To ensure that the installed systems perform in an anticipated manner, it is necessary to test and certify the fitness for use of these systems. The tests are performed on special test sites for this purpose. The first guideline that describes such test scenarios and the general conditions of a full scale test is now older than 10 years. From 2000 to 2006 a group of experts in the field of rockfall protection



**Figure.1.** System TS-500-ZD with hinged connection in Sjomen, Norway



**Figure.2.** Typical situation for a system with fixed rotation next to a road for forestall work and the object of protection more down-slope

from various authorities, institutes and system suppliers of different countries of the European Union drafted the first guideline for European technical approval of falling rock protection kits (ETAG 27). The European Organisation for Technical Approval (EOTA) approved the ETAG 27 guideline in 2008.

## 2 Austrian Test Site Erzberg

The Austrian test site Erzberg opened in the year of 2000 in an inactive area of an open pit mine. It consisted primarily of a cable car with a single bearing rope (Heiss, 2002). At first, the projectiles, which were made of rock, were accelerated by their own weight into the rockfall protection system that was previously installed on the test platform. Standardized concrete forms have since replaced the rock projectiles. The velocity of the block was calculated using positions taken from the single frames captured by high-speed video cameras. As such, it was already possible in 2000 to successfully test a 500kJ rockfall protection system (so called TS-500) in full scale. The subsequent use of rope force sensors have led to improved opportunities in the design of rockfall protection kits. Furthermore the design of the anchoring on construction sites was founded on more realistic values.

In their beginnings, rockfall protection systems were designed with a hinge connection between post and base plate and retaining ropes on the post head. Trumer Schutzbauten started to develop early on systems with fixed-rotation-connection between post and base plate. This makes the requirement of retaining ropes on the uphill-side redundant. One benefit from such systems, besides the obvious reduction of ground anchors required, is that the fence can possibly be emptied after a rockfall event using machinery without any interference from the retaining ropes. In 2003, a 500kJ system (so called TS-500-oA) was successfully tested. In 2004, the upper energy limit with the old cable car was reached by certifying a 1000kJ barrier.

From 2005 to 2006 a nearly complete rebuilding of the test site Erzberg was undertaken, i.e. a new cable car with double bearing ropes was installed. The topography changed by extensive excavation and the test platform changed from a horizontal plane to a more



**Figure.3.** Full scale test at the test site Erzberg using the first cable car



**Figure.4.** 3000 kJ impact on the new test site

realistic slope parallel plane. These building measures were necessary to be able to test all the energy classes of ETAG 27 and to meet the new geometrical requirements. Between 2006 and 2008, rockfall protection systems with hinged connection between post and base plate were tested up to an energy value of 5000kJ and systems with fixed-rotation were tested up to 2000kJ.

### 3 Guidelines and Standards for Rockfall Protection Systems

The first guidelines for rockfall protection systems were established in 1996. Since that time the following guidelines have been approved and used:

- ◇ Norme française NF P 95-307 (1996): Équipements de protection contre les éboulements rocheux - Terminologie
- ◇ Norme française NF P 95-308 (1996): Équipements de protection contre les éboulements rocheux – Écrans de filets
- ◇ BUWAL guideline (2001): Guideline for the approval of rockfall protection kits, additional extensions in 2006
- ◇ WLV guideline (2005): WLV-Richtlinie für den Eignungsnachweis von Steinschlagschutznetzen
- ◇ ETAG 27 guideline (2008): Guideline for European Technical Approval of Falling Rock Protection Kits

#### French Standard NF P 95-307 and NF P 95-308

NF P 95-307 contains general terminology and gives an overview and summary of useful definitions in order to plan protection measurements against such phenomena. NF P 95-308 is more detailed and is focused specifically on rockfall protection fences. It already defines design parameters of rockfall protection fences. The choice verification of the bearing capacity of rockfall protection system either by calculation or by full scale test is open.

#### BUWAL Guideline

The BUWAL guideline that was established in 2001 has a strong focus on the verification of suitability of rockfall fences by testing on a vertical test site using a crane. The

guideline describes explicitly the test procedure for the approval as well as the test criteria, testing methods and requirements for a successful test (BUWAL, WSL, 2001).

The total test scenario consists of 3 test stages: small energies of max. 94 kJ in the boundary section, 50% energy in the middle section and 100% energy with an impact velocity of at least 25 m/s, also in the middle section.

Tested heights, as well as maximum elongations and minimum residual heights, are associated with the tested category/energy class. It is not allowed to construct systems with lower heights than those of the tested category. Once the test has passed, the manufacturers are allowed to offer posts up to 1.5 times longer than the tested lengths, whereby proof of the posts bearing safety must be submitted.

In comparison to other guidelines or standards the residual height defined by the BUWAL guidelines has an alternative definition. Instead of the distance between upper and lower bearing ropes measured perpendicular after the impact, it defines the residual height as the distance between the upper bearing rope and the connecting line of the posts' bases. Because the systems are tested on a vertical test site and the nature of deformations on the system due to the test, a wide opening between the lower bearing rope and the connecting line of the posts' bases occurs. This opening is included in the residual height.

In addition, deformations or breaks following a test on posts, ropes, brake elements, nets and supporting parts need only to be recorded. There are no criteria for a test to be deemed unsuccessful due to deformations or breaks.

#### WLV Guideline

The first version of the WLV guideline was established in the nineteen-nineties (Austrian Service for Torrent and Avalanche Control WLV, 1996). The most recent version (2005) is a composition of general conditions for testing rockfall protection systems independently to the type of test site. To verify the suitability of systems, only the test of the impact with the maximum energy is needed.

The residual height is measured between the upper and lower bearing rope perpendicular to the slope after the test.

Breaks on ropes, nets, posts or components with bearing capacity are not allowed for systems up to 1000 kJ. For systems with higher capacities, only limited breaks are permitted as defined by the independent inspection authority. Plastic strains are allowed but have to be documented in the test report.

Static calculations or models to verify the suitability of systems based on other tests are not permitted. This means that all systems with hinged and rigid bases have to be tested.

Though there are no measures defined for quality control, it is stipulated that all material must at least have the same or better quality as the tested material.

#### ETAG 27

Due to the ETAG27 guideline a major change for rockfall protection system suppliers is happening. There are three primary areas affected:

- ◇ Full scale tests
- ◇ Factory production control (FPC)

◇ CE-marking and conformity attestation

Compared to the previous situation in Austria, it is now necessary to test all rockfall protection kits by conducting three full scale tests, one with maximum energy level (MEL) and two with service energy level (SEL), instead of a single maximum impact. That means the MEL test remains unchanged but two additional SEL tests must be carried out. The SEL tests consist of two impacts with a third part of energy of MEL in the same kit without any repairing or maintenance between tests. This represents recurring events, whereas the MEL tests is a model of a rare appearing impact with the highest energy that shall be resisted.

The reference plane on the test site for the ETAG 27 is the slope under the installed rockfall protection kit. Nominal and residual height are measured between the upper and lower bearing rope perpendicular to the reference plane.

The impact point accuracy of 50 cm around the ideal point in the centre of the middle module is more difficult to obtain for inclined test sites when compared to vertical test sites. This issue is dealt with by conducting pre-tests to establish the flight path.

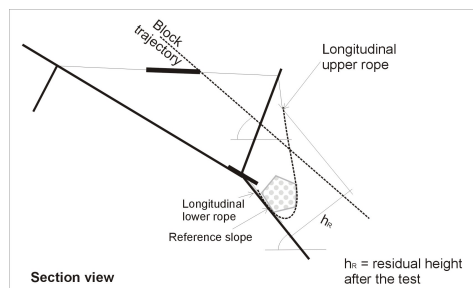


**Figure 5:** Residual height according to ETAG 27

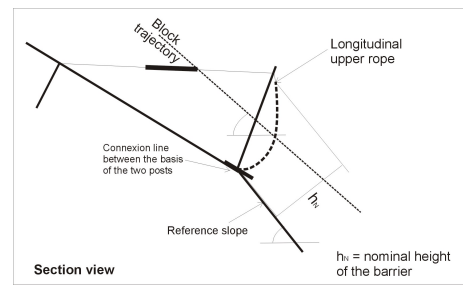


**Figure 6:** Nominal height according to ETAG 27

For defining the characteristics of a rockfall protection kit, three of the main parameters remain the maximum energy level, the residual height and the maximum elongation. There are 9 energy classes ranging from 100 kJ to >4500 kJ while only three classes of residual height: greater than or equal to 50%, between 30 and 50% and less than or equal to 30%. Like the WVL guideline, the residual height is taken as the minimum distance between the upper and lower bearing ropes. The maximum elongation, which is often vital for the implementation of fence structures when constructed near to elements at risk, is declared in the technical approval.

The FPC-test plan brings on the one side quality due to testing with a defined frequency according to a test plan, so defect or inappropriate material is prevented to be put on the market. On the other side, it also leads to higher testing costs, which must be covered by the market price.

The CE-marking with the accompanying conformity attestation causes a strict link between tested material and material to be put on the market. This leads to a higher safety

for the client, e.g. the ordered rockfall protection kit must accord completely to the kit tested in the full scale test. But the loss of flexibility related to special tasks or user defined solutions is also obvious, because the manufacturer no longer complies with its technical approval.

#### 4 Conclusion and outlook

As shown, the ETAG 27 represents the European standard for rockfall protection kits. It is the most comprehensive standard available and will likely be adopted as a global standard if not used as a model for others. This is largely because of its requirements for full-scale testing and factory production control system and so having no similar alternative.

From the technical point of view in the ETAG 27 the highest energy class defined is from 4,500kJ to unlimited. It will be interesting to see what are the next energy values resisted by rockfall barriers. Certainly one limit will be how cost effective this new generation of fences will be when compared to rockfall dams and galleries.

Over the next years, suppliers will be using the time to test their product lines according to ETAG 27 and to get the CE-marking through the accompanying certification. This marking will become a sort of entrance ticket for producers to access the rockfall protection product market.

As more and more certified products enter the market, there will be other criteria that will once again become the deciding factor on which product is favoured. Some questions that will undoubtedly be at the front of the list are:

- Which product is the easiest to install?
- How is it possible to replace single components after an impact?
- How is the barrier emptied or cleaned?
- And finally the most important question, what are the costs for the materials and for all the above?

#### References

- EOTA (2008) ETAG 027 Guideline for European Technical Approval of Falling Rock Protection Kits. Edition February 2008. <http://www.eota.be/>
- Heiss C. (2002) Entwicklung und Prüfung einer Versuchsanordnung für Steinschlagschutzbauten, Diploma Thesis, Mining University Leoben, Austria
- Austrian Service for Torrent and Avalanche Control WLW (1996) Richtlinie für den Eignungsnachweis der Schutznetze, Austria
- BUWAL, WSL (2001) Richtlinie über die Typenprüfung von Schutznetzen gegen Steinschlag. Bundesamt für Umwelt, Wald und Landschaft (BUWAL) und Eidgenössische Forschungsanstalt WSL, 39 S.; Bern
- NF P 95-307 (1996): Équipements de protection contre les éboulements rocheux – Terminologie, AFNOR, December 1996
- NF P 95-308 (1996): Équipements de protection contre les éboulements rocheux - Écrans de filets, AFNOR, December 1996

## A new site in the French Alps for full-scale tests on rockfall protection works: project and realization

Frédéric Rocher-Lacoste<sup>1</sup>, Laurent Dubois<sup>2</sup>, Mathieu Feregotto<sup>2</sup>, Marion Bost<sup>1</sup>

<sup>1</sup> Université Paris Est University, LCPC, Paris, France  
[frederic.rocher-lacoste@lcpc.fr](mailto:frederic.rocher-lacoste@lcpc.fr)  
[marion.bost@lcpc.fr](mailto:marion.bost@lcpc.fr)

<sup>2</sup> CETE de Lyon, Lyon, France  
[laurent.dubois@developpement-durable.gouv.fr](mailto:laurent.dubois@developpement-durable.gouv.fr)  
[mathieu.feregotto@developpement-durable.gouv.fr](mailto:mathieu.feregotto@developpement-durable.gouv.fr)

---

**Abstract.** The construction of a device intended for full-scale tests on rockfall protection works is the achievement of a project driven by the French Ministry in charge of Ecology, Energy, Sustainable Development and Planning (MEEDDM) since 1988. This site is the only one of this type in France. It started working in 2009 and is available for companies, design offices, research departments and universities wishing for tests about high stakes issues: technical approval of falling rock protection kits, research engineering on innovative rockfall protection works, improvement of knowledge on dynamic behavior of materials, *etc.*

**Keywords:** Rockfall, passive protection system, full-scale test.

---

### 1 Introduction

Rockfalls are one of the main natural hazards for people and infrastructures safety, especially in mountain areas. Services in charge of infrastructures and planning make use of passive protection systems like rockfall protection net fences, reinforced embankments, rockfall galleries, *etc.* in order to decrease damages caused by rockfalls.

Important needs have been identified:

- on one hand, concerning justification and harmonization of designing methods of protection works. These methods are at the moment simplified and on theoretical basis, or even empirical;
- on the other hand, concerning improvement of building and maintenance of these protection works.

Services of the French Ministry in charge of Ecology, Energy, Sustainable Development and Planning (MEEDDM) have been working since the end of the 80's on a project of a

permanent device intended for full-scale tests on rockfall protection works and located in France. The purpose is to perform impact tests for:

- research and development on non-rigid structures (soils, geomaterials, reinforced embankments, net fences, wire mesh, new dissipative structures, etc.) or rigid structures (reinforced concrete slabs, elements of works, *etc.*);
- technical approval of net fences, according to the specifications of the European Technical Approval Guide for falling rock protection kits (ETAG 27). This guideline set to perform impact tests on full-scale works, and will gradually replace the current net trap French standard (NF P95-308, December 1996), the transition lasting until December 31 2014.

This full-scale testing device for rockfall protection works was built close to Chambéry in the French Alps. It's the property of the Central Laboratory of Bridges and Highways (LCPC), a research laboratory of MEEDDM. The project was entirely financed by public funds: equity capital of LCPC, and grants from MEEDDM, territorial collectivities (Isère, Savoie and Haute-Savoie Departments) and public companies in charge of French railways (RFF and SNCF). The CETE de Lyon, a technical service of MEEDDM, is responsible for the exploitation of the device. An operational comity, gathering the LCPC and the CETE de Lyon, deals with tests scheduling. These two services work together on technical approval, expertise and research activities concerning rock hazards (trajectory analysis, behavior of reinforced embankments for rockfall protection, behavior of passive anchorages, investigations on sites, *etc.*). Thus, they contributed to the redaction of the ETAG 27. The LCPC is the agency responsible for the CE marking for falling rock protection kits on the French territory, and the CETE de Lyon collaborates with SETRA (an another technical service of MEEDDM), which is notified for the European technical approval of falling rock protection kits.

Three other projects were examined before the current and final one. They were all located on sides of disused quarries in the French Alps, and were based on the principle of a cable car guiding and dropping a boulder onto the tested work. These projects were successively failures, the last one in 2006, because of technical difficulties (such as insufficient accuracy after the drop, or dynamical problems caused into the device structure by the drop) or a lack of funds.

After these failures, the principle of a vertical drop from the top of a high cliff was adopted. This solution is more reliable and enables higher energy impacts than with a cable car.

## 2 Presentation of the site

In 2006, the CETE de Lyon has taken inventory of sites into areas of Grenoble and Chambéry that were likely to host a full-scale testing device for rockfall protection works. A disused quarry located in Chartreuse foothills, close to Chambéry, was chosen for its 80 meters high quasi-vertical cliff (figure 1). Moreover, the cliff is more than 90 meters long, thus enables assembling of net fences with modules up to 20 meters long, at height from 15 to 25 meters above the ground. This ground is an old head of the quarry, quite flat and steady, convenient for heavy plant operations, and also to build protection works that will be tested, like reinforced embankments or rockfall galleries. Regarding the configuration of this site, the construction of a cable car or a pendulum could also be planned for non-vertical impact tests.



**Figure.1.** Picture of the cliff before construction works

The site is the property of an important French cement manufacturer, Vicat. Administrative procedures needed to make the site accessible favorably ended in 2007. After that, Vicat decided to start again the exploitation of the quarry for aggregate production, while in the same time began the construction works of the testing device. From a security point of view, the start of a new exploitation close to the testing site implies a strict management of the coactivity.

In the meanwhile, CETE de Lyon has led structural and geotechnical investigations based on drilling and laboratory testing results. The cliff is made of Tithonian limestone beds, with a vertical shape caused by the folding of geological layers, and with little fractures despite the proximity of a major fault. These more than 15 meters thick bulky limestone beds have high and homogeneous physical and mechanical characteristics, with

compression strength higher than 100 MPa. Thus, conditions for execution and strength of anchorages drilled into the cliff should be good.

### 3 Presentation of the boulder-dropping device

The boulder-dropping device has been designed, built and set up on site by a pooling of two companies, GTS and RB-PIM, from January 2008 to April 2009. It has been designed to lift up and drop boulders weighing up to 20 tons, from heights from 5 to 70 meters above the ground. Maximal impact energy available is thus high (13900 kJ). As a consequence, some impact tests on net fences with absorption capacities from 1000 kJ up to 5000 kJ have been foreseen.

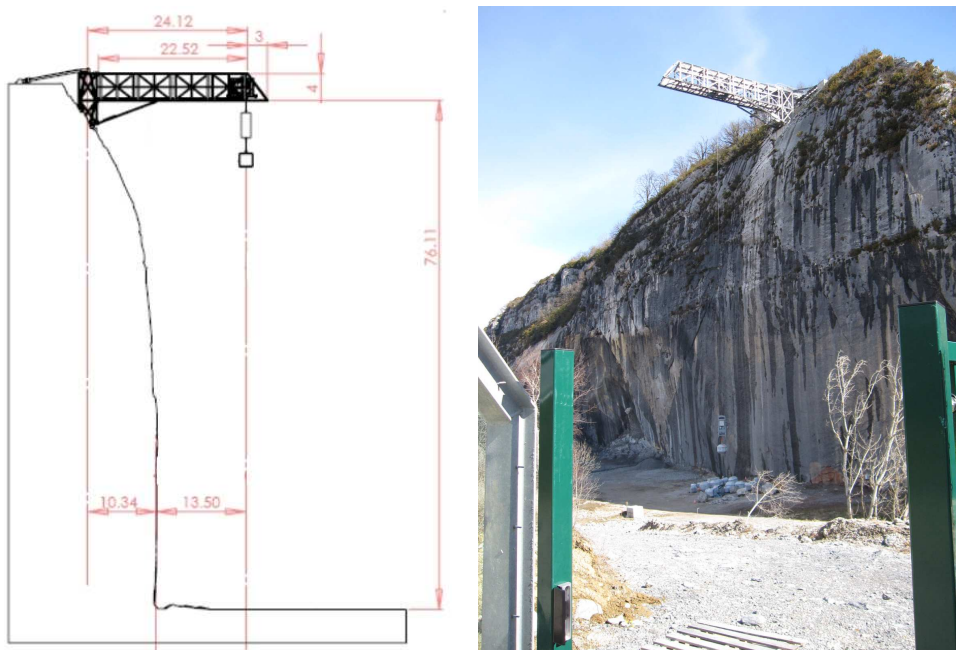


**Figure.2.** (a) Diagram (source : RB-PIM) and (b) picture of the boulder-dropping device

The boulder-dropping device is made up of (figures 2a and 2b):

- a 25 meters boom crane built up with a metal framed structure swiveling around an axis. This axis is grounded on the rock with passive anchorages and a base made of concrete;
- a 5 tons hoist moving inside the boom crane thanks to a trolley. 4 powerful electric engines are necessary to wind up, unwind and lock the dropping cable (diameter of 38 mm);
- a 8.3 tons hook at the end of the dropping cable. Thanks to a counter mass, this device enables the dissipation of 75 % of the energy stored into the cable and the

structure before a drop. The remaining energy is dissipated by the boom crane structure, and by a dry friction damping device located between the swiveling axis and the boom crane.

The whole dropping device is about 80 tons. The structure is made of 7 tons modular elements that can be lifted up from the foot cliff by a high capacity crane and set up at heights progressively.

Movements of the boulder-dropping device are radio controlled from the foot cliff. The overall position of the boulder before the drop (angular position of the boom crane, place of the hoist inside the boom crane, height from the tested work) is known thanks to rotating optical encoders. With wind intensity up to moderate, the drop accuracy is better than the accuracy specified into the ETAG 27 (0.5 meter from the theoretical impact point). The boulder-dropping device cannot be used when the wind speed exceeds 30 km/h. This threshold is seldom exceeded on the site. The drop release is radio controlled from a safe place technically located out of reach from possible splinters.

#### 4 Presentation of complementary equipment

750 kg, 1500 kg, 2500 kg, 4500 kg, 7000 kg and 11500 kg reinforced concrete boulders are available for impact tests on falling rock protection kits with energy level classification of ETAG 27 from 3 to 8. On the ground, these boulders are moved thanks to a special trailer pulled by a powerful tractor (figure 3). In the future, 2500 kg, 5000 kg, 10000 kg and 20000 kg spherical boulders will also be available for tests intended to research works.

Transducers placed on the tested work ( $\pm 500$  kN bridge strain gage extension-compression load cells, piezoelectric, piezoresistive and capacitive accelerometers, strain gages for all bridge configurations, LVDT displacement transducers, etc.) are acquired and logged with a modular data acquisition device thought for dynamic measures.

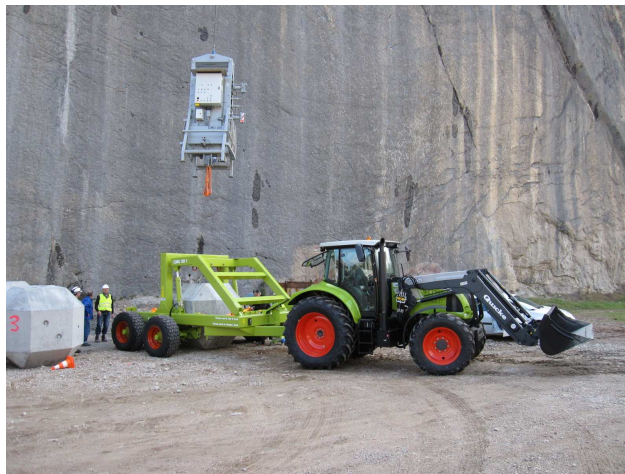


**Figure.3.** Picture of the dropping-hook, the trailer, the tractor and the reinforced concrete boulders

For every channel, trigger of simultaneous acquisition (no multiplexing) is synchronized, and the sample rate applied is the same. The maximum sample rate is equal to 1 MHz divided by the number of channels that will be used.

High-speed cameras (speed equal to 500 frames per second at full resolution (1280x1084), 8 GB of video memory) are used to measure the boulder speed before impact and deformations of the tested work.

The instrumentation set is relevant to the specifications of the ETAG 27. Data acquisition for transducers and high-speed cameras can be triggered with a remote radio control, for instance right before a drop. Thanks to Gigabit Ethernet interfaces, data acquisition device and high-speed cameras are driven from laptops intended to this use. Local networks can be created in order to check workings of the data acquisition device and high-speed cameras, before and during a test, and from the place where the drop is triggered.

## 5 Conclusion and perspectives

Studies and works carried out during the second part of the year 2009 made the site intended for full-scale testing on rockfall protection works operational. First tests performed since the end of the year 2008 on falling rock protection kits were of great interest. They have led to improve equipments and processes, especially safety processes concerning the approach of the impacted work by height workers. Research works will probably start before the end of the year 2010.

The new site of the LCPC for full-scale testing on rockfall protection works is the only one of this type in France. This equipment is available for companies, design offices and research departments. The purpose is to improve the reliability of rockfall protection works.

## References

- AFNOR (1996). Rock falling protection equipments. Net trap (NF P95-308)., pp 1-12.
- EOTA (2008). Guideline for European technical approval of falling rock protection kits (ETAG 27)., pp 1-53.

## Design of rockfall net fence interventions

Daniele Peila<sup>1</sup>, Chiara Ronco<sup>1</sup>, Luca Borio<sup>1</sup>, Sebastiano Pelizza<sup>1</sup>

<sup>1</sup> Dept. of Land, Environment and Geo-technology, Politecnico di Torino, Italy  
daniele.peila@polito.it

---

**Abstract.** The paper presents and discusses the recent issued European Technical Approval Guideline ETAG-027: “Guideline for European Technical Approval of falling rock protection kits”, which defines how to test and assess the performances of a net fence. This guideline gives the procedure useful to define the product “fitting for its intended use” and sets the basis for the certification procedure and CE marking. The design procedure for net fences should consider ETA document information and Eurocodes impositions, particularly the application of safety factors to the actions and resistances. The barriers should be defined and designed using foreseen impact kinetic energy, impact height and deformation level, applying adequate partial safety factors to the known design characteristics of the net fence (energy level defined in ETA, interception height and distance between the fence and the area that has to be protected). The innovations introduced by ETAG 027 are handled and a new possible design approach for falling rock protection kits are described and discussed.

**Keywords:** net fences, regulations, design.

---

### 1 Introduction

The need for protection against rockfall has led in these last days to the development and use of different types of technological solutions that can, on one hand, prevent the blocks from breaking off the rock walls, thus reducing the frequency of the collapses, and, on the other, control, intercept or deviate the blocks during their movement, such as ditches, rockfall shelters, ground embankments and net fences made of metallic meshes (Peckover and Kerr, 1977; Pelizza et al., 2004; Peila et al., 2006).

When the best position with reference to the interception percentage of the trajectories, the corresponding maximum bouncing height and the kinetic energy have been established, a suitable device can be chosen. In the past, many tests were carried out by manufacturers and universities to define the maximum energy that can be safely absorbed by net fences (Duffy, 1999; Peila et al., 1998; Duffy, 1999; Gerber, 1999; Gerber et al., 2008; Peila and Ronco, 2009), but they were developed according to different standards and procedures and the results were not easily comparable. For this reason, the European Organization for Technical Approvals has endorsed the new European Technical Approval Guideline “Falling rock protection kits” (ETAG 027), where the testing procedure for CE marking of

a net fence, named falling rock protection kit in the guideline, has been settled. (Kohlmaier, 2008; Peila e Ronco, 2009).

## 2 Product characterization by full-scale-test

The net fences consist of a sequence of functional modules made up of an interception structure, a support structure and connection components, which are linked to the foundations that are anchored in the ground (Table 1). As requested by the guideline, the certified kit must be made of a minimum of three functional modules. The energy that can safely be absorbed by the kit during block impact is the key points for its certification and its classification. ETAG 027 defines two energy levels as reference values: SEL “Service Energy Level” and MEL “Maximum Energy Level”. SEL is defined as 1/3 of MEL and the kit should be able to retain such a SEL event twice (Table 2).

The tests foresee the launching of a plain or reinforced polyhedral concrete block with a size of at least three times smaller than the nominal height of the kit against the central module of the tested kit. The maximum size of the block must be and, in the last metre of the trajectory before the impact, the block must move with an average speed that is greater or equal to 25 m/s.

SEL is defined as the kinetic energy of a block that impacts the kit twice and which allows the following constraints to be fulfilled: the kit should stop the block during two impacts with the same kinetic energy without maintenance after the first impact (after the first impact the block must be removed); the block should not touch the ground until the kit reaches the maximum elongation during both the first and the second impacts; during the first impact, there should be no ruptures in the connection components and no significant the openings of the mesh finally, the residual height of the kit (defined as the minimum distance between the lower and the upper rope measured orthogonally to the reference slope without removing the impacted block), after the first impact, should be higher or equal to 70% of the height of the kit before the test.

This value was chosen to set a reasonable height of an impacted net fence that can permit a block that rolls along the slope and impacts the already impacted modulus to be intercepted. Furthermore, this value is high enough to prevent the modules next to the impacted one from being slightly perturbed as a consequence of a first the impact.

MEL is defined as the kinetic energy of the block that impacts the kit which must fulfill the following constraints:  $MEL > \text{three times SEL}$ ; the barrier stops the block during the impact and the block does not touch the ground, until the kit reaches the maximum elongation.

The SEL energy value is assumed to be equal to 1/3 of the MEL value. The maximum deformation of the structure and the forces on the foundations are measured during the MEL test and are reported in the ETA.

The development of the ETA not only requires the previously described full-scale tests, but a complete evaluation of the factory production control and an analysis of the accompanying documents (i.e. installation manual, maintenance and handling procedures) are also necessary. The Approved Bodies have to check that the factory production control which has been activated by the manufacturer and the ETA-holder maintains continuous surveillance and that a traceable documentation of all the production processes is available.

The standard conditions for the installation of falling rock protection kits in real sites

should be clearly described in the manufacturer's installation guide, where the producer, under its own responsibility, should provide the technical specifications of all the components and the geometric admissible tolerances, particularly concerning the spacing of the posts and the inclination of the main ropes. It is very important to highlight that the height of the barrier cannot be reduced, with reference to the tested kit, and cannot be raised by more than 1 m for a tested height not less than 4 m and 0.5 m for a tested height lower than 4 m.

| Main parts             | Components   | Function  |
|------------------------|--|---|
| Interception structure | Principal net: made up of metallic cables, wires and/or bars of different types and materials (for example cable nets joined by clamps, submarine nets and ring nets. In the last two cases the rings forming the net are connected to each other). Additional layers: usually with a finer meshwork than the principal net made up of cables and/or wires or other materials. | To bear the direct impact of the mass, deform elastically and/or plastically and transmit the stresses to the connection components, the support structure and the foundations. |
| Support structure      | Posts made of different materials, geometries and lengths (for example, pipes, structural metallic elements) having a hinge at the bottom.   | To keep the erected interception structure. It can be directly connected to the interception structure or through the connection components.                                    |
| Connection components  | Connecting ropes, steel cables, wires and/or bars of different types and materials, junctions, clamps, energy dissipating devices (elements which are able to dissipate energy and/or allow a controlled displacement when stressed).  | To transmit the stresses to the foundation structure during impact and/or keep the interception structure in position.  |
| Foundations            | Cables or bars anchored in the ground with adequate grout (not part of the ETAG).  | To transmit the forces derived from the block impact to the ground.   |

**Table 1.** Net fences main components as reported in ETAG 027.

| Energy level | 0   | 1   | 2   | 3    | 4    | 5    | 6    | 7    | 8     |
|--------------|-----|-----|-----|------|------|------|------|------|-------|
| SEL [kJ]     | -   | 85  | 170 | 330  | 500  | 660  | 1000 | 1500 | >1500 |
| MEL [kJ] ≥   | 100 | 250 | 500 | 1000 | 1500 | 2000 | 3000 | 4500 | >4500 |

**Table 2.** Net fences energy classifications.

### 3 Design procedure for rockfall restraining nets

The design of rockfall protection devices (Peila et al., 2006) is a complex task that requires the designer to take into account many data from the site (i.e. geological, geotechnical and topographical) and from the trajectory forecast. When the best position of the protection devices and the impact energy have been evaluated, on the basis of the trajectory forecast, it is necessary to design and choose the correct net fence on the basis of the design rules in force (for example Eurocode 7 - EN 1997-1:2004).

The first design step is to choose whether to design with a MEL or SEL approach:

- in the case of forecasted low frequency rockfall events and with different fall directions, thus not involving the same modulus, it is possible to adopt the MEL approach;
- if the barrier has to be installed in difficult maintenance positions and it is therefore preferable not to repair it after each block impact, the SEL design approach should be chosen (considering that the design safety factor is three);
- in the case of the possibility of several impacts against the same modulus, that is, in the same direction, the designer's choice could be: installation of two net fences with the alignment defined at a MEL level or one net fence with the alignment designed at a SEL level.

The designer should then verify that:

- the energy that can be dissipated by the net fences is greater than the computed energy of the block:

$$E_{design} - \frac{E_{ETA,netfences}}{\gamma_E} \leq 0 \quad (1)$$

where:  $\gamma_E$  is a safety factor that is suggested as 1.30 if the barrier is designed taking into account the MEL energy level (as used in Eurocode 7 in Design Approach 2) and 1.00 if it is designed taking into account the SEL energy level (as used in Eurocode 7);  $E_{ETA,netfences}$  is the energy certified by ETA (MEL or SEL);

- the interception height ( $h_i$ ) of the net fence is greater than the design interception height ( $h_p$ ), which is determined from the trajectory forecast, taking into account the computed block passage height relative to the slope (95% percentile) in the design position plus a clearance ( $f$ ) that is not lower than half the average size of the block:

$$h_i \geq h_p + f \quad (2)$$

- the maximum barrier elongation towards the valley ( $d_a$ ) multiplied by a safety factor ( $\gamma_E$ ) must be smaller than the design distance between the net fence alignment and the area that has to be protected ( $d_p$ ):

$$d_a \gamma_E \leq d_p \quad (3)$$

This means that the barrier should always be installed at a sufficiently safe distance from the protected area.

The computation of the kinetic energy of the block during the impact is usually carried out using the computed block speed and the design block mass, applying the usual classical physics formulations and the concept of the partial safety factor, as indicated in Eurocode 7 (point 2.4.7.3.3).

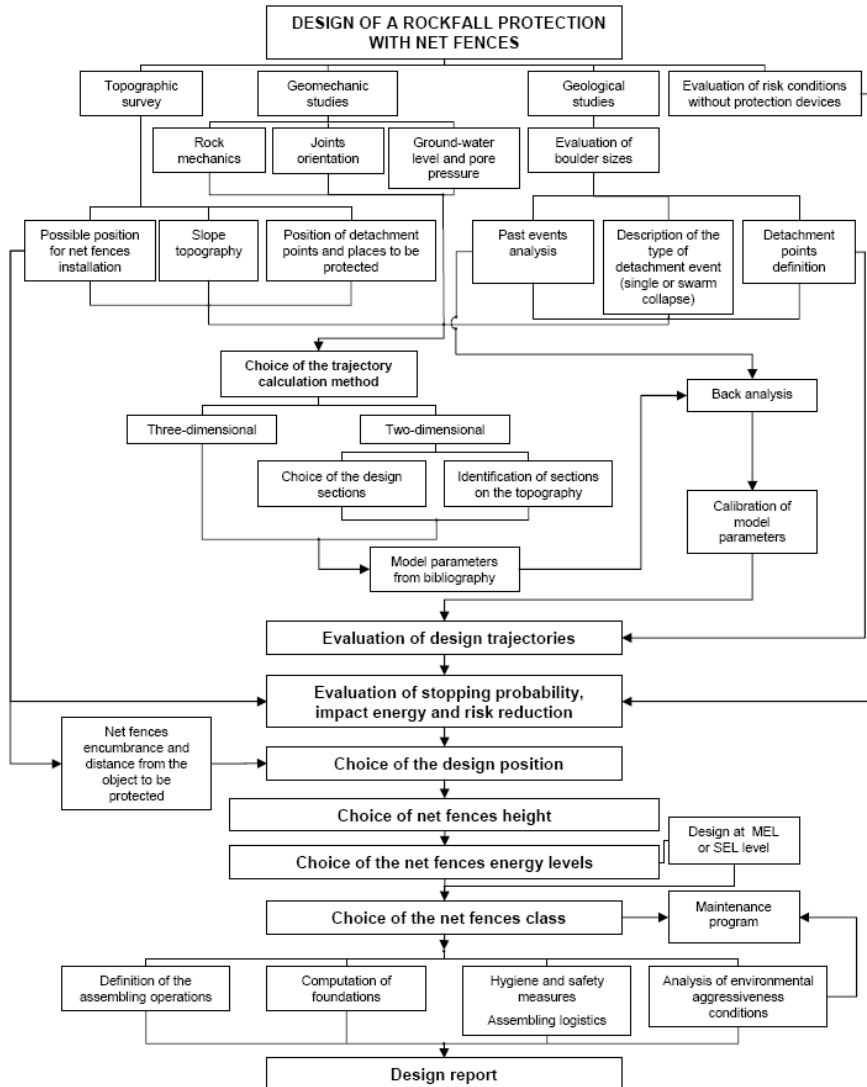


**Figure 1.** Flow chart for the design of a rockfall protection device in an area prone to rockfall (redrawn from Peila et al., 2006).

The design speed of the block ( $v_p$ ) is obtained taking the calculated 95% percentile ( $v_i$ ) of the computed speeds of the falling trajectories, as the characteristic value, multiplied by a safety factor ( $\gamma_F$ ):

$$v_p = v_i \gamma_F \quad (4)$$

where  $\gamma_F = \gamma_{Tr} \gamma_{Dp}$  (EN 1997-1:2004 Annex B; EN 1990:2002), with:

$\gamma_{Tr}$ , is reliability coefficient of the trajectory computation, which takes into account the possibility of deviation of the action values from their characteristic values, for which the following values are suggested:

= 1.00 in the case of statistical computations derived from a back analysis;

= 1.10 in the case of computations based on restitution coefficients obtained from bibliographic information;

$\gamma_{Dp}$  is the partial factor linked to the slope discretization quality, that takes into account the uncertainties involved in modelling the actions, for which the following values are suggested:

= 1.05 for a carefully discretized slope characterized by a precise topographic survey;

= 1.10 for a slope modelled with a simplified 2D cross-section derived from a large scale map.

These partial factors must be considered as suggestions and must be defined and evaluated individually for each problem. The design block mass ( $m_p$ ) can be equal to the product of the design block volume ( $Vol_b$ ) and the rock unit weight ( $\gamma$ ) multiplied by a specific safety factor ( $\gamma_m$ ):

$$m_p = (Vol_b \gamma) \gamma_m \quad (5)$$

where  $\gamma_m = \gamma_{VolF1} \gamma_y$  (EN 1997-1: 2004 Annex B; EN 1990:2002), with:

$\gamma_y$ , the coefficient derived from the rock unit weight evaluation, which can be assumed equal to 1.00

$\gamma_{VolF1}$  is the coefficient derived from the volumetric survey accuracy for the definition of the “design block” which should be chosen on the basis of the “engineering judgement” of the designer, for which the following values are suggested:

= 1.05 for a precise survey of the rock slope, for example obtained with a detailed reconstruction of the rock slope using laser scanning, photogrammetric methods or several direct geological surveys of the slope;

= 1.10 for a survey of the rock slope carried out only with a limited number of site investigations.

## 4 Conclusions

The new ETAG 027 guideline that states how to test and certify a falling rock protection kits will also play an important role in the design of rockfall protection devices since, for the first time, a testing standard has been defined that is the same for all EU Countries, thus making it possible to compare the various products on the basis of the energy level they can adsorb.

Furthermore, other significant information for designers, such as the maximum elongation of the net fences and the forces applied to the foundations, can be obtained during full scale tests and this will lead to an improvement in the design quality of a protection device, as shown by the proposed design procedure.

These data can be combined to provide a robust design with a systematic use of partial safety factors, as prescribed by the geotechnical Eurocode design approach, which represents the official standard in force in Europe for geotechnical works design thus obtaining a design procedure.

## References

- Duffy, J. D.: Barrier testing in North America. A brief summary report, in: Proceedings of Convegno "Previsione e prevenzione di movimenti franosi rapidi", Trento, Italy, 17-19 June 1999, 67-72, 1999.
- EN 1990: Eurocode – Basis of structural design, 2002
- EN 1997-1: Eurocode - Geotechnical design – Part 1: General rules, 2004.
- ETAG 027: Guideline for European Technical Approval of Falling Rock Protection Kits, <http://www.eota.eu/>, access 16/06/09, 2008.
- Gerber, W.: Highly flexible wire net rock fall barriers, in: Proceedings of the Joint Japan-Swiss Scientific Seminar on Impact Loads by Rock Falls and Design of Protection Structures, Kanazawa, Japan, 4-7 October 1999, 37-42, 1999.
- Gerber, W., Baumann, R., and Volkwein, A.: Swiss guidelines for the approval of rockfall protection kits – 7 years of experience, in: Proceedings of Interdisciplinary Workshop on rockfall protection, Morschach, Switzerland, 23-25 June 2008, 34-36, 2008.
- Jaboyedoff, M., Dudd, J.P., and Labiouse, V.: An attempt to refine rockfall hazard zoning based on the kinetic energy, frequency and fragmentation degree, *Nat Hazard Earth Sys*, 5, 621-632, 2005.
- Kohlmaier G.: European Technical Approvals. The way for CE marking of rockfall protection kits, in: Proceedings of Interdisciplinary Workshop on rockfall protection, Morschach, Switzerland, 23-25 June 2008, 43-45, 2008.
- Nicot, F., Cambou, B., and Mazzoleni, G.: Design of rockfall restraining nets from a discrete element modelling, *Rock Mech Rock Eng*, 34 (2), 98-118, 2001.
- Peckover, F. L. and Kerr, W. G.: Treatment and maintenance of rock slopes on transportation routes, *Can Geotech J*, 14(4), 487-507, 1977.
- Peila, D., Oggeri, C., and Baratono, P.: Barriere paramassi a rete: interventi e dimensionamento. GEAM Associazione Georisorse e Ambiente ed., Torino, Italy, 127 pp., 2006.
- Peila, D., Oggeri, C., and Castiglia, C.: Ground reinforced embankments for rockfall protection: design and evaluation of full scale tests, *Landslides*, 4, 255-265, 2007.
- Peila, D., Pelizza, S., and Sassudelli, F.: Evaluation of behaviour of rockfall restraining nets by full scale tests, *Rock Mech Rock Eng*, 31(1), 1-24, 1998.
- Peila D. and Ronco C.: Technical Note: Design of rockfall net fences and the new ETAG 027 European guideline, *NHESS*, 9, 1291-1298, 2009
- Pelizza, S., Peila, D., and Oggeri, C.: Tipologie di intervento per la bonifica di versanti rocciosi, in: Proceedings of Convegno su Bonifica di versanti rocciosi per la protezione del territorio, Trento, Italy, 11-12 March 2004, 9-44, 2004.
- Volkwein, A.: Numerical simulation of flexible rockfall protection system, in: Proceedings of congress on Computing in civil engineering, Cancun, Mexico, 12-16 July 2005, 2005.
- Wieczorek, G. F., Stock, G. M., Reichenbach, P., Snyder, J. B., Borchers, J. W., and Godt, J. W.: Investigation and hazard assessment of the 2003 and 2007 Staircase Falls rock falls, Yosemite National Park, California, USA, *Nat Hazard Earth Sys*, 8, 421-432, 2008.



## Impact load transmission within a half-scale sandwich rockfall protection wall

Adeline Heymann<sup>1,2,3</sup>, Philippe Gotteland<sup>2</sup>, Stéphane Lambert<sup>1</sup>

<sup>1</sup> Cemagref, UR ETGR, Domaine Universitaire BP 76, 38402 St-Martin d'Hères, France  
[adeline.heymanncemagref.fr](mailto:adeline.heymanncemagref.fr) ; [stephane.lambertcemagref.fr](mailto:stephane.lambertcemagref.fr);

<sup>2</sup> 3SR, UMR5521, DU Grenoble Universités, 38041 cedex 9, Grenoble, France  
[philippe.gotteland@ujf-grenoble.fr](mailto:philippe.gotteland@ujf-grenoble.fr)

<sup>3</sup> RAZEL, 3 rue René Razel, 91400 Saclay, France

---

**Abstract.** This contribution presents experiments on cellular sandwich rockfall protection structure. Such structures constitute innovative developments aiming at using the cellular technology, classical in the field of civil engineering, for rockfall protection. In order to explore the mechanical behavior of these systems under dynamic loadings, impact experiments are performed and a numerical model of the structure is developed. The experiments consist of the impact by a 260 kg spherical projectile on a structure composed of gabion cages filled with coarse materials in the front part and fine materials in the kernel part. This structure stands against a rigid concrete wall. In a first time, the methods and results are presented focusing on the transmission of the load (stress) in the impact direction.

**Keywords:** rockfall, protection, dynamic loading

---

### 1 Introduction

Soil structures are used as passive countermeasures against medium to high energy falling boulders. Despite several experimental and numerical studies have been carried out (Yoshida, 1999; Hearn et al., 1995; Peila et al., 2007; Aminata et al., 2008), the design of these dams generally rests on an empirical approach. A thorough analysis of the mechanical response of these structures remains to be done in order to improve their efficiency, fully taking into account the dynamics.

Reinvestigating the principle of a sandwich structure, pioneered by Yoshida (Yoshida, 1999), an intensive study was initiated to develop cellular structures (the REMPARE project). For instance, cells considered to build the structure are gabion cages and the sandwich is obtained using different fill materials. The aim with such a sandwich is to increase the structure ability in dissipating and diffusing the impact energy.

With this aim the behaviour of cells under impact has been first studied using different fill materials (Lambert et al., 2009), before investigating the response of a half-scale structure,

focusing on the load transmission in the direction of the impact. This is the aim of this paper.

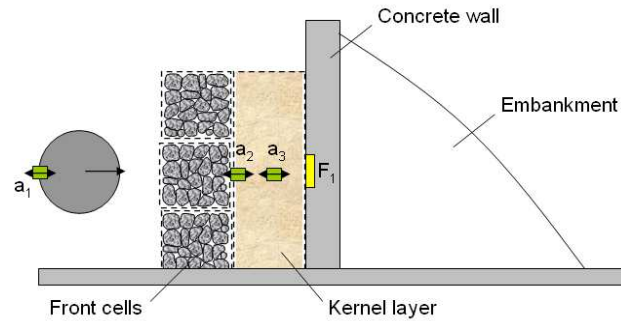


**Figure.1.** sandwich structure used in the experiment and measurement devices ( $a_1$  : accelerometer on the projectile,  $a_2$  : accelerometer at the interface between the front and the kernel layers,  $a_3$  : accelerometer in the middle of the kernel layer,  $F_1$  : stress sensor on the back part wall).

## 2 Materials and methods

### 2.1 Tested structure

The structure consisted in a two-layers sandwich structure leaned on a rigid reinforced concrete wall (Figure 1). The dimensions of this structure were 1.5 m in height, 2.5 m. in length and 1 m. in thickness.

The first layer, or front part, consisted of 15 gabion cells filled with a coarse material. These geocells were cubic in shape, 500 mm in height. The envelope was made up of a hexagonal or double-twisted wire mesh. The mesh height and width were 80 mm and 100 mm respectively, and the wire had a 2.7 mm diameter. The filling material was a crushed quarry limestone, 80 to 150 mm in grain size



**Figure.2.** Overview of the experimental device (a) and the impacted structure during the implementation (b).

The second layer of the sandwich structure, in the kernel part, consisted of a Seine sand cushion. This sand is a well-graded sand which size distribution ranges from 0.2 to 5 mm. For an easier implementation, the material of the kernel is not contained in cells, but dumped in bulk. In order to contain this fine material a non-woven-needle-punched geotextile was used (Figure 2b).

## 2.2. Experimental methodology

These experiments were performed in the CER (Center of Road Study) of Rouen (France). The experimental device (Figure 2a, Figure 3) consists of a concrete wall, 3m in height, leaned on a ground consolidated embankment. This set constitutes the back part support. The dropping device is made of two metallic pylons 7 m in height, linked with a transversal girder where two chain slings are tightened. The lifting is completed by a hand cable winch to reach a maximal height of 4.75 m. The tested structure is subjected to a pendular impact by a 260 kg spherical projectile, 54 cm in diameter, and made of a steel shell filled with concrete (Lambert et al., 2009). The maximal energy developed by the projectile is 10kJ. At the beginning of the impact, the trajectory of the projectile is perpendicular to the front face of the structure.

Two types of measures are carried out: acceleration measured on various locations, and measures of the stress transmitted at the support ( $a_1$ ,  $a_2$ ,  $a_3$  and  $F_1$  on Figure 1). A triaxial piezoresistive accelerometer is placed on the projectile ( $a_1$ ). It allowed determining the time evolution of the impact force  $F_{imp}$  applied by the projectile on the structure. The duration of the impact,  $d_{imp}$ , is deduced from the projectile's acceleration measurements. Accelerometers are also placed at the interface between the front and the kernel layers ( $a_2$ ) and in the middle of the kernel layer ( $a_3$ ). All sensors are placed along the impact direction of the projectile before impact, and at the same height as the impact point. These accelerometers are used to measure the time elapsed between the beginning of the impact and the beginning of the displacement at the point considered as well as estimating the amplitude of the compression wave. A stress sensor is placed on the concrete wall ( $F_1$ ). It provides the time evolution of the stress  $\sigma_{tran}$ , normal to the impact direction on the back part of the structure.

The sample rate was 40 000 Hz. In order to minimize the noise due to high frequency phenomena, signals were submitted to a low-pass Butterworth filter with a cut frequency of 1000 Hz. Then the norm of the acceleration of the projectile was calculated using the

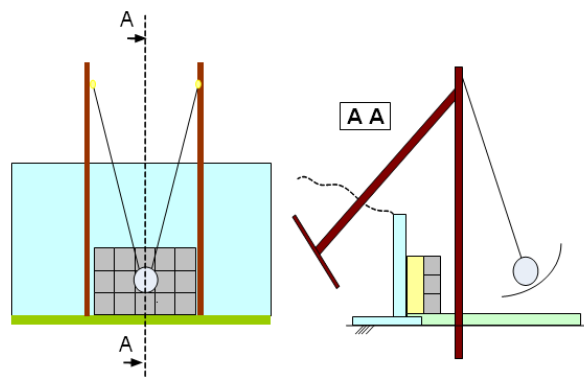


Figure.3. Principle of the experimental device.

three components. The filtering induces a temporal gap between the real and filtered  
 The evaluation of the response of the structure is mainly based on the force applied by the projectile on the structure  $F_{imp}$  and the stress transmitted by the structure to the support  $\sigma_{tran}$ .  
 Four successive impacts increasing the impact energy were carried out (2, 4, 8 and 10kJ). The highest energy impact was repeated twice.

### 3 Results

#### 3.1. Time evolution of the impact force and of the transmitted stress

As shown in Figure 4 (left), the impact force increases with the impact energy. The duration of the impact is about 50 ms, and seems to be independent of the impact energy. The curves of the impact force present a maximum and then a plateau behaviour. With increasing impact energy, the slope of the section preceding the peak increases and the peak occurs earlier. For a 2kJ impact, the maximum of the impact force is 90 kN, and for the first impact at 10 kJ it is 450kN. Comparison of the two 10kJ-impacts show that despite the maximum force for the second impact is higher (490 kN), the two plateau have approximately the same amplitude.

The response of the structure in terms of transmitted stress is pictured in Figure 4 (right). The stress measured at the support increases with the impact energy. For the 2kJ-impact the transmitted force remains little. For other impact energies, a peak occurs approximately 20ms after the impact.

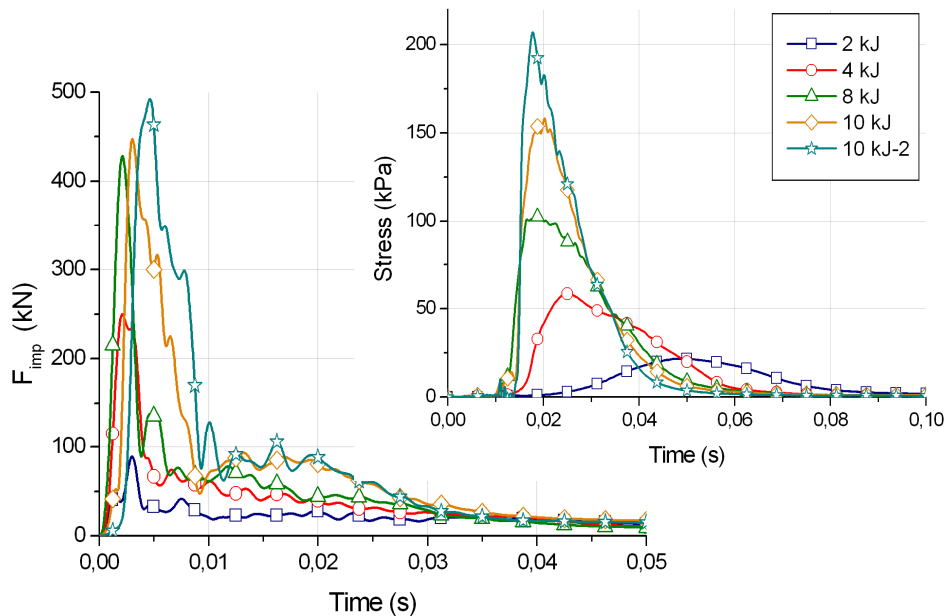


**Figure.4.** (left) Impact force  $F_{imp}$  of the projectile vs. Time for each impact energy;  
 (right) Stress measured at the support vs. Time for each impact energy.

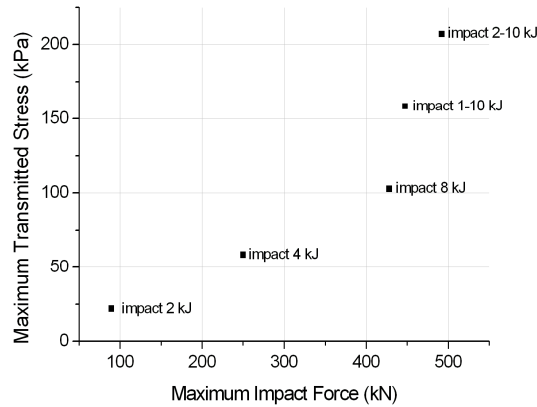


**Figure.5.** Maximum of stress measured at the support vs maximum impact force for each impact energy

As presented in Figure 5, the maximum transmitted stress increases non-linearly with the maximum impact force. It is assumed to be the consequence of the repeated loadings of the structure, since the answer is higher when the material is compacted.

### 3.2. Compression wave propagation

The Figure 6 compares the data from the different sensors in the case of an 8kJ impact. It takes about 2.5 ms for the compression wave to reach the accelerometer  $a_2$ , 5.8 ms for the  $a_3$  accelerometer and 10 ms for the stress sensor.

The respective compression wave velocity can then be estimated: 120m/s in the stones cells, and 66m/s in the kernel layer. These values are rather low.

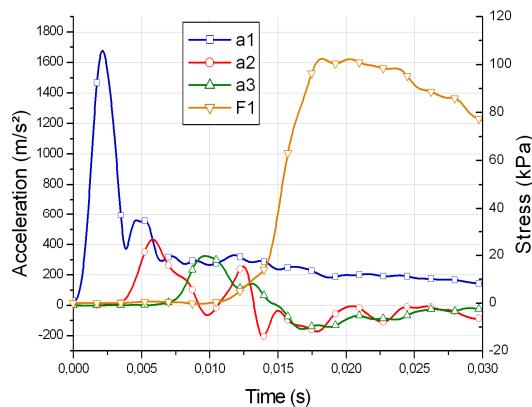


**Figure.6.** Propagation of the compression wave in the structure for an 8kJ impact.

Figure 6 allows also appreciating the variation of amplitude of this compression wave. For this impact, the maximum projectile deceleration is  $1700 \text{ m.s}^{-2}$ , the maximum acceleration measured at the interface between the front and the kernel layers is only  $430 \text{ m.s}^{-2}$  and the acceleration measured in the middle of the kernel is  $330 \text{ m.s}^{-2}$ .

## 5 Conclusion and perspectives

In order to understand the mechanical response of a cellular sandwich structure under a dynamic loading, a series of impact tests was performed. The response of the structure was evaluated thanks to the impact force and the stress transmitted to its back part support. Results show that the impact force and transmitted stress increase with the impact energy. They also show that the maximum of the transmitted force evolves non-linearly with the maximum of the impact force. This is due the compaction of the material by the successive impacts. The measurement device allows appreciating the evolution of the compression wave in terms of velocity and amplitude.

A numerical model of this structure was developed using a discrete element method. The structure is modelled as an assembly of rectangular cells of the same size representing the gabion cages used in the experiments. The peculiar feature of this model is that the constitutive model used for the different cells depends on the proximity to the impact point. Even if the improvement of this constitutive model is in progress by means of experimental studies on the energy transfer inside a sand layer during rock impacts the model provides a correct prediction of the impact force on the projectile (Bourrier et al., 2010).

## References

- Aminata, D., Yashima, A., Sawada, K. and Sung, E. (2008). New Protection Wall Against Rockfall Using a Ductile Cast Iron Panel. *Journal of Natural Disaster Science* 30(1). pp 25-33.
- Bourrier, F., Gotteland, P., Nicot, F. and Lambert, S. (2010). A model for rockfall protection structures based on a multi-scale approach. *Conference Proceedings, Geoflorida*, West Palm Beach, Florida, to be published, 6 pages.
- Hearn, G., Barrett, R. and Henson, H. (1995). Development of effective rockfall barriers. *Journal of transportation engineering* 121(6). pp 507-516.
- Lambert, S., Gotteland, P., and Nicot, F. (2009). Experimental study of the impact response of geocells as components of rockfall protection embankments. *Natural Hazards and Earth System Sciences* 9. pp 459-467.
- Peila, D., Oggeri, C., Castiglia, C. (2007). Ground reinforced embankments for rockfall protection : design and evaluation of full scale tests. *Landslides* 4. pp 255-265.
- Yoshida, H. (1999). Recent experimental studies on rockfall control in Japan. *Conference Proceedings, Joint Japan-Swiss scientific seminar on impact by rock falls and design of protection structures*, Kanazawa, Japan, pp 69-78.

## Impact loads of falling rocks on granular material

Werner Gerber, Axel Volkwein

WSL Swiss Federal Institute for Forest, Snow and Landscape Research, Zuercherstr. 111, CH-8903 Birmensdorf, Switzerland

[werner.gerber@wsl.ch](mailto:werner.gerber@wsl.ch), [axel.volkwein@wsl.ch](mailto:axel.volkwein@wsl.ch)

**Abstract.** This contribution presents results of 54 tests with two different boulders made of concrete, which dropped on two different ground layers. The deceleration of the boulder during the impact was measured with accelerometers. The analysis of data delivered useful results such as maximum deceleration, penetration depth and braking time. This allows the description of the correlation between maximum deceleration, penetration depth and impact velocity. The characteristic of the deceleration of each test was analyzed specially. The normalization of the decelerations shows an independence of the course of deceleration from the drop height respectively from the impact velocity. The results are a useful basis to design earth dam against rockfall or help to calculate the rockfall process in simulations.

**Keywords:** rockfall, impact load, deceleration, braking process, ground layer.

### 1 Introduction

Dynamic load extremes of rockfalls on structures are dependant on the distance over which the impacting mass is stopped. Lower values are observed when braking occurs over a greater distance such as the case of a flexible wire-rope rockfall barrier. Conversely, highest peaks are observed when impacting a concrete gallery or wall with no or just a thin cushion layer. Therefore, an in depth understanding of such impact loads is essential to properly design protection measures. One question is therefore how deep is the penetration and what is the maximum rockfall deceleration on different grounds?

**Table 1.** Drop heights and kinetic energies of all tests

|                               |                            |            |         |            |            |            |
|-------------------------------|----------------------------|------------|---------|------------|------------|------------|
| drop height                   | 2.5 m                      | 5 m        | 7.5 m   | 10 m       | 12.5 m     | 15 m       |
| velocity at impact            | 7 m/s                      | 10 m/s     | 12 m/s  | 14 m/s     | 16 m/s     | 17 m/s     |
| kinetic energy (800 kg)       | 20 kJ                      | 40 kJ      | 60 kJ   | 80 kJ      | 100 kJ     | 120 kJ     |
| kinetic energy (4'000 kg)     | 100 kJ                     | 200 kJ     |         | 400 kJ     |            | 600 kJ     |
| <b>ground layer A (0.5 m)</b> | <b>Test number 1 - 30</b>  |            |         |            |            |            |
| series 1 (800 kg)             | 1, 2, 3                    | 4, 5, 6    | 7, 8, 9 | 10, 11, 12 | 13, 14, 15 | 16, 17, 18 |
| series 2 (4'000 kg)           | 19, 20, 21                 | 22, 23, 24 |         | 25, 26, 27 |            | 28, 29, 30 |
| <b>ground layer B (1.3 m)</b> | <b>Test number 31 - 54</b> |            |         |            |            |            |
| series 3 (4'000 kg)           | 31, 32, 33                 | 34, 35, 36 |         | 37, 38, 39 |            | 40, 41, 42 |
| series 4 (800 kg)             | 43, 44, 45                 | 46, 47, 48 |         | 49, 50, 51 |            | 52, 53, 54 |

The existing guideline in Switzerland (ASTRA 1998) refers to galleries on concrete with variable cushion layer. Egli (2004) calculates the acting forces for a penetration depth of 20 mm on a 20 - 40 cm thick concrete shed. The tests of Schellenberg *et al.* (2007, 2008) showed penetration depths of 4 - 14 cm in a 40 cm cushion layer of compacted gravel banked on different concrete plates. Heidenreich (2004) performed tests under laboratory conditions using concrete blocks with masses of 100 kg, 500 kg and 1000 kg dropped on a cushion layer with a thickness of 1 m resulting in a penetration depth of 5 – 28 cm.

## 2 Experimental set-up

### 2.1 Methods and measurements

Two concrete blocks with masses of 800 kg and 4'000 kg were dropped vertically onto two ground layers A and B. Layer A was 0.5 m and layer B 1.3 m each prepared above bedrock. The drop heights of the blocks varied between 2.5 m and 15 m, producing a kinetic energy range of between 20 and 600 kJ. Each test was repeated three times and a total of 54 tests were carried out (Table 1). On top of the concrete block four accelerometers with a range of  $\pm 500$  g ( $g$  = gravitational acceleration constant) were installed to measure the deceleration of the block two seconds before and one second after impact. The sample rate for all accelerometers was 5000 Hz. The experimental setup can be seen in Figure 1.

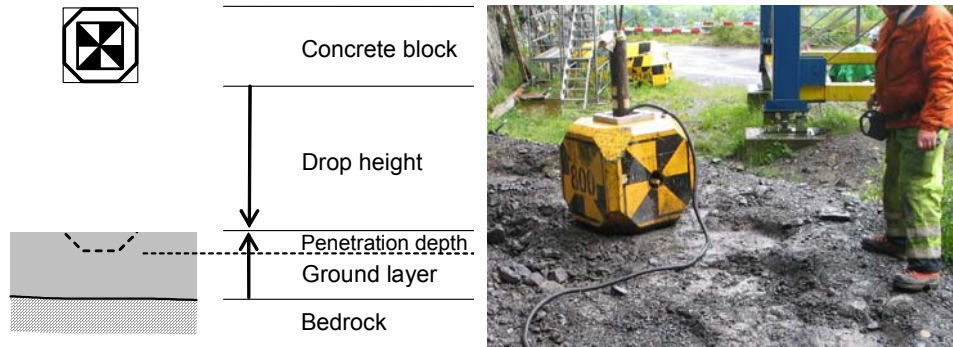


**Figure.1.** Experimental set-up and 800 kg concrete block with accelerometers mounted within a U-shaped steel frame on top

### 2.2 Ground layers and procedure

Three 23-54 kg samples of the ground layer material with a grain size < 63 mm were sieved and analysed according to Swiss code SN 670'008. The analysis indicated a material of sorted gravel with silt and sand (GW-GM), showing average grain size fractions: gravel 74 %, sand 18 % and silt 6 % (details in Table 2).

**Table 2.** Grain size distribution of 3 samples and average

| ground material | grain size  | Sample 1 | Sample 2 | Sample 3 | Average |
|-----------------|-------------|----------|----------|----------|---------|
| gravel          | 2 - 63 mm   | 76%      | 67%      | 79%      | 74%     |
| sand            | 0.06 - 2 mm | 18%      | 22%      | 15%      | 18%     |
| silt            | < 0.06 mm   | 6%       | 11%      | 6%       | 6%      |

In the first series (tests 1-18) the 800 kg block was impacted onto ground layer A. For each impact the block was released onto a fresh portion of the 5 by 7m ground layer. Following this the surface of ground layer A was then raked to level out impact scars in preparation for tests 19-30 using the 4000 kg boulder. In series three (tests 31-42) the same procedure was performed onto ground layer B, while the 4000 kg boulder was used before the 800 kg (tests 43-54). A re-levelling of the impact scars was also conducted between tests with the different boulders.

### 3 Time integration of acceleration measurements

The average of the four acceleration sensors was again averaged over time using a 2 milliseconds mean (11 values) in order to remove the natural vibrations of the sensors. The result was integrated over the time to obtain velocity and displacement curves of the falling boulders (Figure 2). Maximum velocity was reached at the time of the impact and decreases to zero at the point of the maximum penetration depth. Afterwards, the block accelerates upward and drops to the ground a second time.

## 4 Results

### 4.1 Results of braking process

The maximal penetration depths lie between 15 and 30 cm and clearly increase with increasing drop heights. These penetrations have been produced with the 4000 kg block and a ground layer of 1.3 m (test no 31 - 42). For the smaller boulder or the thinner ground layer the penetration depths lie between 7 and 18 cm (Figure 3).

The minimum decelerations of 210 - 700 m/s<sup>2</sup> were also produced with the 4000 kg block and a ground layer of 1.3 m (test no. 31 - 42). The maximum decelerations of 600 – 1620 m/s<sup>2</sup> were measured with the 4000 kg block and a ground layer of 0.5 m (test no. 19 - 30). The decelerations of the tests with the 800 kg block don't show significant differences between the two variable ground layers (Figure 3). The relation between maximum deceleration and penetration reveals strong changes for the 4000 kg block and the two different ground layers but less for the tests with the 800 kg block (Figure 4 left).

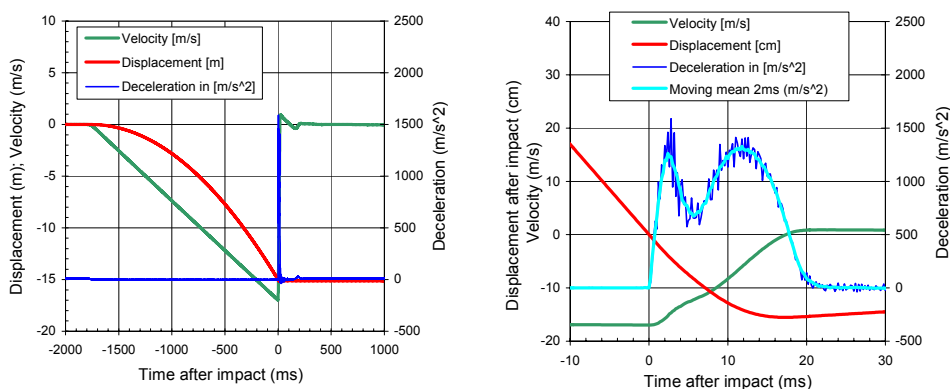


Figure.2. (left) Measured deceleration during 3 seconds and (right) detail during 0.040 seconds

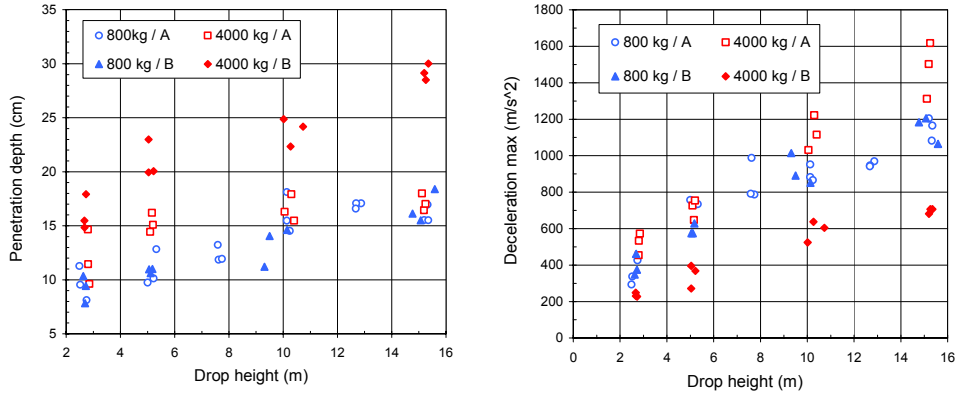


Figure.3. Displacement after impact (Penetration) and (b) maximum of deceleration (54 tests)

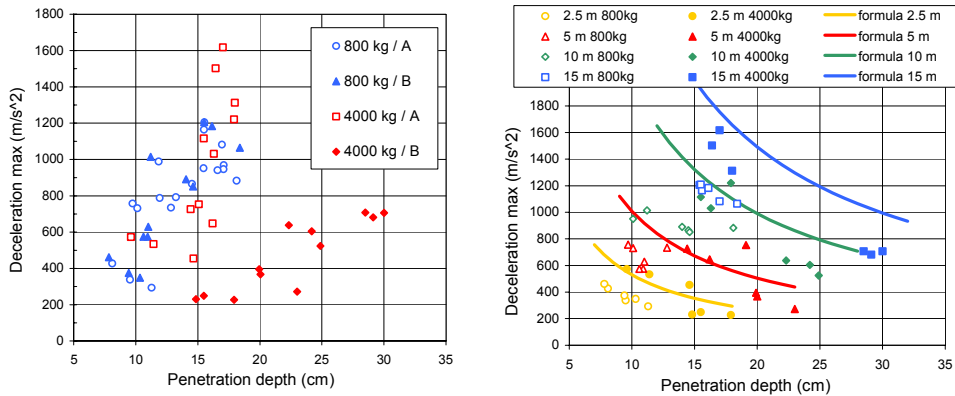


Figure.4. Maximum deceleration as a function of penetration depth (on the right with assumed relationship model for four different falling heights)

#### 4.2 New formula

In Figure 3, penetration and deceleration deal with the drop heights. With increasing drop height penetration and deceleration increase as well. That means that the impact velocity influences these values. The results of the 4000 kg block tests show also a correlation between the penetration and the maximum deceleration. The maximum braking force  $F_{max}$  is therefore assumed as a function of mass  $m$  and maximum deceleration  $a_{max}$ . Thereby, the deceleration  $a_{max}$  itself is a function of impact velocity  $v$ , braking time  $t$  and a constant value  $c$  (Eqn 1). The penetration  $d$  is also a function of impact velocity  $v$ , braking time  $t$  and the reciprocal value  $1/c$  (Eqn 2). The combination of the two equations delivers an estimation for the maximum acceleration in dependency to the impact velocity and the penetration depth (Eqn 3). This new assumption is visualized for four different falling heights on the right side of Figure 4. The calculated values are mostly above the measured one. So, equation 3 is a valuable instrument to gain a first impression of the braking process.

$$F_{\max} = m \cdot \frac{v}{t} \cdot c \quad (1) \quad d = v \cdot t \cdot \frac{1}{c} \quad (2) \quad a_{\max} = \frac{v^2}{d} \quad (3)$$

### 4.3 Normalization of deceleration curves

In order to find a general rule on how to describe the characteristics of a deceleration process, the moving means of decelerations can be standardized by equating both the stopping time and the maximum deceleration to 100%. Two examples for differently shaped deceleration curves are shown in Figure 5 with either two significant local maximum accelerations or one maximum and a plateau-like behaviour of the ground underneath the blocks. Depending on the deceleration curve type the time of maximum deceleration varies between 10 – 30 % or 60 – 75 % of the total braking time.

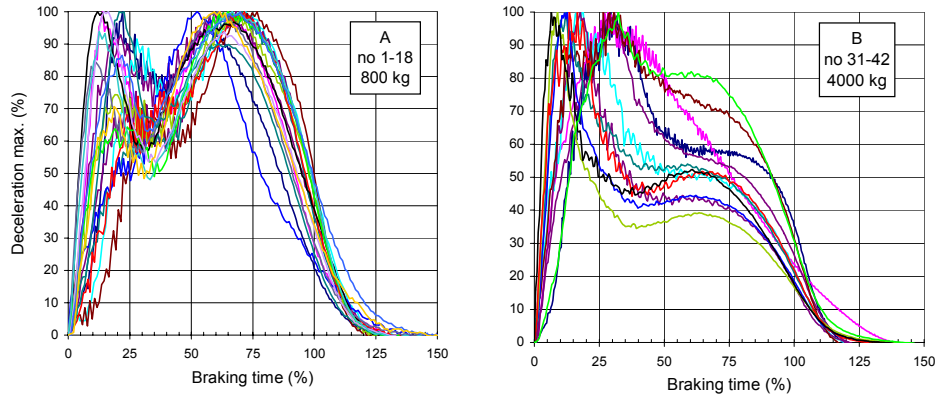


**Figure.5.** Two examples for differently shaped deceleration curves after performing a according normalization: (left) test no 1-18 and (right) 31-42

## 5 Discussion and Outlook

The penetration depth results of the tests with masses of 4000 kg show a clearly difference between the two ground layers in contrast to the tests with the 800 kg block. This surprising result can be explained through the chronology of the different test series. For the third series, the 4000 kg block was used before the 800 kg block tests on the same ground layer B. The re-leveling of the surfaces between tests did not involve a full repacking of the ground layer. Therefore, in comparison to the first and second test series where the 800 kg was used prior to the 4000kg block, the ground B can be argued to have been greater compacted for the tests with the 800 kg boulder. Thus the penetration depths with the 800 kg block don't show significant differences anymore. This observation has illustrated the importance of compaction in the ground layer, and is an important factor during the impact that has to be investigated more in detail. This influence of a ground layer compaction is further illustrated with the results of impact tests conducted by Schellenberg (2004), were impacts onto a gravel cushion layer (40cm) were conducted. In these tests the cushion layer was highly compacted with a vibration plaque and resulted in higher decelerations for same penetration depths in comparison to our results (Figure 6).

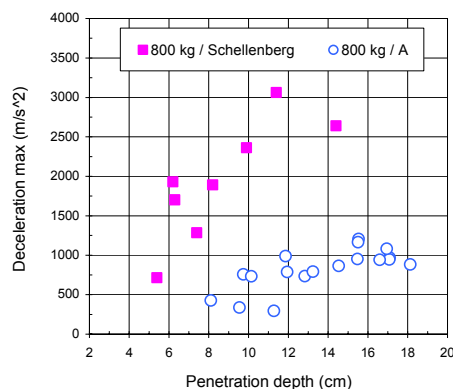


Figure 6. Comparison of test no 1-18 with Schellenberg (2004) compacted gravel layer

Penetration depth as well as maximum deceleration depends on the drop height or the impact velocity, respectively. The higher the velocity the greater the penetration and deceleration. On the other hand, the higher the penetration gets the smaller the deceleration will be. This correlation could be described with the new formula which reflected most of results about penetration depth and deceleration.

The normalization of decelerations shows clearly differences between the single test series. With such an instrument a lot of ground characteristics can be classified allowing a prediction of the ground behaviour due to rockfalls in order to better simulate trajectories or to design earth dams. Future analyses therefore should verify the interrelation of the mentioned parameters. Especially, to verify the assumed constant factor  $c$  containing information on impact velocity, braking time and penetration depth.

Generally, the obtained results help to better design protection systems such as earth dams, embankments and concrete galleries with layer thickness ranging 0.5 - 1.3 m. Additionally, valuable data are produced in order to improve and/or calibrate trajectory simulation of rockfall models. Further experiments are necessary to confirm and to improve the relevant mathematical functions and to calculate the influence of the compaction of the ground layer.

## References

- ASTRA (1998) Richtlinie Einwirkungen auf Steinschlagschutzgalerien. Eidg. Departement für Umwelt, Verkehr, Energie und Kommunikation, Bundesamt für Strassen, Bern.
- Egli, T. (2005) Wegleitung Objektschutz gegen Naturgefahren. *Vereinigung kantonaler Feuerversicherungen (Hrsg.)*, Bern.
- Heidenreich, B. (2004) Small- and half-scale experimental studies of rockfall impacts on sandy slopes. *Ph. D. thesis no. 3059*, Ecole Polytechnique Fédéral, Lausanne.
- Schellenberg, K., Volkwein, A., Roth, A. and Vogel, T. (2007) Large-scale impact tests on rockfall galleries. *Proc. of the 7<sup>th</sup> Int. conf. on shock & impact loads on structures*. Beijing, China. pp. 497-504.
- Schellenberg, K. (2008) On the design of rockfall protection galleries. *Dissertation Nr. 17924*, ETH Zürich.
- SN 670 008a: Identifikation der Lockergesteine. Eingetragene Norm der Schweizerischen Normenvereinigung. *Vereinigung Schweizerischer Strassenfachleute VSS*, Zürich.

## Use of the ultrasound to predicting the collapsible soils

LAOUAR Mohamed Salah<sup>1,2</sup>, ABBECHE Khelifa<sup>2</sup>, MESSAOUD Farid<sup>1</sup>

<sup>1</sup> University of Tebessa /Department of Civil Engineering, Tebessa, Algeria  
[c\\_laouar@yahoo.fr](mailto:c_laouar@yahoo.fr)

<sup>2</sup> University of Batna, Department of Civil Engineering, Batna, Algeria

---

**Abstract.** The majority of the arid regions have surface deposits of loose granular soils. These soils are suspect to undergo a great reduction in their volumes, after the moisture of their structure by giving huge settlements. Such deposits are known as collapsible soils. Most of the work carried out on these soils was devoted to the initial dry density, the water content, the degree of saturation and the applied load. The purpose of this experimental study led on reconstituted soils is the identification of the collapsible after having performed (Influence of the water content and the energy of compaction) In addition, to studying the influence of the ultrasonic speed on the collapse potential, based on having tested various samples with the ultrasound.

**Keywords:** collapsible soils, collapse potential, ultrasound.

---

### 1 Introduction

The collapsible soils are metastable soils of loose open structure, unsaturated nature, being in deposits form. In the dry state, a natural cementing between the grains confers an main inter-granular connection and can support very high loads. However, the saturation, even without additional loading, causes the disintegration of the connections giving a denser structure followed by a sudden collapse of the soil particles. Among the causes of saturation there is the raise of the ground water, water infiltration by the top and canalization leaks. Because of the important collapse potentials and serious consequences which can occur in the construction, this type of soil is considered unstable as foundations sit. These soils are mostly localized in the arid and semi arid region. They relate to a significant number of countries in particular those of the northern hemisphere located between the 30th and 55th parallels as well as countries of South America Abelev (1988). The collapse of Cheria 2009 in Eastern of Algeria constitutes a good example, where a great collapse was recorded, in which tens of constructions were inserted of more than two meters and half in the ground. While waiting to achieve measurements of the technical expertise, the preliminary report charges this catastrophe to a movement in the ground water. A building of three floors with Xining, Qinghai, was destroyed beyond repair because of collapse. This problem occurs because the loess beneath the foundations undergoes a structural collapse when it is flooded.

The literature revealed that the majority of research was devoted to the collapse mechanisms and the identification methods, of treatment and prediction. Marking propose an interval of degree of saturation between 60 % and 65 % beyond which collapse does not appear any more. The same result is confirmed by Ganeshan (1982).

In spite of having a great range of ultrasonic equipment and a large use of this process in various fields, the literature reveals that, except geotechnical marine and some applications, little attention was granted to this technique in the soil mechanics. This experimental work presents in addition to the compression tests, a series of non-destructive tests with the ultrasounds, in the objective to propose a predicting method of the collapsible soils based on ultrasonic tests.

## 2 Characteristics of materials

The tests were carried out on six reconstructed soils made up of sands and of kaolin in various proportions for which the application of the various criteria of collapse, reported by Ayadat and Bellili (1995), shows that those are collapsible. Two types of sands lesser than 2 mm of diameter are used for the soils reconstruction; sand of Dunes of Oum Ali region and sand of stream extracted from Melag stream of El Aouinet region washed and dried at 105 °C during 24 hours. In view of the small percentage of fine particles that they contain, these two types of sands are used for the concretes making. The kaolin used (<80µm) is extracted from of Djebel Debagh Mine of Guelma region of white color used generally in the manufacture of the fine porcelain, pottery and ceramic products. The soils S1, S2 and S3 are reconstructed with sands of Dunes and kaolin, while the soils S4, S5 and S6 are reconstructed with sands of stream and kaolin. The geotechnical characteristics of sands, kaolin and reconstructed soils are presented in Table 1. The literature revealed that a soil is expected to collapse if at least, one of the following criteria is checked:  $A_c < 1$ ,  $I_L < 0$ ,  $I_p \leq 20$ ,  $I_c > 1$ ,  $I_w \leq 1$ . The results presented, shows that these soils are expected to collapse and that the characteristics of consistency of the reconstructed soils depend basically on the initial moisture content.

**Table 1 Characteristics of Materials**

| Materials           | Characteristics  |       |       |       |       |       |       |
|---------------------|--|-------|-------|-------|-------|-------|-------|
| Sand of Dunes       | Grain size distribution ranged between 0.08 and 2 mm with 1.36% of particles < 80 µm. Coefficient of uniformity 3.91. Coefficient of curvature 1.33. Sand equivalent 73.26%. |       |       |       |       |       |       |
| Sand of stream      | Grain size distribution ranged between 0.08 and 2 mm with 3.01% of particles < 80 µm. Coefficient of uniformity 2.19. Coefficient of curvature 0.94. Sand equivalent 68.69 % |       |       |       |       |       |       |
| Kaolin              | % < 2 µm 43%. Liquid limit 65.83%. Plastic limit 39.64%<br>Specific density of grains $G_s$ 2.42   |       |       |       |       |       |       |
| Reconstructed soils | Label  | S1    | S2    | S3    | S4    | S5    | S6    |
|                     | % kaolin   | 15    | 35    | 50    | 20    | 30    | 40    |
|                     | % Sand of dunes  | 85    | 65    | 50    | -     | -     | -     |
|                     | % Sands of stream  | -     | -     | -     | 80    | 70    | 60    |
|                     | $G_s$  | 2.65  | 2.59  | 2.46  | 2.62  | 2.56  | 2.48  |
|                     | $w_L$ (%)  | 16.47 | 26.63 | 35.37 | 18.47 | 28.97 | 33.42 |
|                     | $w_p$ %  | 11.03 | 15.37 | 20.87 | 11.95 | 14.77 | 19.03 |
|                     | $\gamma_d$ max (g/cm <sup>3</sup> )  | 2.04  | 1.95  | 1.84  | 1.95  | 1.82  | 1.75  |
|                     | $w_{opt}$ (%)  | 8.62  | 9.43  | 13.88 | 12.82 | 14.67 | 17.82 |
| % < 2 µm            | 4.91   | 11.73 | 16.74 | 7.03  | 9.84  | 14.12 |       |

### 3 used materials

#### 3.1. Oedometric tests

The oedometer of which essential elements are an oedometer Mold of 50.4 mm diameter and 20 mm height, a frame of consolidation of lever arm of 1/10, and a set of weight.

The compaction tampers which is conceived especially at the laboratory for the compaction of the soil in the oedometer ring. Entirely manufactured of steel, it consists of a Base of 48.42 mm diameter and 3mm thickness attached to a column of guidance of 280 mm length, through which a piston slips. A sliding stopper along the rod makes it possible to adjust drop height of the hammer, and a Hammer in circular shape of dish of 84.422 mm diameter and 8.40 mm thickness. Its weight is 121g, having a centered drilling of 8.45 mm diameter.

#### 3.2 ultrasonic tests

Equipment includes an Analyzer for velocity measurement of the ultrasonic waves, a calibration bar, a Set of two transducers of 54 kHz with cables, acting differently as transmitter or receiver, and a paste pot of contact.

### 4 Tests program

Three series of principal tests were carried out on six reconstructed soils. The table II illustrates the program of these tests.

**Table 3 Tests Program**

| Test Type         | Selected Parameters   | Test Number | Observation  |
|-------------------|---|-------------|--|
| Oedometric Tests  | Water contents: 2%, 4%, 6% and 8%.<br>Compaction degrees: 10, 25, 40 and 60 blows.                | 96          | Realized according to Jennings and Knight procedure. |
| Penetration Tests | Water contents: 2%, 4%, 6%, 8%, 10%, 12% and 14%.<br>Compaction degrees: 10, 25, 40 and 60 blows. | 168         | Realized with the cone Penetrometer.                 |
| Ultrasonic Tests  | Water contents: 2%, 4%, 6% and 8%.<br>Compaction degrees: 10, 25, 40 and 60 blows.                | 96          | Led to the Ultrasonic Analyzer.                      |

### 5 Tests results and interpretation

#### 5.1 Oedometric tests

##### 5.1.1 Depiction of the collapse of the soil

The variation of the moisture contents and energies of compaction are made in the purpose to check whether these soils have the properties of collapsible soils. The variation of moisture content and energies of compaction allow controlling the collapse potential. Curves obtained are similar to that of Knight (1975), as shown in Figures 1. The collapse potential CP (%) is calculated by the relation:

$$CP = \frac{\Delta e_c}{1 + e_0} \times 100\% \quad (1)$$

$$\Delta e_c = e_1 (200 \text{ kPa}) - e_2 (200 \text{ kPa, flooded}); \quad e_0 : \text{Initial void ratio.}$$

The results of these tests show that the collapse potential CP varies for;

Soil S1: from 0.52 % to 7.54 %; Soil S2: from 0.59 % to 8.34 %

Soil S3: from 0.83 % to 8.92 %; Soil S4: from 0.66 % to 7.61 %

Soil S5: from 0.74 % to 7.84 %; Soil S6: from 0.77 % to 7.90 %.

According to the classification suggested by Jennings, and Knight (1975),

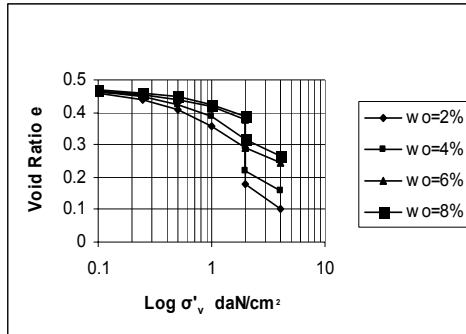


Figure.1. Oedometric Curve Soil 1 (E = 10 Blows)

### 5.1.2 Influence of the water content and the energy of compaction

The high collapse potentials are noted for low initial moisture contents. For a given initial water contents the collapse potential is decreasing with the increase in the energy of compaction (Fig. 2). The decrease of collapse is more obvious that the moisture content increases (Fig. 3). In the same conditions of compactness and moisture content of the soil containing the greatest percentage of kaolin exhibit greatest collapse potential. These results agree with those of Ayadat et al (1999), and confirm the observations of Abbeche (2005). One can conclude that the reconstructed soils at the laboratory hold a similar behavior to those met in situ, therefore suitable for the series of tests suggested.

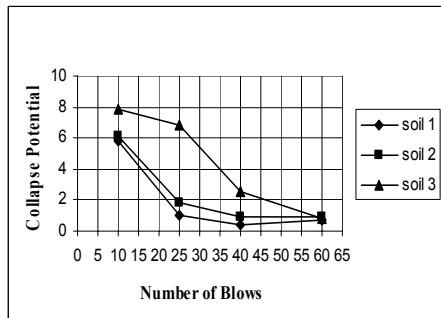


Figure.2. Collapse Potential versus number of blows ( $w_0 = 6 \%$ )

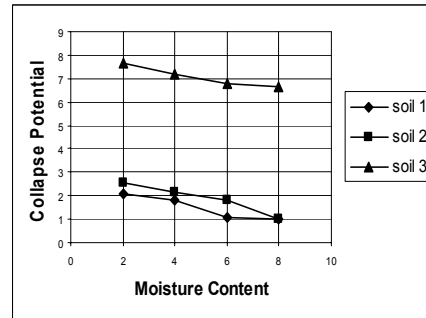
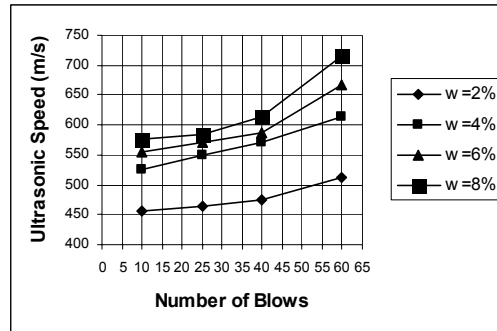


Figure.3. Collapse Potential versus moisture content (E = 25 Blows)

## 5.2 Ultrasonic tests

### 5.2.1 Influence of the moisture content and the energy of compaction

The results of the ultrasonic tests show that ultrasonic speed varies according to variation of the energy of compaction and/or moisture content the (Figures 4). For the same value of the energy of compaction, whatever the soil, the ultrasonic speed is increasing with the growth of the moisture content;



**Figure.4.** Variation of Ultrasonic Speed with number of blows (Soil 4)

The growth of compaction contributes to the increase of speeds, especially when the moisture content comes close to the Proctor optimum. Let us note that curves corresponding to 60 blows present more important speed values compared to other energies of compaction, especially with the increase in the moisture contents. This proves a good state of compactness due to the humidification and the rearrangement of the grains; it is the case of non collapsible soils.

### 5.2.2 Prediction of collapse by ultrasonic test

The figure 5 concretize a vital relationship between ultrasonic speed and potential collapse; the decrease of one is synchronized with the increase of other. In Figure 11, curves have the same shape. They pass by three phases, in the beginning parallel straight lines representing an important fall of the CP with very close speed values. Then, two successive slopes of the curves are noted; in the first, a reduction of the CP corresponds to an increase speeds, in the second, the stabilization of collapse is explained by great values speeds and very close collapse potentials.

From these observations, values of ultrasonic speeds are compared against various water content and energy of compaction. Since the questioned soils have the possibility of collapsing when they are in a loose state; one propose prediction method of collapsible soils based on ultrasonic tests (non destroyed), fast and easy to realize.

Values of ultrasonic speed are limited as follows:

$$V \leq 400 \text{ m/s} \rightarrow \text{Collapse appears;}$$

$$400 \text{ m/s} < V < 1000 \text{ m/s} \rightarrow \text{Collapse can occur.}$$

$$V > 1000 \text{ m/s} \rightarrow \text{Risk of Collapse is isolated.}$$

In the second case the susceptibility of collapse depends on the water content and the state on compactness on the soil. This procedure can be applied to the restructured or intact soil, at the laboratory and even on site. Considering its advantages, the results of the ultrasonic sounding can be generalized with the various types of collapsible soils such as the loesses and other unsaturated soils.

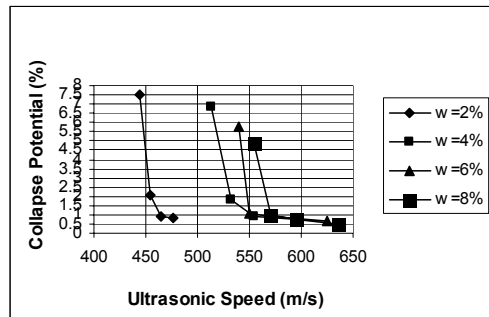


Figure 5. Variation of Collapse Potential with Ultrasonic Speed for w% (Soil 1)

## 6 Conclusions

The principal conclusions which one can draw from this study summarize as follows:

Collapsible soils can be reconstructed in the laboratory by mixing with various proportions the kaolin, such fine particles with sand, led to water contents lower than the optimum of Proctor and than compacted to moderate energies of compaction.

The results obtained clearly show the influence of certain parameters such as; kaolin content, water content and energy of compaction on the collapse potential and the ultrasonic speed. The collapse potential can be excessive if the initial water content is low. For water content lower than the optimum of Proctor, there is energy of compaction beyond which collapse does not occur.

Proposal of a new experimental approach of prediction of collapsible soils based on ultrasonic tests, easy and fast. The results obtained depend on grains size distribution, state of compactness of the soil and water content. The ultrasonic test can be carried out in the laboratory or in situ, on intact or altered samples of an unspecified form. The ultrasonic speed of metastable soils gives an idea of the state of compactness; it is inverse proportion with the potential of depression.

## References

- Abbeche, K., Mokrani, L. and Boumekik, A.: (2005), Contribution à l'identification des sols effondrables, *Revue Française de Géotechnique*. 110, 85–90.
- Abelev, M.Y.: (1988), Loess and its Engineering Problems in the USSR, *Proc. of the Int conf. Engineering Problems of Regional Soils. Beijing, China*.
- Ayadat, T. and Bellili, F.: 1995, Sols susceptibles d'affaissement: Identification mécanique et traitement. *Revue Algérie Equipment*, no20, p p.18-23.
- Ayadat, T. and Ouali. S.: (1999), Identification des sols affaissables basée sur les limites d'Atterberg. *Note Technique. Revue française de géotechnique*.
- Ganeshan, V.:(1982), Strength and Collapse Characteristics of Compacted Residual Soils. *Thesis (M.E), Asian Institute of Technology Bangkok Thailand*.
- Jennings, J. E. and Knight, K.: (1975), The Additional Settlement of Foundation due to Collapse of Sandy Soils on Wetting. In: *Proceeding. 4th International Conference on Soil Mechanics and Foundation Engineering*, 316-319.
- Knight, K. and Jennings, J. E. :( 1975), A guide to construction on or with materials exhibiting additional settlement due to collapse of grain-structure. *Proc. 6th Regional Conf. For Africa on SMFE, pp99-105. Durban, South Africa*.

## Genetic algorithm search for critical slip surface in slope stability analysis

Mendjel Djenatte<sup>1</sup>, Messast Salah<sup>2</sup>

<sup>1</sup> Department of Civil Engineering, LMGHU Laboratory, Faculty of Engineering Sciences, University of Skikda, Algeria.  
[rech\\_mendjel@yahoo.fr](mailto:rech_mendjel@yahoo.fr)

<sup>2</sup> Department of Civil Engineering, LMGHU Laboratory, Faculty of Engineering Sciences, University of Skikda, Algeria.  
[smessast@yahoo.fr](mailto:smessast@yahoo.fr)

---

**Abstract:** the slope stability analysis is usually done using the methods of calculation to rupture. The problem lies in determining the critical failure surface and the corresponding factor of safety (FOS). To evaluate the slope stability by a method of limit equilibrium, there are linear and nonlinear methods. The linear methods are direct methods of calculation of FOS but nonlinear methods require an iterative process. The nonlinear simplified Bishop method is popular because it can quickly calculate FOS for different slopes.

This paper concerns the use of inverse analysis by genetic algorithm (GA) to find out the factor of safety for the slopes using the Bishop simplified method. The analysis is formulated to solve the nonlinear equilibrium equation and find the critical failure surface and the corresponding safety factor. The results obtained by this approach compared with those available in literature illustrate the effectiveness of this inverse method.

**Keywords:** Stability, inverse analysis, genetic algorithm, safety factor.

---

### 1 Introduction

There are many different ways to compute the factor of safety of natural slopes including limit equilibrium, finite element and finite difference methods. In recent years the finite element method has been used for slope stability analysis, but limit equilibrium methods are still common practice.

Many methods have been presented to compute the factor of safety (FOS) using limit equilibrium methods for a homogenous soil layer slopes.

To avoid the difficulty in finding out the global minima, evolutionary methods such as genetic algorithm (GA) is being used, which is more robust in finding out the optimal solution in many complex problems. Gho (1999) has used GA to find out the critical surface and the factor of safety using method of wedges, Sarat Kumar Das (2005) has used real coded GA to find out the critical failure surface and the corresponding factor of

safety for three wedge method, Zolfaghari *et al.* (2005) have used a simple genetic algorithm search for homogenous soil layer, and heterogeneous multi soil layers slope, Mendjel *et al.* (2009) used GA to find out critical circular failure surface at the foot of the homogenous slope, and the corresponding factor of safety using Bishop’s method. McCombie and Wilkinson (2002) developed a simple genetic algorithm to search the minimum factor of safety of a circular failure surface in slope stability analysis. They presented a three variable parameters coding, containing the  $x$  and  $y$  coordinates of the centre of a circle and the *radius* of a circular failure surface. They also showed that replacing the radius with a tangent level or with the coordinates of a point the circle had to pass through (thus creating a four dimensional search space), would usually work better, as the formulation of the problem becomes closer to what determines the fitness of each variable parameters.

The genetic algorithm used in this study is to solve the Bishop method to find the minimum factor of safety and the corresponding critical failure surface in finite slopes.

In this GA the use of three dimensional search space (the  $x$  and  $y$  coordinates of the centre of a circle and the horizontal coordinate of an end or start point of the circle which pass through the slope) could work better, as the formulation of the problem becomes very closer to what determines the fitness of each variable parameters. Because we eliminate the failure surface does not hit the geometry of the natural slope, so that the search space is reduced.

The analysis of the problem can be considered in two stages:

- Presentation of objective function;
- The application of GA in solving the objective function.

## 2 Presentation of objective function

The slope stability analysis method used in this study to develop the objective function is the Bishop method.

The simplified Bishop method also uses the method of slices to discrete the soil mass for determining the FOS. This method satisfies vertical force equilibrium for each slice and overall moment equilibrium about the centre of the *circular* trial surface. In this method it is assumed that only shear forces acting on the sides of each slice are equal. Hence,  $X_1 = X_2$  but the  $E_1 \neq E_2$  (figure 1a, 1b).

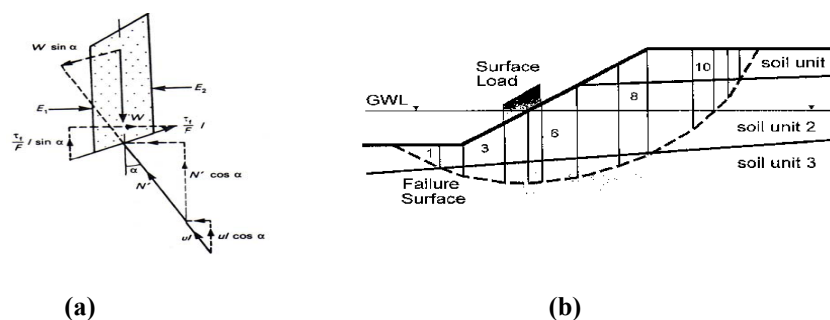


Figure.1. (a) Bishop’s simplified slice (R. Whitlow, 1995) and (b) Division of potential sliding mass into slices.

From (Huang, 1983), R. Whitlow (1995) formulated the equation for Fellenius method as follow:

The equilibrium along the base of the slice:

$$0 = W \sin \alpha - \frac{\tau_f}{F} l = W \sin \alpha - \frac{c' L + N' \tan \phi}{F}$$

The equilibrium in a vertical direction

$$0 = W - N' \cos \alpha - ul \cos \alpha - \frac{c'}{F} l \sin \alpha - \frac{N' \tan \phi'}{F} \sin \alpha \quad (1)$$

After substituting for,

$$l = b \sec \alpha \quad \text{and} \quad N' \text{ from the equation (1)}$$

So that

$$F = \frac{1}{\sum W \sin \alpha} \sum \frac{[c' b + (W - ub) \tan \phi'] \sec \alpha}{1 + \frac{\tan \alpha \tan \phi'}{F}} \quad (2)$$

“The procedure is commenced by assuming a trial value for the F on the right-hand side and then, using an iterative process, to converge on the true value of F for a given trial circle. This is the routine procedure commonly used in programs designed for use on computers.” (R. Whitlow 1995)

In this study an optimisation method was developed to found out the F minimum which satisfies equation (2).

### 3 Genetic algorithm optimization

The GA is a random search algorithm based on the concept of natural selection inherent in natural genetics, presents a robust method for search of the optimum solution to the complex problems. The algorithms are mathematically simple yet powerful in their search for improvement after each generation (Goldberg, 1989). The artificial survival of better solution in GA search technique is achieved with genetic operators: selection, crossover and mutation, borrowed from natural genetics. The major difference between GA and the other classical optimization search techniques is that the GA works with a population of possible solutions; whereas the classical optimization techniques work with a single solution. Another difference is that the GA uses probabilistic transition rules instead of deterministic rules.

In the present analysis a binary-coded GA has been used, in which the GA consists of three basic operators, selection, crossover or mating, and mutation, which are discussed as follow. The first step when applying genetic algorithms is to choose an initial population consisting of members called chromosomes. The candidates of the input space are then coded using binary coding. These are called chromosomes and form an initial population. The basic procedure then becomes: choose an initial population, select the best candidates for next generation, do crossover operation, and mutate.

In the selection procedure, the chromosomes compete for survival in an elitist selection, the size of initial population is selected double that the population of the next generation, thus permitted to have a best initial exploration of the search space and have a considerable effect on the convergence rate. The effects of the size and grid of search

space on the convergence are studied by Levasseur (2007). A fitness value associated with each chromosome is calculated. The population is then sorted in ascending order according to the fitness value, the best individuals are copied to the next generation, and then 1/3 of the population called parent population is selected for the reproduction process. A crossover process with a probability of 2/3 is applied to two selected parent chromosomes. A random position along the length of the chromosome is selected and the values of each binary string are exchanged or crossed by swapping all characters after this position. The two new chromosomes created are known as children of those parents. Mutation is applied to a small proportion of chromosomes, thus introducing the possibility of significant shifts away from the solutions currently being converged on, that overcomes problems associated with local maxima or minima in analyses. Each binary value in a chromosome selected for mutation is swapped with a probability of 0,9. The fitness values of the new population, which include both children and parent chromosomes, are then calculated. The process of reproduction, crossover, mutation and evaluation is repeated as a cycle of generation. A number of cycles are performed until an optimal solution is determined. The program of this genetic algorithm is written in Matlab following the flow chart represented by figure 2.

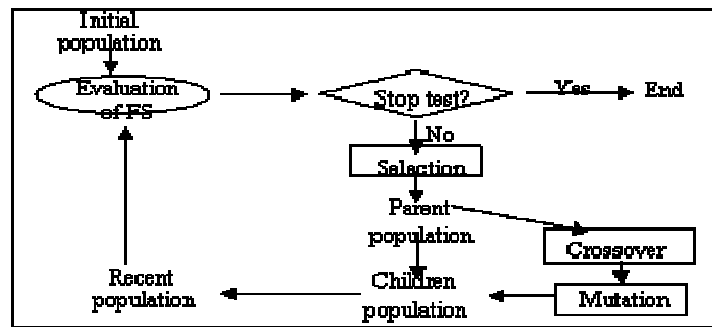


Figure. 2. Principle of optimization with a genetic algorithm (Levasseur, 2007)

### 4 Results and discussion

Two natural slopes as analysed in (Zolfaghari and al., 2005) were considered for the present study. The two dry slopes with its geometry and soil parameters are shown in table1.

Table.1. slopes geometry and parameters

|           | H1<br>m | $\beta 1(^{\circ})$ | C1<br>kN/m | $\phi 1$<br>( $^{\circ}$ ) | H2<br>m | $\beta 2(^{\circ})$ | C2<br>kN/m | $\phi 2$<br>( $^{\circ}$ ) | H3<br>m | $\beta 3(^{\circ})$ | C3<br>kN/m | $\phi 3$<br>( $^{\circ}$ ) | H4<br>m |
|-----------|---------|---------------------|------------|----------------------------|---------|---------------------|------------|----------------------------|---------|---------------------|------------|----------------------------|---------|
| Example 1 | 8,5     | 26,565              | 15         | 20                         | /       | /                   | /          | /                          | /       | /                   | /          | /                          | /       |
| Example 2 | 8,5     | 26,565              | 15         | 20                         | 0,5     | 3,18                | 17         | 21                         | 4,4     | 12,17               | 5          | 10                         | 4,7     |

| $\beta 4(^{\circ})$ | C4 (kN/m) | $\phi 4 (^{\circ})$ | $\gamma 1= \gamma 2= \gamma 3= \gamma 4$ (kN/m) |
|---------------------|-----------|---------------------|---|
| /                   | /         | /                   | 19  |
| 12,06               | 35        | 28                  | 19  |

The first example of a natural slope with a homogenous soil layer is analysed. The factor of safety is calculated for the slope using the genetic algorithm method proposed in this paper. Figure 3 shows how the fitness value (F) is changed and converged to a minimum FOS ( $F=1.741$ ), figure 4 shows the critical circular failure surface.

The result of the present study compared to results calculates in (Zolfaghari and al., 2005) (for: Bishop's method for circular failure,  $F=1.74$ , Morgenstern-Price method for circular failure,  $F=1.76$ , and Morgenstern-Price method for non circular failure,  $F=1.75$ ), shows that the FOS is similar for different methods and failure surfaces. What confirm that all these methods, if used respecting the basic hypothesis, gives satisfactory results.

For the second example of a natural slope with a heterogeneous soil layers, figure 5 shows how the fitness value (F) is changed and converged to a minimum FOS, figure 6 shows the critical circular failure surface.

The FOS calculate in the present study is  $F=1.454$ . The result of the present study compared to those calculates in (Zolfaghari and al., 2005) (for: Bishop's method for circular failure,  $F=1.475$ , for Morgenstern-Price method for circular failure,  $F=1.5$ , and for Morgenstern-Price method for non circular failure,  $F=1.24$ ), shows that the FOS is similar for circular failure for different methods. The small difference between the result in the present study and in the literature is resulted of principle of GA that works with a population of possible solutions not a single solution. The result of this study  $F=1.454$  is few lower than the Bishop's method in the literature on account of the effect of GA parameters (size and grid of search space) which are optimised in this study by limited the search space in three dimensional parameters. The FOS of this study is over than that for non circular failure in the literature.

## 5 Conclusions

In this paper, application of genetic algorithm in analyzing soil slopes using Bishop's simplified method was discussed. The results obtained by this approach compared with those available in literature illustrate the efficacy of this inverse method. The optimization of the GA parameters by eliminate the failure surface does not hit the geometry of the natural slope is reduced search space, so that the factor of safety is improved.

Also a simple circular failure surface is sufficient for a slope in a homogenous soil layer, while for a heterogeneous multi soil layers slope such as in example 2, a simple circular failure surface gives a FOS greater than that in the literature for the non circular failure.

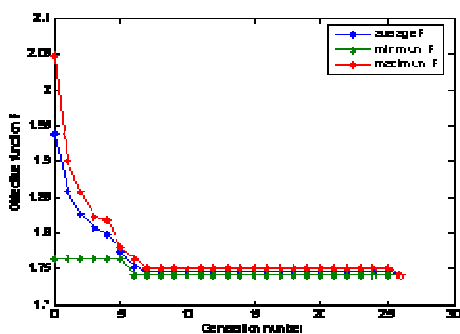


Figure.3. Variation of the objective function with generation number for example 1.

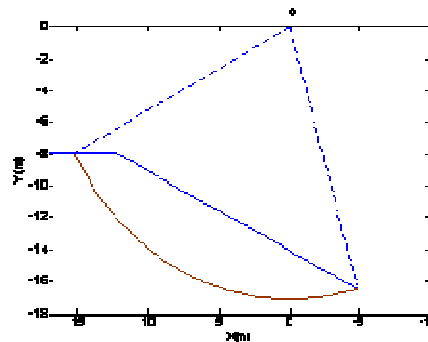


Figure.4. Critical circular failure surface for example 1.

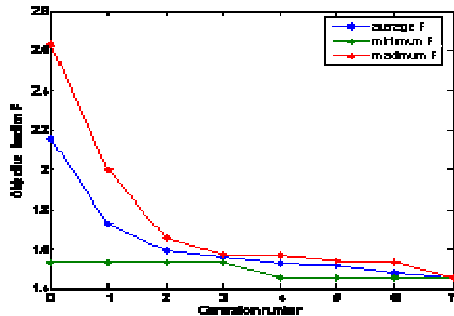


Figure.5. Variation of the objective function with generation number for example 2.

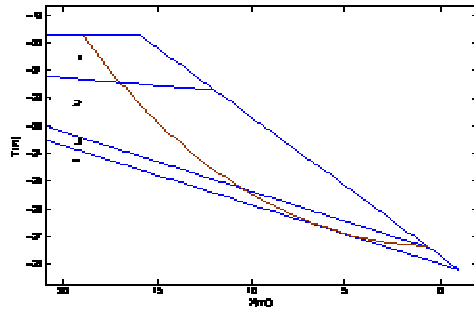


Figure.6. Critical circular failure surface for example 2.

## References

- Goh, A.T.C. M. (1999). Genetic algorithm search for critical slip surface in multiple-wedge stability analysis. *Canadian Geotechnical Journal*, Vol.36, pp. 382-391.
- Goldberg, D.E. (1989). Genetic algorithm in search, optimization, and machine learning. *Addison – Wesley*, Massachusetts, USA.
- Huang, Y.H. (1983). Stability analysis of slopes. *Van Nostrand Reinhold Company*, USA.
- Levasseur, S. (2007). Analyse inverse en géotechnique : développement d’une méthode à base d’algorithmes génétiques. *Thèse de Doctorat*, Université Joseph Fourier – Grenoble I.
- McCombie, P. and Wilkinson, P. (2002). The use of the simple genetic algorithm in finding the critical factor of safety in slope stability analysis. *Computer and Geotechnics*, Vol.29, pp. 699-714.
- Mendjel D., Hamami M. and Messast S. (2009). Identification de surfaces de rupture d’un talus par algorithme génétique 1<sup>er</sup> *Symposium méditerranéen de géotechnique (SMGE’09)*, Alger, pp. 467-471.
- Sarat Kumar Das. (2005). *Slope stability analysis using genetic algorithm*. Research Scholar, Department of Civil Engineering, Indian Institute of Technology Kanpur, India.
- Zolfaghari, AR., Andrew C.H and McCombie P.F. (2005). Simple genetic algorithm search for critical non circular failure surface in slope stability analysis. *Computer and Geotechnics*, Vol.32,pp. 139-152.

## Falling-weight impact test for 2/5 scale model of rockfall protection gallery with/without sand cushion

Hisashi Kon-no<sup>1</sup>, Satoru Yamaguchi<sup>1</sup>, Hiroaki Nishi<sup>1</sup>, Norimitsu Kishi<sup>2</sup> and Yusuke Kurihashi<sup>2</sup>

<sup>1</sup> SRT, CERi for Cold Region, PWRI, Sapporo, Japan  
[konno@ceri.go.jp](mailto:konno@ceri.go.jp), [yamaguchi-s22aa@ceri.go.jp](mailto:yamaguchi-s22aa@ceri.go.jp), [h-nishi@ceri.go.jp](mailto:h-nishi@ceri.go.jp)

<sup>2</sup> CERU, College of Environmental Engineering, Muroran IT, Muroran, Japan  
[kishi@news3.ce.muroran-it.ac.jp](mailto:kishi@news3.ce.muroran-it.ac.jp), [kuri@news3.ce.muroran-it.ac.jp](mailto:kuri@news3.ce.muroran-it.ac.jp)

---

**Abstract.** In this study, in order to investigate impact resistant behavior of rockfall protection galleries, two 2/5 scale gallery models were made, and consecutive falling-weight impact tests with/without sand cushion were conducted up to the ultimate state. From these experiments, the following results were obtained: 1) in case without sand cushion, roof slab is finally collapsed in punching shear failure mode; 2) in case with sand cushion, impact force can be estimated using a design formula with Lamé's constant  $\lambda = 1,000 \text{ kN/m}^2$  which is derived on the basis of Hertz's contact theory; 3) the roof slab with sand cushion has not reached the serviceability limit state until input energy  $E_k = 500 \text{ kJ}$  and is under near the ultimate limit state with punching shear failure at  $E_k = 1,000 \text{ kJ}$ .

**Keywords:** Falling-weight impact test, rockfall protection gallery, sand cushion.

---

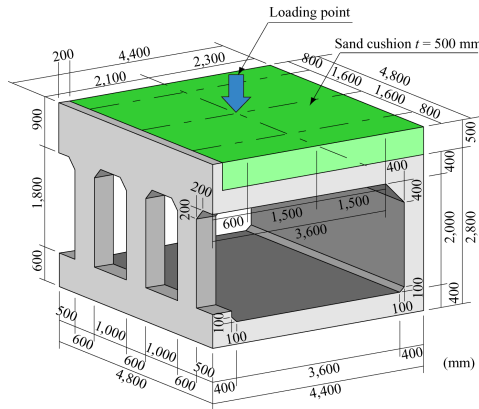
### 1 Introduction

In Japan, many rockfall protection structures have been constructed in the mountainous and coastal area to protect people's lives and vehicles from falling rocks. Those structures are designed on the basis of the allowable stress design concept. However, the trend of the design concept in the world tends to shift from allowable stress design method through limit state design method to performance-based design method. To establish performance-based impact resistant design procedure for reinforced concrete (RC) rockfall protection structures, it is important to accumulate basic knowledge on the impact response behaviors.

From this point of view, in this study, in order to investigate impact resistant behavior of rockfall protection galleries, two 2/5 scale gallery models were made, and consecutive falling-weight impact tests with/without sand cushion were conducted up to the ultimate state. Two kinds of heavy weight masses (10 ton and 2 ton ) were used for the test with/without sand cushion, respectively.

**Table 1.** List of experimental cases

| Experimental cases | Cushion layer | Mass of falling weight $M$ (ton) | Falling height $H$ (m) | Input energy $E_k$ (kJ) |
|--------------------|---------------|----------------------------------|------------------------|-------------------------|
| N-H0.25            | None          | 2                                | 0.25                   | 5                       |
| N-H0.50            |               |                                  | 0.50                   | 10                      |
| N-H0.75            |               |                                  | 0.75                   | 15                      |
| N-H1.00            |               |                                  | 1.00                   | 20                      |
| N-H1.25            |               |                                  | 1.25                   | 25                      |
| S-H1.00            | Sand          | 10                               | 1.00                   | 100                     |
| S-H5.00            |               |                                  | 5.00                   | 500                     |
| S-H10.00           |               |                                  | 10.00                  | 1,000                   |

**Figure.1.** Dimensions of gallery models**Photo.1.** Experimental setup

## 2 Outline of experiment

### 2.1 Rockfall protection gallery model

Figure 1 shows the dimensions of the gallery models used in this experiment. These models are 2/5 scale models of RC rockfall protection galleries constructed in Japan generally, in which the length and width of the block are 4,800 and 4,400 mm, respectively, thickness of roof, base, and wall is 400 mm, dimensions of cross section of column are 600 x 400 mm. Haunch is prepared at each inner side corner as well as real gallery. Thickness of sand cushion layer is 500 mm. At commencement, compressive strength of concrete was 29.7 MPa, and yield strength of steel rebar was 413 MPa.

### 2.2 Experimental procedure

Table 1 shows a list of experimental cases. Nominal name of case is designated by combining with/without cushion layer (N: none, S: sand) and falling height of impacting weight. Photo1 shows experimental setup. In this experiment, two scale models were prepared for conducting the tests with/without sand cushion. Each model was subjected to consecutive impact load at the center of the roof slab until reaching ultimate state. 10 and

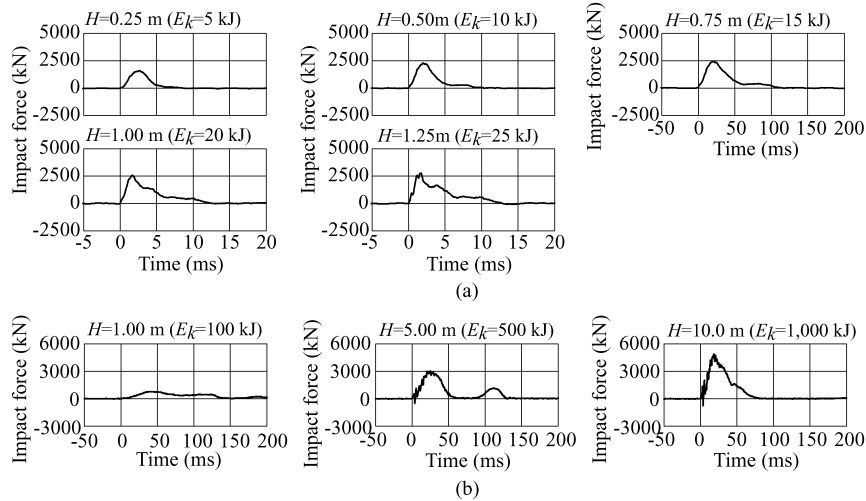


**Figure 2.** Time histories of impact force for the cases of the test: (a) without; and (b) with sand cushion

2 ton heavy weights are used for the test with/without sand cushion, respectively, and those are cylindrical (diameter: 1.25 and 1 m, respectively) and spherical bottom. In this experiment, the weight impact force and displacement at loading point (hereinafter, displacement) were measured and recorded at intervals of 0.1 ms using digital memory recorders. After impact loading at each experimental step, crack patterns developed in the model were sketched.

### 3 Experimental results

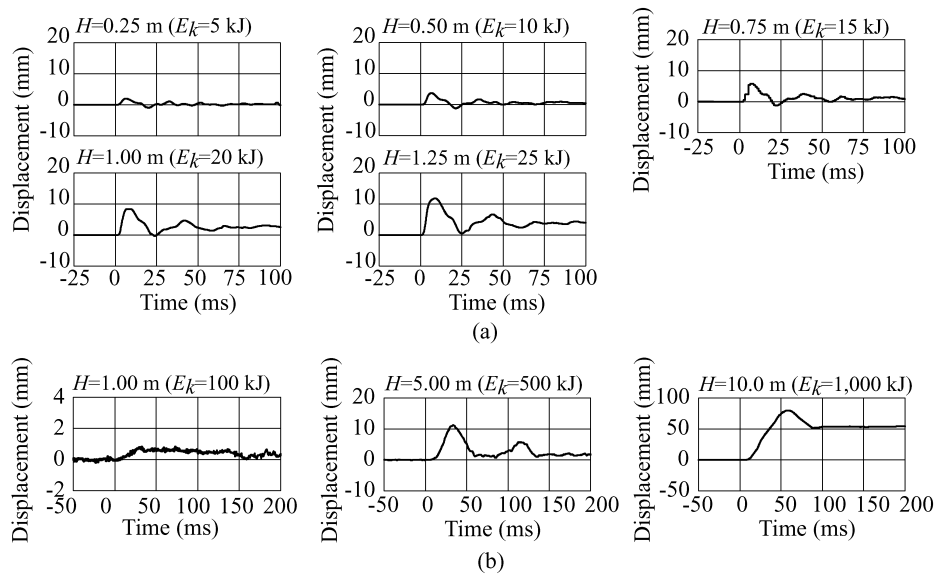
#### 3.1 Impact force

Figure 2 shows the time histories of impact force for the cases of the test with/without sand cushion. In case without sand cushion, the configuration of the time history at falling height  $H = 0.25$  m forms only a half sine curve. In the cases of higher falling height than  $H = 0.50$  m, the configurations are composed by joining a triangle with 5 ~ 7 ms duration time and a trapezoid with low amplitude and long duration time. These duration times increased with increasing falling height. This means that the roof slab may be gradually damaged due to consecutive impact loading.

In case with sand cushion, the configurations of the time histories of impact force at falling height  $H = 1.0$  and 5.0 m are composed of two half sine curves. On the other hand, in the case of  $H = 10.0$  m, the configuration forms only one triangle. This implies that a punching shear cone was formed and the roof slab has reached its ultimate state.

#### 3.2 Displacement

Figure 3 shows the time histories of displacements for the cases with/without sand cushion. In the case without sand cushion, it is observed that the slab is under the damped free vibration. Maximum amplitude and duration under the loading state tend to be gradually increased with an increment in falling height  $H$ . Displacement cannot be



**Figure 3.** Time histories of displacement for the cases of the test: (a) without; and (b) with sand cushion

restored at  $H = 0.75$  m and the residual displacement has been increased after this loading step.

In the case with sand cushion, it is observed that: (1) the roof slab behaves almost elastically at the falling height of  $H = 1.0$  m and the maximum displacement is less than 1.0 mm; (2) after that, the maximum displacement reached about 10 mm but the slab has still behaved elastically at  $H = 5.0$  m; but (3) at  $H = 10.0$  m, the maximum displacement is drastically increased and the displacement cannot be restored without any vibration. It means that the roof slab has been collapsed in the punching shear failure mode.

### 3.3 Relationships between various response value and input energy

Figure 4 shows relationships of each maximum impact force, maximum displacement, and residual displacement with input energy, respectively, in the cases with/without sand cushion. In the case without sand cushion, maximum impact force increased with increasing input energy  $E_k$ . However, the increment decreased in the region of larger input energy than  $E_k = 10$  kJ. This implies that punching shear cone tends to be formed around the loading point of the roof slab. It can be confirmed by observing crack patterns on the bottom surface of roof slab mentioned later. Maximum and residual displacements increased with an increment in input energy  $E_k$  linearly and parabolically, respectively.

In the case with sand cushion, maximum impact force increased with an increment of input energy  $E_k$ . The solid line in the figure is obtained using a design formula for rockfall protection structures based on Hertz's contact theory as follows:

$$P = 2.108 (m g)^{2/3} \lambda^{2/5} H^{3/5} \alpha \quad (1)$$

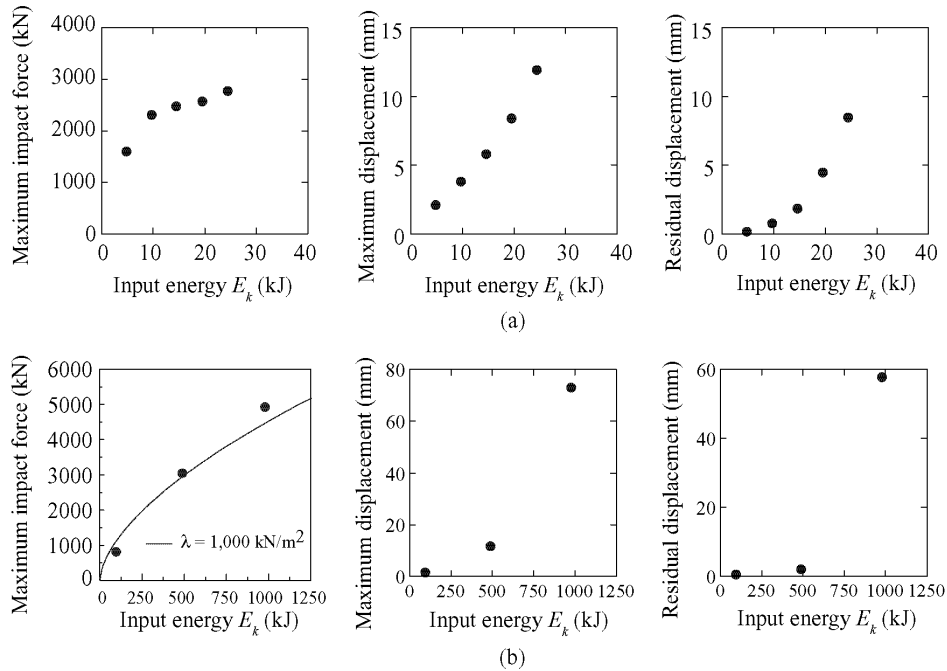


**Figure 4.** Relationships between various response values and input energy for the cases of the test: (a) without; and (b) with sand cushion

where,  $P$ : impact force due to falling rock (kN),  $m$ : mass of falling rock (ton),  $g$ : gravity acceleration ( $\text{m/s}^2$ ),  $\lambda$ : Lamé's constant ( $\text{kN/m}^2$ ),  $H$ : falling height of a rock (m),  $\alpha$ : amplification factor of impact force determined by the ratio between thickness of sand cushion and diameter of falling rock.

From figure 4(b), it is seen that the distribution of impact force can be evaluated using a design formula with Lamé's constant  $\lambda = 1,000 \text{ kN/m}^2$ . Maximum and residual displacements are increased with increasing of input energy  $E_k$ . Those increments in the region of input energy less than  $E_k = 500 \text{ kJ}$  are small but at  $E_k = 1,000 \text{ kJ}$ , both maximum and residual displacements get very large. The model must be collapsed at this stage.

### 3.4 Crack patterns

Figure 5 shows crack patterns developed on the bottom surface of roof slab. In case without sand cushion, cracks are gradually developed in the radial and circumferential directions with increasing of falling height  $H$ . Circumferential cracks may occur by development of punching shear cone and those can find at  $H = 0.75 \text{ m}$ . At  $H = 1.25 \text{ m}$ , the roof slab was completely collapsed in the punching shear failure mode.

In case with sand cushion, cracks are mainly developed in the span direction and diagonal cracks are slightly observed at falling height of  $H = 5.0 \text{ m}$ . At  $H = 10.0 \text{ m}$ , many cracks are developed not only in the span direction but also in lateral and circumferential directions around the loading point. Thus, the roof slab may have collapsed in the punching shear failure mode. At this loading step, the heavy weight penetrated into the

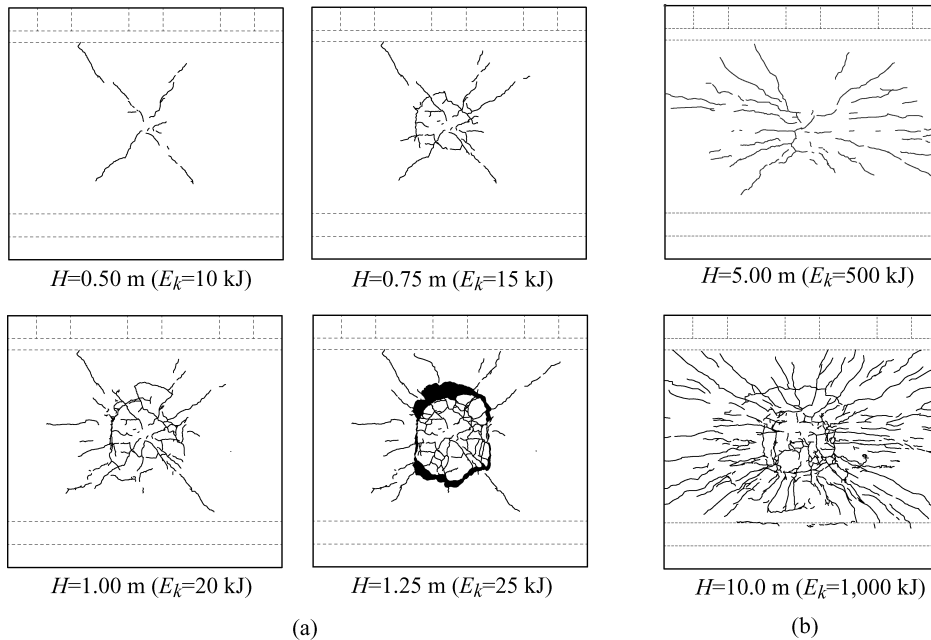


**Figure 5.** Crack patterns for the cases of the test: (a) without; and (b) with sand cushion

sand cushion up to 410 mm depth. This means that the heavy weight almost directly collided the roof slab.

From these results, it is seen that the roof slab has not reached serviceability limit state until falling height of  $H = 5.0$  m. On the other hand, at  $H = 10.0$  m, the roof slab has been under near the ultimate limit state because the slab may collapse in the punching shear failure mode.

#### 4 Conclusions

In this study, in order to investigate impact resistant behavior of rockfall protection galleries, two 2/5 scale gallery models were made, and consecutive falling-weight impact tests with/without sand cushion were conducted up to the ultimate state. From these experiments, the following results were obtained:

- 1) In the case without sand cushion, the roof slab collapsed in punching shear failure mode;
- 2) In the case with sand cushion, impact force can be estimated using a design formula with Lamé's constant  $\lambda = 1,000$  kN/m<sup>2</sup> which is derived on the basis of Hertz's contact theory;
- 3) The roof slab with sand cushion did not reach serviceability limit state until input energy  $E_k = 500$  kJ. At input energy  $E_k = 1,000$  kJ, the slab is under near the ultimate limit state with punching shear failure.

## Weight impact test for rockfall protection wall jointed to steel-pile foundation with H-section steel

Satoru Yamaguchi<sup>1</sup>, Hiroaki Nishi<sup>1</sup>, Hisashi Kon-no<sup>1</sup>, Norimitsu Kishi<sup>2</sup> and Yuji Ushiwatari<sup>3</sup>

<sup>1</sup> SRT, CERl for Cold Region, PWRI, Sapporo, Japan  
[yamaguchi-s22aa@ceri.go.jp](mailto:yamaguchi-s22aa@ceri.go.jp), [h-nishi@ceri.go.jp](mailto:h-nishi@ceri.go.jp), [konno@ceri.go.jp](mailto:konno@ceri.go.jp)

<sup>2</sup> CERU, College of Environmental Engineering, Muroran IT, Muroran, Japan  
[kishi@news3.ce.muroran-it.ac.jp](mailto:kishi@news3.ce.muroran-it.ac.jp)

<sup>3</sup> Koken Engineering, Co., Ltd, Sapporo, Japan  
[ushi@koken-e.co.jp](mailto:ushi@koken-e.co.jp)

---

**Abstract.** In this paper, a rockfall protection wall method is newly proposed in which the wall is jointed to steel-pile foundation with H-section steel embedded in the wall and requiring no excavation of the slope. The wall is attached to a two-layered absorbing system to decrease the impact force due to falling rocks. The absorbing system is composed of Expanded Poly-Styrol (EPS) block and reinforced concrete (RC) panel. The applicability of the system is confirmed by conducting full-scale impact test. From this experiment, the following results are obtained: 1) the absorbing system can effectively absorb the impact force; and 2) the protection wall without the absorbing system is severely damaged while subjected to impact input energy of  $E_k = 62.5$  kJ, but the wall with the system has no crack due to impact energy twice as much of above input energy.

**Keywords:** rockfall protection wall, pile foundation, two-layered absorbing system, impact test.

---

### 1 Introduction

In Japan, there are a number of rockfall protection walls installed along mountainous and coastal roads to protect human's lives and vehicles from falling rocks. Usually, the gravity-type rockfall protection wall made of plane concrete has been constructed. If the foundation cannot have much bearing capacity, the soil must be excavated up to the layer with a good bearing capacity and replaced with a better material. However, if the backyard of the wall has not much space apart from the slope, the slope failure may be brought because the toe of the slope must be excavated.

In this paper, in order to protect human's lives and transportation network from the falling rocks using protective walls without any excavation of the toe of the slope, a new rockfall protection wall system was proposed here as shown in figure 1. The wall is jointed to steel-pile foundation with embedded H-section steel in the concrete wall. Also, a two-layered absorbing system is attached to the wall to absorb the impact force due to falling

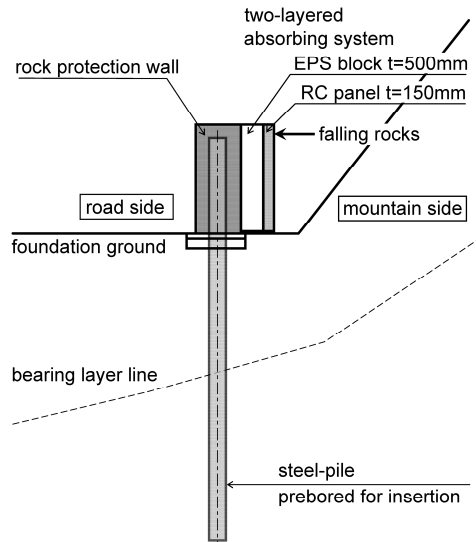


Figure 1. Rockfall protection wall

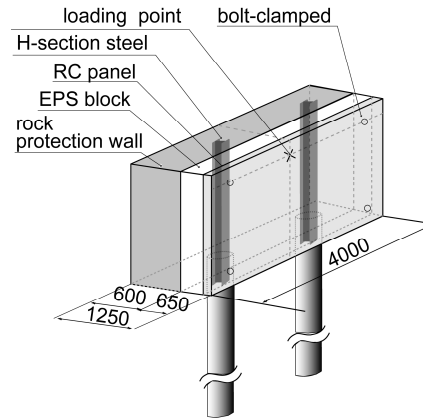


Figure 2. Dimensions/configurations of protection wall with steel-pile foundation

rocks which is composed of RC panel and EPS blocks. Here, the impact resistant capacity of the wall and absorbing performance of the system are discussed by conducting field impact tests.

## 2. Experimental overview

### 2.1 Test setup

Figure 2 shows the configuration and dimensions of the rockfall protection wall used in the field tests. The steel-piles are 400 mm in diameter and 9 mm in thickness. The piles are longer than embedded depth (8.7 m) for the self retaining pile. The foundation soil in the region from ground surface to 3.0 m depth was replaced with sand layer whose standard penetration test (SPT) blow count  $N$  is equal to 2 to follow the real site. The bottom layer of the foundation has SPT blow count  $N = 5$  in the region of 5.7 m depth. H-section steels of H-250 (250 x 250 x 9 x 14 mm) were embedded in the wall and also embedded into the steel piles with filled concrete up to 0.85 m depth from the top edge. Dimensions of the reinforced concrete (RC) wall are 2.0 m in height and 4.0 m in width. Steel reinforcement of diameter  $\phi = 22$  mm and 13 mm was casted at intervals of 250 mm horizontally and vertically, respectively. Thickness of the wall is 0.6 m considering concrete cover for reinforcement and the space between reinforcement and H-section steel. The two-layered absorbing system is composed of a RC panel 150 mm in thickness as the mountain-side front layer and with EPS blocks 500 mm in thickness as the back layer. The single reinforcement bar was casted in the panel and the reinforcement ratio was taken as 1.0 % in both horizontal and vertical directions.

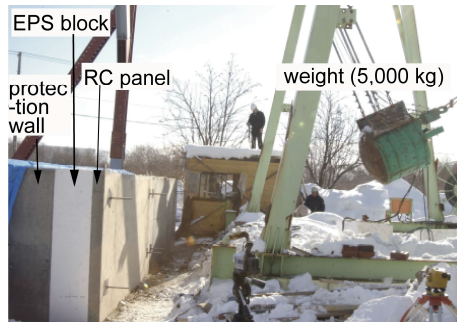


Photo.1. Experimental setup

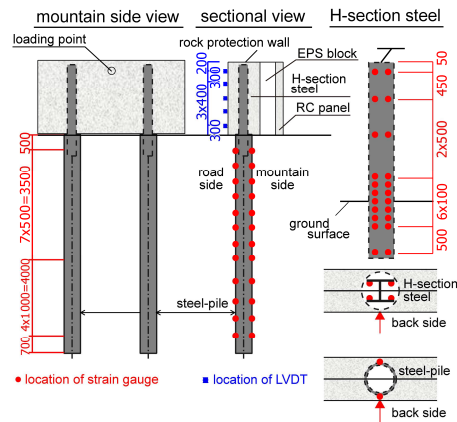


Figure.3. Measuring points

Table.1. List of test cases

| Experimental cases | Two-layered absorbing system | Impact velocity (m/s) | Input energy (kJ) |
|--------------------|------------------------------|-----------------------|-------------------|
| A-V3.5             | Available                    | 3.5                   | 30.6              |
| A-V5.0             |                              | 5.0                   | 62.5              |
| A-V7.0             |                              | 7.0                   | 122.5             |
| N-V5.0             | Unavailable                  | 5.0                   | 62.5              |

## 2.2 Test method

In this experiment, a 5,000 kg impacting weight was freely dropped from a prescribed height onto the mid-span and 1.8 m height from the bottom of the wall using a pendulum movement. The weight is made of steel outer-shell of  $\phi = 1$  m diameter and a spherical base with  $r = 80$  cm radius. It was filled with steel balls and concrete to give a total mass of  $M = 5,000$  kg. Photo 1 shows the experimental setup.

In this field test, the impact force time history  $P$ , the displacement time histories  $D_s$  of the wall and the strain time histories  $\varepsilon_s$  of steel-pile and H-section steel were measured. The impact force  $P$  is estimated by measuring the deceleration of the weight. Dynamic displacements of the wall were measured using Laser-type LVDTs. The strains of the steel-pile and H-section steel were measured by gluing strain gauges. Analog signals from these sensors were continuously converted into digital data and then continuously recorded using digital data recorders. Figure 1 shows the measuring points.

## 2.3 Test cases

The experimental cases conducted in this paper are listed in table 1. In this table, each case is designated using the two parameters with/without the absorbing system (A: with and N: without) and impact velocity, in which digit following the notation "V" represents the impact velocity of the impacting weight. The case with impact velocity  $V = 5$  m/s is the reference as it provides the design value of the impact energy ( $E_k = 62.5$  kJ).

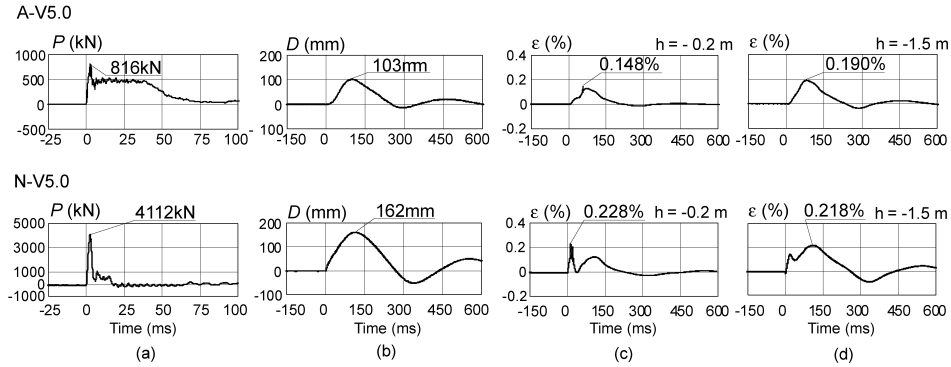


**Figure 4.** Time histories of (a) impact force; (b) displacement at loading point of wall; (c) strain of H-section steel; and (d) strain of steel-pile

The other cases:  $V = 3.5$  and  $7$  m/s, are for a half and twice impact energy of the design value, respectively.

Even though virgin RC panels and EPS blocks were used for each test, the same wall has been used for all cases. In fact no damage was found in the wall when the absorbing system was attached. For comparisons, the wall without absorbing system was tested for impact velocity  $V = 5$  m/s.

### 3. Experimental results

#### 3.1 Time histories of impact force, displacement, and strains of H-section steel and steel-pile

Figure 4 shows time histories of impact force, displacement at the loading point of the wall, and strains of H-section steel and steel-pile for cases of the test with/without absorbing system at impact velocity  $V = 5$  m/s. Each time history of the strain is at the location where the maximum response occurs along the height of H-section steel and steel-pile, respectively.

From figure 4(a), it is observed that: time history of impact force in the case without the absorbing system is jointed a high frequency and high amplitude of half sine shape and a trapezoid over a 15 ms duration. On the other hand, in the case with absorbing system, the configuration of the time history is composed of a high frequency and half sine shape and a trapezoid with over a 75 ms duration. The high frequency component may be initiated at the beginning of impact due to the heavy weight impacting to RC panel which is the mountain-side front layer of the absorbing system. The trapezoid shape may be formed when EPS blocks are deformed plastically. Comparing with the results of the case without absorbing system, the maximum impact force can be reduced to 1/5, and duration time can be prolonged 5 times. From these results, it is seen that absorbing system can rationally decrease the impact force occurred due to the heavy weight impacting the wall.

From figure 4(b), it is observed that the wall is under damped free vibration regardless of existence of absorbing system. Maximum displacement can be decreased up to about 60 % by setting the absorbing system.

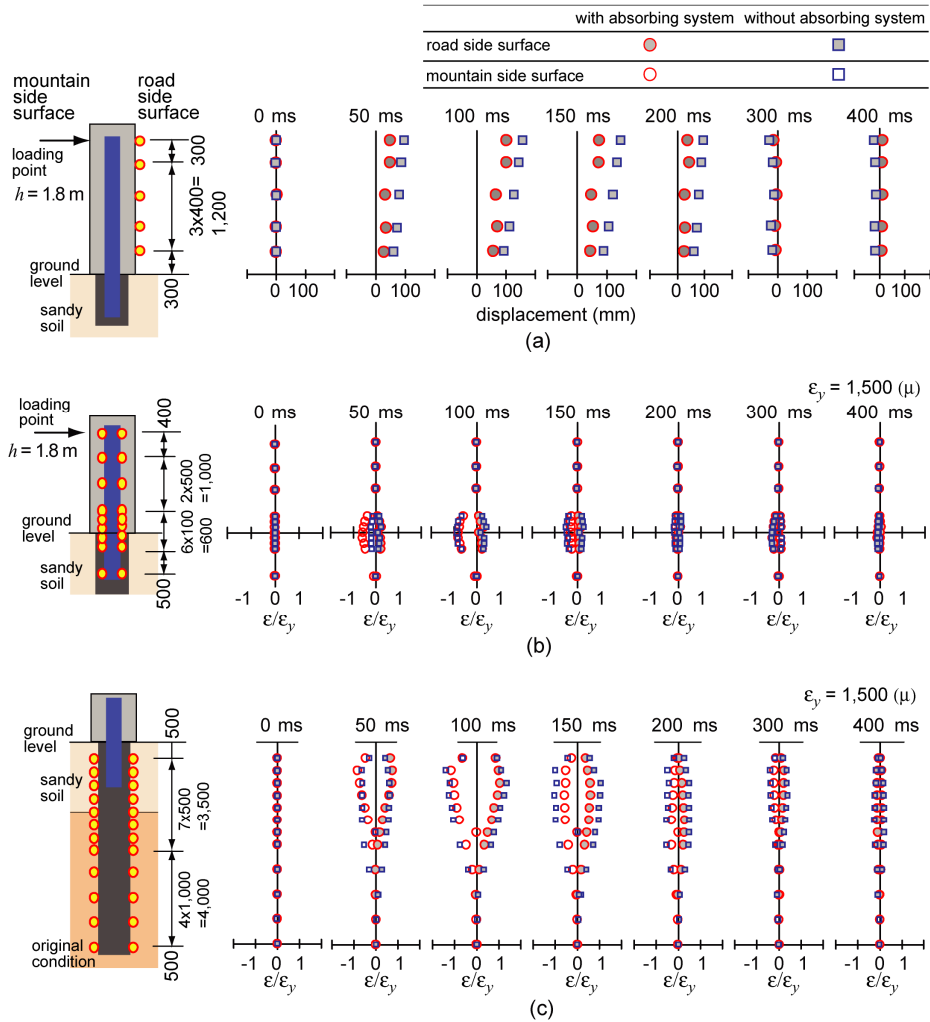


**Figure 5.** Comparison of response distribution both cases with/without absorbing system at each time step: (a) displacement distribution along height of wall; (b) axial strain distribution along height of H-section steel; and (c) axial strain distribution along height of steel-pile.

From figures 4(c) and (d), it is seen that the configurations of time history of strain for H-section steel and steel-pile in the case with absorbing system are composed of a triangle during loading and then damped sine curve at the unloading time. On the other hand, in the case without absorbing system, the configuration is chained a sharp triangle at the loading and then damped sine curve. Comparing maximum strains in cases with/without absorbing system, the value can be reduced by 50 % setting the system.

### 3.2 Displacement and strain distributions

Figure 5 shows the comparison of the response distributions between the cases with/without two-layered absorbing system at each time step which based on the

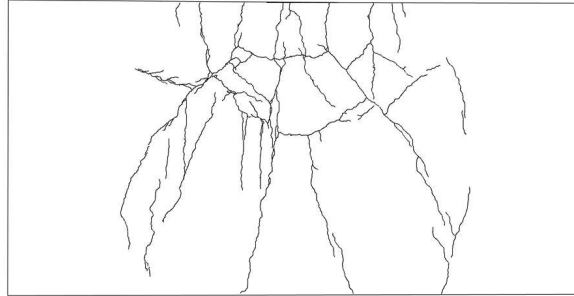


**Figure 6.** Crack distribution on road-side surface of the RC protection wall (N-V5.0)

displacement distribution along the height of wall, the axial strain along the height of H-section steel and the steel-pile. In this figure, strain distributions for H-section steel and steel-pile are plotted by refereeing to yield strain of steel  $\epsilon_y$ .

From this figure, it is observed that: (1) maximum displacement of the wall with the absorbing system is smaller than that the one without; (2) maximum strain of the H-section steel is developed near the ground level, where is the boundary point between H-section steel and steel-pile, in spite of with/without absorbing system (see figure 5b); (3) H-section steel is under the elastic region since the maximum strain is less than 1.0; and (4) maximum strain in the steel-pile is reached at a depth of about 1.5 m from the ground surface at 100 ms after impacting; and (5) the steel-pile in deeper region than 4 m from the ground surface becomes almost fixed boundary.

### 3.3 Crack pattern

Figure 6 shows crack pattern on the road-side surface of the wall without the absorbing system after experiment. From this figure, it is observed that punching shear type and flexural type cracks are developed in the circumferential and vertical directions, respectively. However, in case of the test with two-layered absorbing system, no crack was found on the surface of the wall. Therefore, it is confirmed that setting two-layered absorbing system, impact force can be rationally absorbed even though the impact energy is twice the design value.

## 4 Conclusions

In this study, in order to investigate the impact resistant behavior of rockfall protection wall jointed to steel-pile foundation with H-section steel embedded in the wall, full scale impact loading tests were conducted taking existence of the absorbing system and the impact velocity as variables. From this experiment, the following results were obtained:

- 1) The absorbing system proposed here can effectively decrease the impact force;
- 2) The protection wall without the absorbing system is severely damaged while subjected to impact input energy of  $E_k = 62.5$  kJ, but the wall with the system exhibits no crack after an impact with twice this energy.

## Numerical analysis method for prototype reinforced concrete girders under consecutive impact loading

Norimitsu Kishi<sup>1</sup>, Sara Ghadimi Krasraghy<sup>2</sup>, Hisashi Kon-No<sup>3</sup>

<sup>1</sup> CERU, College of Environmental Engineering, Muroran IT, Muroran, Japan  
[kishi@news3.ce.muroran-it.ac.jp](mailto:kishi@news3.ce.muroran-it.ac.jp)

<sup>2</sup> Institute of Structural Engineering, ETH Zurich, 8093 Zurich, Switzerland  
[ghadimi@ibk.baug.ethz.ch](mailto:ghadimi@ibk.baug.ethz.ch)

<sup>3</sup>SRT, CERI for Cold Region, PWRI, Sapporo, Japan  
[konno@ceri.go.jp](mailto:konno@ceri.go.jp)

---

**Abstract.** In order to establish a rational impact resistant design procedure for reinforced concrete structures based on the performance-based design concept, load-carrying capacity and dynamic response characteristics for each limit state must be precisely evaluated. Here, to accurately evaluate accumulated dynamic response characteristics of the prototype reinforced concrete girders under consecutive impact loading, an application of the equivalent tensile fracture energy concept to the concrete element with large size in the span direction is proposed. The applicability of the concept was discussed by conducting numerical simulations for a girder having 8 m span length taking element size and with/without considering the concept as variables.

**Keywords:** reinforced concrete girder, consecutive impact loading, tensile fracture energy, elasto-plastic analysis

---

### 1 Introduction

In order to establish a performance-based impact resistant design procedure for reinforced concrete members, it is important to establish the evaluation method for each limit state: mainly serviceability and ultimate limit states. In reality, the rockfall protection structures may be subjected to impact of more than a single rock and the damage will be accumulated due to the consecutive impact loading. This implies that the limit states should be evaluated for not only a single but also consecutive impact loading. However, impact tests are not easy to conduct because special techniques for measuring and processing dynamic signals including the high frequency components from the girders are required. It may be possible to establish a rational analysis procedure to project the results beyond the experiments by correlating with numerical simulations. At present, small size reinforced concrete girders/slabs under a single and consecutive impact loading can be accurately analyzed as illustrated by Kishi *et al.* (2009) and Ghadimi *et al.* (2009). Moreover, prototype reinforced concrete girders under a single impact loading can be

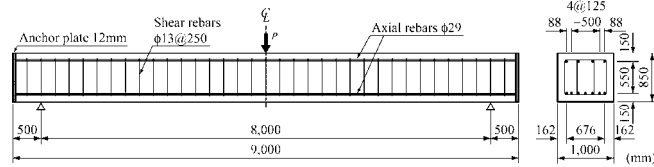


**Figure.1.** Dimensions of reinforced concrete girder and layout of reinforcement

analyzed with coarse mesh by applying an equivalent tensile fracture energy concept (hereinafter,  $G_f$  concept) for concrete element as proposed by Kishi and Bhatti (2010). In order to establish numerical analysis method for prototype reinforced concrete girders under consecutive impact loading, an applicability of the  $G_f$  concept for concrete element is investigated by conducting numerical simulations for the models taking the element size of concrete in the span direction and with/without considering  $G_f$  concept as variables. In this study, LS-DYNA code was used for numerical simulation.

## 2 Test setup

Falling weight experiment on a prototype reinforced concrete girder is used for the numerical simulations. The experimental setup is explained in details by Kishi and Bhatti (2010). Figure 1 shows the dimensions of the girder and layout of reinforcement. The material properties of concrete and reinforcement are given by a compressive strength of concrete  $f_c = 31.2$  MPa, and yield stresses of  $\sigma_y = 401$  MPa and 390 MPa for the bending reinforcement and the stirrups, respectively. Since the static shear-bending capacity ratio  $\alpha$  is greater than one ( $\alpha = 2.89$ ), the girder has collapsed in the flexural failure mode under the static loading.

A 2000 kg weight was freely dropped from a prescribed height onto the mid-span of the girder. The supports were able to rotate freely while their horizontal movement was restrained by supporting devices.

## 3 Outline of numerical simulation

### 3.1 Numerical analysis model

In order to adequately analyze the prototype reinforced concrete girders under consecutive impact loading and to reduce the mesh size dependency, here, an applicability of the  $G_f$  concept for the concrete elements of large size in the span direction will be numerically investigated. To study the applicability of  $G_f$  concept for prototype girders under consecutive loading, the same dimensions and control model used by Kishi and Bhatti (2010) is adopted here. The element size in the transverse direction is 40 – 50 mm long and that in the span direction is 35.7 mm long, which is obtained by dividing the spacing of stirrups (250 mm) into 7 elements.

Figure 2 shows the control FE model of the reinforced concrete girder. Here, due to the two axes of symmetry, only one quarter of the girder is modeled in 3D for numerical simulation. Reinforcement and stirrups are modeled using beam elements. All other components are modeled using eight-node solid element. The 2000 kg impacting weight is modeled following its real shape. The support including the load cells and device for preventing the girder from lifting off are also accurately modeled.

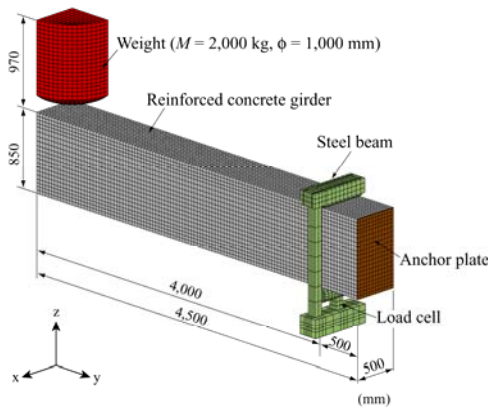


Figure 2. Control model for FE numerical analysis

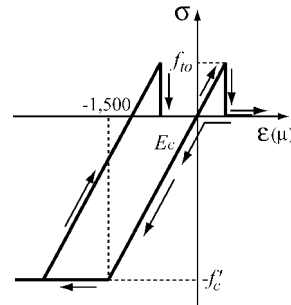


Figure 3. Stress-strain relation of concrete

The number of integration points for solid and beam elements is one and four, respectively. Contact surface elements are defined in order to take into account the interaction between the girder and the bottom surface of the falling weight, as well as between the girder and support elements.

The girder is analyzed by inputting a predetermined impact velocity for the impacting weight. The viscous damping factor is set to  $h = 1.5\%$  based on the numerical simulation for the same girder under a single impact loading by Kishi and Bhatti (2010). The time increment for the numerical calculation is approximately  $0.6 \mu\text{s}$  and is determined by Courant's stability conditions.

### 3.2 Procedure of numerical analysis for consecutive impact loading

In order to numerically and adequately reproduce the dynamic behavior of reinforced concrete girders under consecutive impact loading, the numerical simulations are performed using the following procedures:

- (1) Several falling weights modeled are set on the loading point prior to start the calculation, in which the total number of weights is equal to that of the consecutive loads;
- (2) Numerical analysis is performed by inputting the predetermined impact velocity for the first falling weight, in which  $h = 1.5\%$  is set for the viscous damping factor;
- (3) The numerical analysis is continued from the previous termination point, inputting the critical viscous damping factor for the girder to be in a state of rest;
- (4) The FE model of the previous impacting falling weight is removed;
- (5) Numerical analysis is done by inputting the next predetermined impact velocity for another FE model of weight, in which  $h = 1.5\%$  is set for viscous damping factor; and
- (6) The procedures from (3) to (5) are repeated iteratively until reaching the prescribed final loading.

### 3.3 Modeling of materials

Stress-strain relationship of concrete is defined using a bilinear model in compression and a linear cut-off model in tension as shown in figure 3. In this study, it is assumed that: (1) concrete yields at  $1500 \mu$  strain and its strength is equal to the compression strength  $f'_c$ ;

(2) the tensile stress is released to zero when applied negative pressure reaches the tensile strength of concrete; (3) yielding of concrete is evaluated by using Drucker-Prager’s criterion.

The stress-strain relationship for reinforcement and stirrup is defined by using a bilinear isotropic hardening model. The plastic hardening modulus  $H'$  is assumed to 1 % of elastic modulus. Yielding of steel is estimated on the basis of von Mises yield criterion. The other steel materials used in falling weight, support, load cells and anchor plate are assumed to be elastic.

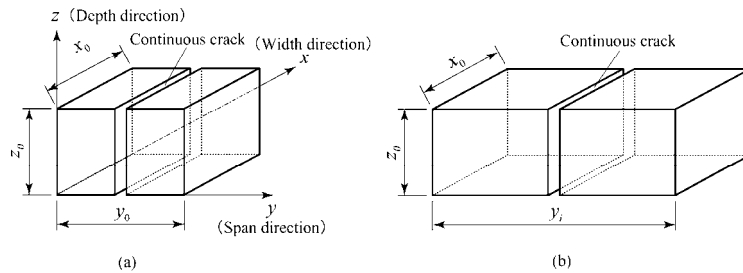


Figure. 4. Continuous crack model in a concrete element: (a) crack model of control element; and (b) crack model of element  $i$  with arbitrary length  $y_i$

### 3.4 $G_f$ concept

In order to evaluate an occurrence of a flexural crack in the concrete element in spite of the length of the element in the span direction, an equivalent tensile fracture energy concept ( $G_f$  concept) has been proposed by one of the authors (kishi and Bhatti, 2010). Here, the concept will be briefly outlined.

Assuming a continuous crack parallel to the  $xz$  plane occurs in the control element with the size of  $x_0$ ,  $y_0$ , and  $z_0$  and an arbitrary element  $i$  having the size of  $x_0$ ,  $y_i$ , and  $z_0$  as shown in figure 4, the tensile fracture energy of the element  $i$  must be set to be equal to that of the control element. Therefore, assuming tensile strength and elastic modulus of the control element as  $f_{t0}$  and  $E_c$ , respectively and setting a fictitious tensile strength of the element  $i$  as  $f_{ti}$ , the following equation can be formulated:

$$G_f = \frac{f_{t0}^2}{2 E_c} x_0 y_0 z_0 = \frac{f_{ti}^2}{2 E_c} x_0 y_i z_0 \tag{1}$$

Thus, the fictitious tensile strength  $f_{ti}$  of the element  $i$  can be obtained as:

$$f_{ti} = f_{t0} \sqrt{\frac{y_0}{y_i}} \tag{2}$$

## 4 Discussion of applicability of $G_f$ concept

### 4.1 Analytical cases

In order to discuss an applicability of the numerical analysis method using fictitious tensile strength for concrete elements, four FE models are prepared listed in table 1. The element sizes are given by dividing the spacing of stirrups (250 mm) into 1, 2, 3, and 7 elements, respectively. In this table, the digit following the notation “MS” represents the

Table. 1. List of numerical analysis cases

| Analysis case  | Element size of concrete in span direction (mm) | Total No. of elements | Total No. of nodal points |
|----------------|---|-----------------------|---------------------------|
| MS250-N/ $G_f$ | 250.0   | 12,757                | 11,234                    |
| MS125-N/ $G_f$ | 125.0   | 17,035                | 15,152                    |
| MS83-N/ $G_f$  | 83.3  | 21,493                | 18,914                    |
| MS35           | 35.7  | 38,875                | 34,832                    |

approximate value (mm unit) of the element size in the span direction and the hyphenated notations “N” and “ $G_f$ ” represent the cases using the normal and fictitious tensile strength of concrete elements considering  $G_f$  concept, respectively. MS35 is the control model for this simulation, with which the rest of results will be compared.

In each case, the fictitious tensile strength  $f_{ti}$  of the concrete element is as follows:  $f_{ti}$  for the cases “N” is 3.12 MPa; and  $f_{ti}$  for the cases MS250/125/83- $G_f$  and MS35 is 1.18 MPa, 1.67 MPa, 2.04 MPa and 3.12 MPa, respectively.

Impact load was numerically subjected onto the mid-span of the girder by consecutively falling the weight from the height of 1.0, 2.5, 5.0, 7.5, and 10.0 m.

#### 4.2 Comparisons of results

Figure 5 shows the comparisons of the time history of impact force, reaction force, and the mid-span displacement (hereinafter, displacement) for three cases of MS250-N/ $G_f$  and MS35 with falling heights of  $H = 1.0$  m and 10.0 m which represent the first and final loading cases. From this figure, it is seen that: (1) the time histories of the impact force generated at a falling height of  $H = 10$  m show different configurations among three cases; (2) the time histories of the reaction force for both cases of MS250- $G_f$  and MS35 are similar to each other but the time history of MS250-N is different from the two other cases; (3) the maximum and residual displacements of both MS250- $G_f$  and MS35 are good agreement each other in spite of height of fall; and (4) however, these in case of MS250-N at  $H = 10$  m are smaller than other two cases.

Figure 6 shows the comparisons of the time history of impact force, reaction force, and

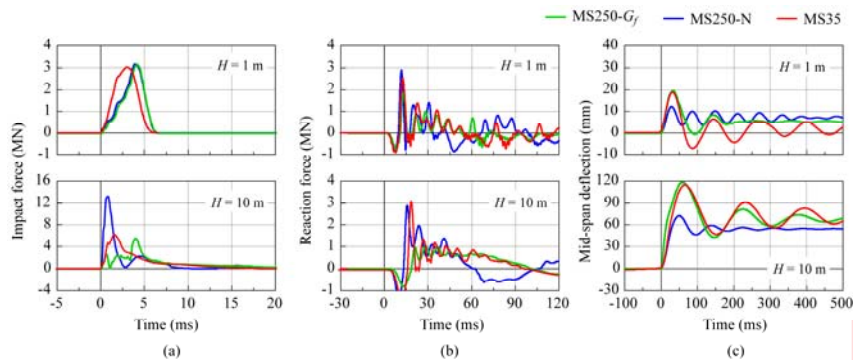


Figure. 5. Comparisons of results among three cases of MS250-N/ $G_f$  and MS35 at  $H = 1.0$  m and 10.0 m: (a) impact force; (b) reaction force; and (c) displacement.

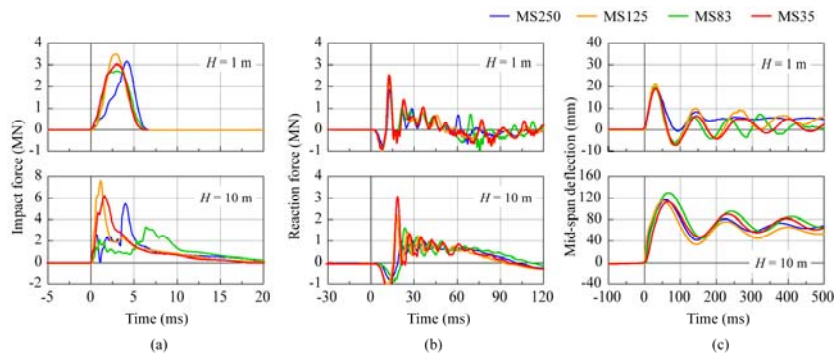


Figure. 6. Comparisons of results among four cases of MS250/125/83- $G_f$  and MS35 at  $H=1.0$  m and 10.0 m: (a) impact force; (b) reaction force; and (c) displacement

displacement for four cases considering  $G_f$  concept for falling heights of  $H = 1$  m and 10 m. From this figure, it is seen that: (1) the time history of the impact force cannot improve even though  $G_f$  concept is considered; (2) maximum reaction forces are different among four cases but the configurations of the time history are almost the same; and (3) vibration frequencies of the displacement after unloading at  $H = 1$  m are a little different among four cases but maximum displacement and residual displacement are almost similar among four cases in spite of the size of concrete elements.

From this comparison, it is confirmed that the maximum and residual displacements of the girder under consecutive impact loading which are very important indexes for impact resistant design can be adequately evaluated by considering  $G_f$  concept.

#### 4 Conclusion

In order to numerically evaluate the dynamic response behavior of the prototype reinforced concrete girders under consecutive impact loading, a numerical analysis method applying equivalent tensile fracture energy concept ( $G_f$  concept) was proposed. The applicability of the proposed method was discussed by conducting numerical simulations for the models with various element sizes of concrete in the span direction. From this study, it is confirmed that applying the  $G_f$  concept, time history of the displacement, and maximum and residual displacements can be rationally evaluated in spite of the length of concrete element.

#### References

- Kishi, N., Kon-No, H., Mikami, H. (2009) Numerical simulation of RC beams under consecutive falling-weight impact loading, *Journal of Structural Engineering, JSCE*, Vol. 55A, 1225-1237, in Japanese.
- Ghadimi Khasraghy, S., Kishi, N., Vogel, T. (2009) Numerical simulation of consecutive rockfall impacts on reinforced concrete slabs, *Proceedings of IABSE Conference*, Bangkok, Thailand.
- Kishi, N. and Qadir, B. A. (2010) An equivalent fracture energy concept for nonlinear dynamic response analysis of prototype RC girders subjected to falling-weight impact loading, *International J. of Impact Engineering*, Vol. 37, No. 1, 103-113.

## Reinforced concrete structures for rockfall protection

Jean Tonello<sup>1</sup>, Jean-Luc Palle<sup>1</sup>

<sup>1</sup> Tonello Ingénieurs Conseils - Groupe BG - [tonello@tonello-ic.com](mailto:tonello@tonello-ic.com)

---

**Abstract.** Engineers considered that a reinforced concrete structure which supports a "dissipative cover" allows ensuring security of the itineraries confronted with rock falls. Such concrete structures are dimensioned accounting for the following effects: (i) weight of the selected cushion layer and (ii) "equivalent static" stress due to the impact on the cushion layer, and accounting for the dissipation of energy in this layer. But taking into account the permanent loads and the impact load always lead to a substantial steel reinforcement of the covering slab. Considering that the covering slab could participate massively and mechanically in dissipation without the contribution of a heavy cushion layer a block-proof roofing has been developed, with special attention paid to the necessary control of the damages on the reinforced-concrete structure.

**Keywords:** reinforced-concrete, elastoplasticity, dissipation, soft impact, fusible supports.

---

### 1 Introduction

Many countries devote a significant part of their investments to the development of their road system. In mountain areas, roadways become a considerable challenge due to specific risks such as frequent rock falls and stone breakup. The direct consequences of this particularity in mountainous areas are: (i) roads often blocked and unusable, (ii) dwellings endangered and (iii) human fatalities.

In this context, rock fall protection galleries are often used, and mainly at the toe of vertical cliffs. Typical these galleries consist of reinforced concrete slab covered with a cushion layer. This soil layer aims at dissipating a large part of the kinetic energy of the falling boulder. To fulfil this function, the soil cover must be thick and its mass is then high compared to the slab mass. As a consequence, the portal and their foundations must be strong enough to withstand the mass of the slab plus the soil layer mass. In mountainous valleys and gorges, this latter point is often critical.

A relatively recent development in this field is the Structurally Dissipating Rock-shed (SDR) (Tonello, 2001) (Delhomme et al., 2005) which doesn't require a cushion layer. Indeed, the proposed structure is made of a reinforced concrete slab supported by specific elements (fuse supports) (Figure 1). The structure is designed so that the impact energy is dissipated by deformation of the fuse supports as well as by damaging the slab concrete.



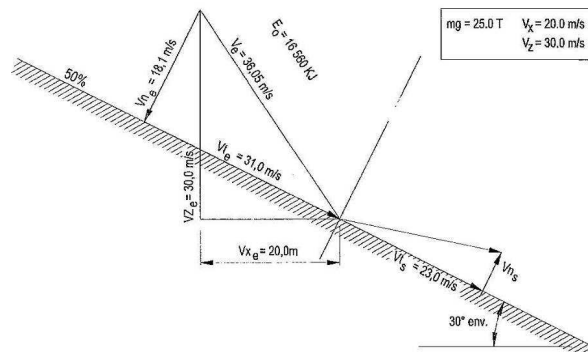


Figure.2 Analysis of velocities and energies,  $E_o = 16560$  KJ,  $E_n = 4180$  KJ,  $E_{rg} = 5725$  KJ

## 2. Sequential approach case of Poniente

As regards the phenomena, we can distinguish three sequences in the functioning:

- the “dissipative impact” with local compaction of concrete in a short instant (a few hundredths of a second) during which reciprocal contact forces of the block-structure pair are developed reducing a level of incident energy and degrading very noticeably velocity of the block/structure complex.

The “developers” of this phase are plastic deformations of recess of surfaces, decohesion of materials, acoustic effects, local increases of temperature, propagations of longitudinal waves.

- the absorbent elasto-plastic work (fig. 3, fig. 4) with a strictly dissipative plastic phase; this phase imposes a play of normal and tangent stresses with the development of “plastic hinges” in the impacted zone and recesses of fuses, if necessary.
- the “restitution” phase during which the structure is capable to serve an elastic work of inverse deformations which is not strictly equal to that from the initial elastic phase because irreversibility appear.

Being capable to create non-negligible accelerations (considerably superior to  $g$ ), the slab ejects a block or deflects it.

Damages of reinforced concrete which are noticed during tests are “accumulations” of successive relative damages during each phase.

Studies and tests are still necessary to identify phenomena. However, retrospection which we now have, which is associated with successive internal improvements (transversal reinforcements) shows that a plate which contains very careful arrangements of details related to reinforcement, offers very large capacities in relation to violent impacts.

What can be noticed, is the ability of the slab to be locally destructurized by the impact phase, conserving in the very nearby zones its flexional capacities.

Secondly, the ability to repair damages, without the loss of performance, is nowadays proved to be the conclusive replica of impacts.

In the domain ( $\epsilon_b \leq 3,5\%$ ;  $\epsilon_s \leq 15\%$ ) and surely beyond it, upgrading of damaged structures is fully possible, profitable and capacity-assured.

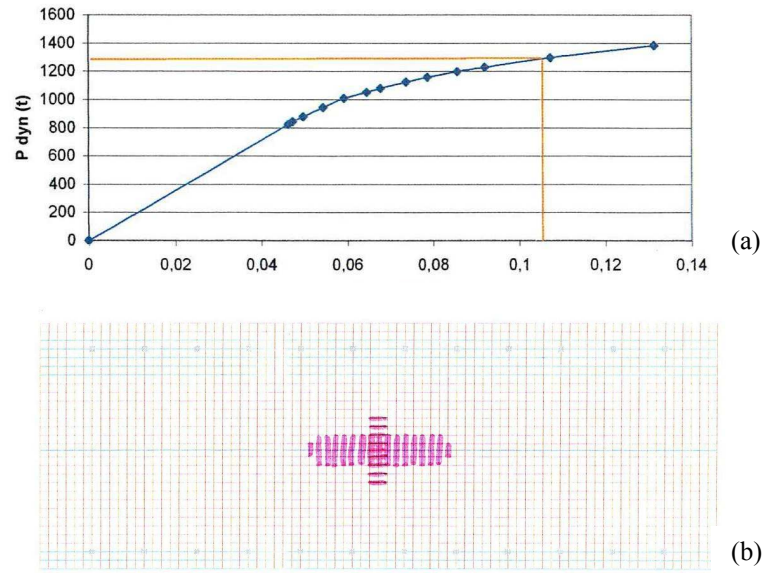


Figure.3. Impact centered on the SDR structure (Poniente), (a) elasto plastic works (b) damaged zone

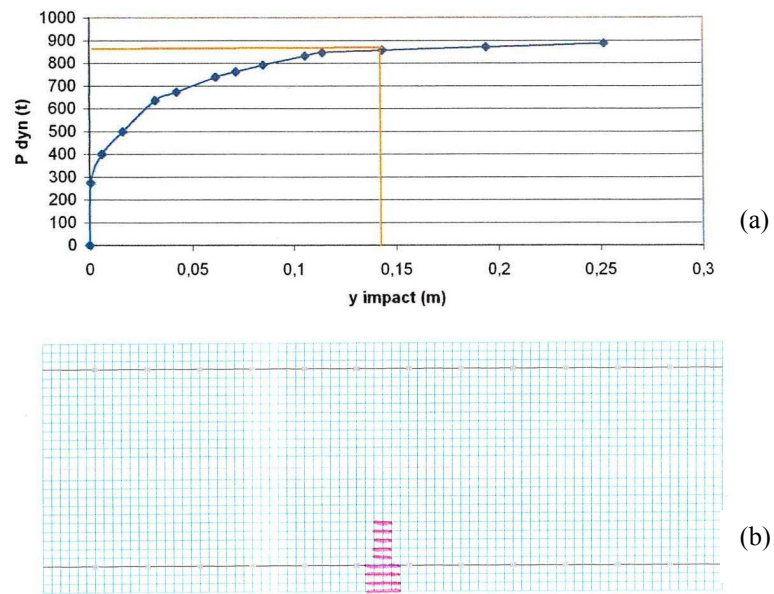


Figure.4. Impact at the boundary PSD structure (Poniente) : (a) elasto plastic works (b) damaged zone

### 3 Experimental tests and Finite elements Analysis

The main innovation of the SDR concept is to make the slab work in its plastic range under high energy impacts, but with low occurrence. The impact energy is dissipated directly by the actuation of the slab, by the cracking of the concrete and the plastic stains in the reinforcements for the central impacts, and by the deformation of the fuse supports for impacts on the edges.

Experimental tests aiming at validate this concept were performed. A tested structure at a 1/3 scale model of the rock-shed of Essariaux (Savoy - France) was realised. It consists of an horizontal slab of 4.8 m out of 12 m with 0.28 m thickness (Figure 5). It is built with a concrete of compressive strength of 30 MPa and is reinforced by a strong density of steel reinforcements HA Fe E 500 (4300 kg of steel for 16 m<sup>3</sup> of concrete). The slab is supported by 22 metal fuse supports: they consist of a steel tube (TUE 220 A, 100 mm in height, 70 mm diameter and 2.9 mm thickness) welded onto two square plates of 100 mm side and 8 mm thickness; these fuses have an elasto-plastic behaviour and blister under a static load of 260 kN. (Perrotin et al, 2002; Perrotin et al., 2004; Delhomme et al., 2005))

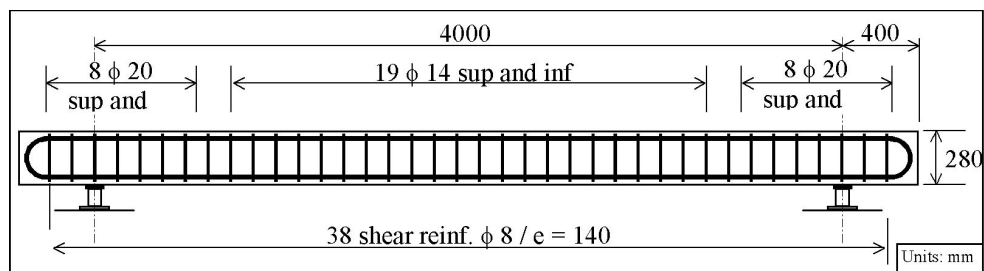


Figure 5. The experimental slab

Using Abaqus, modelling was performed and compared with experimental results for the same level of energy (Berthet-Rambaud 2004) on the global structure, and on special part on the concept such as the fuses (Figure 6).

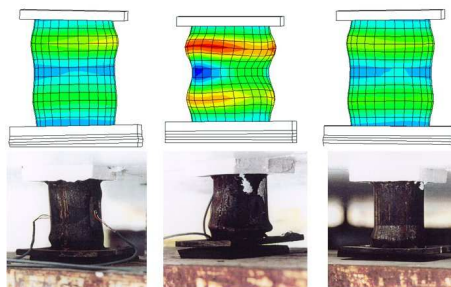


Figure 6. Numerical results compared to experimental tests: compression of fuses

## 5 Conclusions and Perspectives

Over the years, we were able to adapt the SDR structures to site-specific conditions, but also to execution constraints on mountain itineraries which connect villages in the summer and ski resorts in the winter, and lot of structures were built for the Conseil Général de la Savoie (CG73). By avoiding downstream supports and by introducing prefabricated elements in the structure, the SDR were able to adapt themselves to demanding exploitation constraints of concerned itineraries.



**Figure 7.** Example of new development: concept and during construction works.

## 6. References

- Berthet-Rambaud. (2004). Structures rigides soumises aux avalanches et chutes de blocs : modélisation du comportement mécanique et caractérisation de l'interaction phénomène-ouvrage. Phd Thesis. University Joseph Fourier, Grenoble, 285 p.
- Mougin (Locie-Esigec Université de Savoie) / Mazard (Laboratoire 3 S et RNVO Grenoble) / Perrotin (Locie-Esigec) / Delhomme (Locie-Esigec - Tonello IC). (2004). Exploitation analytique et modélisation numérique des essais d'impact sur une dalle pare-blocs structurellement dissipante (PSD).
- Delhomme F. Étude du comportement sous impact d'une structure pare-blocs en béton armé. PhD Thesis, University of Savoie, LOCIE-ESIGEC, France; 2005, 79-97 Chapter 3.
- Delhomme F, Mommessin M., Mougin J.P., Perrotin P., 2005, Behaviour of a structurally dissipating rock-shed: experi-mental analysis and study of punching effects, International Journal of Solids and Structures, Volume 42, Issue 14, Pages 4204-4219
- Perrotin P., Mommessin M., Mougin J-P., Tonello J. 2002, Étude expérimentale du comportement d'une dalle pare-blocs. Revue française de génie civil, Volume 6, n° 5/2002, p. 723-734.
- Perrotin P, Delhomme F, Mommessin M, Mougin J-P. 2004. Behaviour of an impacted reinforced concrete slab: Percussion and punching analysis. Proceedings of the 8th international conference on structures under shock and impact. p. 419-27.
- Tonello J., 2001, Couverture Pare-Blocs Structurellement Dis-sipante, Label Ivor 01.1. Mission génie-civil, Ministère de l'équipement, French Civil-Works Ministry France.

## Rockfall attenuator and hybrid drape systems - design and testing considerations

James Glover<sup>1</sup>, Axel Volkwein<sup>1</sup>, François Dufour<sup>1</sup>, Matthias Denk<sup>2</sup>, Andrea Roth<sup>2</sup>

<sup>1</sup> WSL Swiss Federal Institute for Forest, Snow and Landscape Research, Zuercherstrasse 111, 8903 Birmensdorf Switzerland  
[james.glover@wsl.ch](mailto:james.glover@wsl.ch)

<sup>2</sup> GeobruGG AG, Aachstrasse 11, 8590 Romanshorn, Switzerland  
[matthias.denk@geobruGG.com](mailto:matthias.denk@geobruGG.com)

---

**Abstract.** Rockfall attenuator and hybrid barrier systems combine the performance of standard drape nets and flexible rockfall barriers. The testing of these systems proves a challenge when placed in the framework of Swiss or EOTA guideline for technical approval of rockfall protection kits. The importance of net and rock slope interaction during the attenuating process necessitates a test load that models closer the natural occurrence of rockfall. A series of seven rockfall tests were conducted. Rock boulders up to 1,000 kg were released using a trial net ramp release mechanism. A test hybrid barrier system was installed with a marked impact zone at the top and extended drape section for the remaining slope. Impacting rock boulders enabled observations of system behaviour with interactions of net and rock boulder during its decent. An overview of the testing procedure, release mechanism and the observed results of the rockfall tests are presented herein.

**Keywords:** Rockfall, Protection kits, Full scale testing, Hybrid, Attenuator; Draperies.

---

### 1 Introduction

Rockfall attenuator and hybrid barrier systems combine the performance of standard drape nets and flexible rockfall barriers. In this case, an impact zone constructed of a high tensile spiral rope net intercepts upslope rockfall. Rock blocks are then guided through a tail drape section and contained to the base of slope (Fig. 1). This is beneficial because it avoids costly maintenance and clean out commonly associated with standard rockfall protection kits. They are intended as a low maintenance passive barrier system without the use of dynamic energy absorbing brake elements or lateral restraining anchors (Badger et al, 2008). Instead they use the boulder impacts with the net and its interaction with the slope to attenuate the velocity and trajectory of rockfall.

The testing of these systems proves a challenge when placed in the framework of Swiss or EOTA guideline for technical approval of rockfall protection kits (Gerber, W. 2001, EOTA. 2008). Testing to a prescribed energy rating produced from vertical free fall is not

possible due to their reliance on an open ended system. The importance of net and rock slope interaction during the attenuating process necessitates a test load that models closer the natural occurrence of rockfall. Testing programs to date (Ortiz. et al. 2008, Sassudelli et al. 2007) have focused on material testing for the design of hybrid and attenuator systems. However, a dimensioning concept that identifies system attenuating capacity with respects to rock slope properties and expected hazard has yet to be produced. Marking the first of a series of full scale dynamic testing in Switzerland 2009, a prototype hybrid barrier was impacted horizontally using natural rock boulders with rotation. This is part of a joint research program investigating rockfall attenuator and hybrid barriers.

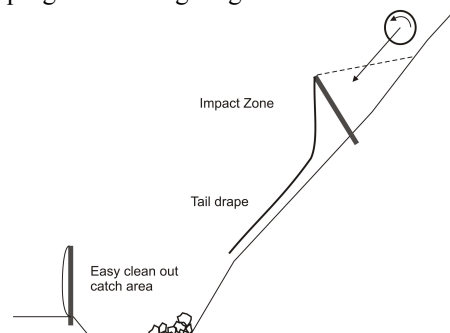


**Figure.1.** Rockfall attenuator and hybrid concept

## 2 Testing

### 2.1 Test site

To facilitate the development of rockfall attenuator and hybrid systems, a full scale test site at MTA Carrière quarry St Léonard (Switzerland) has been realized. A ramp and automated remote release mechanism have been constructed for the artificial release of natural rock boulders at the top of a 50 m long and 50° steep rock slope. It enables vertical potential energy to be guided to horizontal impact with a test barrier, while additionally rotating the test block. The unique test site was selected for its long reaching steep rock slope, which for the first time ever has enabled testing of a full scale hybrid barrier system. A feature of this test site is the ability to select locally a range of natural boulders from the quarry for use as test bodies.

### 2.2 Tested hybrid barrier

The prototype hybrid barrier under testing consisted of drapery 40 m long covering the test slope, it was constructed from high tensile spiral rope net (SPIDER® S4-230) with mesh openings of 23 cm. While the barrier opening is defined with a 6 m long impact zone constructed of high tensile spiral rope net (SPIDER® S4-130) with mesh openings of 13 cm. The net system was hung on a top support rope suspended between two 3 m tall posts with 8 m wide spacing. The posts were further stabilised with rear and front support ropes. No lateral restraint of the tail drape or dynamic energy absorbing brake elements were used (Fig. 2).

### 2.3 Test boulders

Natural rock boulders were selected from the quarry that were of reasonably regular shape This provided a test load that closer modeled rockfall, providing insights into the

influences block angularity on the interaction with the test barrier. Test boulders were individually weighed using a net and electronic weighing device, and ranged 300 - 1200 kg. Three principle planes were traced on the boulders with paint to assist with the video back analysis.



Figure.2. (left) impact zone at the top and (right) 40 m tail drapery

#### 2.4 Apparatus

The ramp consisted of a high tensile spiral rope net stretched between the base of the test net installation and a digger bucket. This was used to accelerate the test boulders to the point of impact with the test barrier. The release point was 9 m above and 9 m to the rear of the test nets generating a 45° net ramp that was stabilized with guy ropes. The release mechanism was a triangular snow net attached to the top of the wire net ramp. Once loaded with the test boulder, the snow net was attached to the digger bucket using an automated remote release hook and primed ready for testing (Fig. 3). On release the mechanism initiated the rotation of the block into the ramp.



Figure.3. Cross sectional view of test site and apparatus. [A] Test hybrid barrier with impact zone at top [B] Release ramp constructed of SPIDER wire net [C] Natural test boulder [D] Release nets constructed of snow net [E] Automated remote release hook

### 2.5 Measurement technique

Video cameras captured the events and enabled a back calculation of the impacting energies, net deflections, and observations of the loading processes. In addition, dynamic force cells sampling at 1 kHz captured the loads experienced in rear and top support ropes of the barrier. A vertical and horizontal measuring post was installed to enable net deflection measurements (Fig. 4).



Figure.4. a) boulder before horizontal impact c) first impact d) maximum net deflection

## 3. Test results

### 3.1 Net ramp and release mechanism

All test blocks were successfully released using the test set up, each impacted with rotation and horizontally into the test barrier, and were guided to the base of slope where they were all contained in the catch area.

The design for the ramp and release mechanism was successful in achieving the desired rotational and horizontal impacts. Test boulders stayed within the bounds of the 3.5 m wide net ramp, even those that were irregular in shape. The ramp was tensioned such that the nets did not sag as an initial condition. This proved ideal for smaller test boulders of 350 kg where the fastest impact velocity was produced at  $\sim 8 \text{ ms}^{-1}$ . On the other hand, larger boulders caused the net ramp to sag much further and consequently losing more kinetic energy prior to impact.

Table 1: Velocity and energy back calculations

| Test number  | T1   | T2  | T3  | T4   | T5   | T6   | T7   |
|--|------|-----|-----|------|------|------|------|
| Mass (kg)  | 310  | 330 | 360 | 635  | 720  | 850  | 1210 |
| Translational impact velocity ( $\text{ms}^{-1}$ ) | 9.0  | 6.5 | 4.7 | 5.8  | 5.8  | 6.5  | 4.3  |
| Impact energy kJ                                   | 13.6 | 7.4 | 4.0 | 10.9 | 12.3 | 18.9 | 11.1 |
| Tail drape velocity m/s                            | 9.5  | 9.6 | 7.4 | 9.5  | 10.9 | 11.1 | 11.9 |
| Horizontal net deflections (m)                     | 2.0  | 1.3 | 0.8 | 1.7  | 1.4  | 2.2  | -    |

### 3.2 Video footage

Back calculations of the footage indicate translational impact velocities of between 4 and  $9 \text{ ms}^{-1}$  were achieved. Table 1 presents these values. Comparing the achieved velocities with boulder weight, a poor correlation is observed. Here larger mass boulders yielded slower impact velocities. Similarly there appeared no correlation with the calculated impact energies. This was observed to be a result of increased ground impacts with heavier boulders and consequently increased energy losses. A solution here is to further tension the launch ramp or increase its angle. Furthermore, the initial impact velocity

appeared to be largely dependent on boulder geometry. This was evident in test three where an oval shaped boulder was used which produced one of the lowest velocities. Conversely, boulder velocities internally to the tail drape demonstrate a positive correlation to boulder mass with increasing mass. This is likely to reflect the 50 m travel distance within the tail drape section. Boulder velocity internally to the tail drape was  $9 - 11 \text{ ms}^{-1}$  exceeding the maximum impact velocity achieved in the impact zone.

### 3.3 Force cells

Force cell data from the top rope are presented Figure 6. The data has been normalised to remove the initial pre-tensioning due to the load of the mesh. Highest loads were experienced during passage of the boulder internally to the tail drape during tests four and six, they represent 1/3 greater force than that recorded for all initial impacts. This is in concordance with the higher boulder velocities observed in this section. The higher forces can be explained through the large scale launching features on the slope initiating secondary impacts mid way down the tail drape. This was assisted by the large 230 mm mesh size openings of the tail drape spiral rope net where angular features on the boulders caught in the large mesh openings, generating a sharp snagging effect. These observations from video footage correlate with the observed peak loads of tests four and six (Fig. 6). The snagging produced a good attenuating affect to the boulder halting them momentarily in their passage, in some cases inducing a negative rotation, although is responsible for most net damage.

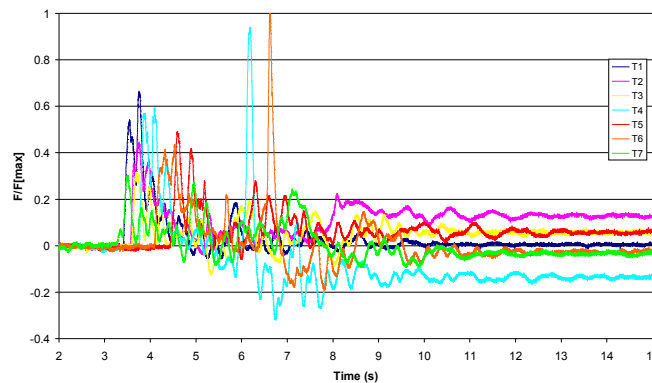


Figure.6. Top rope force cell data with initial static load removed

Comparing remaining tests where now snagging was observed in the tail drape, force cell peaks in the top rope for initial impacts are shown to be 20 – 40 % greater than those in the tail drape section. On average forces were 20 % higher in the top ropes compared to the retaining ropes for the initial impacts. Although the peak loads observed in tests four and six greatly reduced the difference in forces observed to ~ 4 %. This is thought to be a result of the mode and position of these impacts where forces were greater and applied in an orientation nearer parallel to the netting. Here the impact mode is more of a tugging fashion as opposed to the net deflections experienced for initial impacts.

It is clear the presence of the drape reduced the bounce of boulders over the slope terrain, limiting their potential to gain kinetic energy through extended periods of free fall in bounce parabola. It is thought this is a function of net weight and slope angle, and as such it is a goal to quantify this in future testing.

## 5 Conclusions

Till now the use of natural rock boulders in the testing of rockfall attenuator and hybrid barrier systems has not been conducted. A goal of this pre testing series was to simulate closer the occurrence of natural rockfall to generate a suitable impact load for the testing of rockfall attenuator and hybrid barriers. Previous studies have used artificial concrete test boulders of regular shape (Badger et al. 2008, Ortiz. et al. 2008, Sassudelli et al. 2007), and as such the snagging effect has been little observed. This testing series has highlighted that the irregular shape of naturally occurring rock boulders is an essential parameter to be considered in the design of rockfall attenuator and hybrid barrier systems. More over, the results have illustrated the importance of including rotational impact in the testing of hybrid barriers, because of its bearing on the loading in the test net. Protruding features can catch on mesh openings; this concentrates the force on one local point in the net. It is clear from the achieved impact energies and velocities that to fulfill the desired goals for hybrid testing it requires that an attempt is made to release boulders from greater heights and a rethink of release device is needed.

### Acknowledgements:

Grateful thanks to Monsieur Tissières, Monsieur Genolet, and members of MTA Carrière St Léonard for help in realising this test site and excellent assistance during experimentation. We would further like to extend these thanks to the community of St Léonard and Canton Valais. Thanks are also accorded to Sébastien Cheseaux PARAVALANCHE (Leytron) and Geobruigg AG (Romanshorn), for expert installation of barrier systems and materials supply respectively. Authors would like to acknowledge the part financial support of the Commission of Technology and Innovation (CTI) of the Swiss Federal Office for Professional Education and Technology (OPET) through this project [CTI-Project Nr. 10044.1].

### References

- Badger, T.C. et al. (2008) Hybrid Barrier systems for Rockfall Protection Proceedings of the IDWRP, Switzerland
- EOTA. (2008) Guideline for European technical approval of falling rock protection kits (ETAG 027), February 2008, Brussels
- Gerber, W. (2001) Guideline for the approval of rockfall protection kits Swiss Federal Research Institute WSL Berne
- Ortiz, T. & Arndt, B. (2008) Implementation & Developments of Hybrid Rockfall Barrier Systems in Colorado 59<sup>th</sup> Highway Geology Symposium Santa Fe, New Mexico
- Sassudelli, F. et al. (2007) Recent Rockfall barrier testing in Italy: Structural component tests and dynamic testing of barrier kits and hybrid barrier/drape systems in the framework of European technical guidelines Assoc. of Environ & Engr. Geologists Program pp. 122

## New energy dissipating device for rockfall protection barriers

Ayman Trad<sup>1,2</sup>, Ali Limam<sup>1</sup>, Philippe Robit<sup>2</sup>

<sup>1</sup> Université de Lyon, INSA de Lyon, Laboratoire LGCIÉ, Lyon, France  
[ali.limam@insa-lyon.fr](mailto:ali.limam@insa-lyon.fr)

<sup>2</sup> GTS, Travaux Géotechnique et de Sécurisation, Lyon, France  
[probit@gts.fr](mailto:probit@gts.fr)

---

**Abstract.** With the transformation of the earth's climate and due to the global warming, the risk of rock fall events increases, especially in the Alpine region where many roads and highways are exposed. To protect traffic against this phenomenon, many protective measures have long been applied. Commonly used measures, are flexible protective net barriers able to interrupt and slow down the fall of rocks.

**Keywords:** natural risks, rock fall nets, cable nets, finite element method, experimental tests, energy dissipators.

---

### 1 Introduction

In recent years, different types of wire-nets have been developed. An innovative concept is proposed by the company GTS. This wire-net system is constituted of pear shaped cells, which conduct to an orthotropic behaviour. These cells are connected with rigid or fuse clamps.

The energy absorbing capacity of wire-net systems has been increased by a factor of ten over the last ten years. In comparison with concrete sheds and barriers, the energy absorbing capacity of the flexible systems is 30 % higher and the investment costs are ten times smaller, (Grassel et al. 2003).

As a result of the development of this type of protection, the European Organization for Technical Approvals (EOTA), released in February 2008 a new guideline for falling rock protection kits, (ETAG 27, 2008), which defines how to test and assess the performance of the kits. This guideline introduces new concepts of residual capacity, both in terms of energy and in terms of residual height, and as a result changes the design procedures of these devices. The validation of protection kits is done by testing the entire structure with real scale experiments, and a characterization of each element of the tested kit is required. This contribution focuses on the energy dissipators.

## 2 Braking devices

The function of the rockfall protection barrier is to absorb the kinetic energy of the impacting block, and ensure its retention. The role of the net is to diffuse the efforts to the braking devices which absorb the energy and slow down the velocity of the block. Quasi-static and dynamic tests are done to validate the behavior and the energy absorbed by different types of dissipators used by the company GTS.

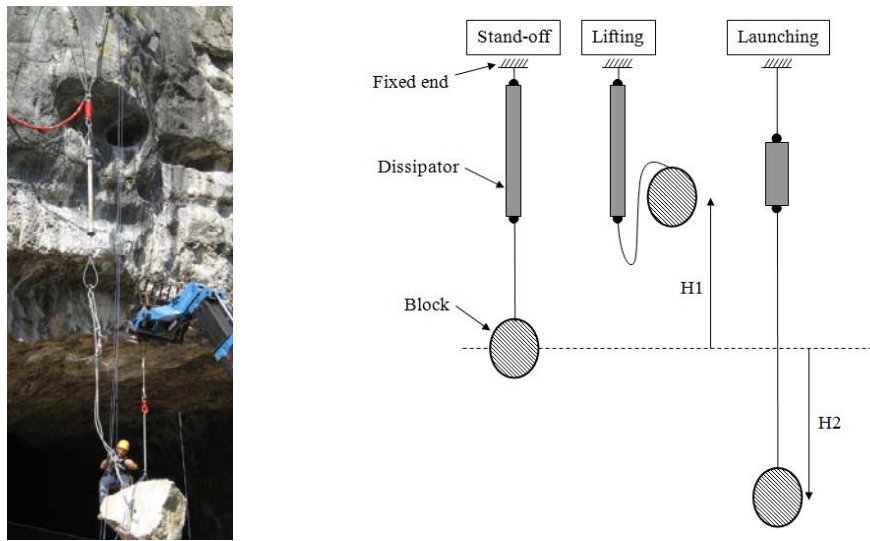


**Figure.1.** Dynamic tests on the energy dissipators

The dissipators working by friction are the most common. GTS has designed and developed a braking device working on this principle, Figure 2.



**Figure.2.** GTS braking system working by friction

The problem of this type of dissipators is the decreasing of performance during the braking due to the wear and the temperature rise, the behavior is shown in Figure 3.

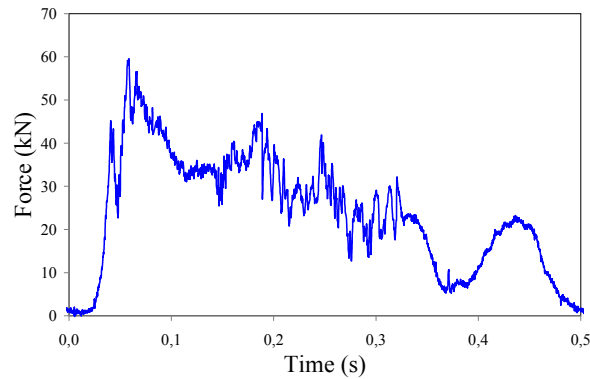


**Figure.3.** Behavior of the dissipators working by friction

The second type of brakes is considered to dissipate energy by ductile tearing of a metal or propagation of cracks (Figure 4). Two steel bars are positioned inside a tube of mild steel, which is notched at one end to initiate the crack propagation. These two bars are connected to cable loads which permits to induce complete tear of the tube by crack propagation.

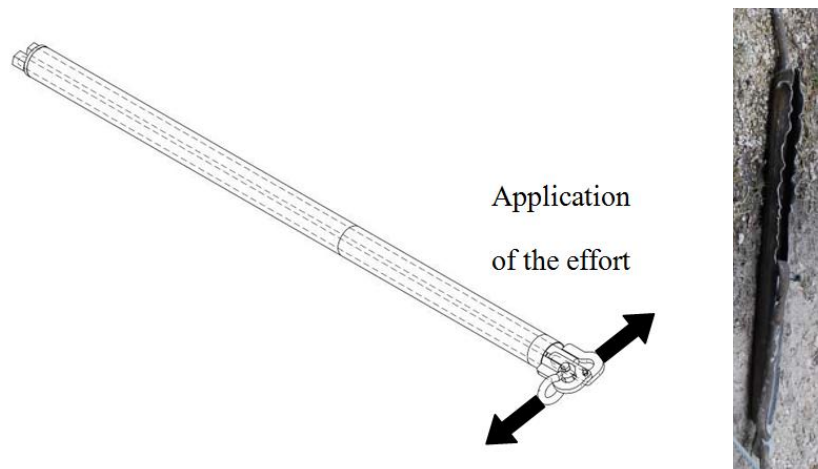


**Figure.4.** GTS braking system working by tearing

At low speed (less than 1cm/s), the tear propagates along the tube, sometimes with a helical crack propagation, induced by the twisting of cables and the possibility of rotation of the tube. This effect is considered as positive because the curvilinear length, and implicitly the absorbed energy, is more important than the length of the tube. When the speed is around 15m/sec and more, random failures of the steel bars subjected to high torsion terminates the process of tearing dissipation making the system unreliable.

Another braking system based on the principle of buckling of tubes was developed by the LGCIE laboratory of "INSA de Lyon" and the company GTS.

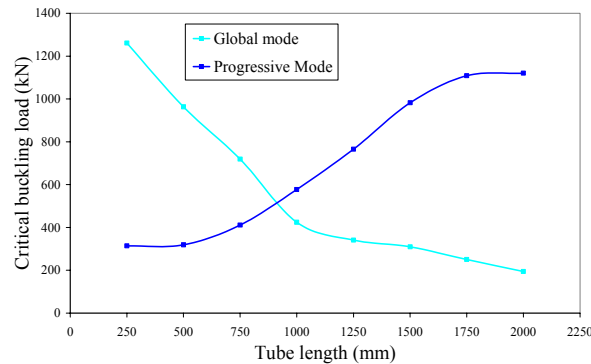


**Figure.5.** The effect of the tube length on the buckling mode

The tubes are generally effective components in energy absorption point of view, if we are able to block the beam mode. The proposed new concept, permits to inhibit the global mode (beam mode) which allows to consider a significant length and to increase the absorbed energy by progressive buckling: a cable pass through the tube ensures the compression loading via two bearing plates, and prevents the global buckling mode even though the tube is well above the critical length.

The stress-strain curve of the material used (steel S235 or aluminum ALU 6060 T5) is obtained by a uni-axial tensile test. A numerical simulation is conducted with CAST3M code, which is based on FEM method. Incremental calculation using multilayer shell elements (seven integration points through the thickness), taking into account large displacements and plasticity with isotropic strain hardening, allows us to obtain the fundamental equilibrium path. Plastic bifurcation check permits to obtain the buckling load and various buckling modes, and therefore to isolate the geometric parameters (length, thickness and section) used to separate the two different critical modes (beam and shell) and the zone of interaction between these two modes (Al Ghalib, 2003).

A particular case is presented here after. The considered section is  $100 \times 100 \times 4$  mm, the aluminium grade is ALU 6060 T5. Figure 5 shows the characteristic of the buckling mode depending on the tube length. If the length of the tube is less than 750 mm the tube will always buckle in a shell fashion, if it exceeds 1000 mm we obtain a beam mode. Between 750 and 1000 mm there is a transition zone between the two modes.

Figure 6 shows the load deflection curves obtained numerically, the bifurcation point and the associated buckling mode.

Contacts between cable, plate and tube, sliding and friction are complex and difficult to model, especially when the folds of buckling confine the crossing cable, inducing friction and blocking the wavelengths associated with global buckling. A simple way to inhibit these global modes and thus achieving systematic shell mode via numerical modeling is to mesh a quarter of the tube: the imposed symmetries can thus block the global modes.

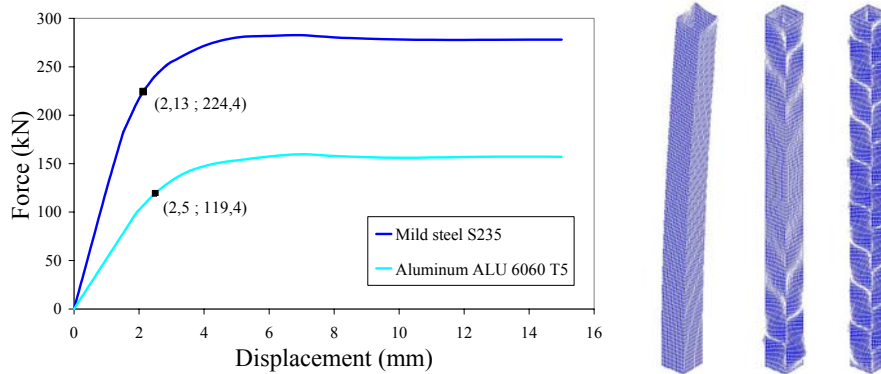


**Figure.6.** Comparison between Aluminum and Steel (a 80x80x2 mm tube) and different modes obtained (global and progressive)



**Figure.7.** Progressive buckling of an aluminum dissipator

To validate this new concept, a series of quasi-static and dynamic tests has been conducted. The quasi-static crushing tests are conducted on a specific traction compression machine. Example of a crushed tube under quasi static load is shown in Figures 7.

The load-deflection curve of the crushing tests presents several oscillations that correspond to the initiation, propagation and collapse of each fold (Figure 8). The mean braking load is constant with a slight gradual increase at the end; this is due to the frictional forces obtained by the sliding of cables inside the tube. The different loading peaks characterize the different folds of the tube during the progressive buckling mode. The final phase of the behaviour corresponds to the pure traction on the cable after the total collapse of the tube.

Dynamic tests are conducted on site, close to service conditions of the system, with an impact velocity near 20 m/s. The dynamic loadings are induced by the free fall of a block. Different blocks are available, with a mass varying between 0,5 and 3 tons, the maximum free fall height being 20 meters, which corresponds to a maximum energy of 600 kJ.

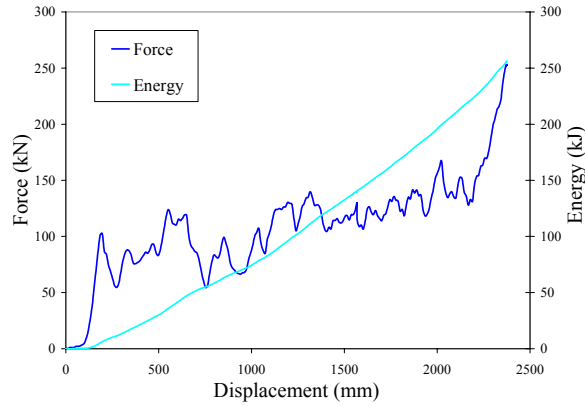


**Figure.8.** Behavior and absorbed energy of a dissipator

Here below in Figure 9 and 10 we clarify the effect of the impact velocity and impact energy (SEL : service energy level and MEL : maximum energy level) for the case of  $80 \times 80 \times 2$  mm mild steel absorber.

As a result of the quasi-static and the dynamic tests we found that this type of braking devices working by buckling of tubes is the best between the tested types, the advantages are:

- A configurable braking force, depending on the material and the section of the tube;
- A constant average braking force throughout the braking;
- An excellent reproducibility of results;
- A low impact of the speed in the range of work considered;

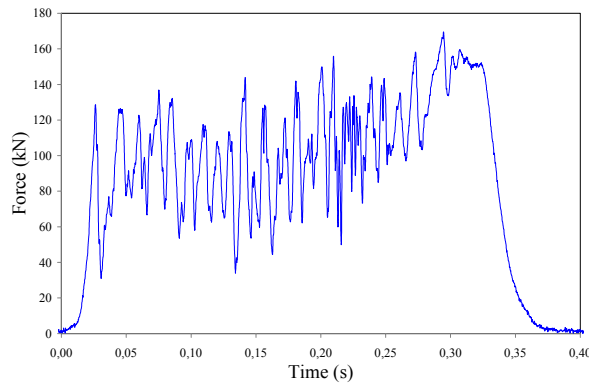


**Figure.9.** Impact velocity = 18 m/s, impact energy = 240 kJ (96 % of the dissipation capacity for this absorber - MEL conditions). Mean braking force = 107 kN, maximum braking force = 170 kN

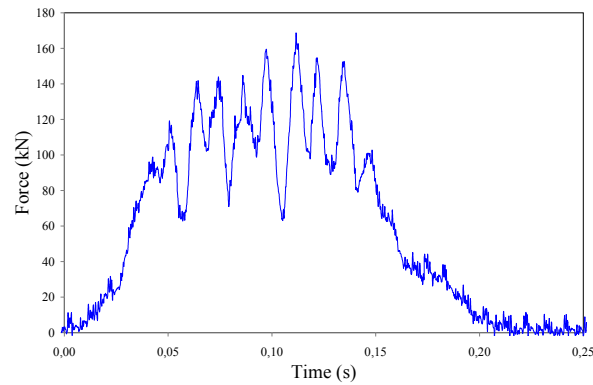


**Figure.10.** Impact velocity = 10 m/s, impact energy = 85 kJ (34 % of the dissipation capacity for this absorber - SEL conditions). Mean braking force = 112 kN, maximum braking force = 168 kN

#### 4 Real scale tests

Finally, real scale tests must be done on the rockfall barrier to validate its functionality specially the energy dissipators, the holding of anchors and posts, the deceleration and stop block according to the specifications defined by the new guideline for European technical approval (ETAG 27). A test of a barrier class 6 - 3000kJ is prepared, the tests are conducted on the testing station developed by the LCPC on Montagnole - France (Figure 11).



**Figure 11.** Testing station of LCPC

The test site consists of a crane mounted on top of a cliff 80 m high with a capacity of 20 tons thus a potential of 15000 kJ. The final validation test is still in progress.

## 5 Conclusion and perspectives

A new braking system working by buckling of tube is proposed and validated via numerical simulations and experimental tests. Further studies are needed to optimise the behaviour of this dissipator. Full scale tests in Montagnole and dynamic simulations are in progress to validate and optimise the energy absorbed by each class of the rockfall protection barriers.

## References

- Al Galib D. (2003). Comportement statique et dynamique de structure fusibles susceptibles d'absorber les énergies d'impact en cas de crash. Ph.D. Thesis, INSA of Lyon 258p.
- Bertrand D., Nicot F., Gotteland P., Lambert S. (2008). Discrete element method (DEM) numerical modeling of double-twisted hexagonal mesh. *Can. Geotech. J.*, Vol. 45, p 1104-1117.
- ETAG 27 (2008). Guideline for European Technical Approval of Falling Rock Protection Kits, 53 p.
- Grassl H., Volkwein A., Bartelt P. (2003). Experimental and Numerical Modeling of Highly Flexible Rockfall Protection Barriers. 12th Pan-American Conference on Soil Mechanics and Geotechnical Engineering, Cambridge, Massachusetts, USA.
- Nicot F., Cambou B., Mazzoleni G. (2001). Design of Rockfall Restraining Nets from a Discrete Element Modelling. *Rock Mech. Rock Engng.*, Vol. 34 (2), p 99-118.
- Trad A., Limam A., Robit P. (2009). Etude expérimentale et numérique du comportement des filets de protection, *Revue de Mécanique Appliquée et Théorique*, Vol. 2, 1. , pp 71-84.
- Trad A., Robit P., Limam A. (2009), Essais de freins, Technical report, G.T.S. - Travaux Géotechniques et de Sécurisation, 29 p.

## Dissipating devices for rockfall protection kits

Benoît Boutillier<sup>1</sup>, Abdelmoumen Marzouk<sup>2</sup>

<sup>1</sup> HC Systec, Groupe HC, Le Pont de Claix, France  
[benoit.boutillier@groupehc.com](mailto:benoit.boutillier@groupehc.com)

<sup>2</sup> HC Systec, Groupe HC, Le Pont de Claix, France  
[hc.systec@groupehc.com](mailto:hc.systec@groupehc.com)

---

**Abstract.** The present study deals with dissipating devices used in rockfall protection kits. These elements are the main elements in a dynamic structure that has to stop the rocks that are falling with high energy. These devices are essential to stop the rocks as the structure can not intercept them without rupture from low energy (around 250kJ).

In this experiment, we have studied the behavior of different types of devices in real size tests with different parameters such as the diameter of cable or the tightening of nuts and bolts. The obtained results show interesting information to improve the design of rockfall protection kits.

**Keywords:** rockfall, protection, energy, dissipating devices, break.

---

### 1 Introduction

To protect against falling rocks, net protection kits are commonly used. This type of barrier is constituted of net sets, posts, cables and elements to dissipate the energy of the falling block (figure 1). To improve the design of rockfall protection kits, it is important to improve the performances of the dissipating devices. The performances of breaks can be divided into 4 characteristics as follows:

- Dissipation of energy per meter of displacement;
- Release strength;
- Forces applied to the connection during the impact;
- Possibilities to manage different types of devices with the minimum of items.

To improve the characteristics of dissipating device, we changed different parameters of two types of breaking system and tested them in real conditions independently of a structure. The results present interesting information to improve the design of rockfall protection kits.

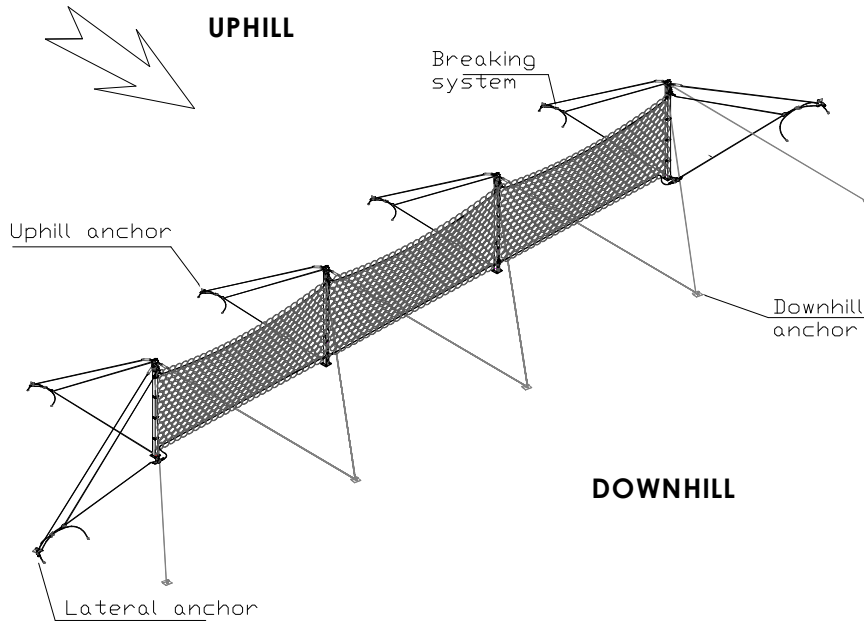


Figure.1. Example of rockfall protection kits with dissipating device

## 2 Dissipating devices

The tested dissipating devices are divided into two types of system: the *Simple Break* device – SB and the *Monobloc Break* device – MB. The system is composed of a set of cables tightened by some nuts and bolts between 2 types of steel plates. The steel of the plates has different mechanical properties. The dissipation will occur when the cable glide between steel plates tightened by nuts and bolts.

### 2.1 Simple Break device - SB

This type of break is composed of 2 cables and a set of steel plates, nuts and bolts (figure 2). The cables glide in opposite directions.

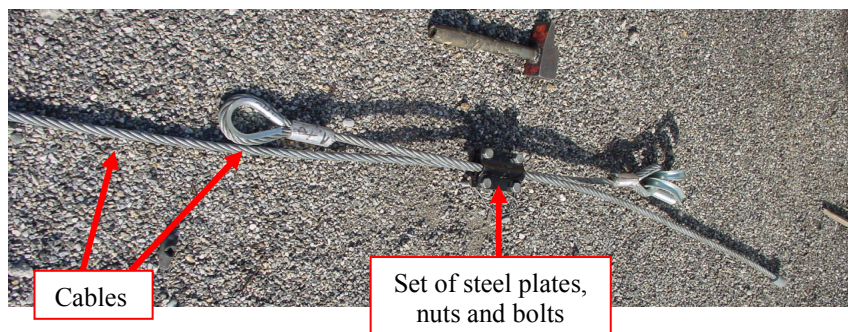


Figure.2. Example of *Simple Break* device – SB device

### 2.2 Monobloc Break device - MB

This type of break is composed of 2 cables with 2 strands and a set of steel plates, nuts and bolts (figure 3). The cables glide in the same direction.

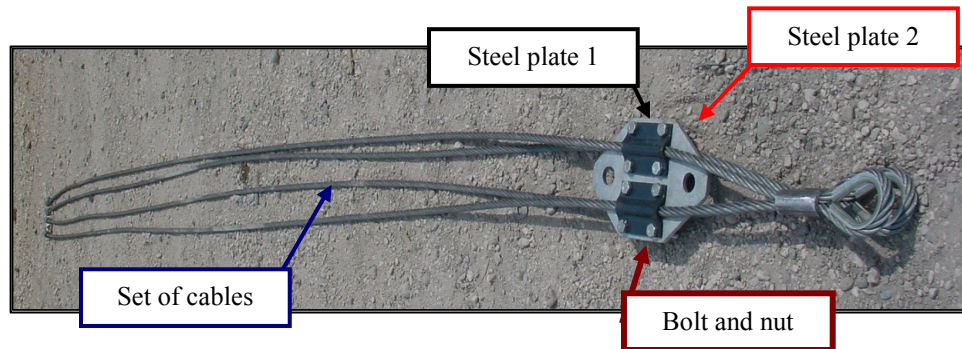


Figure.3. Example of *Monobloc Break* device – MB device

## 3 Tests

### 3.1 Protocol and parameters

Figure 4 presents tests to determine the characteristics of dissipating devices. One device is hooked up to an anchor. Under the break, a block (in concrete or a rock) is hung up. After lifting it with a crane, the block is released and is stopped by the breaking system. Videos of the tests are also recorded. A sensor is installed between the anchor and break to measure the applied forces, the measurement is done with a frequency of 1000Hz minimum. After the test, the displacement of the system is measured to determine its real capacity of dissipation.

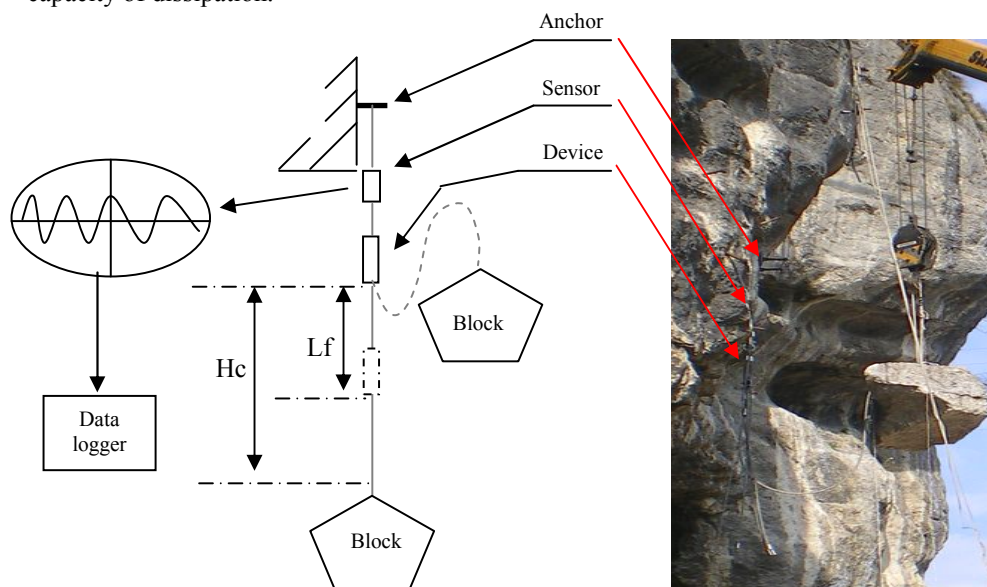


Figure.4. Real size test protocol for dissipating devices

Tests were done to improve the performances of these breaks; consequently, we have to determine the influence of different parameters. The main characteristic to improve is the dissipation per meter of displacement. It means raising the friction between cables and steel plates. This can be obtained with different solutions, by increasing

- the pressure applied by the steel plates on cable with the torque of nuts and bolts;
- the surface of friction (by increasing the diameter of cable);
- the length of friction.

For the latest, we used different solutions according to the type of break. For SB device, we added a new set of steel plates, nuts and bolts (left of figure 5). This device is called SBL device.

For MB device, the middle steel plate was extended and another set of steel plate 1 and bolts were also added (right of figure 5), it is called MBL.

Tables 1 and 2 present the total of tests done during this experiment.



Figure.5. 2 steel plates 1 for SB device (left) - Longer steel plate 2 for MB device (right)

Table.1. Parameter variations for tests

| Element       | Parameter           | Values  |
|---------------|---------------------|---|
| Steel plate 1 | Quantity            | 1 or 2 plates (SBL device, fig.5)                     |
| Steel plate 2 | Length of the plate | Standard or longer (MBL device, fig. 5)               |
| Cable         | Diameter            | D16mm or D20mm  |
| Bolt and nuts | Tightening          | Confidential data<br>7 values for each type of system |

Table.2. Number of tests according to parameter values

| Device                | Parameter                        | Quantity of tests |
|-----------------------|----------------------------------|-------------------|
| <i>Simple Break</i>   | Torque – 6 values                | 24                |
|                       | Cable diameter – 2 values        |                   |
|                       | Quantity of sets of steel plates |                   |
| <i>Monobloc Break</i> | Torque – 7 values                | 28                |
|                       | Cable diameter – 2 values        |                   |
|                       | Length of steel plates           |                   |

### 3.2 Results and comments

More than 50 tests were done for all of the parameters. The measurements of displacement of the system were also performed after each test. The energy applied and then the energy dissipated per meter of extension for each break was determined with the energy of the block and the displacement of the device (cf. Figure 6 and 7).

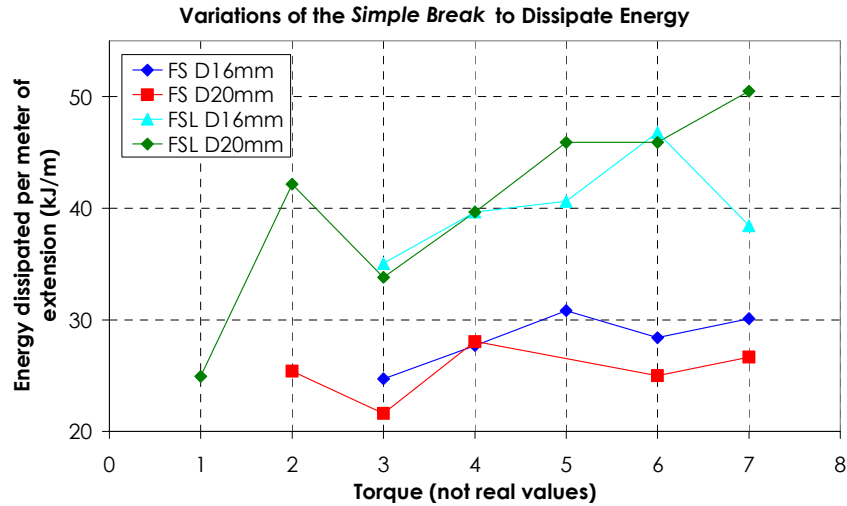


Figure.6. Variations of dissipated energy of SB and SBL devices according to different torque

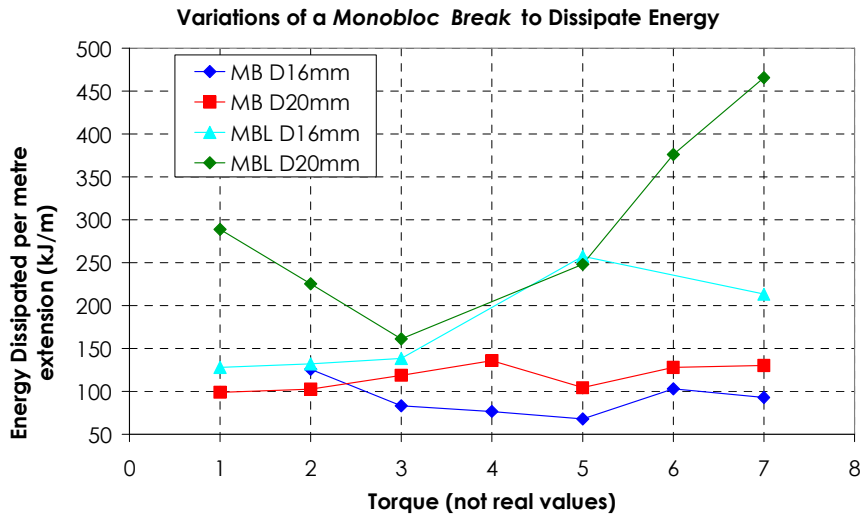


Figure.7. Variations of dissipated energy of MB and MBL devices according to different torque

The applied forces on anchor were also recorded with a minimum frequency of 1kHz. The average values for each type of dissipating device (for all torque values) are presented in table 3. The comparison of the variation of applied forces with the one of the dissipated

energies shows a different variation. For example, between MB16 and MBL20, a coefficient of 2.3 is applied for forces, whereas a coefficient greater than 3 is obtained in dissipated energies. It means the performance of dissipation increase more quickly than the forces applied to connection elements.

This study completes previous tests done in 2002 and 2004 for standard breaks: SB16 and MB16 (Hert, 2002; Boutillier, 2004); and real size tests were also done on a complete structure of 250kJ (Boutillier, 2008), during which the same results were obtained.

**Table.3.** Average values of applied force on anchor during dissipation (for example SB16 = Simple Break cable of D16mm)

| Break               | SB16 | SB20 | SBL16 | SBL20 | MB16 | MB20 | MBL16 | MBL20 |
|---------------------|------|------|-------|-------|------|------|-------|-------|
| Force (kN)          | 80   | 105  | 110   | 130   | 140  | 235  | 220   | 320   |
| Dissipation (kJ/ml) | 28   | 26   | 40    | 42    | 95   | 117  | 174   | 290   |

#### 4 Conclusion and perspectives

Very interesting results on dissipating devices were obtained with this study for each type of break. Even for each tightening only one test was done, the results showed some parameters such as diameter of cable and length of friction have real influence on the dissipation of energy.

These results are very important in the context of the new European standard, ETAG 27. These data opened new possibilities to develop new designs of rockfall protection structures for low and high energy level.

#### References

- Hert, D. (2002) Study on dissipating devices, test in real size conditions – Phase 1, *Confidential report*.
- Boutillier, B. (2004) Study on dissipating devices, test in real size conditions – Phase 2, *Confidential report*.
- Boutillier, B. and Idoux L. (2008) Rockfall protection barrier: A comparison between full scale tests and numerical modelling, Rockfall conference, Morschach.

## Discrete element simulation of an innovative metallic net dedicated to rockfall protection: a multi-scale approach

David Bertrand<sup>1</sup>, Ayman Trad<sup>1,2</sup>, Rémi Chauvel<sup>1</sup> and Ali Limam<sup>1</sup>

<sup>1</sup> INSA de Lyon, L.G.C.I.E. (Laboratoire de Génie Civil et d'Ingénierie Environnementale), Site Coulomb 2, 69621 Villeurbanne cedex, France  
E-mail: name.surname@insa-lyon.fr

<sup>2</sup> Travaux géotechnique et de sécurisation - G.T.S.  
29, rue des tâches, 69800 Saint Priest, France

---

**Abstract.** This paper focuses on a specific rockfall protection fence. Metallic nets are widely used in order to protect roads or infrastructures against rocks falling on a slope or coming from cliffs. Rockfall nets are particularly well suited to stop the blocks whose kinetic energy can reach 5000 kJ before impacting the defense structure. The main objective of these protection structures is to dissipate the block energy. The G.T.S. company proposes a new metallic fence and innovative energy dissipating systems have been developed. Discrete element simulations and experimental test have been performed in order to explore the mechanical response of the system under quasi-static and dynamic loadings. Several scales of study have been considered (the mesh, the net and the entire structure). The model calibration is described and a parametrical study is proposed to enhance the braking system under impact loading.

**keyword:** Metallic nets ; Rockfall protection structure ; Discrete element method ; Experimental tests ; Numerical simulations ; Dynamic.

---

## 1 Introduction

As a consequence of the urbanization of mountainous areas, more and more people are threatened by natural hazards such as falling rocks. Practitioners have a wide range of strategies and technologies to propose protection solutions (see for instance *Calvetti et al.* (1997), *Ikeda et al.* (1999), *Gotteland et al.* (2005), *Bourrier et al.* (2008), *Lambert et al.* (2009)). This study deals with passive protection systems (netting system) whose goal is to stop the boulder propagation after the cliff collapse. The net technology have been developed by the firm G.T.S. (France). This company proposes a new metallic fence and innovative energy dissipating systems (Figure 1a). Experimental tests (*Trad et al.*

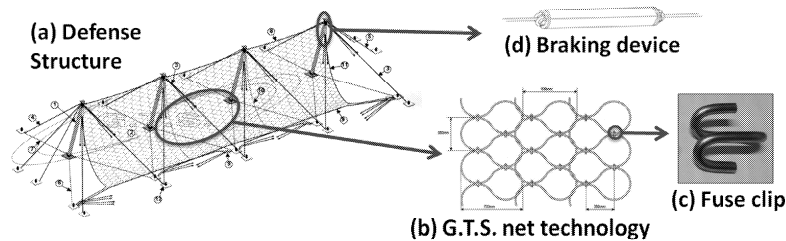


Figure 1: Metallic net technology : Entire defense structure (a), G.T.S. net (b), clip fuse (c) and braking device (d).

(2009b)) and numerical simulations (Discrete Element Simulations) have been performed in order to characterize the mechanical behavior of all structural elements of the net.

## 2 Structure technology

The G.T.S. net is woven using a single cable (Figure 1b). The production of the mesh is carried out thanks to fuse clips (Figure 1c). Moreover, the energy transfer to the cliff anchorages is reduced using a new braking device. The energy dissipation is carried out using frictional and buckling effects (Figure 1d).

## 3 Numerical modeling

The discrete element method (Cundall *et Strack*, 1979) is well suited to model these kind of netting systems (Bertrand *et al.* (2008)). The numerical method is based on particles interactions. The net is modeled by positioning spherical particles at cable and clip intersections. Then, the detection of interacting particles is carried out and finally suited interaction models are implemented into the code. The interaction models are initially assessed from experimental results (tensile tests) carried out both at the cable scale and at the clip scale. Moreover, two sizes of fuse clip are considered: A fuse clip at scale 1 and another one at scale 1/2. The first one has been used in order to perform tensile tests at a local scale of the net (*i.e.* the mesh scale) and the second one has been used for experimental punching tests on the net.

## 4 Study Scales

First of all, quasi-static experimental tests have been used to calibrate the numerical model at the mesh scale and at the net scale. Tensile tests have been performed at the mesh scale and punching tests at the net scale. After calibration, the numerical results are in rather

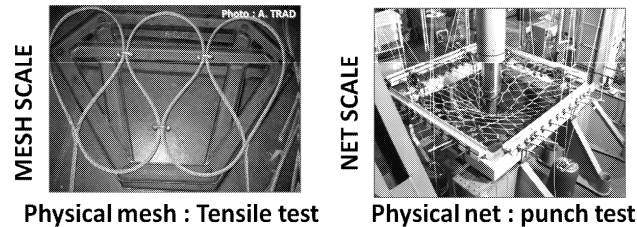


Figure 2: DEM modeling of the mesh (left graph) and of the net (right graph).

good agreement with the experimental measurements. Secondly, the entire structure has been modeled in order to explore its behavior under impact.

#### 4.1 Mesh scale - Tensile test

The figure 2 (left graph) depicts the tensile test performed at the mesh scale. The diameter of the cable is  $\phi = 12$  mm and fuse clips have been considered. The figure 3 (upper graph) shows a comparison between the numerical results and the experimental curves. In order to get this agreement between numerical and experimental results several parameters have been changed. On the one hand, in the case of fuse clips, the stiffness has been multiplied by two and the force at failure has been increased by 20%. On the other hand, the stiffness of the cable has been divided by 2.5 and the force at failure increase of 10%.

#### 4.2 Net scale - Punching test

The figure 2 (lower graph) depicts the punch test performed at the net scale. It consists in applying a normal force to the net plane of  $2 \times 2$  m<sup>2</sup>. Experiments are conducted on a half-scale model of the net. The cable diameter is 6 mm. Mesh and fuse clip sizes are reduced by half. A comparison between numerical results and experimental data is carried out on figure 3 (lower graph). Such as for the numerical model calibration at the mesh scale, interaction model parameters have been changed to fit the experimental curve. On the one hand, in the case of the cable, the stiffness has been divided by 2.5 and the maximum allowable force has been increased by 20%. On the other hand, the fuse clip stiffness has been multiplied by  $4/3$  and the force at failure has been increased by 40%.

#### 4.3 Discussion

In both cases, differences between experimental and numerical macroscopic responses can be explained from the behavioral dissymmetry of tested systems (mesh and net). This latter experimental feature is not taken into account in the numerical modeling. However, from an energetical point of view, agreements between experiments and numerical results

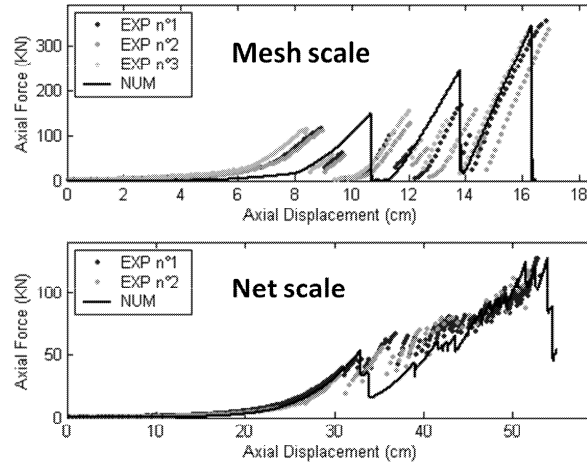


Figure 3: Mechanical response at the mesh and net scales. Numerical and experimental results comparison. The upper (resp. the lower) graph shows the evolution of the axial force as a function of the axial displacement for the tensile test at the mesh scale (resp. for the punch test at the net scale).

are good. Thus, because the energy dissipation is one of the main relevant parameter linked to the structure function (energy dissipation), it is supposed that the model is able to represent correctly the dynamical response of the entire structure under impact.

## 5 Dynamic behavior

The dynamical behavior of the net is explored by considering a spherical boulder impacting the defense structure at the center of the net. Experimental tests have brought interesting information concerning the energy dissipation capacity of the braking device using friction and buckling effects. The mechanical features of the latter have been implemented into the code.

### 5.1 Experimental test and modeling

Experimental tests have been performed in order to assess the energy dissipation ability of this kind of braking device (*Trad et al. (2009a)*) and the figure 4 shows the model proposed to represent it. After a linear increase by the force applied on the braking system, buckling phenomenon develops and leads to regular force oscillations until cable failure. From an experimental point of view, the energy dissipation of a braking system is around 240 kJ. The simulated structure is shown on figure 5. Supporting cables, beams, anchorage and the 6 braking devices are taken into account. Beams are modeled as rigid bodies.

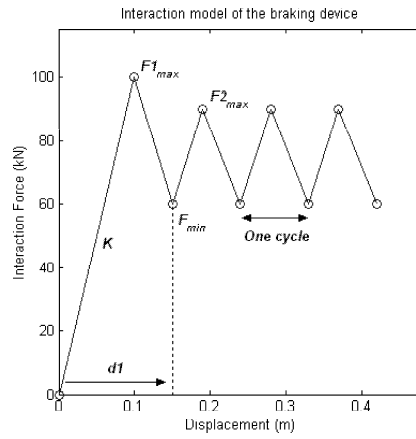


Figure 4: Interaction model proposed to describe the mechanical behavior of the braking system and associated parameters.

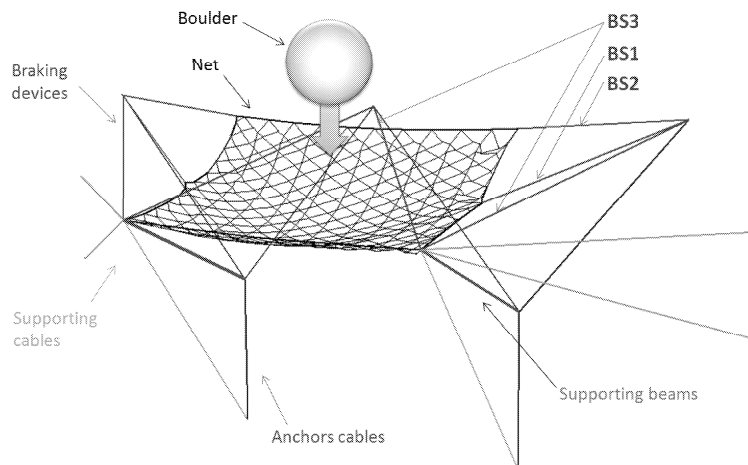


Figure 5: DEM modeling of the entire rockfall protection net where BS1, BS2 and BS3 point out brake's description.

| Parameter       | $C_{ref}$ | $C_1$ | $C_2$ | $C_3$ | Meaning                                  |
|-----------------|-----------|-------|-------|-------|--|
| $F1_{max}$ (kN) | 100       | 40    | 60    | 140   | Max. allowable force                     |
| $F2_{max}$ (kN) | 100       | 40    | 60    | 140   | Max. allowable force after the first pic |
| $F_{min}$ (kN)  | 60        | 24    | 36    | 84    | Min. allowable force after the first pic |
| $K$ (kN/m)      | 1000      | 1000  | 1000  | 1000  | Loading stiffness                        |
| $d1$ (cm)       | 15        | 15    | 15    | 15    | Displacement after the first cycle       |
| $N_c$ (-)       | 32        | 58    | 43    | 31    | Number of cycles                         |
| $E_d$ (kJ)      | 239       | 238   | 241   | 240   | Max. dissipated energy                   |

Table 1: Modeling parameters of the braking device used for the simulation campaign.  $C_i$  is related to the simulation  $i$  ( $i \in \{ref, 1, 2, 3\}$ ).

## 5.2 Impact simulation

In a sake of simplicity, the boulder is supposed to be spherical, its radius is 50 cm and its masse is 1300 Kg. The reference kinetic energy of impact is 409 kJ which correspond to a free falling height of 32 m. Several simulations have been performed to explore the influence of the maximum allowable force which can be supported by the braking system (*i.e.*  $F1_{max}$ ). Table 1 summarizes the parameters used for the simulation campaign. For each run, braking systems can absorb the same amount of energy than the experimental one. Eight brakes are considered in the structure model and their locations are given in the figure 5.

## 5.3 Brakes energy dissipation

The figure 6 shows the influence of  $F1_{max}$  on the mechanical response of the braking device and represents the evolution of the force as a function of the displacement inside BS1 and BS2 (on both sides of the net). The numerical results related to the BS3 brakes are not presented because they are not loaded during the impact. Indeed, a centered impact induces the distension of the cables on which the BS3 brakes are fastened and thus no energy dissipation can occur. Furthermore, the higher  $F1_{max}$ , the less the energy dissipation is. If  $F1_{max}$  is high, the magnitude of the forces transmitting through the anchorage cables do not reach  $F1_{max}$  and the buckling triggering do not occur. Thus, only elastic energy is stored inside brakes and there is no energy dissipation. The difference of brake response depending on the side of the net considered (n°1 vs. n°2) is due to the geometrical dissimetry of the structure model.

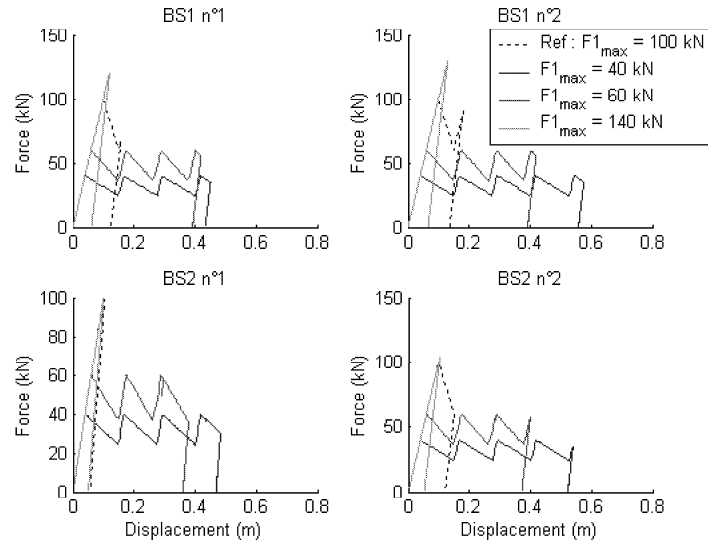


Figure 6: Mechanical response of brakes BS1 and BS2 from the simulation campaign (Table 1). n°1 (on the left) and n°2 (on the right) refers to both sides of the net.

## 6 Conclusion and perspectives

This paper presented a numerical approach to model a specific rockfall protection net using fuse clips and friction/buckling braking systems to dissipate energy. The DEM has been used and a multi-scale approach allowed exploring the mechanical response of the net under quasi-static (tensile and punching test) and dynamic (impact) loadings. Globally, numerical results are encouraging. After calibration, simulations are able to reproduce the experimental data at both scales (mesh and net).

For the tensile test on the mesh and the punch test at the net scale, a very similar mechanical behavior is observed. The main difference comes from the intrinsic symmetry of the numerical model (geometry and force distribution). For the impact test, the proposed study was carried out to explore the influence of the braking device features on the global energy dissipation of the rockfall protection structure. To dissipate energy inside the braking devices, these latter have to be design such as a weak structural element in order to concentrated the energy dissipation. In the opposite case, if the net is not able to absorb all the incident energy, the boulder would perforate the net. The calibration of numerical simulations was carried out from an heuristic point of view and it allows to justify the relevance of the numerical model to simulate the experiments. The validation of a numerical model makes it possible to perform parametrical studies dedicated to enhance the net efficacy.

As perspectives, the spatial heterogeneity of the stiffness and the strength of the net could

be taken into account. This intrinsic feature of real nets controls the failure modes. It's a random process which has to be considered from an average point of view. It will certainly improve the numerical description of the mechanical response.

## References

- Bertrand, D., F. Nicot, P. Gotteland, et S. Lambert, Discrete element method (dem) numerical modeling of a double-twisted hexagonal mesh, *Canadian Geotechnical Journal*, 45, 1104–1117, 2008.
- Bourrier, F., F. Nicot, et F. Darve, Physical processes within a 2d granular layer during an impact, *Granular Matter*, 10 Issue: 6, 415–437, 2008.
- Calvetti, F., R. Genchi, L. Nesta, et R. Nova, Numerical simulation of rock block impacts on rigid sheds, *Numerical Models in Geomechanics*, pp. 635–640, 1997.
- Cundall, P., et O. Strack, A discrete numerical model for granular assemblies, *Geotechnique*, 29 (1), 47–65, 1979.
- Gotteland, P., D. Bertrand, S. Lambert, et F. Nicot, Modelling an unusual geocomposite material barrier against a rockfall impact, *Proc. of the 11<sup>th</sup> Int. Congr. of IACMAG Torino (Italy)*, pp. 529–536, 2005.
- Ikeda, K., N. Kishi, R. Kawase, H. Konno, et O. Nakano, A practical design procedure of three-layered absorbing system, *Joint Japan-Swiss Scientific Seminar on Impact Load by Rock Falls and Design of Protection Structures - Kanazawa (Japan)*, 113–119, 1999.
- Lambert, S., D. Bertrand, F. Berger, et C. Bigot, *Proceedings of the international symposium on protection and simulation methods for geohazard mitigation (IS-Kyoto2009)*, in , pp. 133–138, Kyoto, Japan, 2009.
- Trad, A., P. Robit, et A. Limam, Essai de frein, *Tech. rep.*, G.T.S. - Géotechnique et Travaux Spéciaux, 2009a.
- Trad, A., P. Robit, A. Limam, D. Bertrand, et F. Delhomme, Etude du comportement des filets de protection : approches expérimentale et numérique (mef), in *XXVII<sup>èmes</sup> rencontres AUGC 2009*, vol. 03, édité par Association Universitaire de Génie Civil, p. 14, 2009b.

## A numerical model for the design of low energy rockfall protection nets

Franck Bourrier<sup>1</sup>, Christophe Bigot<sup>1</sup>, David Bertrand<sup>2</sup>, Stéphane Lambert<sup>3</sup>, Frédéric Berger<sup>1</sup>

<sup>1</sup> Cemagref - UR EMGR, Grenoble, France  
[franck.bourrier@cemagref.fr](mailto:franck.bourrier@cemagref.fr), [christophe.bigot@cemagref.fr](mailto:christophe.bigot@cemagref.fr), [frederic.berger@cemagref.fr](mailto:frederic.berger@cemagref.fr)

<sup>2</sup> LGCIE - INSA, Lyon, France  
[david.bertrand@insa-lyon.fr](mailto:david.bertrand@insa-lyon.fr)

<sup>3</sup> Cemagref - UR ETGR, Grenoble, France  
[stephane.lambert@cemagref.fr](mailto:stephane.lambert@cemagref.fr)

---

**Abstract.** The analysis of impact experiments on low energy rockfall protection structures allowed building a model based on the Discrete Element Method for the design of these structures. The simulations held using this model highlighted that the efficiency of the structure is strongly depending on the impact conditions. The identification of relevant impact conditions for the design of rockfall protection structures is therefore a difficult task in which using numerical models is of great interest.

**Keywords:** Rockfall, Protection structures, Discrete Element Method, Impact.

---

### 1 Introduction

In mountainous regions, the frequent silvicultural interventions (wood felling, opening of forest roads...) required for forest management can temporarily turn a site previously associated with low rockfall hazard to a potentially dangerous site. In this context, there is a real need for the development of temporary rockfall protection structures for the duration of forestry works.

The innovative temporary protection solution proposed consists of a rockfall catchment fence made of a cable supported wire mesh tightened between two trees. These fences should be installed as close as possible from the probable rock departure points. The impacting rock velocity therefore remains smaller than 25m/s which is the maximum velocity of rocks on forested slopes (Dorren et al., 2005). Thus, considering the range of mass of the rocks to be stopped, the kinetic energy is expected to be less than 200kJ which is a low value for rockfall protection structures. The efficiency of these temporary structures is investigated based on real scale impact experiments complementarily with discrete modeling of the structure. The results from the experiments are qualitatively

analyzed to build a relevant model of the impact of a rock on low energy protection nets. The model is then used to investigate the efficiency of these structures depending on the impact conditions.

## 2 Experiments

The experiments consisted in impacting protection nets with boulders of varying mass. The nets were composed of a 25m long and 3m high fence connected to two support trees by three horizontal cables fixed by cable clips (figure 1a). The diameters of the upper and of the bottom cables were 12mm and the intermediate cable had a 8 mm diameter. Vertical rods fixed between the horizontal cables (figure 1a) prevent the distance between the cables from reducing and ensure vertical rigid boundaries to the fence.

17 impact experiments were performed on four nets having the previously exposed characteristics using rocks ranging from 30 to 500kg. For this purpose, a zip wire was installed perpendicularly to the structure to convey a trolley supporting impacting rocks that were dropped just before the impact on the fence at velocities ranging from 14 to 17m/s. The tension in the upper cable of the fence and the tree acceleration were continuously measured during the impact using a dynamic force sensor. In addition, a qualitative analysis of the damages and deformations of the mesh was performed after each impact.

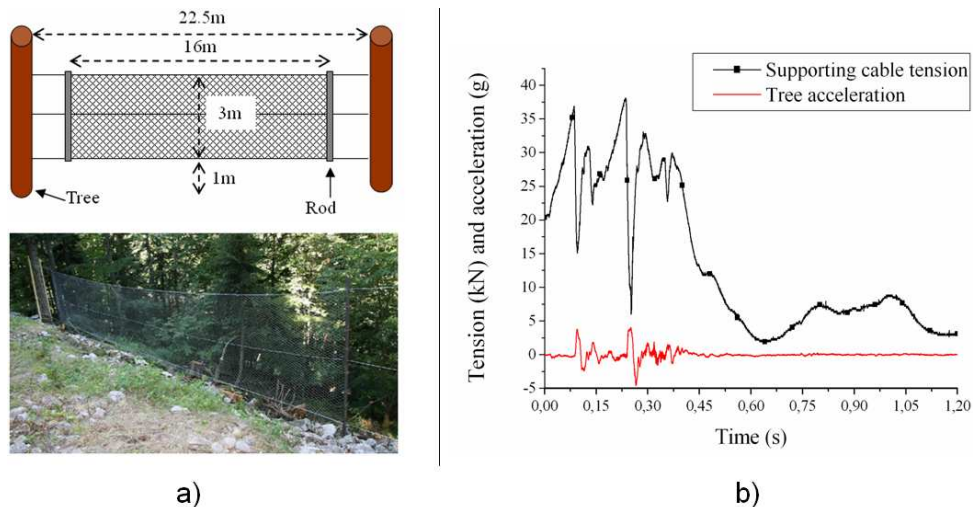


**Figure.1.** a) Description of the structure used in the experiments. b) Time evolution of the tension in the cable and of the acceleration of the tree measured during an impact

The experimental results showed that, during the impact, the tension in the cable increased rapidly (figure 1b) until the cable clips fixing the horizontal cables slip. The clips' slipping was related with a threshold of the upper cable's force around 30kN disturbed by sudden forces drops (figure 1b). The slipping of the cable clips resulted in differences in the static tension in the cable before (20kN – figure 1b) and after (approx. 5kN – figure 1b) impact. The time evolution of the trees acceleration (figure 1b) suggests that tree

displacements were minor and mainly related with the sudden variations in the cable tension. The qualitative analysis of the experiments also showed that the rupture of the wires of the mesh only slightly propagates through the mesh during the impact which is in accordance with previous results (Agostini et al., 1987).

### 3 DEM simulation of the impact on low energy protection nets

The protection net was modeled using the Discrete Element Method (DEM). The DEM is classically used to model the behavior of a collection of interacting particles under static or dynamic loadings. The DEM is also well suited to tackle impact problems inducing large strains and damage of the structure. Rockfall protection nets were previously modeled using this method (Hearn et al., 1995 ; Nicot et al., 2001).

The model of the structure is based on a DEM model of wire netting meshes developed by Bertrand et al. (2008). The initial model was adapted to account for the geometry of the fence, the modeling of the cables and rods, and the boundary conditions. The wire netting mesh is described as a set of spherical particles located at the intersections of the wires of the mesh (figure 2). First, the interaction between the boulder and the mesh particles is modeled by contact forces applied both on the projectile and on the mesh particles in contact. The force applied to the projectile is therefore the sum of all contact forces with the wire netting mesh particles. In addition, interaction forces representative of the mechanical behavior of the wires of the mesh are applied between adjoining mesh particles. These forces are calculated from the distance between the particles using elasto-plastic models characterized from experimental results. Additional details on these interaction models can be found in Bertrand et al., 2008. The resultant force on each particle of the mesh is therefore the sum of the contact force with the projectile and of the interaction forces with the adjoining mesh particles.

The supporting trees are assumed to be rigid compared with the structure. Only the bottom, the top cables, and the vertical rods are therefore modeled (figure 2). To model the vertical rods, the vertical boundary particles of the mesh are fixed one towards the others (figure 2). In addition, the horizontal supporting cables are modeled by adding interaction forces between the horizontal boundary particles of the mesh (figure 2). These forces are calculated from the distance between the particles using an elastic model fully characterized by the cable diameter and the Young modulus ( $E_{cable} = 140000\text{MPa}$  ; Irvine, 1981). Finally, the cable clips and the part of the cable connecting the mesh to the trees are modeled by interaction forces between particles located at the corners of the mesh and fixed particles located on the trees. These interaction forces are determined using an elasto-frictional model which accounts for the slipping of the cable clips during the impact. If the interaction force is lower than a threshold value  $F_{slip} = 40000\text{N}$ , it is calculated using the elastic model for the horizontal cables. If the threshold value  $F_{slip}$  is reached, the interaction force is equal to  $F_{slip}$  for any distance between the particles.

In a first phase, a simulation under gravity loading is held to reach the static equilibrium of the structure. Second, the impact is simulated. A spherical projectile is then located at the impact point and initial kinematical conditions are applied to the projectile. For each impact simulation, the time evolutions of the forces in the cables and on the projectile are recorded as well as the projectile trajectory and the number of broken wires of the mesh.

As the model developed is not yet usable for real-scale simulations because of excessive computational durations, a simulation campaign was performed to investigate the influence of the parameters related with the rock kinematics (velocity, incidence angle,

rotational velocity, mass, impact point) during the impact of rocks on a 4m long and 2m high net. Simulations were done for different rock masses ranging from 25 to 100kg and for translational velocities ranging from 5 to 20m/s. The rotational velocity of the boulder was nil at the beginning of the simulations. Simulations were performed for three impact points (point 1: in the centre of the wire mesh, point 2: horizontally centered and at a 3/4 height of the mesh, point 3: at a 1/4 height of the mesh vertical and horizontal distance from the top left corner of the mesh). Finally, the incidence angle  $\alpha^{in}$ , that is the angle between the incident velocity and the horizontal direction in the  $yz$  plane (figure 2), varied from  $-40^\circ$  to  $40^\circ$ .

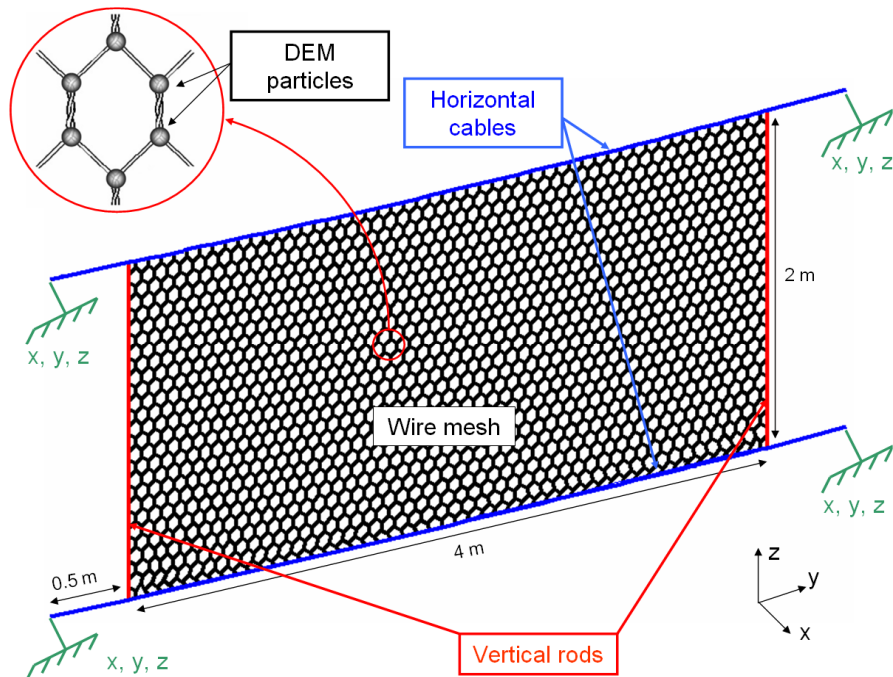


Figure.2. Overview of the DEM model of the protection net.

## 4 Results

The simulation results first show that the interaction between the projectile and the structure can be divided into a tension phase followed by a restitution phase. During the tension phase, an increase in the tension of the horizontal cables occurs conjointly with an increase in the force applied to the projectile (figure 3a). Once the threshold value  $F_{slip}$  for the tension of the horizontal cables is reached, the tension in the cable remains constant whereas the force applied to the projectile keeps increasing more slowly (figure 3a – from 0.75s to 1.1s). During the tension phase, large strains first occur in the mesh until it reaches a position allowing the stretching of the mesh that can potentially lead to the breakage of several wires. One can note that the breakage of the wire mesh exclusively occurs during this phase and is always limited to the wires near the impact point. If the wire mesh does not break, a restitution phase starts when the kinetic energy of the

projectile reaches a minimum value (figure 3a). This phase is marked by decreases in the force applied to the projectile and in the tension inside the cables (figure 3b). Finally, one can note that, included for normal impacts, the direction of the velocity after impact is significantly changed because all velocity components are strongly different before and after impact (figure 3b).

The simulations also show that, for a given incident kinetic energy, the projectile is stopped by the structure or not depending on the impact conditions. This can be deduced from the evolution of the horizontal displacement of the projectile during one simulation

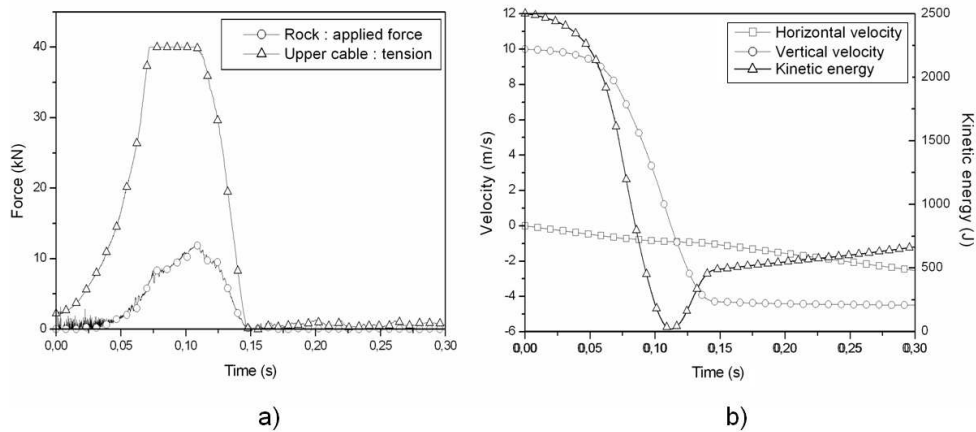


**Figure.3.** a) Time evolution of the forces applied to the projectile and tension inside the upper horizontal cable and b) Time evolution of the vertical, horizontal velocity components and of the kinetic energy of the projectile in the case of a normal impact ( $\alpha^{in} = 0^\circ$ ) by a 50kg projectile impacting the centre of the fence

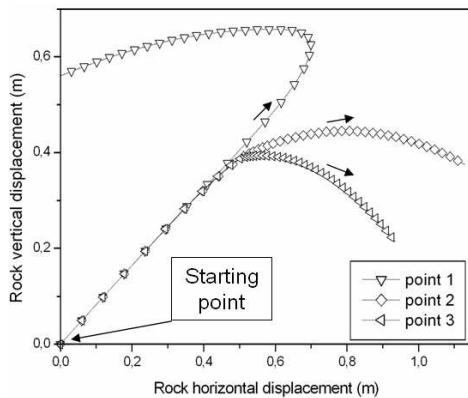


**Figure.4.** Displacement of the projectile for different impact locations in the case of a 50kg projectile with a 10m/s incident velocity and an  $\alpha^{in} = 40^\circ$  incidence angle.

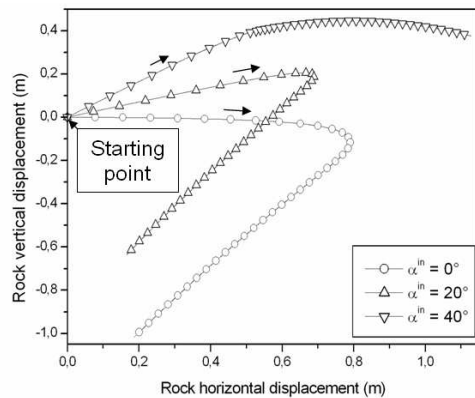


**Figure.5.** Displacement of the projectile for different incidence angles in the case of a 50kg projectile with a 10m/s incident velocity

(figure 4 and 5): if the horizontal displacement of the projectile decreases after increasing, the projectile is stopped; if it always increases, the projectile passes through the structure. In particular, the results highlight that the structure efficiency is strongly depending on the incidence angle (figure 4). Structure breaking can be observed for high incidence angles whereas it is not observed for normal impacts (figure 4). Moreover, the structure efficiency is also related with the location of the impact point (figure 5). Structure breaking are not observed for impacts in the centre of the structure (point 1 – figure 4) whereas it is observed on other points nearer the mesh boundaries (points 2 and 3 – figure 5). These two examples clearly demonstrate that the approach consisting in using normal impacts in the centre of the structure for design purposes can be misleading.

## 5 Conclusion

In this paper, an approach based on the qualitative analysis of experimental results allowed defining a model usable for the design of temporary rockfall protection nets from a DEM model of wire netting meshes. A simulation campaign allowed identifying the mechanisms occurring during the interaction between the projectile and the protection structure. In addition, counter-intuitive results - related with the influence of the impact conditions on the structure efficiency - emphasized the potential difficulties to determine relevant impact conditions for design purposes. These difficulties can be overcome by using numerical simulations.

## References

- Agostini R., Cesario L., Conte A., Masetti M., Papetti A. (1987) *Flexible gabion structures in earth retaining works*. Officine Maccaferri S.p.a, Bologna.
- Bertrand D., Nicot F., Gotteland P., Lambert S. (2008) DEM numerical modelling of double-twisted hexagonal wire mesh, *Canadian Geotechnical journal*, Vol 45, pp 1104-1117.
- Dorren L.K.A., Berger F., Le Hir C., Mermin E., Tardif P. (2005) Mechanics, effects and management implications of rockfall in forests, *Forest ecology and management*, Vol 215, pp 183-195.
- Hearn G., Barrett R. K., Henson, H. H. (1995) Development of effective rockfall barriers, *Journal of transportation engineering*, Vol. 121, n° 6, pp 507-516.
- Irvine M. (1981) *Cable structures*, MIT Press, Cambridge.
- Nicot F., Cambou B., Mazzoleni G. (2001) Design of Rockfall Restraining Nets from a Discrete Element Modeling, *Rock mechanics and rock engineering*, Vol 34, n° 2, pp 99-118.

## Hydration induced meso-stresses in concrete and their consequences on the cyclic behavior

C. La Borderie<sup>1</sup>, M. Matallah<sup>1,4</sup>, T.D. NGuyen<sup>1</sup>, M. Briffaut<sup>2</sup>, F. Benboudjema<sup>2</sup>, JM. Torrenti<sup>3</sup>

<sup>1</sup> LaSAGeC, UPPA, Allée du parc Montaury, 64600 Anglet, France.

<sup>2</sup> LMT, ENS Cachan, 61 Avenuedu Prsident Wilson, 94235 Cachan. France

<sup>3</sup> LCPC 58, boulevard Lefebvre 75732 Paris Cedex 15. France

<sup>4</sup> RISAM, Univertsité de Tlemcen, BP 230 Algérie.

---

### Abstract.

The hydration process of concrete involves heating, progressive hardening, shrinkage. It is well known that this process can create cracking of large structures, but, depending on the concrete mixture used, leaves usually small specimens elastic. In the Case of small specimens, strain mismatch between past and aggregates generates autogeneous stresses in concrete. Even if this state of stress does not affect the elasticity properties of concrete it modifies the initial conditions of any concrete structures. We propose to compute the initial state of stress in concrete at the mesoscopic level and show that this state of stress is at the origin of a part of the inelastic strains that go with damage and the so called “crack closure stress” under cyclic loading.

**keyword:** Hydration, Damage, Cyclic behaviour

---

## 1 Introduction

Durability and service life of massive concrete structures are significantly influenced by the early age behaviour. Evaluation and description of cracks which may occurs at early age are therefore essential. Over the last decade, besides rather empirical formulations [7][4], numerical material models were developed for the description of the mechanical behaviour of concrete at early age [8][1]. Theses models are basically drawn from the experimental studies.

The hydration process is characterized by : a thermal expansion (due to the heat released by exothermic chemical reactions) and shrinkage (autogeneous and drying shrinkage). Due to these chemical reactions and the formation of hydration products, the materials properties are continuously evolving. The structure of concrete is related to the formation of hydrates product during the chemical reaction. So, from these physical considerations, a practical approach will be to consider the hydration degree as a fundamental parameters

to study the early age behaviour[9]. It is also well known that during the hydration process, the cement paste is the only evolving component of concrete. Considering concrete as a multi-scale composite is therefore unavoidable.

In this paper a finite element analysis is performed to simulate the early age behaviour for concrete at mesoscopic scale. Concrete is considered as a bi-phasic material. The numerical modelling process is driven by the degree of hydration. Based on the experimental studies, the evolution of the mechanical properties that describe strength and stiffness of the cement paste are related to the hydration degree. The cracking behaviour is simulated using a damage-plastic model.

The simulations are performed with the Cast3M finite element code [Cast3M] on a small specimen. We propose to compute the initial state due to the hydration process. This initial state is at the origin of ,at least, a part of inelastic strains which induce damage. Under cyclic behaviour, the initial stress state modifies the so called “the crack closing process behaviour”. The aim of these first results is to show that the hydration influences the behaviour of concrete even for small specimen. The hydric process is not modelled in these first computations and we suppose that there is water enough for hydrating the cement. The early age creep is neither modelled, the shrinkage parameters for the cement paste are chosen smaller than the classical values in order to avoid complete cracking of concrete.

Firstly, we recall the theoretical formulations. Furthermore, the numerical simulation of the hydration process are presented. Finally the effect of the early age state on the cyclic behaviour is illustrated.

## 2 Theoretical fundamentals

### 2.1 Chemo-thermal model

The hydration of cement paste is a thermo-activated process. Its evolution is modelled by the following relations [10][8].

$$\dot{\xi} = \tilde{A}(\xi) \exp\left(-\frac{E_a}{RT}\right) \quad (1)$$

in which  $\dot{\xi}$  is the rate of the degree of hydration,  $\tilde{A}(\xi)$  is the normalized affinity.  $E_a$  is the activation energy ( $Jmol^{-1}$ ) (considered as constant).  $R$  is the constant of perfect gaz ( $8.314Jmol^{-1}k^{-1}$ ) and  $T$  is the temperature in Kelvin.

The evolution of temperature is obtained from the energy balance equation, which includes the release of heat due to the hydration reaction :

$$C\dot{T} = \nabla(k\nabla T) + L\dot{\xi} \quad (2)$$

Where  $C$  is the volumetric heat capacity,  $k$  is the thermal conductivity ( $Wm^{-1}k^{-1}$ ) and  $L$  is the latent heat of hydration ( $Jm^{-3}$ ).

## 2.2 Endogenous and thermal shrinkage model

As concrete hardens, autogeneous shrinkage develops. Autogeneous shrinkage is therefore related to the evolution of hydration. Experimental results show that autogeneous shrinkage evolution is linear with respect to the hydration degree as soon as a threshold has been overcome [5]. Autogeneous shrinkage  $\varepsilon_{au}$  can be modelled by [10]:

$$\dot{\varepsilon}_{au} = -k\dot{\xi}I \quad \text{for } \xi > \xi_0 \quad (3)$$

$k$  is a constant parameters,  $I$  is the unit tensor and  $\xi_0$  is a threshold.

The thermal strain  $\varepsilon_{th}$  is related to the temperature variation, due to the release of heat by hydration, and the coefficient of thermal expansion  $\alpha$  (considered as constant) :

$$\dot{\varepsilon}_{th} = -\alpha\dot{T}I \quad (4)$$

## 2.3 Damage-plastic model

### 2.3.1 Damage part

The fichant's plastic damage model is used [2]. For the isotropic version of this model, the relationship between stress and strain reads :

$$\sigma_{ij} = (1 - d)\tilde{\sigma}_{ij} = (1 - d)C_{ijkl}\varepsilon_{kl}^e \quad (5)$$

Where  $d$  is the damage variable,  $C_{ijkl}$  is the initial stiffness tensor. The evolution law of the scalar damage variable is given through the normality rule using the following loading function :

$$f = \varepsilon - \varepsilon_{d0} - \chi \quad (6)$$

Where  $\varepsilon_{d0}$  is the damage threshold.  $\chi$  is a hardening parameter. The evolution law is written as

$$d = 1 - \frac{\varepsilon_{d0}}{\varepsilon} \exp[B(\varepsilon_{d0} - \varepsilon)] \quad (7)$$

$B$  is a parameter that controls the slope of the softening curve.,

### 2.3.2 Plastic part

In order to allow a fracture energy regularization, the plastic part of the model is modified. The Nadai plastic criterion is replaced with a drucker prager one :

$$\begin{cases} F_t = \alpha_t J_2(\tilde{\sigma}_{ij}) + \beta_t I_1(\tilde{\sigma}_{ij}) - w(p) - w_0 \\ F_c = \alpha_c J_2(\tilde{\sigma}_{ij}) + \beta_c I_1(\tilde{\sigma}_{ij}) - w(p) - w_0 \end{cases} \quad (8)$$

Where  $I(\sigma)$  and  $J_2(\sigma)$  are the first and the second invariant.  $(\alpha_t, \beta_t), (\alpha_c, \beta_c)$  are four constant parameters.  $w_0$  is the elastic domain in the stress space.

For the plasticity hardening, a linear plastic evolution is considered :

$$w = q * p + w_0 \quad (9)$$

Where  $p$  is the effective plastic strain and  $q$  is a constant parameters.

## 2.4 Evolution of the model parameters with respect to the hydration degree [9]

### Young Modulus

$$E(\xi) = E_\infty \bar{\xi}^\beta \quad (10)$$

with  $\bar{\xi} = \langle \frac{\xi - \xi_0}{\xi_\infty - \xi_0} \rangle_+$  in which  $\xi_0$  is the mechanical percolation threshold. It is kept constant and equal to 0.1.

$\xi_\infty$  is the final hydration degree.  $E_\infty$  is the final Young Modulus,  $\beta$  is a constant equal to 0.62.

$\langle \rangle_+$  is the positive part operator.

### Poisson ratio

$$\nu = (0.18 * ((\sin(\pi * \xi)/2)) + (0.5 * (\exp(-10 * \xi)))) \quad (11)$$

### Tensile strength

$$f_t(\xi) = f_{t\infty} \bar{\xi}^\gamma \quad (12)$$

where  $f_{t\infty}$  is the final tensile strength.  $\gamma$  is taken equal to 0.46

The evolution of the tensile strain threshold is computed from the evolution of  $f_t$  and  $E$ .

$$\varepsilon_{d0}(\xi) = \frac{f_t(\xi)}{E(\xi)} = \frac{f_{t\infty}}{E_\infty} \bar{\xi}^{\gamma-\beta} = \varepsilon_{d0\infty} \bar{\xi}^{\gamma-\beta} \quad (13)$$

### Fracture energy

The fracture energy is represented by the stress-crack opening displacement curve under tension. Using the damage-plastic formulation, the fracture energy is given by :

$$G_f = h \frac{f_t}{B(1 - \mathcal{H})} \quad (14)$$

with

$$\mathcal{H} = \frac{E}{E + \frac{q}{dF_t/d\bar{\sigma}}} \quad (15)$$

The length scale which is introduced into the model is the element size  $h$ . For the numerical simulation, the damage parameter  $B$  is function of  $h$  and controls the slope of the strain softening curve. The parameter  $B$  is given by :

$$B = h \frac{f_t}{G_f(1 - \mathcal{H})} \quad (16)$$

So, using the evolution equation of  $f_t$  and  $G_f$ , we propose the evolution of  $B$  as :

$$B(\xi) = B_\infty \bar{\xi}^{\gamma - \alpha} \quad (17)$$

With  $B_\infty = h \frac{f_{t\infty}}{G_{f\infty}(1 - \mathcal{H})}$ , and  $\alpha = 0.8$

### 3 Numerical Simulation of the hydration process :

The formulation proposed has been implemented in the Finite Element Code Cast3M. An elementary test is proposed for validation. An original method to mesh the mesoscopic geometry of concrete is used with a diffuse representation of the material [6]. The test is performed on a  $(100 * 100) \text{ mm}^2$  specimen in 2D plane stresses (Figure 1).

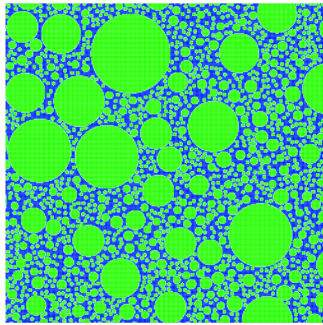


Figure 1. Mesoscopic mesh

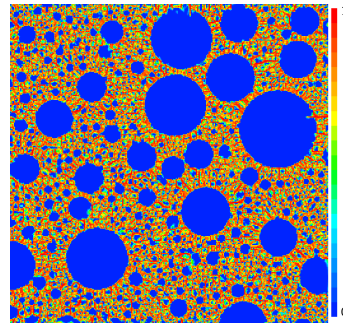


Figure 2. Damage field

Figure 2 shows the damage field. As the creep behaviour has not been taken into account we choose a small value for the shrinkage parameters  $k = 3e - 3$  (compared with that given by the experimentation  $k = 6e - 3$  [11]).

### 4 Numerical simulation of the mechanical behaviour under cyclic loading

In the case of cyclic loading, during the load reversals, micro cracks close progressively and the tangent stiffness of the material should increase. In the damage model proposed in section 2.3, the unilateral condition is taken into account by a separation of the stress tensor into positive and negative parts. In case of cyclic loadings the stress is given :

$$\sigma = (1 - d)\tilde{\sigma}_+ + (1 - d)^\alpha \tilde{\sigma}_-$$

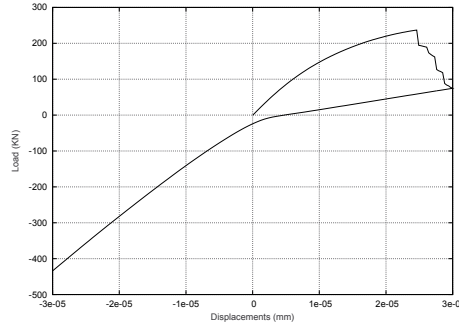


Figure 1: Global behavior under cyclic loading

Where  $\sigma_+$  and  $\sigma_-$  are the positive and the negative part of the stress tensor.  $\alpha$  is a constant parameter and  $d$  the damage variable.

If we consider the damage model without plasticity. As the closing process is driven by the stress tensor sign, the crack closure stress is equal to  $\sigma_c = 0$  Mpa.

If we consider now the specimen tested above. The behaviour at early age computed is considered as an initial state (stresses, internal variables, displacements). The specimen is subjected to a loading cycle (tension-compression cycle). Figure 2 shows the global behaviour.

Due to the presence of the initial stress state. The crack closing stress is modified. The crack closing stress takes a negative value, different from that imposed by the model ( $\sigma=0$ ).

## 5 Conclusion

A numerical Thermo-Hydro-Mechanical procedure has been presented in this article. Based on the experimental observations, the early age behaviour is driven by the degree of hydration  $\xi$ . Implemented in a Finite Elements code (Cast3M), the procedure gives the initial state of concrete (stress, strain, internal variables). Regarding the cyclic behaviour, the initial stress state due to the hydration process seems to play an important role. The value of the crack closure stress is modified. A negative value is obtained instead of the classical one imposed by the model ( $\sigma = 0$ ). Experimentally, the material recovers its stiffness completely at a compression stress state. Taking the early age behaviour as an initial state seems to be a good solution to reproduce the experimental crack closure effect.

## References

- [1] F. Benboudjema and J.M Torrenti. Early-age behavior of concrete nuclear containment. *Nuclear Engineering and Design*, 238:2495–2506, 2008.

- [2] S. Fichant, C. La Borderie, and G. Pijaudier-Cabot. Isotropic and anisotropic description of damage in concrete structures. *Mech. Cohes.-Frict Mater.*, 4:339–359, 1999.
  - [3] M. Matallah, C. La Borderie, and O. Maurel. A practical method to estimate crack openings in concrete structures. *Int. J. Nume. Analy. Meth. Geomechanics*, Accepted.
  - [4] G. Meschke. Consideration of aging of shotcrete in the context of a 3d viscoplastic material model. *Int. J. Num. Meth. Eng.*, 39:23–43, 1996.
  - [5] P. Mounanga, V. Baroghel-Bouny, A. Khelidj and A. Loukili. Autogenous deformations of cement pastes. part i: Temperature effects at early age and micro-macro correlations. *Cement Concrete Res.*, 36:110–122, 2006.
  - [6] T.D. Nguyen, C. Lawrence, C. La Borderie, M. Matallah and G. Nahas. A mesoscopic approach for a better understanding of the transition from diffused damage to localized damage. *EJECE*, Soumis, 2009.
  - [7] Y-Z Niu, C-L Tu, R-Y Liang, and S-W Zhang. Modelling of thermodynamical damage of early-age concrete. *J. Eng. Mech.*, 121(4):717–726, 1995.
  - [8] R. Lackner and H.A. Mang. Chemoplastic material model for the simulation of early-age cracking: from the constitutive law to numerical analysis of massive concrete structures. *Cement Concrete Compos.*, 26:251–562, 2004.
  - [9] G. De Schutter. Finite element simulation of thermal cracking in massive hardening concrete elements using degree of hydration based material laws. *Computers & Structures*, 80:2035–2042, 2002.
  - [10] F-J. Ulm and O. Coussy. Couplings in early age concrete: from material modeling to structural design. *Int. J. Solids Struct*, 35(31/32):4295–4311, 1998.
  - [11] I. Jaouadi. Étude numérique et expérimentale du retrait endogène de la pâte de ciment au jeune âge *Thèse de Doctorat. École Polytechnique Fédérale de Lausanne*, 2008.
- [Cast3M] Cast3M. Finite element code <http://www-cast3m.cea.fr>.



## Impact characterization on a concrete slab using the inverse method

Pascal Perrotin<sup>1</sup>, Zoheir Boukria<sup>2</sup>, Abdel Bennani<sup>3</sup>, Ali Limam<sup>4</sup>

<sup>1</sup> LOCIE (CNRS FRE3220-Université de Savoie, VOR), Polytech Annecy-Chambéry, France, pascal.perrotin@univ-savoie.fr

<sup>2</sup> LOCIE (CNRS FRE3220-Université de Savoie, VOR), Polytech Annecy-Chambéry, France, Zoheir.Boukria@univ-savoie.fr

<sup>3</sup> LBMC (UMR-T9406, Université de Lyon1, INRETS), France, abdelkrim.bennani@iutb.univ-lyon1.fr

<sup>4</sup> LGCIE (Université de Lyon, VOR), INSA Lyon, France, ali.limam@insa-lyon.fr

---

**Abstract.** It is very difficult, if not impossible, to estimate the load of structures in current use by direct measures. In these cases and in geometry and simple boundary conditions, inverse methods can estimate the effort. Identifying the impact force on structures is the inverse of the direct problem: measured responses are used on a given structure to identify the causes, i.e., the original impact forces.

This study will develop an experimental method to identify the impact force on a reinforced concrete slab, using the transfer function obtained experimentally between the strain response and the force history applied to a point of the structure and will use the Tikhonov method for the inverse problem. To locate the impact force, we used an experimental method based on the minimization of an objective function created from the transfer functions between several impact locations, forming a mesh structure, and several measuring points. Characterizing the impact means locating the impactor and identifying the load.

**Keywords:** Inverse problem, impact, localization, identification, concrete slab Tikhonov regularization.

---

### 1 Context and introduction

In France, a new type of rock-shed (Figure 1) called a Structurally Dissipating Rock-shed (SDR) (Delhomme et al 2005) was invented to optimize this type of structure. The SDR consists of a reinforced concrete slab supported on specific fuses. Unlike traditional galleries, the SDR dissipates the energy from the impact of rock falls by the actuation of the slab and by plastic deformation of the reinforcement, concrete damage, and/or buckling support fuses. Consequently, the SDR is likely to be damaged during its life cycle.

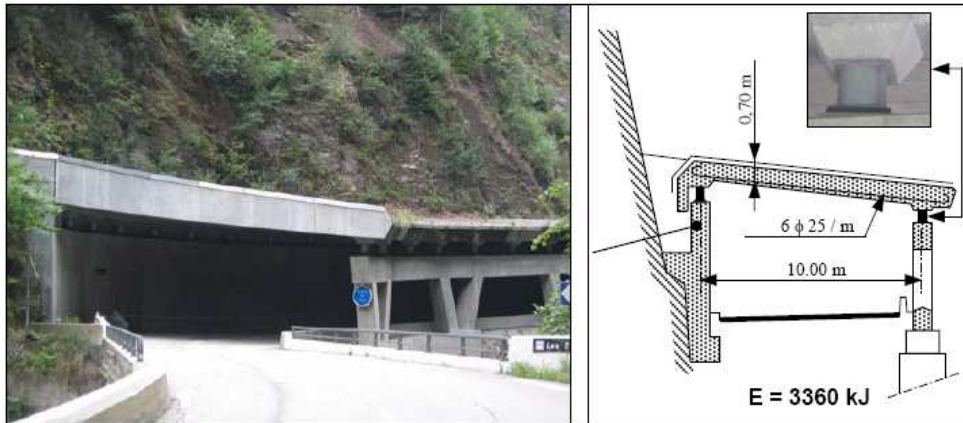


Figure. 1. Structurally Dissipating Rock-shed

Monitoring this kind of rock-shed has led to the development of new analysis and control methods. The first step in these methods locates and identifies the rock fall impact. Then the damaged areas on the slab are determined. In addition, it is possible to evaluate rock fall activity using these structures as hazard sensors (Figure 2). Thus for each impact, the impactor on the slab must be located and the corresponding loads determined.

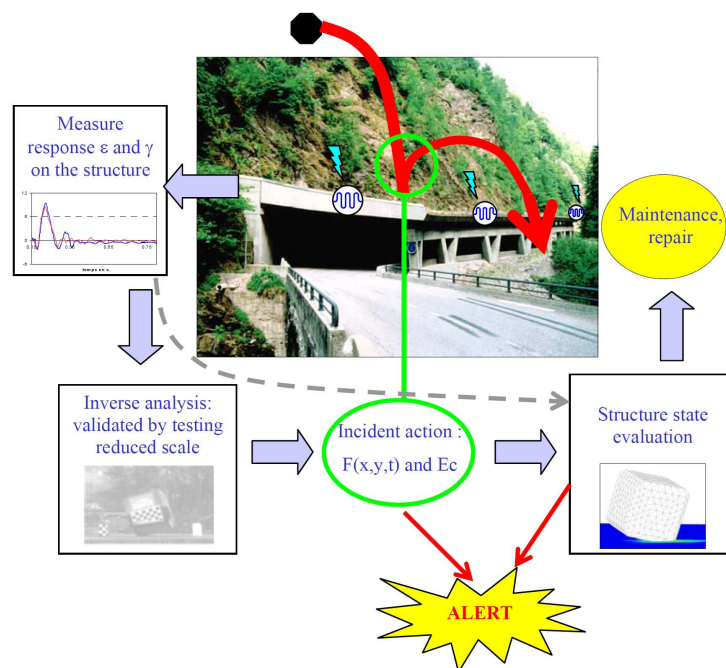


Figure. 2. Use of a PSD as a hazard sensor

To locate impacts, as in the field of acoustics and seismology, the technique used is based on the method of arrival time differences. This technique is highly dependent on how precisely the absolute or relative time of arrival of the first wave can be determined. Accuracy depends on the structure dimensions, the speed of wave propagation and the heterogeneities encountered. In our case, this technique did not provide good results for the location and it was not adapted to characterizing force. For these reasons, we used the approach called "inverse methods". Yen and Wu (Yen and Wu 1995) developed a method based on inverse methods to locate and identify the impact force from the strain recorded at many points on a rectangular plate of linear material. A reciprocal relationship between all pairs of constraints was developed to locate the source, without knowing the force beforehand. The history of the force is then determined after impact force location.

## 2 Identify impact force: theory

### 2.1 The inverse problem

The theory of impact force identification consists in finding the function of the applied load. The principle is very simple, as Gerardin (Gerardin et al. 1993) and Jacquelin (Jacquelin et al. 2003) explained.

The approach is based on determining the transfer function. The transfer functions can be determined analytically, experimentally or numerically. An experimental determination with a vibration test or impacts has the advantage of being applicable to all types of structures (beam, plate or column), even with complex boundary conditions of any kind. The response of the structure can be accelerations, deformations or displacements.

In expression (1), we consider a linear relationship between the applied force at point  $j$  and the response recorded at point  $i$ . Transfer function (2) can be obtained from a pair (force, response). Then the forward transfer function can be used with a new answer to reconstruct the original force.

$$(E)_i = [H]_{i,j} (F)_j \tag{1}$$

$$[H]_{i,j} = \begin{pmatrix} H_{ij}(\Delta t) & 0 & \dots & 0 \\ H_{ij}(\Delta 2t) & H_{ij}(\Delta t) & \dots & \\ H_{ij}(\Delta 3t) & H_{ij}(\Delta 2t) & \dots & \dots \\ \vdots & \vdots & \dots & \dots & 0 \\ H_{ij}(n\Delta t) & H_{ij}((n-1)\Delta t) & \dots & \dots & H_{ij}(\Delta t) \end{pmatrix} \tag{2}$$

In the time domain, the solution to the problem is reduced to solving the linear system.

$$e = \min_{\{f\}} \|\{E\} - [H]\{f\}\|^2 \tag{3}$$

However, the matrix  $[H]$  can be poorly conditioned and the system becomes very sensitive to small changes in response. Therefore, a physical solution for each response may not be found, possibly leading to an unstable solution (Figure 3).

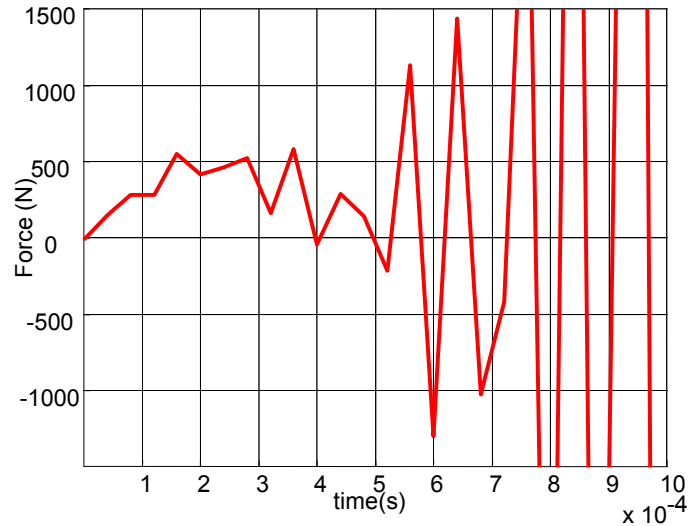


Figure 3. Unstable result

The problem must be regularized for a physically acceptable solution.

## 2.2 Regularization method

To obtain a stable solution, there are several regularization methods, direct ones such as the Tikhonov method and TSVD (truncate singular value decomposition), iterative methods such as the conjugate gradient, etc.

The regularization method used herein is the Tikhonov method (Tikhonov 1977), which proceeds by optimizing an error function constructed from two terms.

$$e = \min_{\{f\}} \left\| \{E\} - [H]\{f\} \right\|^2 + \beta \|f\|^2 \quad (4)$$

To obtain equation (4), Tikhonov proposed to add a term, the force vector norm weighted by a parameter  $\beta$ , to make the method less sensitive to measurement uncertainties. The complexity of the regularization method is to determine an optimal value for the regularization parameter  $\beta$  that ensures sufficient precision and robustness. The optimal setting should minimize the error between the forces identified and the actual forces. To determine the regularization parameter  $\beta$ , there are various methods including the L-curve method (Hansen 1999) and the GCV method (Wahba 1990). In this paper only the L-curve method is used. The L-curve is perhaps the most convenient graphical tool for analysis of discrete ill-posed problems and is based on plotting the norm of the solution, designated by SN (semi-norm) in abscissa, and the residue called RN (residual norm) in ordinate.

$$RN = \left\| \{E\} - [H]\{f\} \right\|^2 \quad (5)$$

$$SN = \left\| \{f\} \right\|^2 \quad (6)$$

The optimal regularization parameter corresponds to the point of maximum curvature (Figure 4).

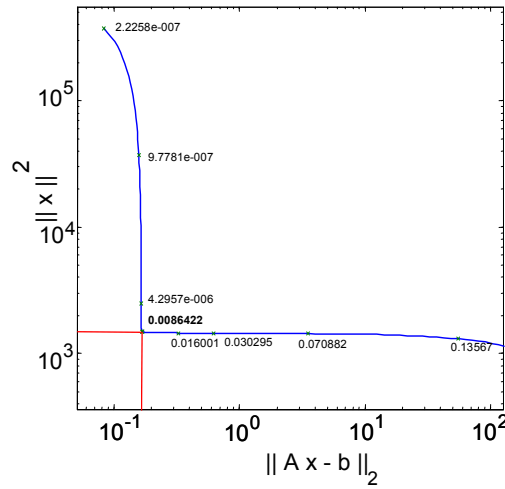


Figure 4. a L-Curve

### 3 Experimental setup and application to identify the impact force

To validate this approach, we used a reinforced concrete slab (Figure 5):

- 10 cm thick, 2 m long, and 1.5 m wide
- concrete C35/45
- a type ST10 welded steel mesh (20-cm mesh with 5.5-mm-diameter strands) for the side impact and ST40C (10-cm mesh and 7-mm-diameter strands) on the other side

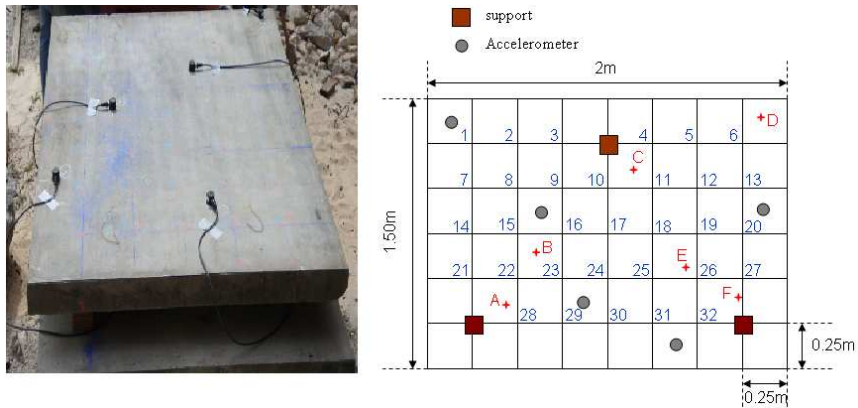


Figure 5. Experimental setup

We created a grid on a reinforced concrete slab, equipped with five accelerometers over the slab and an impact hammer to record the impact force. The impact force and accelerations at various points were recorded continuously using a data acquisition system with a 25-kHz frequency rate.

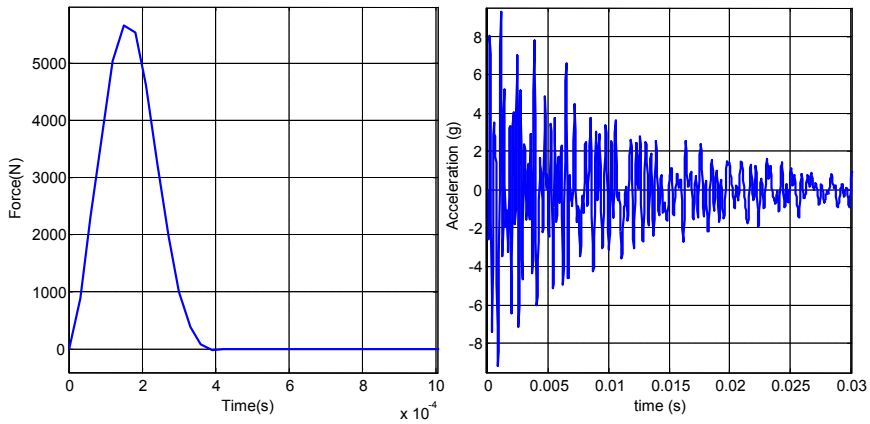


Figure. 6. Impact at point 3 and record on accelerometer 2

This first impact was used to create the transfer function between these two points. Then a new impact force can be found using a new acceleration.

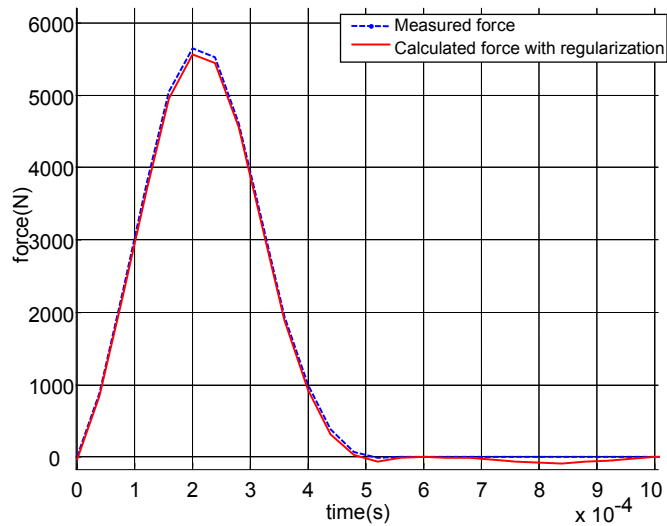


Figure. 7. Comparison between the recorded force and calculated force with the regularization

In figure 7, both types of impact forces are very close. This very good result could not be obtained without using regularization.

#### 4 Impact localization and identification

The problem of impact characterization (localization and identification) on a structure becomes more complex when the impact location is unknown. To solve this problem, we used the Hu and Fukunaga method (Hu and Fukunaga 2005) based on the minimization of an objective function created from the transfer functions between every possible impact

location forming a mesh on the slab (Figure 5), and several measuring points (at least three sensors).

We began the procedure with the localization:

- from recordings of different sensors, a impact force was recalculated for each mesh point, using formula (4). The procedure was explained in the previous paragraph.
- to determine the localization effort, we began by calculating the function G (Equation 7). Then the location (x, y) was obtained for the lowest value of G.

$$\underset{x,y}{\text{minimize}} G = \sum_{i=1}^m \frac{\| [H_i] \{ \tilde{f}_e \} - \{ E_i \} \|^2}{\| \{ E_i \} \|^2} \tag{7}$$

Figure 8(a) illustrates the error function obtained for all the points on the mesh. For one of these points, the error function was lowest: this is the impact point. In figure 8(b), Formula 4 was used to recalculate the impact force; a very good estimation compared with the real effort can be observed.

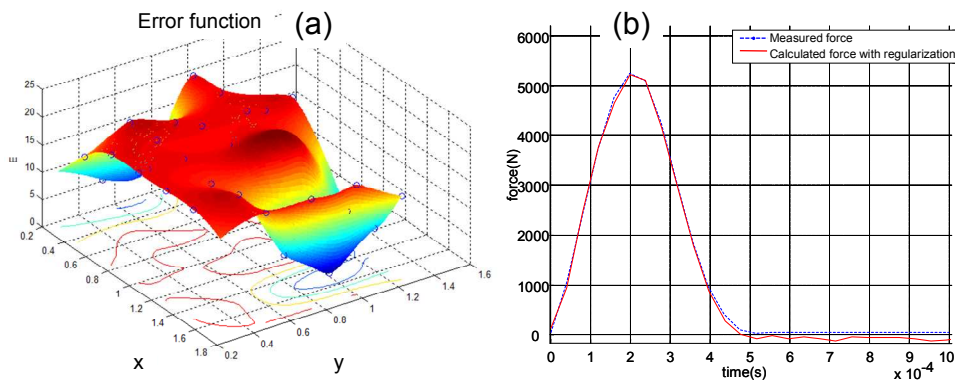


Figure. 8. Analysis

## 5 Conclusion and perspectives

In this study, it was shown that it is possible to identify and locate the impact force experimentally for a reinforced concrete slab, using the measured responses and transfer functions. An experimental determination by means of a vibration test or impact has the advantage of being applicable to all types of structure, including complex structures, with arbitrary boundary conditions. Using the Tikhonov regularization method and the L-curve method to determine the optimal regularization parameter, we obtained good results. Using experimental transfer functions created between different impact points forming a grid on the structure and strains recorded on different sensors, we located the impact force on the grid and could thus reconstruct the impact force. The next experiment will test the robustness of the method by relaxing the grid and looking at its optimality in terms of the number of sensors and their position, and use the SDR structure as a hazard sensor.

## References

- Delhomme F., Mommessin M. Mougin J.-P. and Perrotin P. (2005) Behavior of a structurally dissipating rock-shed: experimental analysis and study of punching effects", *International Journal of Solids and Structure*, Volume 42, Issue 14, July 2005, Pages 4204-4219
- Yen C. S. and Wu E. (1995), On the inverse problem of rectangular plates subjected to elastic impact, part I: Method development and numerical verification, *Journal of Applied Mechanics*, Vol 62, no.3, 692-698.
- Yen C. S. and Wu E. (1995), On the inverse problem of rectangular plates subjected to elastic impact, part II: Experimental verification and further applications, *Journal of Applied Mechanics*, Vol 62, no.3, 699-705.
- Gérardin M and Rixen D. (1993) *Théorie des vibrations: application à la dynamique des structures*, MASSON, Paris, 1993.
- Jacquelin E., Bennani A. and Hamelin P. (2003) Force reconstruction: analysis and regularization of a deconvolution problem, *Journal of Sound and Vibration*, 265: 81-107.
- Tikhonov A.N and Arsenin, V.N. (1977), *Solutions of ill-posed problems*, Wiley, 1977.
- Wahba G. (1990), *Spline Models for Observational Data*, CBMS-NSF Regional Conference Series in Applied Mathematics, Vol. 59, SIAM, Philadelphia, 1990.
- Hansen, P.C. (1999), *The L-curve and its use in the numerical treatment of inverse problems*, Tech. Report, IMM-REP 99-15, Dept. of Math. Model. Tech. Univ. of Denmark, 1999.
- Hu N. and Fukunaga H. (2005) A new method for health monitoring of composite structures through identification of impact force, *Journal of Advanced Science*, 17(1&2): 82-89.

## A new device to simulate explosion blast on reduced-scale structures

Philippe Berthet-Rambaud<sup>1</sup>, Ali Limam<sup>2</sup>

<sup>1</sup> MND Engineering, Sainte-Hélène du Lac, 73800, France  
[philippe.berthet-rambaud@groupemnd.com](mailto:philippe.berthet-rambaud@groupemnd.com)

<sup>2</sup> LGCIE, INSA de Lyon, France  
[ali.limam@insa-lyon.fr](mailto:ali.limam@insa-lyon.fr)

---

**Abstract.** DaisyBell® was initially designed to artificially release snow avalanches: this totally autonomous and mobile system is normally used with an helicopter to secure dangerous accumulations on slopes after a snowstorm. It consists in injecting and igniting a stoichiometric several hundred liters mixture of oxygen and hydrogen in a metallic volume. Thanks to the cone-shaped structure, this generates a shock wave along a vertical axis to the ground : depending on the distance, aerial overpressure can reach more than 1 bar with a wave speed of more than 1000m/s at impact. Used under a fixed structure, it becomes an explosion laboratory to allow a new kind of tests about the behavior of several tens of centimeters samples subjected to (eventually repetitive) blasts. Preliminary tests were performed using simple metallic membranes to validate an experimental protocol before to initiate dynamic inverse analysis development.

**Keywords:** explosion, blast, buckling, rupture, experiments.

---

### 1 Introduction

Preventive release is one of the main strategy used by ski resorts and transport networks against snow-avalanches in winter (Perla 1978): it consists in eliminating/cleaning snow accumulations (due to snowfalls or wind) before they grow to control their release and limit avalanche size and development. It uses artificial explosion of either solid explosives (Gubler 1978) or gas mixture to generate a blast wave on the snowpack and initiate the snow flow.

In order to improve these techniques, TAS and MND Engineering, two companies of the French MND Group ([www.groupemnd.com](http://www.groupemnd.com)) have recently develop the DaisyBell® system (Berthat-Rambaud *et al* 2008). Normally used under an helicopter to combine mobility and efficiency, DaisyBell® is able to produce more than sixty shots with one set of gas bottles. Safe, completely autonomous and very easy to control, why not use it also in a more scientific and research way as a ‘‘controlled explosions source’’ ? With the

experience of more than 10000 explosions during last winters and the set up of more than 25 machines, DaisyBell® is now available and ready for that.



**Figure.1.** DaisyBell normally used during an avalanche release operation

## 2 DaisyBell®: principles and main features

DaisyBell® project is born from a desire for a gas system movable and operable autonomously to make explosions. The first problem was to solve the need for a sufficient gas mixture confinement. If other systems use a latex balloon, they raise technical difficulties with complex mechanisms to connect gas reserves to successive balloons. Moreover, using balloons means capacity and autonomy constraints to limit the number of possible shots.

This has led to this basic idea: to replace the balloon temporary volume by a permanent metal one. At the beginning of the development, a flap system was foreseen to be closed during the gas injection and opened just before the ignition. Using an oxygen-hydrogen mixture was the second initial idea. This mixture is lighter than the air, so a system directed towards the bottom could be designed. Moreover, the explosion of an oxygen-hydrogen stoichiometric mixture is hardly explosive with maximum energy.

Different types of bells have been tested to:

- ◇ Choose the best shape and check its compatibility with the initial containment of the gas mixture injected from the top
- ◇ Check the ability to make a sufficient explosion

◇ Sort the explosion consequences according to the mixture parameters: proportion, volume.

These consequences of an explosion must ensure a compromise between the efficiency of the wave directed towards the ground and the reaction on the system and consequently on the suspension system.

Figure 2 shows drawings of the three tested volumes: the first one was too large and could not confine correctly the gas mixture during injection without a supplementary closing system. The second one was the first to be equipped with a cylindrical upper room: its smaller shape limits the turbulences and the external rejections of gas before the explosion to ensure, in every case, the explosion. Therefore, the advantage is not to have to close the opening during injection, and consequently not to need a flap system. Finally, the cone was retained: it is easier and simpler to make with the same advantages as before. Being still too heavy, the height of the definitive bell was reduced further by 25 cm.

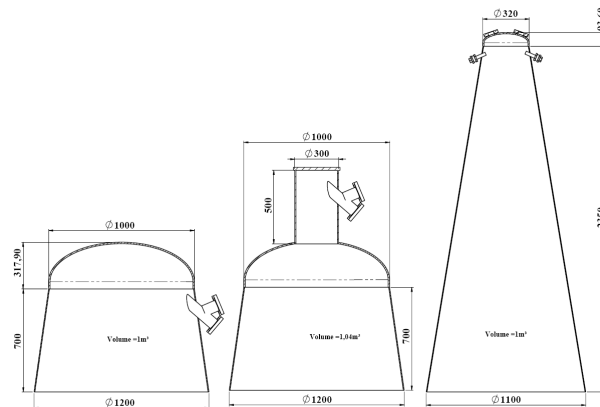


Figure 2: three tested shapes

In parallel, the injection and mixing of the two gases was deeply studied using CFD means (Tonello and Berthet-Rambaud 2009) to ensure first an optimal filling (distribution, homogeneity) and so the better explosion: the two gas are injected separately in a helicoidal mixer with a several bars pressure to then enter in a spreader with multiple drilled injectors. With a streamflow of about 1800 l/min, the cone is filled within only 5 seconds. Finally, two spark plugs used in racing car motors provide the explosion ignition. Systems of check valves prevent the explosion from going to the gas reserves.

Technically, the initial 200-bar pressure in each gas bottle is reduced by a double-expansion system linked to a calibrated hole: this combination enables to maintain with precision the injected flow. Gas circuits are opened via electric valves, one for oxygen and a redundant pair for hydrogen. The control system is placed in a protected box, remotely controlled by radio. The firing procedure is semi-automatic as the operator just needs to remain pressing on two buttons to automatically carry out the operations: simultaneous injection of both gases during 5 seconds and ignition of the sparks. In case of trouble and to exploit human reflexes, the simple release of at least one button stops the procedure. It

can be started again within 30 seconds or the system will ask for the draining of the volume. It consists in saturating the mixture with oxygen to make it non-explosive: it can be activated to secure the system at any moment in case of problem. Energy is provided by 24V batteries.

A system of laser distance measurement has been added to inform operators of the vertical position of DaisyBell to the ground. All in all, the system weighs about 340 kilos without gas reserves: depending on their type, bottles will add between 60 to 140kg to allow between 30 to 60 shots. After one explosion, the system is directly ready again only after a recovering time of 10s. to prevent over-warming and without additional operation.

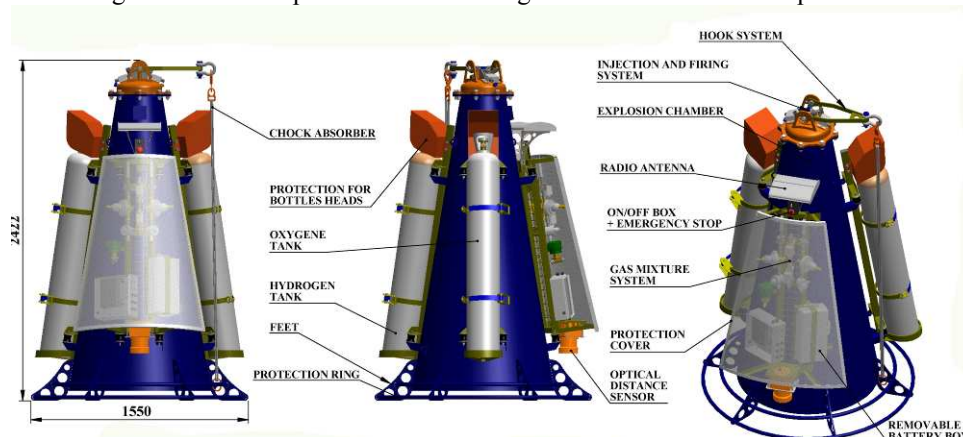


Figure 3: the DaisyBell® system (© TAS 2009)

### 3 DaisyBell® as a static source of controlled explosions

Hung under a crane, DaisyBell® becomes a generator of shockwave. The shape of the cone and the position of the spark plugs will direct the explosion vertically to the ground. Near the symmetry axis, this shock wave can be considered as roughly horizontal (in fact, lightly hemispheric). That means that structures of several tens of centimeters can be tested under direct and quite uniform blast.

Of course, the intensity of the pressure peak depends on the distance with the opening of DaisyBell. Maximum aerial overpressure can reach at least 1 bar but can also be reduced to some millibars by decreasing the gas volume and/or increasing the distance with the tested structure. These two parameters

In comparison to experiments with solid explosive, the main advantage is that, except for the noise, operators do not need any particular protection if they respect a minimum distance of some tens meters: at this location and for usual position height, they are subjected only to the remaining wave reflected on the ground. The fact that there is no solid explosive eases the set up of experiments with acceptable safety procedures. Especially, no particular preparation is needed for DaisyBell itself: as soon as bottles and batteries are connected, it is ready to work! Ageing tests showed also that it is possible to

perform more than two hundred shots a day... you just need to find the right site and/or comprehensive neighbors to do that! Finally, and in comparison to solid explosives (Formby and Wharton 1996), explosions are much more regular and controlled.

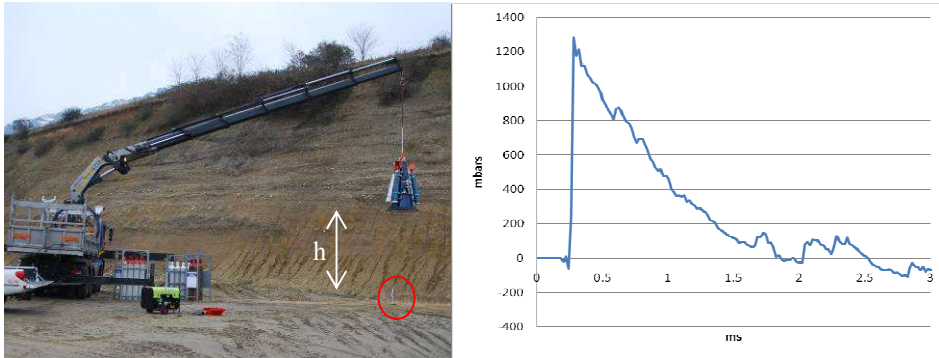


**Figure 4:** Experimental device and measured aerial overpressure for  $h=1.5\text{m}$ , distance between the basis of the cone and the sensitive zone of the sensor (circle)

#### 4 Preliminary structural tests

Preliminary tests were performed with a 0.2mm thick aluminium shell as a 20cm high 16cm diameter pipe with closed extremity. This sample was placed vertically and subjected to the explosion (figure 5).

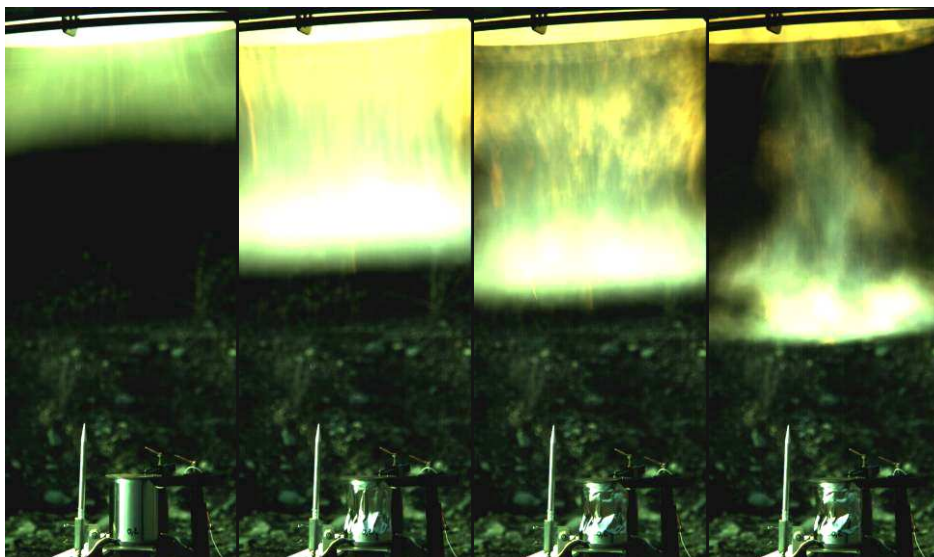


**Figure 4:** DaisyBell® blast on a 0.2mm thick aluminium pipe (one picture every 2 ms)

The corresponding pressure (figure 4) was measured with the free field blast pressure sensor 137A22 from PCB Piezotronics: this pressure probe is specifically designed for military applications and is mounted in an axial direction to the blast source with the sensing surface in a vertical plane (Walter 2004). Data acquisition is done using an autonomous National Instruments CompaqDaq system with a 50kHz rate per channel. In parallel, a Ranger HR Fastec Imaging high speed camera is used at 1000 fps.

This result leads to a partial buckling of the pipe. In parallel, inertia effects and the presence of internal air should have prevented a complete crash of this structure.

## 5. Conclusions

DaisyBell®, new system of avalanche prevention release, has also many advantages to become a controlled explosion source for scientific and research purpose. Mobile and autonomous, it is able to generate and reproduce oxygen-hydrogen explosions in a vertical direction to test (reduced scale) structures and materials, from conceptual shells to real glass or windows. A first experimental protocol has been tested to confirm these capabilities and to initiate new research program on structures subjected to blast and extreme loading.

## References

- Berthet-Rambaud P., Noel L, Farizy B, Neuville JM, Constant S, Roux P (2008), development of an helicopter-borne gas device for avalanche preventive release *In Proceedings of the International Snow Science Workshop, Whistler, BC*
- Formby S.A., Wharton R.K (1996), Blast characteristics and TNT equivalence values for some commercial explosives detonated at ground level, *Journal of Hazardous materials*, 50, 183-198.
- Gubler, H. (1977). Artificial release of avalanches by explosives. *J. Glaciol.*, 19(81). 19-429.
- Perla, R. (1978). Artificial release of avalanches in North America. *Arctic and Alpine Research*, 10(2), 235-340.
- Tonello N, Berthet-Rambaud P (2009), Analysis of a Novel Explosive Avalanche Release System at Maximum Load, *STAR European Conference*.
- Walter P.L. (2004). Introduction to Air Blast Measurements Part 1. Technical Note. *PCB Piezoelectronics*

## Dynamic Behavior of a Tensegrity Ring

Jean-François Dubé<sup>1</sup>, Julien Averseng<sup>1</sup>, Bernard Crosnier<sup>1</sup>

<sup>1</sup> Laboratoire de Mécanique et Génie Civil (LMGC-UMR5508), Université Montpellier 2, France

[dube@lmgc.univ-montp2.fr](mailto:dube@lmgc.univ-montp2.fr), [averseng@lmgc.univ-montp2.fr](mailto:averseng@lmgc.univ-montp2.fr), [crosnier@lmgc.univ-montp2.fr](mailto:crosnier@lmgc.univ-montp2.fr)

---

**Abstract.** Tensegrity structures are light, transparent and rigid lattice structures. These structures are made up of a discontinuous set of bars in compression inside cables in tension ensuring the continuity of the structure. Their stability and rigidity is ensured by a state of selfstress that keeps the various elements in tension or compression. The “Design and Structures” team of the Mechanical and Civil Engineering Laboratory (LMGC) are specialized in the study of light structures to which the tensegrity structures belong. These structures have the characteristic to lend themselves easily to deployment. This is why we currently study a spreadable tensegrity ring that constitutes a basic link of tensegrity tube. This paper relates to the study of the vibratory behaviour of a 2.3 m wide and 1.6 m high pentagon-based tensegrity ring.

**Keywords:** dynamic behaviour, tensegrity, selfstress state, numerical simulation, experimental test, unilateral behaviour.

---

### 1 Introduction

Tensegrity systems appeared in the fifties (Fuller 1973; Snelson 1973) as a new class of reticulate space systems. They are defined nowadays (Motro 2002, 2003) as a discontinuous set of compressed components maintained in a stable equilibrium by a continuous set of tense components. The whole system is in a selfstressed stable equilibrium without any boundary conditions. Selfstress is much like the pressure of air contained inside the tense skin of an inflatable object. This equilibrium between tense (usually cables) and compressed components stabilizes the system and permits optimization of materials. Tensegrity systems present great interests for artists, architects and engineers who design lightweight and transparent structures (Quirant et al. 2003; Sanchez 2005) (Figure1).

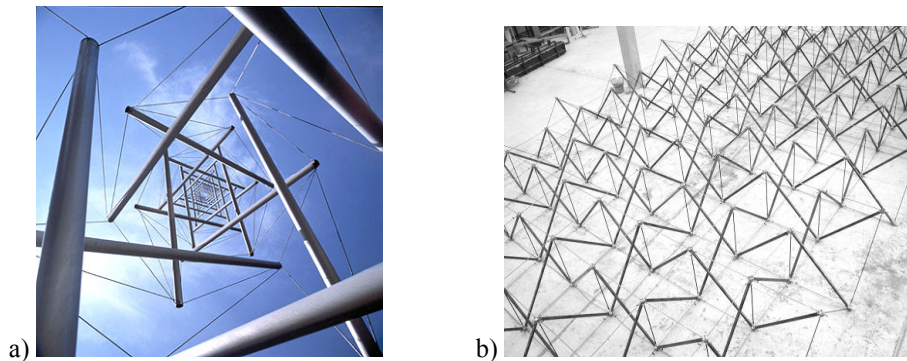


**Figure.1.** a) Needle Tower (Kenneth Snelson, 1968), b) Tensarch project (Motro 2002).

Researchers prospect for tensegrity applications in various fields: architecture, robotics (Aldrich 2004), spatial conquest (Tibert 2002) or biomechanical modelling (Ingber 1998; Baudriller 2006). The capability of folding and deployment of these systems permits also to envisage satellite antennas, scaffolding or deployable footbridges (Pellegrino 1993).

To create new selfstressed shapes, two approaches are possible. The first one consists in looking for a form and a structure that are compatible with some given geometrical or mechanical constraints (Tibert 2003). The second one supposes that the geometry is known and consists in verifying that a compatible selfstress state, in which cables are strained and struts are compressed, exists (Quirant 2003). This latter approach is used in this paper.

Anthony Pugh introduced many physical models of tensegrity structure (Pugh 1976). For some of them, compressed elements are not discontinued struts but constitute a set of interconnected struts, leading to stiffer systems. René Motro proposed recently a method of fabrication and demonstrated the foldability of pentagon-based tensegrity rings (Motro 2006). A life-size module of this type was built in order to demonstrate the feasibility of such systems and study the kinetic of deployment in quasi-static real conditions (dubé 2009). In this paper, we present a vibration analysis of this module.

## 2 The tensegrity ring

The geometrical basis of this structure is a pentagon-based straight prism (Figure. 2). It comprises 30 cables and one continuous set of 15 struts. Each lateral face of the prism contains one strut (lateral strut). Additional nodes are located in the horizontal plane that passes at mid-height of the prism. They are positioned outside the prism, on lines that go from one summit of the mid-section to the opposite side perpendicularly. From these points, a couple of intermediate struts join one point of the superior base and a point of the inferior base. The layer cables form the sides of the two bases of the prism. For each external point, four cables (intermediate cables) are connected to the points of the bases. We differentiate two groups of intermediate cables : coplanar cables with one lateral strut and those not coplanar with lateral strut. They are called respectively intermediate cables 1 and intermediate cables 2.

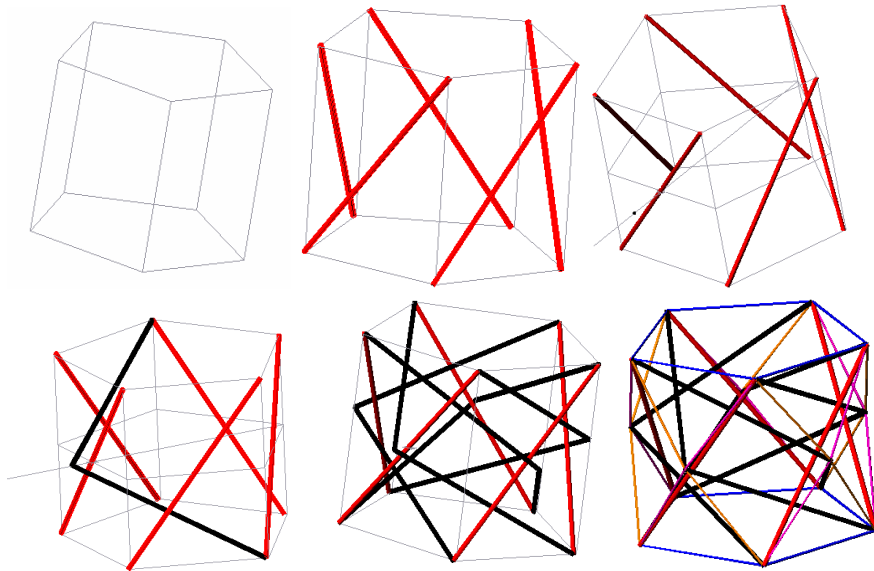


Figure 2. Geometrical construction of the pentagon-based tensegrity ring.

Three parameters define the global geometry of the system: the radius  $R$  of the circles that circumscribe the bases of the prism, the height  $H$  of the prism and the radius  $R'$  of the circles that circumscribe the intermediate nodes (Figure 3). In order to keep geometrical regularity, we choose the basic pentagon and the intermediate one of equal size ( $R=R'$ ). We can determine the relationship between  $R$  and  $H$  by imposing a condition of unicity on the length of lateral and intermediate struts. Thus, geometry of the structure depends only on one parameter (Eq. 1):

$$H = 4R \sqrt{\frac{\cos(2\pi/5)}{3}} \tag{1}$$

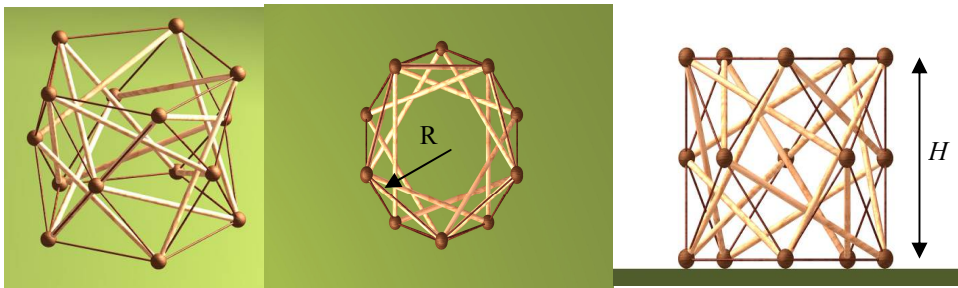


Figure 3. Perspective view, top view and side view of tensegrity ring.

In this paper, we give some information about the behaviour of the tensegrity ring under loads. Then we will present our prototype design and realization. Finally, we give a comparison between simulation and experimental folding carried out on this structure.

## 2 Selfstress state

### 2.1 Theory of selfstress state

System equilibrium is obtained when all nodes are in equilibrium. The static equilibrium of a node  $i$  is written as:

$$\sum_{j \neq i} T_{ij} + F_i = 0 \quad (2)$$

$T_{ij}$  is the internal force vector of the element linking node  $j$  to node  $i$ , and  $F_i$  is the external force vector directly applied to node  $i$ . The internal forces  $T_{ij}$  are a function of the deformation of each element;  $x_i, y_i, z_i$  are spatial coordinates of node  $i$ , and  $l_{ij}^0$  the length of the element connecting nodes  $i$  and  $j$  in the reference configuration. When we introduce

the force density coefficient  $q_{ij} = \frac{T_{ij}}{l_{ij}^0}$  of each element  $(i, j)$  (Pellegrino 1986), the

projection of Eq. 2 on three orthogonal axes  $(x, y, z)$  gives:

$$\left\{ \begin{array}{l} \sum_{j \neq i} q_{ij}(x_j - x_i) + F_i^X = 0 \\ \sum_{j \neq i} q_{ij}(y_j - y_i) + F_i^Y = 0 \\ \sum_{j \neq i} q_{ij}(z_j - z_i) + F_i^Z = 0 \end{array} \right. \quad (3)$$

The system of equations obtained by applying Eq. 3 to all the nodes of the structure is:

$$\mathbf{A}\mathbf{q} = \mathbf{f} \quad (4)$$

with  $\mathbf{A}$  for the equilibrium matrix of the structure (dimension  $b \times 3n$ ),  $\mathbf{q}$  for the vector describing the force densities in  $b$  elements, and  $\mathbf{f}$  for the vector of the external forces acting on  $n$  nodes.

Selfstress state ensures the stability and the rigidity of the tensegrity system. It is then the whole set of internal forces occurring in the initial state, without external loading. This state of equilibrium corresponds to a field of force densities  $\mathbf{q}_0$  satisfying:

$$\mathbf{A}\mathbf{q}_0 = 0 \Leftrightarrow \mathbf{q}_0 \in \ker \mathbf{A} \quad (5)$$

Thus, the selfstress state can be expressed on the basis of the subspace  $(\ker \mathbf{A})$ , noted as  $\mathbf{S}$ , which is composed of  $s$  fundamental selfstress states. Numerical techniques are developed to accurately determine the selfstress basis.

Direct determination of the fundamental selfstress states, starting from  $\mathbf{S}$ , poses numerical problems that are addressed by Quirant (Quirant 2000). Every selfstress state meeting the unilateral conditions for tensioned-only members is called "compatible". A compatible selfstress state can result from a linear combination of several compatible states, or directly from linear combination of the elements defining the subspace  $\mathbf{S}$  (Quirant 2007).

The dual of the subspace  $\mathbf{S}$  is the space of mechanisms  $\ker \mathbf{A}^T$ , noted  $\mathbf{D}$ , which contains all the displacement fields for which the length of every element remains constants at order 1

or more. These mechanisms, that mobilize no deformation energy, are also identified as soft vibration modes.

In our case, the compatible selfstress states and mechanisms are determined with dedicated MATLAB based software, TENSEGRITE 2000.

**2.2 Tensegrity ring selfstress state**

The pentagon-based tensegrity ring analysis results in 6 selfstress states and 0 mechanism. From the selfstress base, one state that holds the struts in compression and the cables in tension can be extracted. In this state, the value of the normal stress is different for each group of similar elements (Figure. 4). It varies only with the geometry of the system (Table 1 and Table 2).

|   |        |
|---|--------|
| Reference length of struts              | 200 cm |
| Reference length of layer cables        | 135 cm |
| Reference length of intermediate cables | 102 cm |
| Radius of circumscribe circle           | 115 cm |
| Height of the module                    | 148 cm |

**Table.1.** Geometrical properties of module.

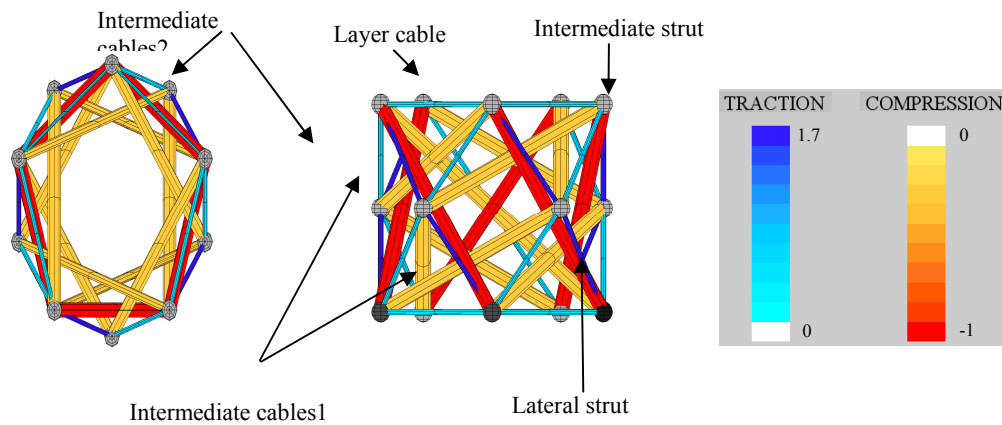


**Figure.4.** Graphic view of the selfstress state and the different type of elements.

|                      |           |
|----------------------|-----------|
| Intermediate strut   | -0,34 N/m |
| Lateral strut        | -1,00 N/m |
| Layer cables         | 0,5 N/m   |
| Intermediate cable 1 | 1,70 N/m  |
| Intermediate cable 2 | 0,64 N/m  |

**Table.2.** Selfstress coefficients for the compatible selfstress state.

It is of course possible to combine this compatible selfstress state with the five other ones if a dissymmetry and heterogeneity of the tension for each elements group is required.

After assembly, the method proposed by Averseng (2002) for the experimental tension setting, is used in order to set this chosen selfstress in the structure.

### 3. Vibration tests

Previous vibration tests were carried out on a double layer tensegrity grid (Dubé 2008, Angellier 2009). They showed that the selfstress level influences rather little the vibrating modes. Angellier identified a law in power 0.25 of the tension level in the elements. Other tests showed that even the higher modes were related to the selfstress level. The study carried out here must make it possible to check if one finds the same results for a tensegrity ring. The experimental tests are carried out in parallel to numerical simulations with the code CAST3M in which the trusts are modelled by finite elements beams and the cables by finite elements bars. A second code adapted to lattice system in which all elements are modelled by finite element bars is also used. For the experimental tests, the structure is posed on three simple supports and an excitation is introduced on the node 9 of the middle layer (figure 5).

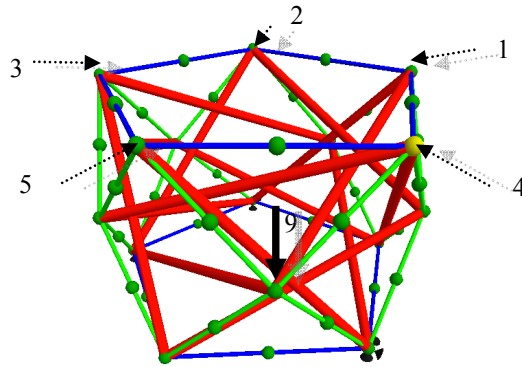


Figure.5. Node numbers for upper layer and input force.

We impose a sinus excitation whose frequency varies from 2 Hz with 50 Hz. The vertical acceleration of all the nodes is measured and the transfer function for each node is determined.

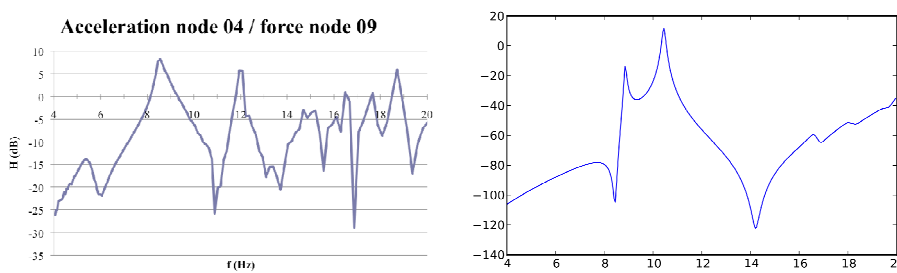


Figure.6. Frequency response function between node 9 and node 4 : experimental results and computation.

The first results show that the numerical simulations give vibration frequencies for the first modes in a good accordance with vibratory measurements. The modal deformations are comparable for the first mode. The numerical simulations make it possible to visualize

that the first two modes are modes of structure whereas the higher order modes correspond to vibrations of the bars and cables (figure 6).

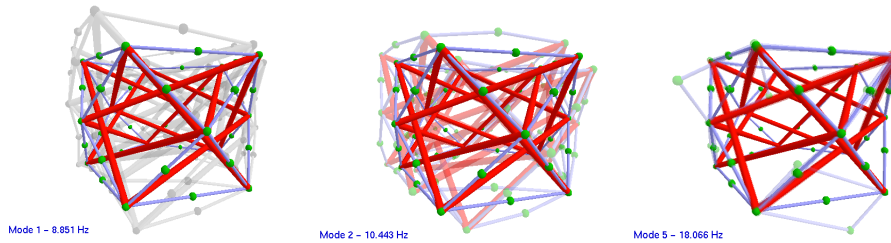


Figure 6. Structural modes (1 and 2) and a higher local mode (5).

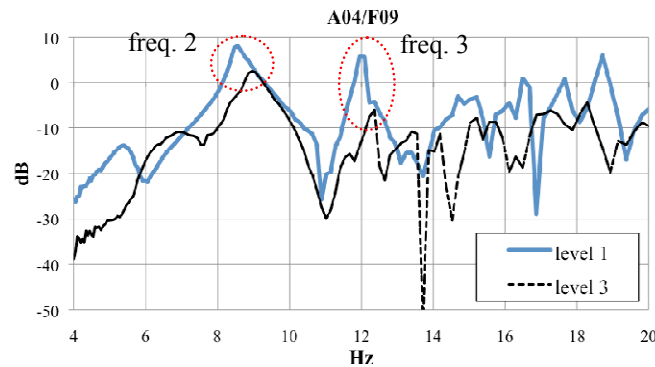


Figure 7. Experimental frequency response between node 9 and node 4 with selfstress level 1 and selfstress level 3.

|                               |          |                |                |
|-------------------------------|----------|----------------|----------------|
| tension in intermediate cable | 269 N    | 315 N          | 354 N          |
| frequency 1                   | 5.47 Hz  | not identified | not identified |
| frequency 2                   | 8.53 Hz  | 8.85 Hz        | 8.93 Hz        |
| frequency 3                   | 11.87 Hz | 12.15 Hz       | 12.22 Hz       |

Table 3. Frequencies evolution function tension in intermediate cable.

To study the evolution of the eigen modes according to the level of selfstress, the intermediates cables are tightened. The tension is measured using a tensiometer developed at the laboratory. The increase of the cables tension generates, in addition to a frequency increase, an attenuation in the amplitude of the global eigen modes and a relative amplification for many local modes (figure 7.). Indeed the first identified mode with 5,47 Hz is less distinct for the tests carried out with higher tension levels. The modes of higher order, after 9Hz, reveal many local modes of bars which mask the global modes. The evolution of the global eigen frequencies, for the three considered levels, does not correspond to a function of square root of the tension (table 3). This result was already obtained with double layers tensegrity grids (Angellier 2009). Indeed, the selfstress structure behaves like the assembly of a classical structure with a tended structure.

## 5 Conclusion and perspectives

The tensegrity ring has a vibratory behaviour similar to a tensegrity grid. The influence of the selfstress level remains limited in majority to the local modes of the elements. One second trial run with higher selfstress levels may allow to confirm this conclusion. In parallel, the numerical simulations make it possible to find the same behaviour appreciably as the experiment. It is then easier to visualize the eigen modes. Indeed the number of measurement points is limited by the handling time. With the numerical simulation, we can also locate the various local eigen modes by increasing the number of elements used to describe cables and struts. There remains to characterize the evolution of damping according to the selfstress level. These first tests are in the course of examination. More important levels and different boundary conditions will supplement them. The numerical models could then be qualified to study larger structures using the principle of tensegrity rings.

## References

- Abedi, K. and Shekastehband, B. (2004). Investigation into Stability Behavior of Tensegrity Structure. *Extended Abstract, IASS Symposium IASS Symposium*, Montpellier, France, 108-109.
- Angellier, N., Jaen, J., Dubé, J.F., Crosnier, B. (2009). Etude du comportement dynamique d'une structure de tenségrité en fonction des niveaux d'autocontrainte. 9<sup>ème</sup> Congrès de Mécanique, Marrakech, 4p in CDROM.
- ANSYS (2005). Basic analysis guide ANSYS Release 10.0. ANSYS, Inc. Ltd.
- Aldrich, J. B. (2004). Control synthesis for a class of light and agile robotic tensegrity structures. Doctoral thesis, Dept. of Mechanical and Aerospace Engineering, Univ. of California, San Diego.
- Averseng, J., Kazi Aoual, M. N. and Crosnier, B. (2002). Tensegrity systems selfstress state implementation methodology. 5<sup>th</sup> *Int. Conf. on Space Structures*, Guilford (U.K.), 19-21.08.02 G.A.R. Parke, P. Disney eds, Telford, T., pp. 31-38.
- Baudriller, H., Maurin, B., Cañadas, P., Montcourrier, P., Parmeggiani, A., Bettache, N. (2006). Form-Finding of complex tensegrity structures application to cell cytoskeleton modelling. *Comptes Rendus de l'Académie française des Sciences -Mécanique*, vol. 334 (11), pp. 662-668.
- Dubé, J-F., Angellier, N. and Crosnier, B. (2008). Comparison between experimental tests and numerical simulations carried out on a tensegrity mini grid, *Engineering Structures*, vol. 30, n°7, pp. 1905-1912.
- Dubé, J-F., Quirant, J., Cevaër, F., Nguyen, A.D., Motro, R. (2009). Anneau detenségrité pliable-dépliable. *Annales du BTP* N°5/2009.
- Farrugia, P., Nooshin H., Disney, P. and Parke, G. A. R. (2004). Spatial foldable rings. *Extended Abstract, IASS Symposium*, Montpellier, France, pp.70-71.
- Fuller, R.B. (1973). *The dymaxion world of Buckminster Fuller*. Anchor Books, New York.
- Ingber, E.D. (1998). The architecture of life. *Sci. Am.*, 278(1), pp. 30-39.
- Kébiche, K., Kazi Aoual, M. N. and Motro, R. (1999). Geometric nonlinear analysis of tensegrity systems. *J. of Engineering Structures*, vol. 21, pp. 864-876.
- Luo, Y., Fu, G. and Chen, T. (2004). Testing study of flat four-prism Tensegrity system. *Extended Abstract, IASS Symposium*, Montpellier, France, pp. 226-227.
- Motro, R. and Raducanu, V. (2002). Tensarch Project. 5<sup>th</sup> *Int conf on Space Structures*, University of Surrey, Guildford.
- Motro, R. (2003). *Tensegrity. Kogan Page Science*, ISBN : 1903996376.

- Motro, R., Maurin, B., Silvestri, C. (2006). Tensegrity rings and the hollow rope. *Extended Abstract, IASS Symposium*, Beijing, China, pp. 470-471.
- Pellegrino, S. and Calladine, C. R. (1986). Matrix analysis of statically and kinematically indeterminate frameworks. *Int. J. of Solids and Structures* 22, pp. 409-428.
- Pellegrino, S., Kwan, A. S. K. and You, Z. (1993). Active and passive cable elements in deployable masts, *International Journal of Space Structures*, 8 (1-2), ISSN0266-3511, pp. 29-40.
- Pugh, A. (1976). An introduction to tensegrity. *University of California Press*, California, USA.
- Quirant, J. (2000). Systèmes de tenségrité et autcontrainte : qualification, sensibilité et incidence sur le comportement. Thesis, Laboratoire de Mécanique et Génie Civil, Université Montpellier 2.
- Quirant, J., (2007). Selfstressed systems comprising element with unilateral rigidity : selfstress states, mechanisms and tension setting, *Int. J. of Space Structures*, vol. 22 (4), pp. 203-214.
- Quirant, J., Kazi-Aoual, M.N., Motro, R. (2003). Designing tensegrity systems: the case of a double layer grid. *Int. J. Engineering Structures*, vol. 25 (Issue 9), pp. 1121-1130.
- Sanchez, L. R. (2005). Contribution à l'étude mécanique des systèmes de tenségrité. Thesis, Laboratoire de Mécanique et Génie Civil, Université Montpellier 2.
- Snelson, K. (1973). Tensegrity Mast. Bolinas California, *Shelter Publications*.
- Tibert, G. and Pellegrino, S. (2003). Review of Form-Finding Methods for Tensegrity Structures. *Int. J. of Space Structures*, 18(4), pp. 209-223.
- Tibert, G. (2002). Deployable tensegrity structures for space application. Thesis, Dept. of Mechanics, Royal Inst. of Technology, Stockholm, Sweden.



# Damage mechanics applied on the seismic behavior of concrete structures

Shahrokh Ghavamian\* — Ludovic Jason\*\* — Justine Bonenfant\*

\* NECS, 196 rue Houdan, 92300 SCEAUX, France  
sg@necs.fr

\*\* CEA, DEN, DM2S, SEMT, LM2S, CEA SACLAY F-91191, Gif sur Yvette  
ludovic.jason@cea.fr

---

*ABSTRACT.* The seismic behavior of reinforced concrete structures is generally evaluated through modal spectral approaches, based on linear elastic analysis. In the case of seismic reevaluation of existing structures using traditional methods, since the nonlinear behavior of materials is not taken into account, these techniques often lead to an overestimation of the needs in reinforcement. In this contribution, it is proposed to highlight how including nonlinearity in the mechanical behavior of concrete and steel can improve the seismic evaluation of RC structures. For this purpose, a pushover technique is applied on an office building. Contrary to a classical approach, the progression of the failure mode and the mechanical degradation can be obtained and used to accurately elaborate the best retrofitting strategy. Some improvements of the constitutive laws are nevertheless needed if the use of this type of approaches is to be extended to more complex structures. However, the maturity of most constitutive models is not enough to allow industrial applications and may limit the use of this technique to experts from research centers.

*KEY WORDS:* seismic evaluation, reinforced concrete, structures, nonlinear behavior

---

## 1. Introduction

Many solutions are available to simulate the material nonlinear behavior, especially for concrete or reinforced concrete. Constitutive laws are developed to represent different effects: local or global scale, continuum mechanics or discrete approach, isotropic or anisotropic behavior, monotonic or cyclic loadings. With the increase in computation capacity, it should be possible to achieve an appropriate description of many industrial problems. Nevertheless, the real situation is probably less optimistic.

Despite the scientific improvements on the understanding of the material behavior, the developments of appropriate theoretical approaches and the implementation of the associated numerical models, combined with the increase in the computer capacity, the applicability of recent approaches is not totally demonstrated. The questions on the reliability of the models, their range of validity, their numerical robustness or the definition and calibration of their parameters are not fully satisfying for industrial

applications. That is why the transfer to civil engineers remains difficult. While, the interest for industrial applications is strong.

In this contribution, after a brief presentation of the existing models, the particular case of an industrial application using a nonlinear behavior is presented. It concerns a seismic evaluation of an office building for which a retrofitting solution is proposed. From this study, it is shown how taking into account the failure mode and the mechanical degradation through a nonlinear constitutive law enables to elaborate the best optimized retrofitting strategy. On the contrary, a classical approach based on an elastic linear analysis leads to a retrofitting solution which is much more intrusive and expansive and less respectful for the environment.

## 2. State of the art

In this part, a brief presentation of the approaches used for seismic diagnosis is proposed. From the choice of a nonlinear simulation, some available techniques are also presented. Finally, the isotropic damage constitutive law chosen for the application is described.

### 2.1 Seismic evaluation

When considering the seismic behavior of reinforced concrete structures, the methods can generally be divided into three parts: modal spectral analysis, equivalent static method (linear or nonlinear) and transient approach (linear or nonlinear).

In the first case, the analysis is based on a linear elastic modal technique. The fundamental modes of vibration of the building are computed by taking into account inertial and static loadings. From the vibration frequencies the seismic loading (acceleration) is obtained. It is added to static forces and the final stresses are computed by a linear elastic simulation to perform the design of the new building or to evaluate the capacity of an existing structure. Nevertheless, this type of computation does not take into account the energy dissipation related to the nonlinear behavior of the material. One solution is to determine a « coefficient of behavior » that reduces the seismic forces. But the choice of this coefficient is not totally well defined, and concerns the entire structure without any distinction between weak and strong sections.

Transient computations represent an appropriate alternative because they provide a more detailed estimation of the behavior and enable to study a large range of structures (even an irregular geometry for example). Moreover, these methods can be applied either with a linear or a nonlinear constitutive law. But in this case, they require a significant computational cost and are thus rarely applied.

The engineering use of these types of analyses is based on an elastic material behavior. But, even if the behavior coefficient enables to reduce the forces and thus reduce the required amount of steel reinforcement, the accuracy of the results is not totally satisfying for existing buildings. The pushover method can represent an interesting alternative, since the estimated capacity of the structure is taken into account through a nonlinear structural analysis. It is less costly than transient approach and enables to use nonlinear constitutive laws (Fajfar (2000), FEMA 273, ATC 40). The structure is submitted to an increasing lateral monotonic load, up to failure. This allows you to obtain a more realistic path of degradation of the structure taking into account post-elastic material behavior and stress redistribution. From the global behavior curve, the possible equilibrium point is determined, where the resistance of the structure balances seismic loading. Contrary to modal spectral methods, the aim is not to define the differences between existing and a

required steel reinforcement design solution but to characterize the “real” capacity of the structure with regard to in place rebars.

To use this technique, a representative robust and “simple” (for the calibration of the parameters especially) constitutive law is needed. In the context of seismic studies, it is indeed essential to be sure that the computation will be performed to the end and it will then provide suitable and sufficient information. It is to be noted that this paper focuses on the global retrofitting of reinforced concrete structures. That is why the chosen model has to be able to represent the mechanical degradation and the global behavior but does not need to characterize accurately the crack characteristics (crack opening for example).

**2.3 Description of concrete constitutive law**

Many approaches have been developed to represent the mechanical behavior of reinforced concrete structures. They are based on theoretical models that can be classified, depending on the way the mechanical degradation is described (directly by discrete approaches or from internal variables with continuum models for example). Many solutions seem thus available to solve the industrial problem. In the following, a brief description is proposed.

For the purpose of this analysis, the isotropic damage law, initially developed by Mazars (1984), is chosen. Given the type of loading (stress state), the numerical robustness and the availability of the model in different finite element codes (well documented law and calibration technique from classical elementary tests), this model is appropriate for the study. Its simplicity also offers acceptable cost in computation. The mechanical behavior is described through a scalar variable  $D$  (for Damage) representative of the microcracking of concrete. The degradation is applied on the elastic stiffness as bellow. Mazars proposes the use of an equivalent strain indicator based on the tensile state of the material to determine the cracking and crack evolution. where  $\langle \varepsilon_i \rangle_+$  designs the positive principal strains. The loading surface  $g$  is defined also.

$$\sigma_{ij} = (1 - D)C_{ijkl}\varepsilon_{kl} \quad \varepsilon_{eq} = \sqrt{\sum_{i=1}^3 \langle \varepsilon_i \rangle_+^2} \quad g(\varepsilon, D) = \tilde{D}(\varepsilon) - D$$

$D$  is equal to the maximum value of  $\tilde{D}$  during the history of loading,  $D = \text{Max}_t (\tilde{D}, 0)$ . The evolution of  $\tilde{D}$  is controlled by a law that distinguishes tension and compression (due to a concrete compressive strength which is ten times higher than the tensile one) by introducing two scalar variables  $D_t$  and  $D_c$ :

$$\begin{aligned} &\text{if } \varepsilon_{eq} \geq \varepsilon_{D0} \\ &\tilde{D}(\boldsymbol{\varepsilon}) = \alpha_t(\boldsymbol{\varepsilon})D_t(\varepsilon_{eq}) + \alpha_c(\boldsymbol{\varepsilon})D_c(\varepsilon_{eq}) \\ &D_{t,c} = 1 - \frac{\varepsilon_{D0}(1 - A_{t,c})}{\varepsilon_{eq}} - \frac{A_{t,c}}{\exp[B_{t,c}(\varepsilon_{eq} - \varepsilon_{D0})]} \\ &\alpha_{t,c} = \left( \frac{\sum_{i=1}^3 \langle \varepsilon_i^{t,c} \rangle_+ \langle \varepsilon_i \rangle_+}{\varepsilon_{eq}^2} \right)^\beta \\ &\text{else } \tilde{D} = 0 \end{aligned}$$

$\varepsilon_{D0}$  is a model parameter and represents the initial threshold from which damage initiates.  $D_t$  et  $D_c$  represent the tensile and compressive parts of damage.  $A_{t,c}$  et  $B_{t,c}$  are four model parameters. The weights  $\alpha_t$  and  $\alpha_c$  are computed from strains. In tension,  $\alpha_t = 1$  and  $\alpha_c = 0$ . In compression,  $\alpha_t = 0$  et  $\alpha_c = 1$ .  $\beta$  reduces the damage effect when the material is loaded in shear.

The damage evolution is finally determined by Kuhn–Tucker conditions:

$$g \leq 0, \quad \dot{D} \geq 0, \quad g\dot{D} = 0$$

Concerning steel, the constitutive model used is a classical elasto-plastic kinematic linear hardening model.

### 3. Damage mechanics applied to the seismic behavior of a reinforced concrete structures

#### 3.1. Presentation of the structure

The office building considered in this contribution is a 9 story reinforced concrete structure. Figure 1 illustrates the geometry. The thickness of the walls and the slabs are respectively equal to 18 and 25 cm. The bracing of the building for the horizontal loads is obtained by the shear walls. Nevertheless, during the design, the actions have been underestimated, with consequently too many openings in the walls and insufficient steel reinforcement.

To propose a retrofiting solution, a traditional engineering approach would be carried out with a modal spectral technique to evaluate the stresses and to determine the required steel ratios. These would have then been compared with the existing rebars to determine the presence of any weak area critical to the stability of the structure.

For the purpose of a pushover analysis, the FE model is enriched with the existing reinforcement. Figure 2 illustrates the mesh, where the slabs are represented using shell elements. Steel reinforcement of slabs and walls are represented by special shell elements with unidirectional behavior along each rebar direction.

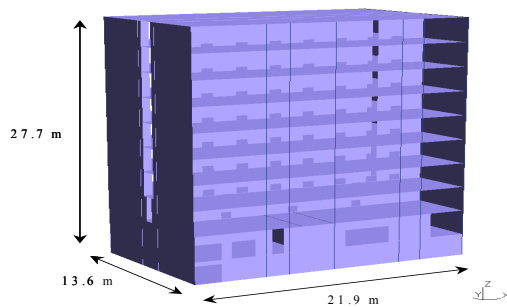


Figure 1. Building geometry

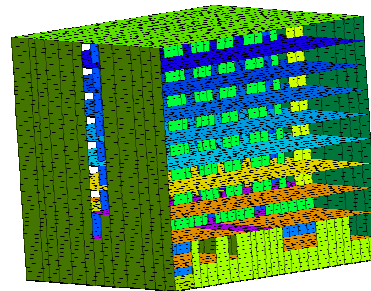


Figure 2. Finite element mesh

The static loadings are the body weight of structural elements, permanent loads  $G$  (between 100 and 250 kg/m<sup>2</sup>) and operating loads  $Q$  (250 kg/m<sup>2</sup>). The mass associated to these loads are also taken into account to evaluate the seismic loading. After having applied the gravity loads, a pushover lateral load is gradually applied on the part of the

building out of ground. The vertical distribution of the lateral load is determined by the shape of the principal mode of vibration in the chosen direction (X and Y).

The lower part of the building under ground, soil-structure interaction is taken into account by considering appropriate boundary conditions.

Nonlinearities are considered to take place in all walls and slabs (absence of beams and columns). Considering the nonlinear material models, all numerical parameters were chosen to fit characteristics specific to the project: elastic modulus, Poisson ratio, tensile and compressive strengths of concrete, elastic modulus and yielding stress of rebar steel. These are summarized in the following table. It has to be noticed that other material properties are also used to determine the softening of concrete. While normal values were used here, more specific values may be chosen upon available experimental data.

|          | E<br>(MPa) | $\nu$<br>(-) | $\rho$<br>(kg.m <sup>-3</sup> ) | $f_c$<br>(MPa) | $f_t$<br>(MPa) | $f_e$<br>(MPa) |
|----------|------------|--------------|---------------------------------|----------------|----------------|----------------|
| Concrete | 32 000     | 0.2          | 2 500                           | 25             | 2.1            |                |
| Steel    | 200 000    | -            | 7 850                           | -              | -              | 400            |

Table 1. Concrete and steel properties

**3.2. Results of the simulation**

The pushover method enables to determine the global behavior of the structure. Figure 3 presents, as a function of the horizontal top roof displacement, the total force applied on the wall.

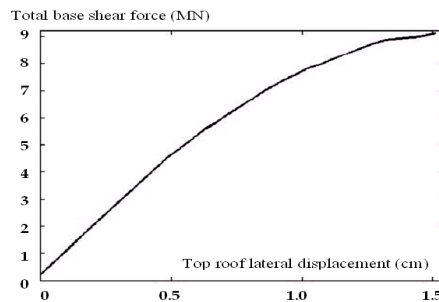


Figure 3. Capacity diagram: foundation shear force versus top roof displacement

This shows a monotonic evolution, quite linear at the early stages before reaching a maximum displacement that corresponds to one of the failure modes of the structure, which corresponds to excessive tensile strain in rebars. Other failure modes could be: concrete crushing, shear cracking, interstory drift, loss of foundation. Here, the large strain in steel is caused by the failure of the wall due to strong shear force (Figure 4). This is the key feature of a nonlinear analysis that provides access to the failure mechanism of the structure.

The pushover method consists in comparing the capacity diagram of the structure to seismic load demand diagram, and determines the equilibrium point (demand point).

At demand point loading, Figure 5 illustrates the damage distribution (D variable of the concrete constitutive model), which indicates the mechanical degradation of concrete. When D=0, concrete is at its full capacity, while at D=100% it loses all its mechanical properties.

From Figure 5 we can observe that:

- For longitudinal walls (left image) concrete damage is rather spread all over the structure. At almost every story, each wall is damaged through their entire width. This behavior is very probably due to door openings that significantly affect the stiffness these walls to resist shear forces.
- For transversal walls (right image) degradations are more localized at lower stories where bending moment are the greatest.

As mentioned before, the main interest of nonlinear analysis is to be able to predict the maximum load capacity of the structure, and identify structural weaknesses, in order to elaborate the best retrofitting solutions. Here one retrofitting solution could be the increase in thickness of walls from 18 to 33cm with an additional 18 cm<sup>2</sup>/m reinforcement in both horizontal and vertical directions. Moreover, from damage distribution results it appears that the retrofitting may be applied only to stories 2 to 4. Including these changes in the FE model, another pushover analysis allows to appreciate the strength capacity improvement reached (see Figure 6).

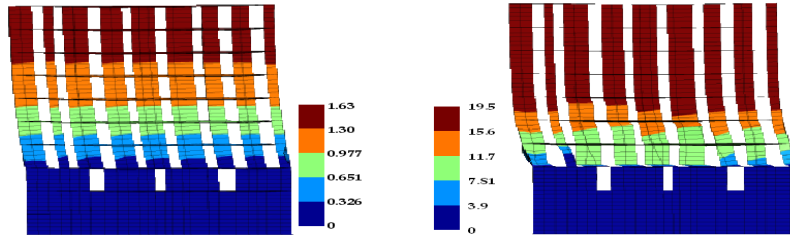


Figure 4. Deflection of the model (cm). Left: at the moment of the first failure point (see Figure 3), Right: at a loading point way above the failure point

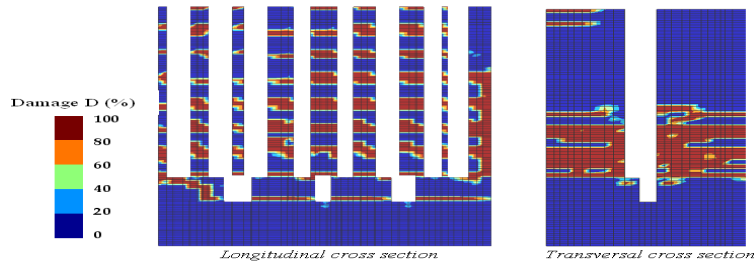


Figure 5. Damage distribution at demand point

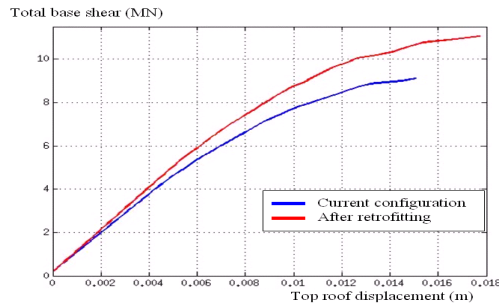


Figure 6. Effect of retrofitting on the demanding diagram

As expected, the retrofitting increases both shear force capacity and slightly the ductility of the structure to ground motions along the X direction. Figure 7 shows the damage distribution at the new demanding point.

For the sake of comparison, the same building studied by traditional linear elastic modal spectral analysis and the use of a behavior factor of 2 concluded to a generalized insufficient reinforcement. The difference in retrofitting cost between the two approaches was then roughly estimated to at least one million euros. To this one could add the organization difficulties of the job site and employee relocation (more important in case of generalized retrofitting) and environmental impact.

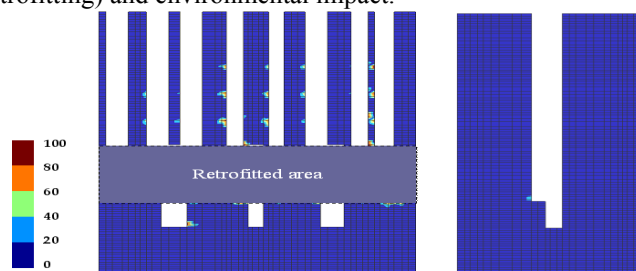


Figure 7. Damage distributions after retrofitting

#### 4. Conclusions

With significant increase in risk management and sustainable development issues related to construction works, the attraction for the use of advanced simulation tools and techniques is becoming more and more obvious. This is even stronger in earthquake mitigation, where structures are submitted to severe conditions.

Most international building codes allow four types of approaches: simplified static equivalent approaches, spectral analyses, time history analyses and non linear pushover methods. While for new projects linear elastic analysis is in most cases sufficient to encounter for seismic action, this is mostly not the case for existing structures where these methods could lead to wrong diagnosis or overestimation in retrofitting needs. The pushover approach, presented in this contribution, provides, in the case of regular buildings, more realistic results than modal spectral models and is more useable than time history methods (computational costs). Pushover analyses have thus proved to be efficient for regular structures and investigation are still going on for more complex situations.

The example shown in this contribution indicates the interest of performing simulations using nonlinear constitutive laws. Such studies lead to both the capacity of the structure to withstand a given ground motion, and provide indication on structural weaknesses. Such analysis techniques also allow to evaluate the efficiency of retrofitting solutions and thus their optimization. In this project the economical benefit appears quite clearly, with the proposal of a less aggressive retrofitting solution allowing to maintain the building functional for most of its occupants.

However, the situation is more complicated when it comes to a wide range of industrial applications, since the validity of nonlinear constitutive models are constrained to specific areas (loading conditions, geometrical configurations,...). The cost in preparing appropriate FE modeling, and computation are usually put forward by engineers to explain why these techniques are not used and finally limited to analysis performed by experts from research centers. The experience shows that quite often strong difficulties

arise: lack of reliable information on models and their validity, lack of input data calibration techniques, numerical robustness, and cost. That is why, in spite of significant improvements in computation capacities (size and speed), nonlinear application still require great amount of time, human and hardware resources to ensure reliable studies.

### 5. Références

- ATC 40, "Seismic evaluation and retrofitting of concrete buildings" – Volume 1, *Applied Technology Council, Reoirt n° SSC 96-01*, November 1996.
- FEMA 273, "NEHRP guidelines for the seismic rehabilitation of buildings", *Federal Emergency Management Agency*, October 1997.
- Fajfar P. "A nonlinear analysis method for performance based seismic design", *Earthquake Spectra*, vol. 16, 2000, p. 573-592.
- Mazars J., "Application de la mécanique de l'endommagement au comportement non linéaire et à la rupture du béton de structure", Thèse d'Etat, Université Pierre et Marie Curie, 1984.

## ISS modelling and its contribution to the seismic response of RC structures

Stéphane Grange<sup>1</sup>, Panagiotis Kotronis<sup>2</sup>, Jacky Mazars<sup>1</sup>

<sup>1</sup> Laboratoire Sols, Solides, Structures - Risques (3S-R) UJF/INPG/CNRS UMR 5521  
Domaine Universitaire BP 53 38041 Grenoble cedex 9, France  
Stephane.Grange@ujf-grenoble.fr, Jacky.Mazars@grenoble-inp.fr

<sup>2</sup> Research Institute of Civil Engineering and Mechanics (GeM), UMR CNRS 6183  
Ecole Centrale de Nantes, 1 rue de la Noë, BP 92101, 44321 Nantes Cedex 3, France  
Panagiotis.Kotronis@ec-nantes.fr

---

**Abstract.** This paper presents a simplified modelling strategy aiming at simulating the dynamic behaviour of reinforced concrete (RC) structures considering Soil-Structure Interaction (SSI). The presentation of a non linear interface element able to compute SSI by simulating a rigid shallow foundation is carried out. The new element is based on the “macro-element” concept. The foundation of the structure is supposed infinitely rigid and its movement is entirely described by a system of global variables (forces and displacements) defined in the foundation’s centre [Grange *et al.* , 2008], [Grange *et al.* , 2009]. This SSI element is available in various finite element codes (e.g. FEDEASLab or Cast3m). It can be coupled with multifiber Timoshenko beam elements to simulate the behaviour of the RC upper structure. The use of macro-elements combined with multifiber beam elements allows mitigating vulnerability of structures and evaluating the displacements that occur during an earthquake. Validation of the proposed modelling strategy is provided using experimental results.

**keyword:** foundation; plasticity; uplift; macro-element; soil structure interaction; RC walls.

---

## 1 Introduction

In civil engineering, boundary conditions have to be correctly modeled in order to reproduce numerically the non linear behavior of a structure. Soil-Structure Interaction (SSI) can not be neglected. This is particularly true for slender structures like tall buildings or bridge piers. Their behavior is different whether the structure is on a solid rock or on a soft soil.

However, simulating SSI often necessitates the use of detailed and complex 3D finite element models for the soil and the structure, leading to a great number of degrees of

freedom and thus to significant computational costs. This is the reason why various simplified modelling strategies have been recently developed.

The macro-element concept was applied for the first time in geomechanics in [Nova *et al.*, 1991]. It consists in condensing all nonlinearities into a finite domain and works with generalized variables (forces and displacements) that allow simulating the behaviour of shallow foundations in a simplified way. The macro-element developed in [Grange *et al.*, 2008], [Grange *et al.*, 2009] is inspired from [Crémer *et al.*, 2002] and it reproduces the behavior of a 3D shallow foundation of circular, rectangular or strip shape, submitted to cyclic or dynamic loadings. It takes into account the plasticity of the soil and the uplift of the foundation. A brief outline of the formulation of the macro-element follows.

## 2 Mathematical description of the macro-element

The associated generalized variables (displacement and force vectors) are dimensionless. They are defined hereafter (for any  $a, a'$  defines the corresponding dimensionless variable): vertical force  $V'$ , horizontal forces  $H'_x, H'_y$  and moments  $M'_x, M'_y$ , but also the corresponding displacements, vertical settlement  $u'_z$ , horizontal displacements  $u'_x, u'_y$  and rotations  $\theta'_x, \theta'_y$ . Torque moment ( $M'_z$ ) is not taken into account (figure 1).

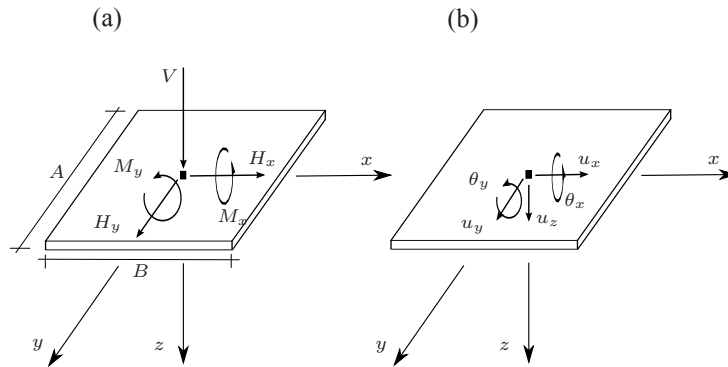


Figure 1: Generalised variables: (a) forces and (b) displacements for a rectangular foundation.

The elastic part of the constitutive law is defined as  $\underline{\mathbf{F}} = \underline{\mathbf{K}}^{\text{el}} \underline{\mathbf{u}}^{\text{el}}$ , where the displacement  $\underline{\mathbf{u}}^{\text{el}}$  and force vectors  $\underline{\mathbf{F}}$  are dimensionless. The elastic stiffness matrix  $\underline{\mathbf{K}}^{\text{el}}$  is calculated using the real part of the static impedances. It is considered diagonal, i.e. there is not coupling between the different directions of the loading.

The failure criterion for the plasticity mechanism is defined for an overturning mechanism with uplift [Salençon *et al.*, 1995]. The adaptation in 3D is done by adding the two terms related with the horizontal force and moment according to the other axis and assuming axial symmetry. One finally obtains the following 5D surface:

$$f_c(\underline{\mathbf{E}}, \underline{\boldsymbol{\tau}}, \rho, \gamma) \equiv \left( \frac{H'_x}{\rho a V'^c (\gamma - V')^d} - \frac{\alpha_1}{\rho} \right)^2 + \left( \frac{M'_y}{\rho b V'^e (\gamma - V')^f} - \frac{\alpha_2}{\rho} \right)^2 + \left( \frac{H'_y}{\rho a V'^c (\gamma - V')^d} - \frac{\alpha_3}{\rho} \right)^2 + \left( \frac{M'_x}{\rho b V'^e (\gamma - V')^f} - \frac{\alpha_4}{\rho} \right)^2 - 1 = 0 \quad (1)$$

The coefficients  $a, b$  define the size of the surface in the planes  $(H' - M')$ .  $c, d, e$  and  $f$  define the parabolic shape of the surface in the planes  $(V' - M')$  and  $(V' - H')$ . These parameters can be fitted to different experimental results found in the literature.  $\underline{\boldsymbol{\tau}} = [\alpha_1, \alpha_2, \alpha_3, \alpha_4]$  is the kinematics hardening vector composed of 4 kinematics hardening variables and  $\rho$  the isotropic hardening variable. The variable  $\gamma$  is chosen to parametrize the second intersection point of the loading surface with the  $V'$  axis and its evolution along the  $V'$  axis. The evolutions of the hardening variables are obtained considering experimental results and numerical simulations of foundations under cyclic loadings from the model of Crémer [Crémer *et al.*, 2002].

An evolution of this variables linked to the distance  $\Delta$  between the loading point and the failure criterion leads to a perfect tangency of the loading surface and the failure criterion without any interpenetrations between the surfaces (see figure 2 where, for instance:  $H^* = \frac{H'}{a V'^c (1 - V')^d}$ ).

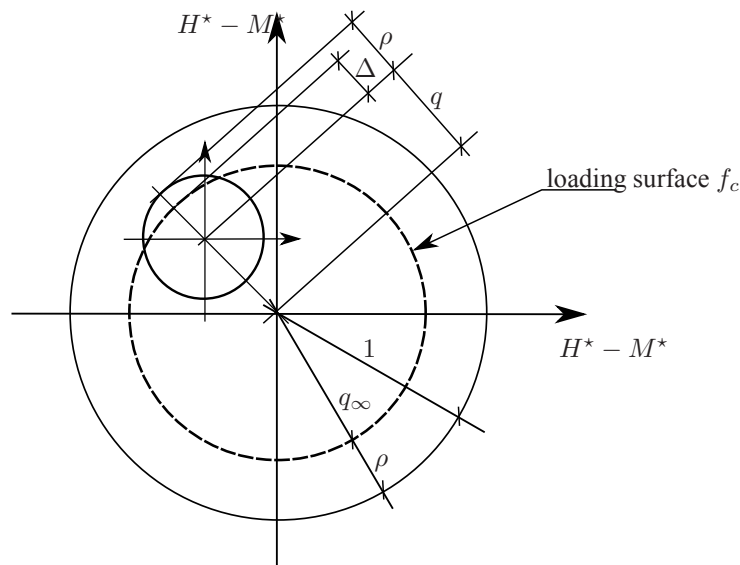


Figure 2: Definition of the distance  $\Delta$  in hyperplan  $(H^*_x, M^*_y, H^*_y, M^*_x)$ .

The failure criterion is given by equation (1) considering  $(\alpha_1, \alpha_2, \alpha_3, \alpha_4, \rho, \gamma) = (0, 0, 0, 0, 1, 1)$ .

The flow rule used is associated in the  $(H'_x, M'_y, H'_y, M'_x)$  hyperplane and non associated in the  $(H'_x, V')$ ,  $(M'_y, V')$ ,  $(H'_y, V')$ ,  $(M'_x, V')$  planes.

Uplift behavior can be treated with a non-linear elastic mechanism following the  $M - \theta$  relationship proposed by Cr mer. A Newton algorithm solver is computed in order to solve the three non-linear equations system governing the uplift mechanism. Let's remind that uplift mechanism is essential for computing a negative vertical displacement of the center of the foundation. For further details see [Grange *et al.* , 2009].

### 3 Numerical results

A model using Timoshenko multifiber beams [Kotronis *et al.* , 2005], [Mazars *et al.* , 2006] and concentrated masses is chosen to reproduce the structure (3). Six beam elements are used for the piles P1 and P3 and nine elements for the pile P2. The mesh is refined at the base of the piles where damage tends to be important. 40 concrete fibers and 80 steel fibers (representing the reinforcement bars at their actual position) are used in each section. Details of the model are provided in [Grange *et al.* , 2010]. Concrete is simulated using a uniaxial damage mechanics law [La Borderie , 1991] and steel with the classical Menegoto Pinto model [Menegoto *et al.*, 1973]. The desk being from prestressed concrete, its behaviour is assumed linear and it is discretised using linear beam elements. The loading is applied according to the  $z$  axis. Calculations are made with FEDEASLab, a finite element MATLAB toolbox [Filippou *et al.* , 2004].

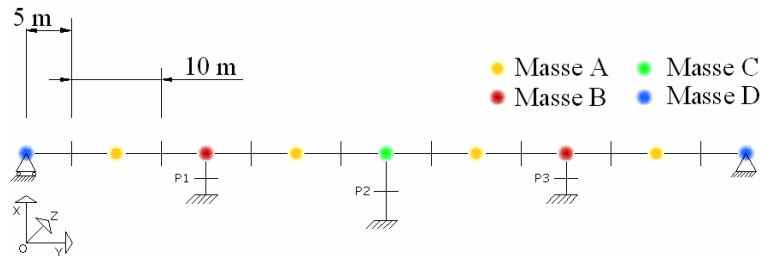


Figure 3: Viaduct - SSI: model using multifiber beam elements and concentrated masses.

Rectangular shallow foundations are numerically introduced at the base of each pile in two different ways, via macro-elements or linear springs. The dimensions of the foundations are:  $L_z = 4.2m$ ,  $L_y = 2.1m$ . The stiffness of the springs is such that they accumulate the same energy as the non-linear SSI macro-element. A class B soil is considered according to the Eurocode 8 classification. Its characteristics are given in table 1.

Numerical results are presented in 4. Three types of boundary conditions are considered: linear springs (EL), macro-element (ME) and embedded (Fixed). Results are similar in terms of internal forces. Nevertheless, maximum displacements at the top of the piles are found significantly increased (multiplied by 2) for the cases considering SSI (EL and

Table 1: Viaduct - SSI: Characteristics of the class B soil.

| soil            | Shear modulus $G_0$<br>velocity $V_s$ | cohesion $c$<br>and friction<br>angle $\phi$ | Stiffness and<br>damping   | ultimate<br>bearing<br>stress $q_{max}$ |
|-----------------|---------------------------------------|--|--|---|
| Class B<br>soil | $V_s = 360m/s$<br>$G_0 = 259.2MPa$    | $c_u = 370kPa$<br>$\phi_u = 0$               | $K_{\theta\theta} = 144484.1MNm/rad$<br>$K_{zz} = 1845.5MN/m$<br>$K_{hh} = 2260.2MN/m$<br>$C_{\theta\theta} = 23.17MNms/rad$<br>$C_{zz} = 3.61MN/s/m$<br>$C_{hh} = 2.95MN/s/m$ | $q_{max} = 2100MPa$                     |

ME). Non-linearities are concentrated principally at the base of each pile. In other words, the resisting moment of concrete guides the behavior of the structure. The resisting force of the pile is reached before the resisting moment of the system soil+foundation. The procedure is similar as if the piles were embedded in the soil, except for the displacements that are amplified.

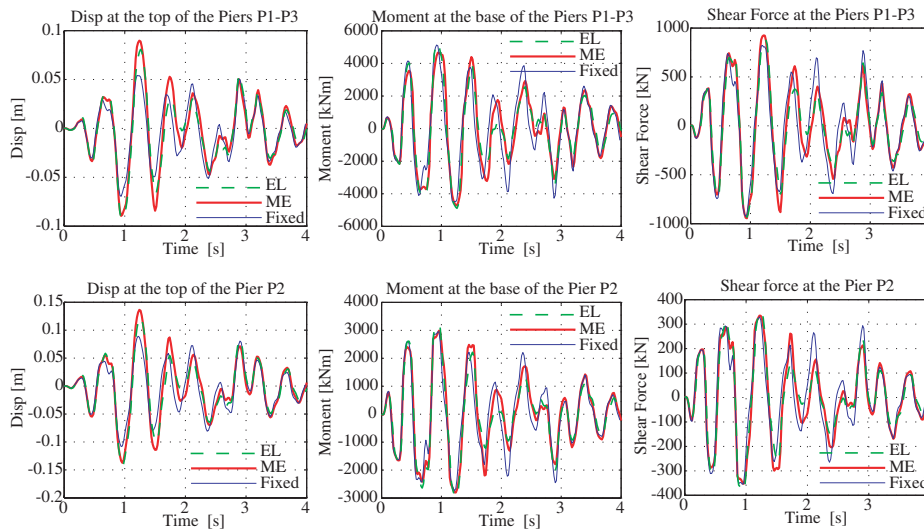


Figure 4: Viaduct - SSI: comparisons of the displacements, moments, shear forces for a class B soil.

## References

- Crémer C., Pecker A., Davenne L., Modelling of nonlinear dynamic behaviour of a shallow strip foundation with macro-element, *Journal of Earthquake Engineering*, vol. 6, n 2, (2002), p. 175-211.
- Filippou F., Constantinides M., FedeesLab Getting Started Guide And Simulations Examples, Report, Dpt of civil and Env. Engng. UC Berkeley, (2004).
- Grange S., Botrugno L., Kotronis P., Tamagnini C., The effects of Soil-Structure Interaction on a reinforced concrete viaduc, *Earthquake Engineering and Structural Dynamics*, (2010), accepted for publication.
- Grange S., Kotronis P., Mazars J., A macro-element for a circular foundation to simulate 3D soil-structure interaction, *International Journal for Numerical and Analytical Methods in Geomechanics*, vol. 32, n 10, (2008), p. 1205-1227.
- Grange S., Kotronis P., Mazars J., A macro-element to simulate 3D soil-structure interaction considering plasticity and uplift, *International Journal of Solids and Structures*, vol. 46, (2009), p. 3651-3663.
- Kotronis P., Mazars J., Simplified modelling strategies to simulate the dynamic behaviour of r/c walls, *Journal of Earthquake Engineering*, vol. 9, issue 2, (2005), p. 285-306.
- La Borderie C., Phénomènes unilatéraux dans un matériau endommageable: modélisation et application à l'analyse des structures en béton, Thèse de doctorat, Université Paris 6, (1991).
- Mazars J., Kotronis P., Ragueneau F., Casaux G., Using multifiber beams to account for shear and torsion. applications to concrete structural elements, *Computer Methods in Applied Mechanics and Engineering*, vol. 195, issue 52, (2006), p. 7264-7281.
- Menegoto M., Pinto P., Method of analysis of cyclically loaded reinforced concrete plane frames including changes in geometry and non-elastic behaviour of elements under combined normal force and bending, IABSE Symposium on resistance and ultimate deformability of structures acted on by well-defined repeated loads, final report, Lisbon, (1973), p. 328p.
- Nova R., Montrasio L., Settlements of shallow foundations on sand, *Géotechnique*, vol. 41, n 2, (1991), p. 243-256.
- Salençon J., Pecker A., Ultimate bearing capacity of shallow foundations under inclined and eccentric loads. Part II: purely cohesive soil without tensile strength, *European Journal of Mechanics, A/Solids*, vol. 14, n 3, (1995), p. 377-396.

## Seismic Vulnerability reduction: Numerical modeling of FRP reinforcement using multifiber beams elements

Cedric Desprez<sup>1</sup>, Saber El Arem<sup>1</sup>, Panagiotis Kotronis<sup>2</sup> and Jacky Mazars<sup>1</sup>.

<sup>1</sup> Laboratoire Sols Solides Structures et Risques (3S-R) UJF/INPG/CNRS UMR 5521  
Domaine Universitaire BP 53 38041 Grenoble cedex 9, France.  
Cedric.Desprez@hmg.inpg.fr, Jacky.Mazars@hmg.inpg.fr

<sup>2</sup> Research Institute of Civil Engineering and Mechanics (GeM), UMR CNRS 6183  
Ecole Centrale de Nantes, 1 rue de la Noë, BP 92101, 44321 Nantes Cedex 3, France.  
Panagiotis.Kotronis@ec-nantes.fr

---

**Abstract.** This paper presents a simplified modeling strategy for reproducing the behavior of beam-column structures reinforced with Polymer Reinforced Fibers (FRP). A 1D concrete constitutive model has been recently proposed, suitable for both monotonic and cycling loadings [1]. The model is inspired on two well-known concrete laws, one based on damage mechanics theory (La Borderie concrete damage model) and one based on experimental studies (Eid & Paultre's confined concrete model). Spatial discretization is done using multifiber Timoshenko beam elements. Validation of the strategy is provided using two case studies: a retrofitted bridge pier and a vulnerability analysis on an existing building.

**Keywords.** FRP, seismic loading, vulnerability, concrete, damage mechanics, retrofitting.

**Acknowledgement.** The authors gratefully acknowledge the support of the Sherbrooke civil engineering department and the French ANR ARVISE research project.

---

### 1 Introduction

Nowadays, Reinforced Polymer Fibers (FRP) are often used in retrofitting of civil engineering structures. Their role is mainly to confine existing columns and to increase the bearing capacity of beams or walls through axial reinforcement. This paper deals with a simplified model to simulate the behavior of FRP confined columns and beams or walls. A uniaxial (1D) concrete constitutive model, suitable both for monotonic and cycling loadings, is presented. Two case studies are used for validation: a retrofitted bridge pier and a vulnerability analysis on an existing building.

### 2 Modeling tools

In order to decrease the number of degrees of freedom and thus to simplify the finite element mesh, Timoshenko multifiber beam elements are often used to discretise RC specimens [2]. This approach is also adopted for the calculations presented in this paper. Shear is considered linear, allowing thus using 1D constitutive laws. Regular concrete is

modeled using La Borderie’s model [3]. Based on damage mechanics, it takes into account the opening and closing of cracks. In order to reproduce the behavior of confined concrete under monotonic loading, the predictive model of Eid & Paultre [4] is adopted. It is a global model taking into account internal (due to Transverse Shear Reinforcement TSR) and external (due to FRP) confinement (Figure 1). The cyclic behavior of steel is simulated using the classical Menegotto-Pinto model.

### 3 Simulating RC Columns confined with FRP

#### 3.1 RC columns confined with FRP: principle of modeling

In concrete columns, the main mechanical effect of the internal and external confinement is to reduce the development of lateral expansions that cause the most part of the damage. A simplified way to take this effect into account using a 1D damage mechanics law is to adapt the damage evolution law due to compression. The proposed strategy consists in adapting the damage evolution of the La Borderie model to fit the evolution proposed in Eid & Paultre’s model [1].

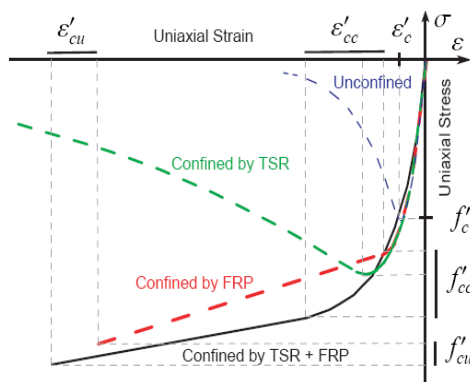


Figure 1 . Monotonic model for confined concrete available for different confinement ratio (Eid & Paultre)

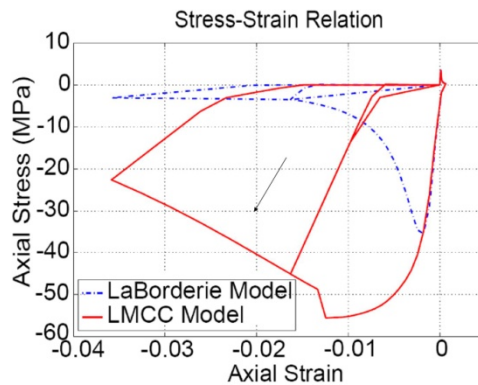


Figure 2 . Cyclic model for confined concrete (LMCC model)

#### 3.2 Case study: Bridge pier under axial and flexural load.

##### Experimental setting

A RC mockup, representative of an existing bridge (1/3 scale) with partial retrofitting, has been recently cyclic tested at the University of Sherbrooke. The bridge pier contains 3 identical columns of 2.1m height and a transverse beam (Figure 3). Only the two outer columns are retrofitted with FRP (the central column and the beam are not retrofitted). The axial load on each column varies from 10% to 20% of its estimated capacity in uniaxial compression during the cycles. The lateral imposed displacement is cyclic with increasing intensity. During the test, the force-displacement curve is measured (Figure 4).



Figure 3. Bridge pier mockup with partial retrofitting.

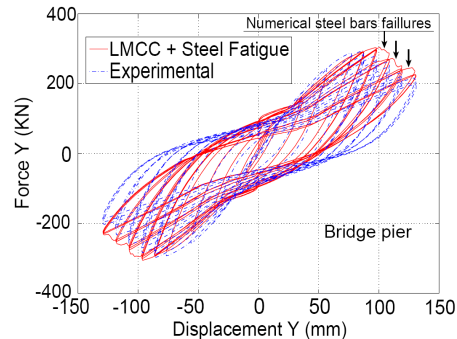


Figure 4. Numerical result Vs experimental data.

### *Numerical modeling*

Each column is modeled using Timoshenko multifiber beam elements. They are considered fixed at the bottom. The transverse beam is assumed elastic with a reduced section to take into account the initial cracks in concrete. Each multifiber section contains 24 concrete fibers and 15 fibers representing the longitudinal steel bars. Material parameters are based on experimental tests [5]. The material model used for the unconfined concrete (central column) is the La Borderie model; for the confined concrete (outer columns) the LMCC model and for the steel bars the Menegotto-Pinto model. In Figure 4, numerical results show relatively good agreement with the experimental data in terms of maximum values but also hysteretic cycles.

## **4 Seismic vulnerability analysis of an existing RC building: Simulating RC elements axially retrofitted by FRP**

### **4.1 Axial reinforcement with FRP: principle of modeling**

FRP reinforcement, bonded on one side of a RC element (beam, wall...), has a function similar to the one of an external reinforcement bar (Figure 5). Using multifiber beams, one can easily numerically reproduce this contribution by adding a specific fiber in the multifiber beam section (Figure 6). The role of FRP is then simulated adopting a linear elastic brittle material law. Concrete and steel are again modeled again using La Borderie and Menegotto-Pinto models respectively.



Figure 5. Beam retrofitting with FRP bonding on lower side.

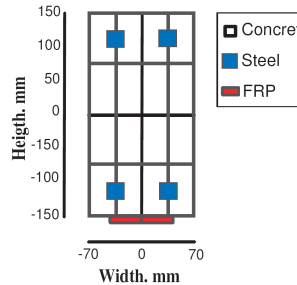


Figure 6. FRP addition in multifiber beam section



Figure 7. Grenoble city hall

#### 4.2 Case study: RC building

The proposed method is used to simulate the nonlinear behavior of an existing structure (Figure 7) before and after retrofitting. This building is a reinforced concrete structure constructed in 1966. Only the tall tower (which is separated from the rest of the building) is considered (Figure 8). The dimensions are, 43m long, 13m large, and 50m height. The structure is composed of four very stiff rectangular elements (containing the stairs and elevators), slabs, beams and columns.

The building has been modelled using nonlinear multifiber beams for the vertical elements and linear shell elements for the horizontal slabs. The linear dynamic behavior of the model has been validated by in-situ ambient vibration records [6].

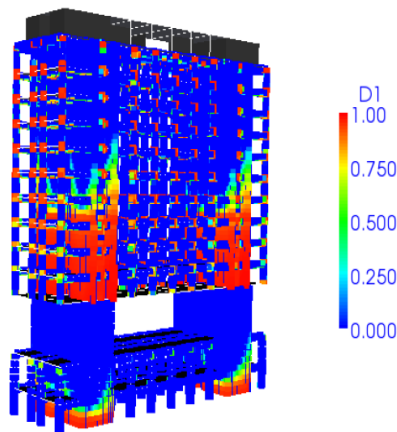


Figure 8. Model (no retrofitting): Damage due to traction (D1) in concrete.

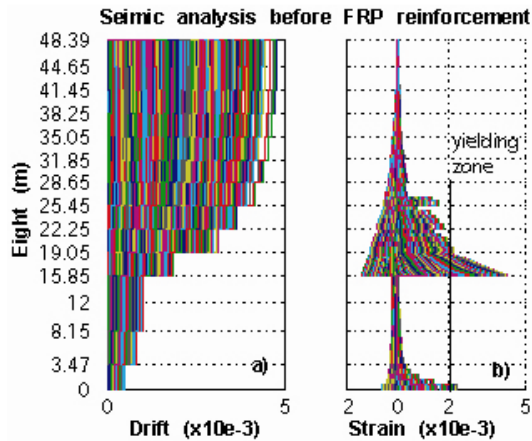


Figure 9. Model (no retrofitting): Maximum drift ratio (a) steel strain (b).

**4.2.1 Vulnerability analysis (without retrofitting)**

The first part of the study concerns the analysis of the seismic vulnerability of the structure before applying the FRP retrofitting. A synthetic three-directional signal based on EC8 design code is used for the dynamic nonlinear simulations. Figure 8 presents the results of the numerical analysis in terms of damage, drift ratio and steel strain. More specifically: The behavior of the structure is found mainly flexural without significant torsional effects. This beam-type behavior allows a flexural reinforcement using FRP. Damage due to traction is concentrated on four large areas but no damage due to compression appears. The steel stress-strain evolution shows that plastic hinges are developed in the building.

**4.2.2 Vulnerability analysis (with retrofitting)**

The second part of the study considers the structure this time (numerically) retrofitted. More specifically, FRP is applied at the four principal piers. The design of the FRP sheets is chosen such as to avoid the plastic behavior of steel bars. According to the results of the previous calculation (Figure 9), FRP is added on the first floor, at the base of the structure and on the five first floors of the upper part. After retrofitting, a classical nonlinear static analysis (pushover) shows that the flexural capacity increases (Figure 10). Indeed, FRP sheets allow reducing the strain localization due to plastic behaviour of reinforced steel bars. However, modifications on the structural dynamic response are surprisingly. FRP allows decreasing the steel strains but new localization patterns appears (e.g. above the last reinforced floor), Figure 11. Moreover, displacements and drift ratio values are slightly modified. One can clearly see the necessity of having numerical tools, as the one presented in this paper, in order to be able to proceed to nonlinear vulnerability studies.

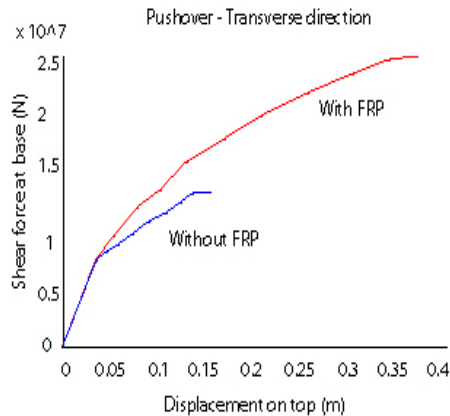


Figure 10. Pushover in the transverse direction: bearing capacity before and after retrofitting.

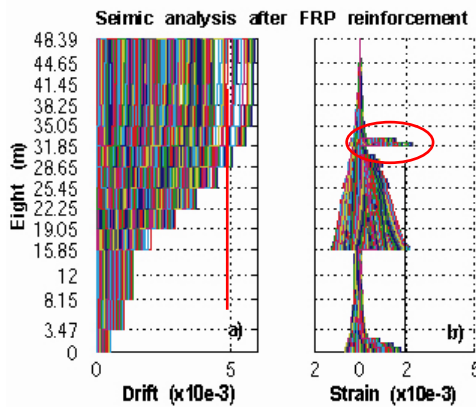


Figure 11. Model (with retrofitting): Maximum drift ratio (a) steel strain (b).

## 5 Conclusion

In this work, a simplified modeling strategy is presented in order to reproduce the nonlinear cyclic behavior of FRP RC structures. More specifically:

- Multifiber beam elements are used for the spatial discretization.
- A modification of the evolution law for the damage variable of the La Borderie model is adopted [1]. The new evolution is based of the Eid & Paultre concrete model. Validation is provided using the experimental results of a retrofitted bridge.
- Extra fibers are added on the multifiber beam element discretization to reproduce the FRP axial reinforcement. A vulnerability analysis on an existing building is performed to validate the approach.

The modeling strategy developed in this paper can serve as a simplified tool to do comparative studies on the vulnerability of RC structures before and after FRP retrofitting.

## References

- [1]. **Desprez, C, et al.** 2009. *Retrofitting reinforced concrete structures with FRP: Numerical simulation using multifiber beam elements*. Rhodes, Greece : Proceedings of COMPDYN, ECCOMAS Thematic Conference on Computational Methods in Structural Dynamics and Earthquake Engineering.
- [2]. **Mazars, J, et al.** 2006. *Using multifiber beams to account for shear and torsion : Applications to concrete structural elements*. 52, , Computer Methods in Applied Mechanics and Engineering, Vol. 195, pp. 7264-7281.
- [3]. **La Borderie, C.** 1991. Phénomènes unilatéraux dans un matériau endommageable: Modélisation et application à l'analyse des structures en béton. Thèse de doctorat. Université Paris VI, Paris, France.
- [4]. **Eid, R et Paultre, P.** 2008 *Analytical model for FRP-confined circular reinforced concrete columns*. 2008, Journal of Composites for Construction, Vol. 12, pp. 541-552.
- [5]. **Roy, N.** 2006 *Réhabilitation parasismique performantielle des ponts avec des polymères renforcés de fibres de carbone; Thèse de doctorat*. Université de Sherbrooke, Canada (Quebec).
- [6]. **Michel, C, et al.** 2009. *Full-scale dynamic response of an RC building under weak seismic motions using earthquake recordings, ambient vibrations and modeling*, Earthquake Engineering & Structural Dynamics, <http://dx.doi.org/10.1002/eqe.948> (Early View).

## Seismic vulnerability of quasi-symmetric structures with reinforced concrete shear walls

Miloud Hemsas<sup>1</sup>, Sidi Mohammed Elachachi<sup>1</sup>, Denys Breysse<sup>1</sup>

<sup>1</sup> Université Bordeaux 1, Laboratoire Ghymac, Av des Facultés, 33405 Talence, France  
[d.breysse@ghymac.u-bordeaux1.fr](mailto:d.breysse@ghymac.u-bordeaux1.fr)

---

**Abstract.** The evaluation of the seismic vulnerability of structures is a key element for preventing or reducing the seismic risk. In this study, we focus on the structural scale for a given type of buildings that of quasi-symmetric buildings made of bearing reinforced concrete walls. The structure is discretized in macro-elements, each macro-element being representative of a given structural scale. The performance level under seismic loading is estimated using the capacity theory, based on a static analysis also called “pushover”. The structural performance is considered as a probabilistic property, since both the spectral model of seismic action and the material properties have random dimensions (variability of the seismic signal, of the soil conditions, heterogeneity of concrete...). Monte-Carlo simulations have been performed in the frame of a parametric study such as to identify the distribution curves for vulnerability and to determine what are the more influential parameters. This study shows that a simplified modelling (macro-elements) which accounts at best for dynamic aspects is useful and enables to get relevant indicators. Fragility curves obtained for quasi-symmetric buildings made of bearing reinforced concrete walls seems consistent with the standard level of loading used in seismic codes and they can be used as well for structural design as for seismic retrofitting of existing buildings.

**Keywords:** Structural wall, Macro-element, Pushover, Inelastic spectra, Monte-Carlo, fragility function.

---

### 1 Introduction

The vulnerability assessment of structures which consists, a seismic action being given, to estimate damage (and its uncertainty) at the scale of a structure, a city or an agglomeration, is a key element for earthquake prevention and mitigation strategies. According to the scale of study, several vulnerability models and methodologies to reduce seismic risk have emerged. HAZUS (FEMA, 1999) and Risk-UE (Risk-UE, 2003) for example, form part of them. They allow to carry out damage assessment for different typologies of structures (in masonry infill, reinforced concrete, steel frames...), through the establishment of vulnerability curves (also called fragility curves).

In this study we consider a single type of structure and we are interested in the determination of vulnerability curves for only one typology: that of the quasi-symmetrical reinforced concrete structure with structural walls. The developed methodology is valid as

well for the design of new buildings (for a given level of seismic safety) as for the reassessment and retrofitting of existing buildings for seismic conformity.

## 2 Earthquake damage and vulnerability curves

### 2.1 Methodology and aims

The structure is discretized into a set of macro-elements, each macro-element being representative of a structure's floor (Hemsas et al., 2007).

The performance level is obtained by building the capacity curve which consists in drawing in the plan of the spectral accelerations ( $S_a$ ) versus the spectral displacements ( $S_d$ ), on one hand the global constitutive law of the structure (obtained from a Pushover analysis) and on the other hand the seismic demand curve (response spectrum which can be either a lawful spectrum, an envelope of the spectra of many earthquakes or the response spectrum of a particular earthquake). The intersection between these two curves gives the point of performance of the structure.

The analysis of the performance of the structure, in the Spectral acceleration-Spectral displacement ( $S_a$ ,  $S_d$ ) format, is deterministic if one knows its mechanical and geometrical characteristics as well as the applied loading. However, the representative response spectrum of the seismic action is random (fundamental period, higher modes effects...). In the same way, the materials properties are also random (variability due to concrete's heterogeneity, error of models and inaccuracy of measurements...).

With the vulnerability concept is associated the fragility concept (Risk-UE, 2003). It consists in representing the limits of performance levels in a probabilistic way according to a parameter ( $S_a$  or  $S_d$ ) representing the entire spectrum of damage states that a building may experience when it is subjected to earthquake ground motions of increasing severity (damage potential). At a given solicitation level, and for the four defined performance levels, four curves are plotted which lead to the probability of exceeding a defined damage level (Slight, Moderate, Severe, Collapse).

### 2.2 Proposed approach for estimating vulnerability

The approach used to estimate structural damage states is based on the capacity spectrum method (Freeman, 1998). It is divided into four main steps :

- determining and reproducing the global behaviour of a structure by a non-linear static (pushover) analysis. The shape of the applied seismic actions to the structure is in general, triangular or trapezoidal, with intensities proportional to the first mode of the structure. The proportionality factors can be the masses of each floor.
- defining and reproducing the seismic load: selection of an accelerogram for a direct dynamic analysis or choice of a response spectrum, if the study is static (or pseudo-dynamics).
- converting at the same time the elastic demand response spectrum which defines the seismic demand and the capacity curve which defines the potential performance of the structure, into a capacity spectrum in terms of spectral displacement  $S_d$  versus spectral acceleration  $S_a$ , then to determine its performance point (intersection of the two curves).
- identifying spectral displacements according to the preset damage levels. Spectral displacement (corresponding to the performance point of the studied structure) is used to evaluate the seismic vulnerability by determining for each damage level the specified

probability of occurrence of this given level of damage. In the case of the structures treated in this study (with shear walls), the damage occurs mainly through the formation of a plastic hinge at the base of the building (Paulay and Priestley, 1992).

### 2.3 Capacity curves and estimate of the performance point

The estimated performance level achieved during a given seismic action is obtained from the capacity curve and the demand spectrum. They are defined in the  $(S_a-S_d)$  format, where  $(S_d)$  is the maximum displacement of the response of an equivalent single-degree-of-freedom (SDOF) system which reproduces the desired mode displacement, usually the fundamental mode of vibration of the structure, and  $(S_a)$  is the maximum acceleration. Obtaining the capacity curves consists into two changes of variables:

- the seismic force  $F$  (the base shear  $V_b$ ) of the structure in the first mode is transformed into spectral acceleration of the equivalent model  $(S_a)$ ,
- and the actual roof displacement  $u_N$  (displacement of the  $N$ th-floor if the structure has  $N$  floors) is transformed into spectral displacement of the equivalent model  $(S_d)$ , using the following equations:

$$S_a = \frac{F}{M_1^*} \quad S_d = \frac{u_N}{\Gamma_1 \phi_{N,1}} \quad M_1^* = \frac{\left( \sum_{j=1}^N m_j \phi_{j,1} \right)^2}{\sum_{j=1}^N m_j \phi_{j,1}^2} \quad \Gamma_1 = \frac{\sum_{j=1}^N m_j \phi_{j,1}}{\sum_{j=1}^N m_j \phi_{j,1}^2} \quad (1)$$

in which  $M_1^*$  is the effective modal mass of the structure, related to the amplitude of the first mode of vibration and the masses  $m_i$  at the floor  $i$ ,  $\phi_{j,1}$  is the amplitude of displacement at the of the  $j$ -th floor corresponding to the first mode of vibration and  $\Gamma_1$  is the modal participation factor corresponding to the first mode of vibration. Note that the assumed displacement shape is normalized, the value at the top being equal to 1.

In the proposed approach, we adopt the non-linear response spectrum obtained directly from the elastic linear spectrum by using the equations  $R_\mu-\mu-T_n$  (which is intended to take into account the relationship between the reduction factors  $R_\mu$ , the ductility demand  $\mu$  and the period of vibration of the structure  $T_n$ ). This procedure was introduced into the developed code (Hemsas et al., 2007).

The identification of the performance point is shown on Figure 1 for medium and long structure's period. Both the demand spectra and the capacity curve have been plotted in the same graph. The intersection of the radial line corresponding to the elastic period  $T^*$  of the idealized bilinear system with the elastic demand spectrum  $S_{ae}$  defines the acceleration demand (strength) required for elastic behavior and the corresponding elastic displacement demand  $S_{de}$ . The yield acceleration  $S_{ay}$  represents both the acceleration demand and the capacity of the structure. In both cases ( $T^* < T_C$  and  $T^* \geq T_C$ ) the inelastic demand in terms of accelerations and displacements corresponds to the intersection point of the capacity curve with the demand spectrum corresponding to the ductility demand  $\mu$ . At this point, the ductility factor determined from the capacity curve and the ductility factor associated with the intersecting demand spectrum are equal.

### 3 Assessment of the vulnerability and identification of the damage levels

The evolution of the damage in a structure or a structural component can be characterized by a Damage Index (DI) which is a mathematical model for quantitative description of the damage state. Therefore many damage models have been developed, but, to the knowledge of the authors, no specific proposal concerning reinforced concrete walls has been developed.

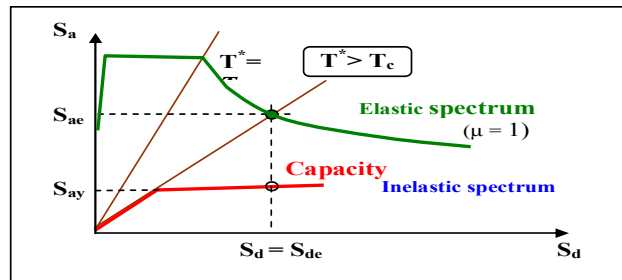


Figure 1. Elastic, inelastic spectrum and capacity curve in (Sa-Sd) format, in the medium and long period ranges.

The simplest Damage Index, following (Park et al., 1985), is defined as:

$$DI = \frac{\delta_m - \delta_y}{\delta_u - \delta_y} \tag{2}$$

where  $\delta_m$  is maximum displacement experienced by the structure (performance point);  $\delta_u$  is the ultimate displacement (total collapse) and  $\delta_y$  is the yielding displacement. Based on the structural damage levels, equivalence between the damage index  $DI$  previously defined and the state of damage (from  $DI \leq 0.1$  for no damage to collapse) are given in (Park et al., 1985). Using the definition of Damage Index and the capacity curve, one can determine the correlation between Park and Ang damage index and inter-story drift  $\Delta_i$ . The statistical distribution used to represent the fragility functions of the structure is a Log-normal distribution which represents adequately the combination of variables whose effects are multiplicative.

The conditional probability of being in, or exceeding, a particular damage state,  $ds$ , given the spectral displacement,  $S_{d_s}$  is defined:

$$P[ds|S_d] = \Phi \left[ \frac{1}{\beta_{ds}} \ln \left( \frac{S_d}{S_{d,ds}} \right) \right] \tag{3}$$

where:  $S_{d,ds}$  is the median value of the spectral displacement at which the structure reaches the threshold of the damage state  $ds$ ; and  $\beta_{ds}$  is the standard deviation of the natural logarithm of spectral displacement for damage state  $ds$ , and  $\Phi$  is the standard normal cumulative distribution function.

The median value of the spectral displacement at which the building reaches the threshold of the damage state,  $S_{d,ds}$  is obtained by multiplying the inter-story drift  $\Delta_{ds}$  by the height of the building and by a fraction of the building height  $H$ . Thus, one can compute and plot the corresponding functions using Equation 3.

### 4 Case study

In this study and at the scale of the structure, we are interested by one typology that is a quasi-symmetrical reinforced concrete structure braced by shear walls. A simplified modeling strategy based on the concept of macro-elements has been developed and validated through comparison with experimental results (Hemsas et al., 2009). The structure is discretized into a set of macro-elements, each macro-element being representative of a floor of the structure. The structural wall considered is based on a prototype five storey building (scale 1/4) designed using flexural strength requirements of the Uniform Building Code (UBC, 1994); however, detailing requirements were determined using a displacement-based evaluation (Wallace, 1995). The model wall had a rectangular cross section with dimensions of (0.102 m x 1.22 m), and a height of 3.66 m. It is composed of 8 macro-elements ( $N=8$ ) stacked upon each other. Each macro-element has eight uniaxial sub-elements ( $m=8$ ) distributed along the length of the wall (Figure 2).

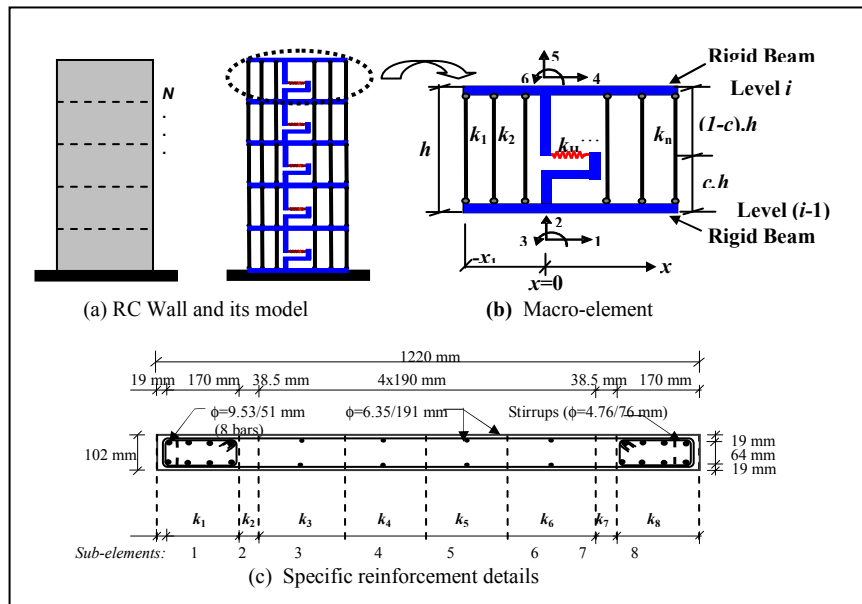


Figure 2. Macro-element modeling of the structural wall and its specific reinforcement details.

The direct Monte-Carlo simulation technique requires a large number of simulations to achieve an acceptable level of confidence in the estimation of the vulnerability curves. That's why the Latin hypercube Sampling (LHS) technique which allows the reduction of the number of simulations and a significant reduction of the variance of the estimators has been preferred. This technique uses stratified sampling of the input variables.

The step-by-step procedure to assess the vulnerability curves of the structure is highlighted in the following steps.

**Step 1:** Generate the random variables by the LHS technique (McKay, 1979). Tables 1 and 2 give the different values of the mechanical characteristics of the structure as well as the applied seismic action which is represented by a non-linear displacement response spectrum. In Figure 3 is presented a set of spectra generated in the  $(S_a-S_d)$  format.

| Concrete                        | Parameters                              | Mean | st. dev. |
|---------------------------------|---|------|----------|
|                                 | compressive strength $f_{cc}$ (MPa)     | 32   | 5        |
| tensile strength $f_{ct}$ (MPa) | 3                                       | 0.1  |          |
| Steel                           | yield strength $f_{stV}$ (MPa)          | 430  | 12       |
|                                 | strain-hardening ratio $\alpha$ (%)     | 2    | 0.2      |
|                                 | ductility ratio $f_{act} \epsilon_{su}$ | 25   | 5        |

**Table 1.** Variability of mechanical characteristics of the structure

| Spectral response | Parameter         | Mean | Standard deviation |
|-------------------|-------------------|------|--------------------|
|                   | $PGA$ ( $m/s^2$ ) | 0.6  | 0.06               |
|                   | $T_b$ (s)         | 0.15 | $0.02T_b$          |
|                   | $T_c$ (s)         | 0.30 | $0.05T_c$          |
|                   | $R_m$             | 2.5  | $0.01R_m$          |

**Table 2.** Variability of the seismic action (Response spectrum)

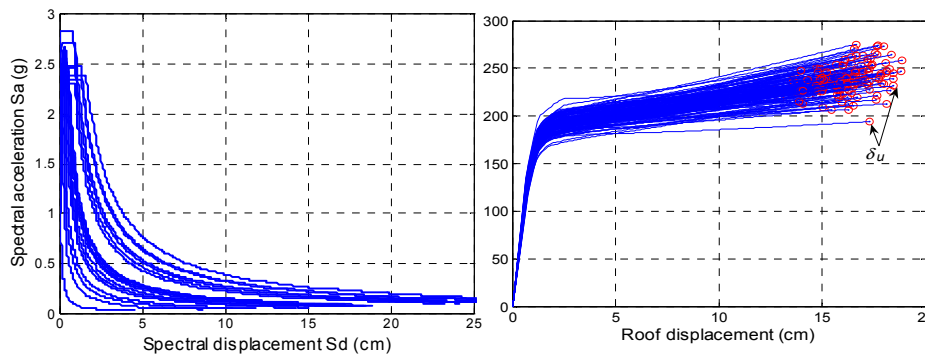


**Figure 3.** Response spectrum (20 simulations) **Figure 4 .** Pushover curves, MC. simulation (LHS)

**Step 2:** Establish the pushover curves. The outcome of the pushover analyses (in terms of the base shear - roof displacement) is a family of capacity curves presented at Figure 4 (example of 50 simulations).

**Step 3:** For each curve, determine the performance point in the  $(S_a-S_d)$  format. The non-linear capacity spectrum method "MSNL", inspired from the method N2 developed by Fajfar (Fajfar, 1999), is considered in this study (Hemsas et al., 2007). Indeed, this method

consists in determining two essential parameters: corresponding spectral displacement  $S_d$  and inter-story drifts  $\Delta_i$ .

**Step 4:** Evaluate the damage state of the wall by means of the damage index defined according to the equation 2.

**Step 5:** Establish a correlation between the damage index  $DI$  (step 4) and the inter-story drift  $\Delta_i$  (step 3) from the determination of mean and standard deviation values.

**Step 6:** From the defined states of damage index, one can identify the mean and standard deviation values of inter-story drift at threshold of damage state  $DI$ . The median value of spectral displacement at which the building reaches the threshold of the damage state  $S_{d,ds}$ , is obtained by multiplying the inter-story drift by the height of the building and by the fraction of the building height at the location of push-over mode displacement. Once the parameters of fragility function,  $S_{d,ds}$  and  $\beta_{ds}$  are obtained, one can compute and plot the fragility functions using equation 3.

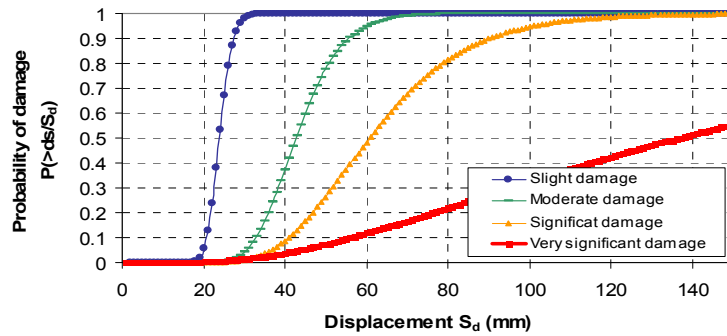


Figure 5. Fragility curves, Monte-Carlo simulation

**Step 7:** Knowing maximum spectral displacement  $S_d$  (calculated from non-linear capacity spectrum method "MSNL"), it is possible to determine the probability of damage according to the four levels of damage. Therefore, for any displacement of  $X$  cm, we can quantify the probabilities of having respectively P1% of damage of level 1 (slight damage), P2% of damage of level 2 (moderate damage), P3% of damage of level 3 (significant damage), P4% of damage of level 4 (very significant damage going until collapse). Thus for example, for a spectral displacement of 6 cm, the probabilities that this structure is on levels 1, 2, 3 or 4 are respectively 100%, 95%, 47% and 12%.

## 5 Conclusion

A simplified method based on performance based design allowing the assessment of the vulnerability curves was presented. Vulnerability curves were established for quasi-symmetrical reinforced concrete structures braced with shear walls.

This study shows that a simplified modeling (by using macro-elements), allowing a better sight of dynamic aspects, is interesting on a global level and allows to obtain good indicators. The fragility curves determined for the quasi-symmetric reinforced concrete structures (braced by shear walls) seem coherent with the level of seismic regulatory solicitation and can be used as well for the design of new structures as for the setting in conformity seismic of existing structures.

The results presented here constitute examples of use for the evaluation of the damage and constitute a first estimate of the levels of risks and a decision-making aid of the authorities in the definition of the seismic risk of constructions (Risk mitigation plan...). The direct prospects for this work are the application of the methodology developed and its validation to other typologies of structures.

## References

- Freeman, S.A. 1998. "Development and use of capacity spectrum method". Proceedings of the 6th U.S. National Conference on Earthquake Engineering, Seattle, CD-ROM, Oakland: EERI.
- FEMA, 1999. "HAZUS Earthquake loss estimation methodology". Federal Emergency Management Agency, Washington, D.C., 1999.
- Fajfar, P. 1999. "Capacity spectrum method based on inelastic demand spectra". *Earthquake Engineering and Structural Dynamics* 28: 979-93.
- Hemsas M., Elachachi S.M., Breysse D. 2007, "Analyse performantielle des murs voiles soumis a une action sismique", 7ème Colloque National AFPS, 4-6 Juillet 2007, Paris.
- Hemsas M., Elachachi S.M., Breysse D. 2009, "Modélisation par macro-éléments du comportement non-linéaire des murs voiles en béton armé", *European Journal of Environmental and Civil Engineering*, n°05, 613-638.
- Mac Kay M.D., Conover W.J., Beckman R.J., 1979, "A comparison of three methods for selecting values of input variables in the analysis of output from a computer code", *Technometrics*, 221, 239-245.
- Park YJ, Ang AHS, Wen YK. 1985, Seismic damage analysis of reinforced concrete buildings. *Journal of Structural Engineering ASCE*;111(4): 740-57.
- Paulay, T., & Priestley, N. 1992, *Seismic Design of Reinforced Concrete and Masonry Buildings*. Wiley & Sons, New-York, Etats-Unis.
- Risk-UE, 2003, "An advanced approach to earthquake risk scenarios with applications to different european towns, WP4 : Vulnerability of current buildings". European Project.
- UBC, 1997, "Uniform Building Code". International Conference of Building Officials, Whittier, California, USA.
- Wallace, J.W., 1995, "Seismic Design of Reinforced Concrete Structural Walls: Part 1: A Displacement-Based Code Format", *Journal of Structural Engineering, ASCE* 121(1), 75-87.

## Towards Implicit Performance Based Seismic Design Rules.

Frederic Legeron<sup>1</sup> and M. Neaz Sheikh<sup>2</sup>

<sup>1</sup> Professor of Civil Engineering, Université de Sherbrooke, Canada  
[frederic.legeron@usherbrooke.ca](mailto:frederic.legeron@usherbrooke.ca)

<sup>2</sup> Senior Lecturer, School of Civil, Mining and Environmental Engineering, University of Wollongong, Australia  
[mshikh@uow.edu.au](mailto:mshikh@uow.edu.au)

---

**Abstract.** Performance based design of bridges for earthquake resistance is still not explicitly used in design. However, most codes specify a level of performance for bridges under various earthquake inputs. In principle, design rules suggested in the code should meet stipulated performance criteria. However, it has been highlighted in the past that design rules are not directly related with stipulated performance criteria. After the presentation of performance criteria and their relation with post-earthquake functional requirements, the article examines the case of the Canadian Bridge Design Code (CAN/CSA-S6-06). Performance of bridges designed with this code is predicted and compared to expected levels. It is shown that compliance with design rule does not guarantee an adequate performance. Some implicit design rules are proposed to design new bridges.

**Keywords:** reinforced concrete bridges, performance-based design, seismic design of bridges.

---

### 1 Introduction

Major seismic events during the past few decades have continued to demonstrate the destructive power of earthquakes, with failures to structures such as bridges, as well as giving rise to great economic losses. Economic losses for bridges very often surpass the cost of damage and should therefore be taken into account in selecting seismic design performance objectives.

The structural engineering community in its transition to performance-based seismic design codes has proposed several methodologies for performance-based seismic design or upgrading. Design codes have adopted different approaches to achieve required performance objectives. However, the performance objectives in the design codes are defined qualitatively in terms of design principles called the “seismic design philosophy”. It is not clear how design requirements are related to design principles and economic considerations.

To assess code requirements, a vast amount of experimental evidences would be necessary. However, such experiments are normally very expensive. Numerical techniques could be an alternative to these expensive experiments, as they can simulate the experimental behaviour reasonably well when modeled properly (Legeron et al., 2005). A numerical modelling technique is used in this paper after being thoroughly

compared with a number of experimental results. With this method, performance of bridges designed by Canadian code (CAN/CSA-S6-06) is compared for the stated performance objectives. Based on these results, some implicit design rules are proposed for the seismic design of bridges.

The article is organized in three parts: (i) definition of performance criteria and relation with post-earthquake functional requirements and methods to predict the performance of bridges; (ii) prediction of performance of bridges designed with the Canadian Code for bridges S6-06; (iii) presentation of implicit rules of seismic design to comply with cost-effectiveness and post-earthquake functional requirements.

## **2 Definition of bridge performance and relation with post-earthquake functional requirements**

### **2.1 Performance limit state**

Current seismic design codes define different levels of damages depending on the importance of the bridge and the return period of the earthquake event. The performance principles stated in the design codes are just descriptive. Table 1 provides actual performance level that might be related to code based performance principle and are in line with recent development of performance-based seismic assessment (Hose et al., 2000; Lehman et al., 2004). Both qualitative and quantitative performance levels are described in Table 1 and are associated with engineering parameters. The level of performance is related to post-earthquake serviceability and repair needs.

### **2.2 Analytical Model for Seismic Performance Assessment**

An analytical model for seismic performance assessment of bridge pier has been developed in Sheikh et al., 2007. The model forms an analytical tool that reproduces most of the important features of reinforced concrete bridge piers under the action of an earthquake event. The model can well predict the force displacement characteristics of bridge piers considering both flexural and shear behaviour. To evaluate the capability of the model, the experimental results of 10 columns tested under cyclic loading by Lehman et al. (2004) have been used. The response of the 10 columns tested by Lehman et al (2004) are very well predicted globally (overall response) as well as locally (local limit states), as demonstrated in Guiziou (2006). Other predictions performed on shear sensitive columns have demonstrated that the model is also effective in this case (Sheikh, 2007).

## **3 Performance of bridges: example of a bridge designed according to Canadian Code for Bridges S6-06**

Canadian Code for bridges S6-06 has adopted performance requirements as a general principle. Bridges are classified as “lifeline” for critical bridges, “emergency” for the bridges that would need to be used in case of a 475-yr return period earthquake, and “other” bridges being all the ones that can be damaged during an earthquake of 475-yr return period. They are summarized in Table 2 taken in the commentary of the S6-06.

**Table 1.** Performance level and relation with functional post-earthquake requirements

| Limit states (LS) | Operational performance level | Post earthquake serviceability | Qualitative performance description   | Quantitative performance description   | Repair                             |
|-------------------|-------------------------------|--------------------------------|---|--|------------------------------------|
| 1A                | Fully Operational             | Full service                   | Onset of hairline cracks  | Cracks barely visible  | No repair                          |
| 1B                |                               |                                | Yielding of longitudinal reinforcement  | Crack width <1 mm  | Limited epoxy injection            |
| 2                 | Delayed Operational           | Limited service                | Initiation of inelastic deformation; onset of concrete spalling; development of longitudinal cracks   | Crack width: 1-2 mm<br>$\epsilon_c = -0.004$   | Epoxy injection; concrete patching |
| 3                 | Stability                     | Closed                         | Wide crack width/ spalling over full local mechanism regions; buckling of main reinforcement; fracture of transverse hoops; crushing of core concrete; strength degradation | Crack width >2 mm<br>$\epsilon_c = \epsilon_{cc50}$ (initial core crushing)<br>$\epsilon_c = \epsilon_{cu}$ (fracture of hoops)<br>$\epsilon_s > 0.06$ (longitudinal reinforcement fracture) | Extensive repair / reconstruction  |

$\epsilon_c$ =axial strain of concrete;  $\epsilon_{cc50}$ =post peak axial strain in concrete when capacity drops to 50% of confined strength;  $\epsilon_{cu}$ = ultimate strain of concrete;  $\epsilon_s$ =tensile strain at fracture

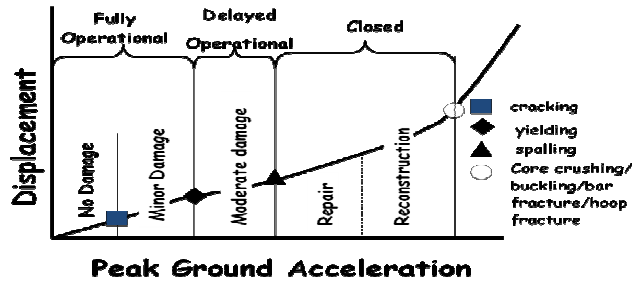


**Figure.1.** Relation between serviceability of a bridge and performance limit states

Application rules of the code use a constant force-reduction factor  $R$  to account for ductility and overstrength, and seismic forces are multiplied by an importance factor  $I$  equal to 1 for “other” bridges, 1.5 for “emergency” bridges and 3.0 for “lifeline” bridges. The seismic acceleration is determined based on the level corresponding to the 475-year return period earthquake multiplied by the importance factor,  $I$ .

Due to space restriction for this paper, the result of only one four-span bridge with three single circular column 7-m in height is shown here. The bridge has a constant span length of 30 m for a total length of 120m. The design peak ground acceleration is varied from 0.2

to 0.4g, corresponding to a return period of 475 years. The bridge is designed with the appropriate importance factor. As the seismic load is very different from  $A=0.2$  and  $I=1.0$  to  $A=0.4$  and  $I=3.0$ , the size of the single column pier had to vary. As the pier is a single column, use of a reduction factor of 3 was used in the design of column as it is stated in S6-06. Varying the size of the pier would lead to a very different period of structures and a variation of seismic loads regardless of  $A$  and  $I$ . As well, behaviour of single columns can be very different as axial load level decrease with increased diameter of column, and longitudinal reinforcement ratio changes. In order to compare behavior we choose to keep the longitudinal reinforcement ratio constant at about 1%. This would ensure that all piers have a satisfactory behavior under seismic loads and it is also reasonable to assume that the diameter of the column is adjusted according to seismic input. Modelling of the bridge piers has been carried out according to the methodology developed in the previous section. P- $\Delta$  effects have also been taken into consideration. The pushover analysis is conducted in order to find out the failure mechanisms and the output is converted into tip displacement ( $\Delta$ ) as a function of peak ground acceleration ( $PGA$ ). Figures 2 shows the results of the calculation for the bridge under consideration with  $A=0.2$  and  $0.4$  and  $I=1.0$  to  $3.0$ .

It can be observed from the figures that design rules do not always necessarily meet the stipulated seismic performance levels. It is clear from Figure that for low level of earthquake shaking ( $A=0.15-0.2g$ ), the “other bridge” did not meet the no-collapse performance level, although it has met the repairable performance level in the event of a design earthquake (475-year return period). As well, the performance is often at the limit of what is accepted by the code in term of performance, and use of higher reduction factors  $R$  could result in poor performance of the bridge and probably unacceptable. Notably, the Canadian Code S6-06 specifies a reduction factor  $R=5$  for multibent. In the longitudinal direction, the multibent pier would perform as the single column and the use of  $R=5$  may result in unsatisfactory performance, not only for the ‘other bridges’ but for ‘lifeline bridges’ too. Hence, proper evaluation of response modification factor and importance factor is essential and is a subject of further research.

#### 4. Implicit Design Rules for Performance Based Design of Bridge

Specifying performance in a design code is very satisfactory on an intellectual and engineering level as it is an assurance of a proper performance at an optimal cost. However, this would suggest an iterative procedure where reinforcement is assumed and checked for performance and if performance is not satisfactory, design is changed accordingly. Performance calculation requires a complex method that is not available to most bridge designers. Specification of performance requirements for large, complex and very important bridges is necessary; large projects designed in North America in the past few years have proposed project specific performance criteria. For most standard bridges, important or not, the use of explicit performance criteria and iterative design procedure is not a viable option. Most design offices are still struggling with current design rules, so it is questionable how they would react to more complex rule. For the time being, the use of a reduction factor ( $R$ -factor) that takes into account the behavior of the structure combined with an importance factor ( $I$ ) is very interesting for design of standard bridges as it enable a fast and efficient design. Even for complex and very important structures this could

provide an initial design that could be checked and modified after proper calculation of performance hence reducing the lengthy iteration process.

**6. Conclusions**

A performance based approach is proposed for optimal seismic design of bridges considering life cycle cost, based on performance limit states that can be related directly to the post-earthquake functionality and repair cost. The methodology could be used for design of a new bridge or retrofiting of an existing one. However, in the methodology, cost of death and injury is not included as such data is scarce. Maintenance cost is also not included as the design earthquake event has insignificant influence on maintenance cost. This study resulted in the proposal of an implicit approach to design bridges for seismic loads that provide an adequate level of safety and post earthquake serviceability included in a life cycle analysis wanting an optimal economic approach.

More research is necessary to confirm these results for other types of bridges and a more refined analysis accounting for seismic input, dividing in zone of high, moderate and low seismicity, type of seismicity (typicall earsten and western for North America) and soil conditions. This is the objective of ongoing collaborative research between University of Sherbrooke and University of Wollongong.

**Acknowledgements**

Part of this research has been supported by the Natural Sciences and Engineering Research Council of Canada under the Strategic Research Networks program. The researchers gratefully acknowledge their financial support.

**Table.2.** Functional Performance Requirement in Canadian Code S6-06.

| Return period                              | Bridge                              |                                     |                              |
|--|-------------------------------------|-------------------------------------|------------------------------|
|  | Lifeline                            | Emergency-route                     | Other                        |
| Small to moderate earthquake               | All traffic<br>Immediate use        | All traffic<br>Immediate use        | All traffic<br>Immediate use |
| Design earthquake (475-year return period) | All traffic<br>Immediate use        | Emergency vehicles<br>Immediate use | Repairable damage            |
| Large earthquake (1000-year return period) | Emergency vehicles<br>Immediate use | Repairable damage                   | No collapse                  |

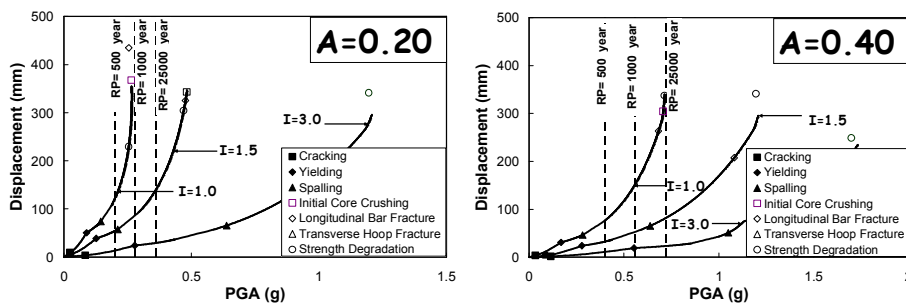


**Figure.2.** Prediction of bridge performance

**Table 3.** R-factor for the three categories of bridges

| Type of bridge   | R for 475-yr return period (I=1.0) | R for 1000-yr return period (I=1.5) | R for 2500-yr return period (I=2.0) |
|------------------|------------------------------------|-------------------------------------|-------------------------------------|
| Other bridge     | 3.0 (extensive damage)             | 4.5 (no collapse)                   | NA                                  |
| Emergency bridge | 1.5 (full traffic)                 | 3.0 (extensive damage)              | 4.5                                 |
| Lifeline bridge  | 1.0 (elastic)                      | 1.5 (full traffic)                  | 2.0 (limited traffic)               |

### References

- ATC-32. (1996). Improved seismic design criteria for California Bridges: Provisional Recommendation, *Applied Technology council, Redwood City, California 94065*.
- Berry, M.P. and Eberhard, M.O. (2005). Practical performance model for bar buckling. *Journal of Structural Engineering* **131(7)**, 1060-1070.
- CAN/CSA-S6-06, 2006. Canadian highway bridge design code. *CSA International, Toronto, Ontario, Canada*.
- Cornell, C.A., Jalayer, F., Hamburger, R.O. and Foutch, D.A. (2002). Probabilistic basis for 2000 SAC Federal Emergency Management Agency steel moment frame guidelines. *Journal of Structural Engineering* **128(4)**, 526:533.
- Hoshikuma, J., Kawashima, K., Nagaya, K., and Taylor, A.W. (1997). Stress stain model for confined reinforced concrete in bridge piers. *Journal of Structural Engineering* **123(5)**, 624-633.
- Hose, Y., Silva, P. and Seible, F. (2000). Development of a performance evaluation database for concrete bridge components and systems under simulated seismic loads. *Earthquake Spectra* **16(2)**, 413-442.
- Légeron, F., Paultre, P. and Mazars, J. (2005). Damage mechanics modeling of nonlinear seismic behavior of concrete structures. *Journal of Structural Engineering* **131(6)**, 946-955.
- Lehman, D., Moehle, J., Mahin, S., Calderone, A. and Henry L. (2004). Experimental evaluation of the seismic performance of reinforced concrete bridge columns. *Journal of Structural Engineering* **130(6)**, 869-879.
- Mander, J.B., Priestley, M.J.N. and Park, R. (1984). Seismic design of bridge piers, Research Report 84-2, *Department of Civil Engineering, University of Canterbury, Christchurch, New Zealand*.
- National Institute of Building Science (NIBS). (1999). Earthquake loss estimation methodology, HAZUS 99: technical manual. *Report Prepared for the Federal Emergency Management Agency, Washington D.C., USA*.
- New Jersey Department of Transportation (NJDOT). (2001). Road user cost manual. *New Jersey Department of Transportation, USA*.
- Guiziou, C., Sheikh, M.N. and Legeron, F. (2006). Optimal performance for cost effective seismic performance of bridges. *Internal research report, The University of Sherbrooke, Sherbrooke (Quebec), Canada*. 100 pp.
- Sheikh, M.N., Vivier, A. and Legeron, F. (2007). Seismic vulnerability of hollow core concrete bridge pier. *Proceedings: the 5th international conference on concrete under severe conditions of environment and loading (CONSEC'07)*, Tours, France, June 4-6.
- Sheikh, M.N. and Legeron, F. (2008). Optimal target performance for cost effective design of bridges. *Proceedings: the 14th World Conference on Earthquake Engineering*, Beijing, China, October 12-17

## From concrete modeling to infrastructure risk management, what can be learned from experience?

B. Gerard & S. Crouigneau  
OXAND SA, Avon, France

---

**ABSTRACT:** Due to their ageing, civil infrastructure performances must be reconsidered in regards of the risks increasing with time. Several recent catastrophic events remind us that these structures can fail. Fortunately, these events are rare. Nevertheless, their impacts can be huge considering population safety, availability and economy. New items are also at the origin of the demand for a better understanding of the performance of infrastructures: environmental issues, climate change, etc. This paper develops the concept of risk analysis and its applications to civil and oil & gas infrastructure. Systemic approaches are necessary to evaluate correctly one or a portfolio of structures. Practical applications and past years feedback show their efficiency for risk assessment and management of civil infrastructure.

The authors conclude on some key recommendations for future research developments in order to develop sustainable life-cycle management of high stakes infrastructure.

---

### 1 Introduction

December 2003, Roissy airport, failure of terminal E: few deaths. December 2005, failure of the Concord bridge in Montreal area: few deaths. Summer 2007, failure of a bridge in Cincinnati area: several deaths. It is obvious that these situations are different. Nevertheless, it shows clearly that a misunderstanding of the structures behaviour, combined to a lack of methodologies for prevention, can have contributed to the existence of such events.

That could be just the summit of the iceberg. Indeed, several reasons can be at the origin of an increase of risks if nothing is done:

- ageing of materials;
- service life extension of existing infrastructure;
- increase of traffic or new conditions of operation;
- more requirements to prevent climate change and environmental issues;
- reduction of maintenance and preventive budgets;
- loss of expertise and experience due to the ageing of the populations.

When **analyzing failures and their origin**, it is considered that the problematic becomes more and more complex because of the heterogeneity of situations, scientific and technical disciplines involved. It is also rare that only one mechanism is the cause of the failure: this is more generally a **succession, or combination, of many events** that can explain the accidents.

Due to these facts, decision-making tends to be based on risk approaches. A risk approach considers a systemic vision of the studied system (the bridge and its access including users and all actions which impact the bridge – sun, wind, pollution, etc.).

## 2 RISK APPROACH: DEFINITION

The risk is not a vague concept but a value that can be quantified through criticality:

Criticality of Risk =  $f(P,G)$

P: probability for an event to appear during a given period of time

G: gravity, or severity (consequence of the event). Usually, the maximum of impact is considered when dealing with safety, availability, economy and environment but other stakes can be considered. If the gravity is defined in terms of cost, the risk is expressed in terms of cost (like annual cost of the risk in euros for example).

N.B.: other parameters such as ‘detectability’, ‘uncertainty’, etc. can also be taken in account in the criticality calculation.

The most important part in order to prognose a structure’s behaviour is the accurate and exhaustive identification of the different events that can occur at the **present time and in the future**. Different methodologies can be used to achieve this; the best are those which are the most complete.

Risk management includes several steps:

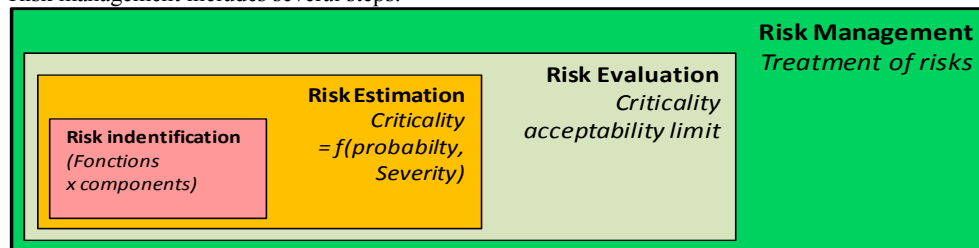


Figure 1 - The different steps of a risk management process

We are now going to show some applications of this approach on concrete case studies.

## 3 Case study 1: Marine concrete structure (Crouigneau et al. 2008)

A massive dry dock was built in the 70’s in a French harbour and aimed at receiving huge tankers for

reparation. This dry dock could be isolated from the sea thanks to a **dock-gate made of prestressed concrete**. This dock-gate consists of a massive box divided into compartments and can be easily operated by filling or emptying those

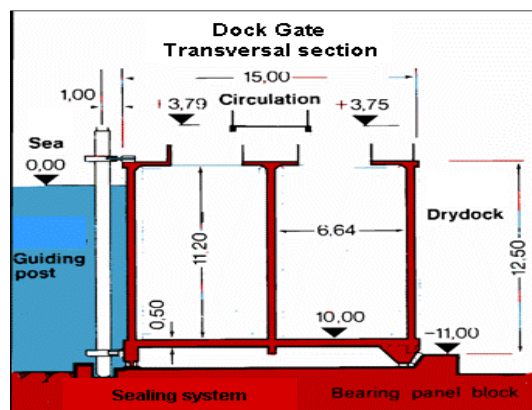


Figure 2 - ‘Aground position’ of the dock-gate.

compartments with seawater. When the dock-gate is filled, it behaves like a gravity dam and can be used to close the dry dock (see Figure 2). When it is empty it floats and can be quickly moved apart to let the various ships go in and out of the dry dock.

Objectives of the port authority were to obtain formal and objective decision-making indicators, based on a technical and financial global approach, considering two different operation scenarios for the next 10 years:

- Scenario 1: the dry dock is exploited for ship repair, which implies a high frequency of the dock

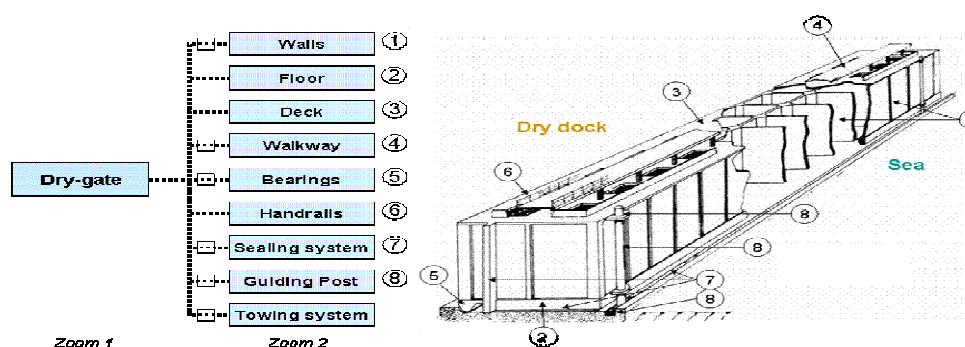


Figure 3 - Decomposition of the 'dock gate' system in components

gate use, with a minimum of 120 opening-closing operations a year;

- Scenario 2: the dry dock is exploited for building new civil engineering structures, which implies a lower frequency of the dock gate use, with about 10 operations a year.

### 3.1 Advantages of Risk analysis to help the infrastructure owner: a systemic approach for a global vision

Recent studies have dealt with risks on coastal structures (Sorensen et al., 2004), with survey optimization (Billard et al. 2006, 2007) and monitoring for reliability (Yanez-Godoy et al., 2006). Risk analysis approach has also appeared during decommissioning works (Kroon, 2004): it clearly stands as a **robust and well-experienced** methodology to optimise infrastructure management.

The methodology used by OXAND consisted in an adaptation of FMECA (Failure Mode Effect and Criticality Analysis) enriched by ageing assessment and functional prediction in time. This methodology allows obtaining exhaustive and objective decision-making indicators.

### 3.2 Functional analysis

First step of the study is to **split up the system into its components** according to their environment, solicitation, geometry or material.

This aims at being exhaustive in the later identification of potential failure modes. The first degree of decomposition (see 'zoom 2' on Figure 3) includes structural elements (walls, floor and deck) so as equipments (handrails, sealing, etc.).

The next step is to define **the expected functions of the dock gate** and to link them to one or several components.

Expected functions of the Dock gate were identified (for instance: “Dock gate must seclude the dry dock when closed” or “Dock Gate must be accessible for maintenance”). Those functions imply resistance to conditions including normal operation loadings, accidental loadings, environment, time...

### 3.3 Failure modes identification and estimation

The exhaustive list of potential failure modes is built thanks to a crossing between the components and the expected functions of the dock gate. For each component, an analysis of the different causes which could lead to a failure of the associated function is carried out.

**More than 50 failure modes can be reached thanks to such a methodology when a brainstorming session with experts would rise only 20.**

In this study, the criticality of failure modes was calculated with three parameters:

The probability of occurrence or frequency of a failure mode,

The gravity or severity of a failure mode, which means its level of consequence for the owner,

We added an extra parameter: the uncertainty, aiming at giving a degree of trust to the frequency estimation rate.

To assess the frequency of failure modes concerning mechanical resistance, OXAND calculated among others the different initial **safety margins** (for each component, as initially built) and compared them to the current **residual estimated resistance**. OXAND used the **SIMEO™ Consulting** software (example of results shown in **Erreur ! Source du renvoi introuvable.** to take into account the ageing mechanisms (especially carbonation and chloride attacks). This software enables numerical simulations of ageing structures with physico-chemical and mechanical characteristics of materials.

To assess the severity of failure modes, different consequence levels were qualified regarding what could be perceived as minor, slight, serious or major for the port. This has been formalized

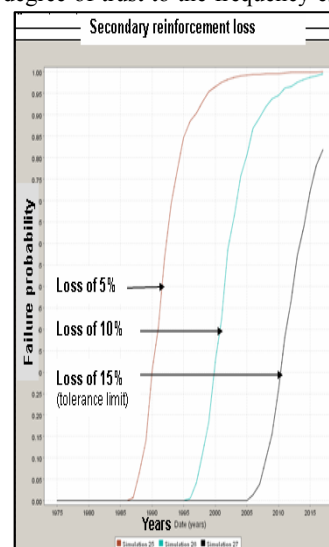


Figure 4 - Example of simulation using SIMEO Consulting to quantify probability of

In a **severity grid developed in collaboration with the port.**

Two major stakes were considered: **the safety and the availability of the dock gate operation.**

### 3.4 Risk evaluation: results and management recommendations

#### 3.4.1 Failure modes ranking

This **Erreur ! Source du renvoi introuvable.** illustrates the risk profile prognosis of the Dock Gate by 2017 considering the two foreseen operation scenario.

Two major conclusions can be drawn:

- Few failure modes are very critical (in red);

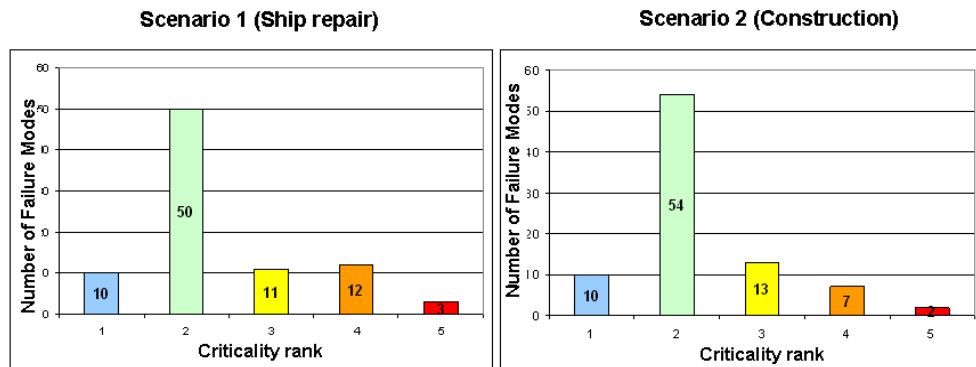


Figure 5 - Ranking of failure modes depending on criticality quantification.

The dispatching between the two risk profiles is very similar.

Notice: The difference between the two risk profiles is due to the equipments' wearing (e.g.: horizontal rubber joints, bearings made of ekki-wood) caused by a more repeated use of the gate with the scenario 1.

#### 3.4.2 Recommendations: Identification of appropriate maintenance actions

A list of recommendations was built, based on the risk ranking and on the infrastructure's owner acceptability of risks. **The cost estimation of maintenance actions indicates a difference of about 25% between the two operation strategies for the next ten years (see Figure 7).**

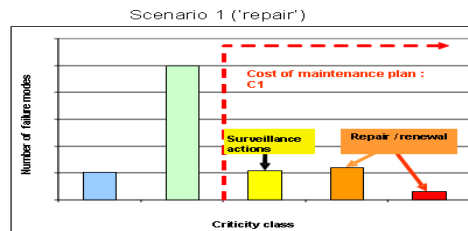


Figure 6 – Dock-gate study: Use of risk mapping for maintenance recommendations of scenario 1.

The recommended actions were finally planned in a ten years maintenance program, integrating operation constraints.

#### 4 Case study 2: Well integrity management for CO2 Sequestration

Carbon capture and storage has been validated by the IPCC (IPCC 2005) as part of a portfolio of measures to mitigate climate change, and pilot projects multiply all around the world. But while the conditions for the deployment of this technology seem always closer, key points remain to be unlocked: before launching large-scale operations, further investigations about the implied risks are required to ensure safety.

Well integrity versus time appears as one of the main issues. Casing corrosion and cement plugs leaching processes influence well integrity and as results, well sealing could fail. Consequently, the degradation of the casing and cement of wells increase the risk of a leakage with time. Oxand proposes an innovative quantitative Performance & Risk (P&R™) assessment methodology for well integrity, based on regular assessment and prevention of potential CO2 leaks. This methodology provides the operators a decision-making tool and a strong support for demonstrating safety to regulators. This methodology is supported by the modelling of the well behaviour (steel and cement material in contact with underground water and fluids).

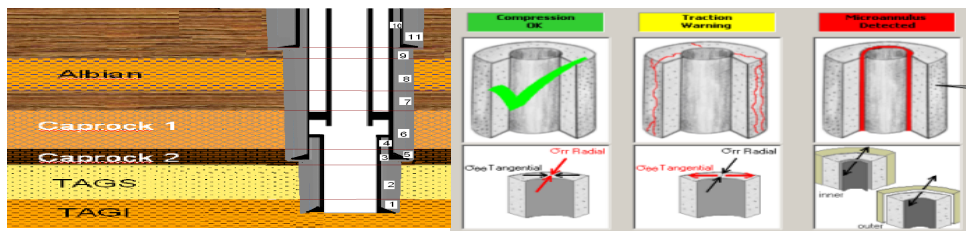
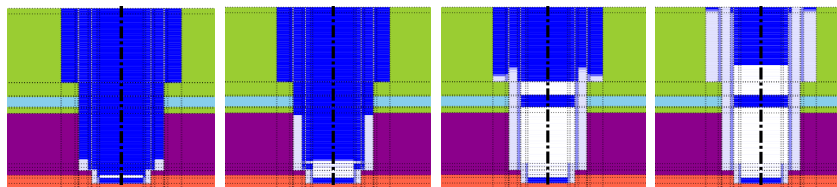


Figure 7 - Simeo™-Stor: modelling of well integrity and risk assessment (Simeo is the generic trade mark of software developed by Oxand for ageing and risk management).



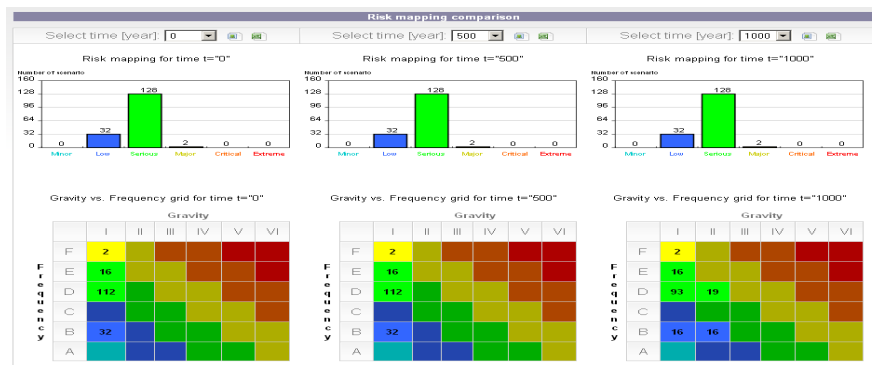


Figure 8 – On the top: Illustration of the evolution of water saturation in a well versus time. CO<sub>2</sub> is moving from the bottom (-3000 m depth) to the surface. Due to ageing and corrosion, this simulation shows the impact of degradation on the migration of CO<sub>2</sub> in external cement annulus (Simeo™-Stor simulations); At the bottom: Evolution of risk mapping

Performance of the site is assessed in terms of CO<sub>2</sub> containment. The methodology focuses on the Risks of both contamination of subsurface formations and hazardous releases on surface (GERARD 2006).

By combining the scenario of leakage and the probability of each scenario to appear, it is possible to estimate the impact of leakage on the environment and people. Those results allow assessing the prevention strategy by identifying the main mechanisms involved in risk levels. Several strategies are available: modification of cement mixtures for well plugging, monitoring the CO<sub>2</sub> release with time, modification of the casing design for future wells, etc.

The proposed Performance & Risk assessment methodology enables:

Predicting the evolution of the well integrity over short, medium and very long time scales (up to 5000 years);

Risk mitigation and safety control planning.

## 5 Conclusions

It has been shown that industry is looking for decision making indicators. Risk management approach presents an important growth in practice because of its capability to communicate easily recommendations considering owner stakes. Models offer a great opportunity to risk managers to anticipate their risks and to engage prevention programs.

Considering two different applications in two different market sectors (harbour field and oil & gas), quantification of damaging mechanisms -and their impact on the function of a technical system- allows to assess accurately the best strategies for designing high performance structures or maintenance programs (when considering existing infrastructures).

The link between decision makers and scientific knowledge is possible through such innovative approaches.

## 6 References

Billard Y., Bernard O., Lasne M., Schoefs F., Risk analysis for survey optimisation of harbours. Proceeding of the Third International Colloquium of the Network for Integrating Structural Analysis, Risk and Reliability, Glasgow, 2006, papers 028-109 on CD-Rom, 9 pp.

Billard Y., Bernard O., Lasne M., Capra B., Schoefs F. et Boreo J., Risk analysis and reliability of repaired concrete quays. Proceeding of 10th International Conference on Applications of Statistics and Probability in Civil Engineering, 2007, Tokyo, paper on CD-Rom, 8 pp.

Crouigneau Sophie, Loïc BOURDON, Yvan BILLARD, Jean-Luc PERSON, Franck SCHOEFS, Risk analysis to support operation and maintenance of an ageing dock-gate for the port of Marseille, MEDACHS08 international conference, Construction heritage in coastal and marine environment - Damage, diagnostics, maintenance and rehabilitation, Lisbon, Portugal, 2008.

Gérard B., Frenette R., Auge L., V. Barlet-Gouedard, J. Desroches, L. Jammes (2006) "Well integrity in CO2 environments: Performance & Risk, technologies", Proceedings of the CO2SC Symposium 2006, Lawrence Berkeley National Laboratory, Berkeley, California.

IPCC (2005) IPCC Special Report on Carbon Dioxide Capture and Storage. Cambridge University Press, Cambridge, United Kingdom and New York, NY, USA, 442 p.

Kroon I.B., Comparative Risk Assessment for Decommissioning Decision Support. International Forum on Engineering Decision Making, Stoos, Switzerland, 2004.

Sorensen J.D., Burcharth H.F., Risk-based optimization and reliability levels of coastal structures. International Forum on Engineering Decision Making, Stoos, Switzerland, 2004.

Yanez-Godoy H., Schoefs F, Nouy A., Rguig M., Voisin D., Casari P., Extreme storm loading on in-service wharf structures: interest of monitoring for reliability updating. European Journal of Civil Engineering, 2006, Volume 10 n°5/2006, pp. 565-581.

## An experimental analysis of the bond-slip cracking in corroded reinforced concrete structures

Yves Berthaud, Frédéric Ragueneau & Tran B. Hop

LMT-Cachan, ENS-Cachan, CNRS, Université Pierre & Marie Curie, PRES Paris UniverSud  
[berthaud@lmt.ens-cachan.fr](mailto:berthaud@lmt.ens-cachan.fr)

**Abstract.** This contribution presents experimental analysis allowing identifying the effects of corrosion on the behavior on reinforced concrete structures. An experimental campaign is presented concerning a focus on the steel-concrete bond. Novel techniques based on digital images correlation are used.

**Keywords:** reinforced concrete, corrosion, steel-concrete bond

---

### 1 Introduction

The effects of corrosion on reinforced concrete structures are nowadays known as one of the main factors leading to a severe decrease of the performance of reinforced concrete structures (durability, serviceability ability and structural safety). The stakeholders need quantitative indicators of the performance of existing structures in order to schedule optimally a maintenance strategy. Therefore, efficient and robust constitutive equations have to be developed to better understand and model the mechanical behaviour of existing reinforced concrete structures. The local mechanisms involved can be summarized as follows:

- the decrease of the steel rebar section due to the oxides expansion and brittleness increase due to picking in case of corrosion due to chlorides penetration
- cracking and delamination of the concrete cover. The lateral pressure generated by the rust products on steel-concrete interface drives this mechanism.
- concerning the steel-concrete bond, evolution of the residual mechanical load bearing capacity due to decohesion induced by rust between the materials.

The use of continuum damage allows accounting, at the representative elementary volume, for micro-cracks growth (Ragueneau *et al.* 2006). Within the issue of corroded reinforced concrete structures analysis, experimental results are presented allowing identifying such constitutive equations. New experimental results concerning the effects of corrosion on the steel-concrete bond sleep behaviour are presented in this contribution.

### 2 Experimental set-up

Classical experimental tests performed on reinforced concrete specimens do not allow a direct identification of the material properties of the interface. The specimens are

structures in fact: like ties, pull-out specimens or three point bending tests (Eligehausen *et al.* 1983, Malvar 1992, Bamonte *et al.* 2002). The stress analyses on the interface for all these tests show very strong inhomogeneities. Moreover, physical measures on the interfaces are prevented by the concrete cover.

The wish to perform digital images analyses on the interface guided us to surrender the classically axi-symmetric specimen for plane stresses plates instead of circular ones. Due to boundary conditions, lateral confinement appears in most of classical tests leading to a non homogenous state of stresses on the interface and to an important confinement preventing a pure measure of the shear failure on the interface. The new boundary conditions allowed by the plate geometry of the specimen prevent any occurrence of lateral parasite stresses introducing an interface confinement (Ouglova 2004, Ouglova *et al.* 2008).

Different interfaces have been studied depending on the rugosity of the steel surface, using smooth, corroded or ribbed bars.

Fig. 1 shows the geometry of the specimen. The three steel bars are fixed on the Instron traction machine with free rotation end. A picture of the complete experimental set-up showing the boundary condition and the numerical camera can be seen in Figure 1. The specimen geometry has been adapted to account for lateral stresses on the mechanical behaviour of the interface. Two parallel rigid plates have placed along the sample with four bolts allowing imposing a controlled lateral pressure.

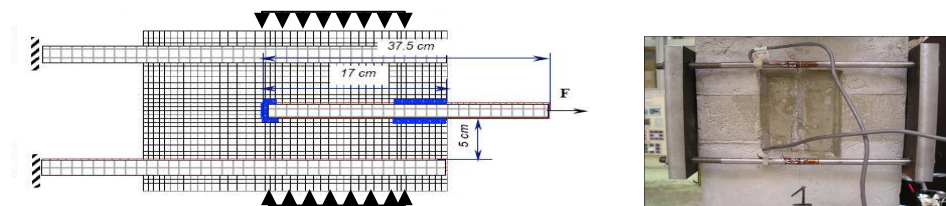


**Figure 1:** Improved specimen geometry accounting for lateral pressure

In order to evaluate the role of the corrosion on the mechanical behaviour of the steel concrete interface, the samples have to be exposed to accelerated corrosion procedure. The aim of this section is to present the experimental procedure used in this work to control the level of corrosion induced.

The known methods to accelerate corrosion are following: (1) acceleration by cyclic test of fog; (2) acceleration by cycles wetting-drying; (3) acceleration by electric current: an intensity of electrical current is applied between the reinforcement (anode) and counter electrode (cathode). The last method seems to be adapted to this study because it is the fastest one and it gives, moreover, a homogeneous corrosion on the surface of reinforcement but keeps the induced corrosion within the 'natural' values which can be found in practice (Auyeung *et al.* 2000, Cabrera 2006, Lee *et al.* 2002).

The set up for the accelerated tests is composed of a current supply, an ohm-meter, an electric resistance and a counter electrode (cathode). The cathode is made of carbon fiber fabric (an excellent conductor which does not corrode and is practically not dissociated by the action of the electric field). A wet sponge provided the electrical contact between the specimen and the counter electrode. To prevent the corrosion of parts of the central bar

embedded in the concrete, a Teflon coating was applied to these parts. The current density ( $500 \mu\text{A}/\text{cm}^2$ ) is applied through the counter electrode located alternatively underneath or beneath the central bar of the specimen.

The magnitude of corrosion was measured after mechanical test using loss of thickness of steel, which can easily be converted in level of corrosion (%). The measurement of loss of steel thickness rather than level of corrosion was chosen because it is an intrinsic data for the steel surface and does not depend on bar geometry. An attempt was made to induce corrosion up to 0.7 % (the loss of thickness  $> 40 \mu\text{m}$ ) but the concrete cracked for this corrosion level. After apparition of a longitudinal crack in the concrete above the central bar the current – induced corrosion process was stopped. Faraday's law and the weight-loss method are used to calculate the loss of thickness of steel of the bar as well corrosion levels.

### 3 Experimental results

#### 3.1 Influence of rugosity

Regarding three different kinds of rugosity on the interface: smooth, corroded and ribbed, figure 2 shows the experimental responses in terms of load-displacement curves.

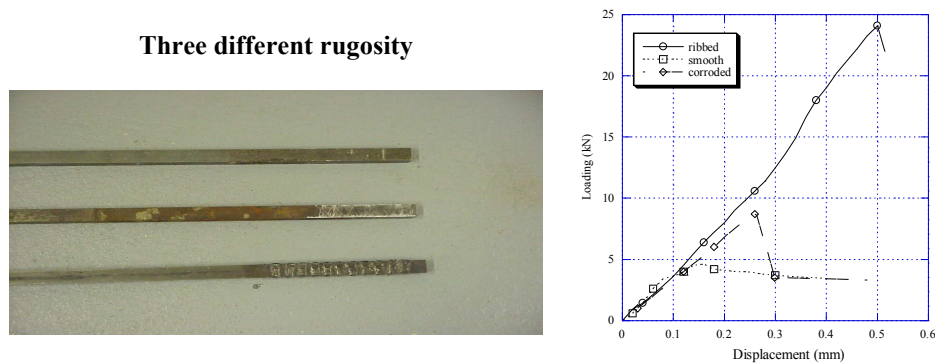


**Figure 2:** Influence of the rugosity on the mechanical behaviour

#### 3.2 Influence of corrosion

The influence of the level of corrosion on the residual mechanical bearing capacity of the steel concrete interface is presented in figure 3. It shows that the maximal average bond stress increases with the corrosion level less than 0.36 % ( $e_{corr} = 10.45 \mu\text{m}$ ). It has been observed by some researchers that surface of the bar becomes rougher by the products of corrosion for small level of corrosion, which increases friction between the bar and the surrounding concrete. Also, the pressure provoked by the growth of oxides in steel – concrete interface which tends to increase the reactionary confinement and the mechanical interlocking of concrete around the bar.

#### 3.3 Influence of lateral stresses

The effects of lateral confinement have been obtained by imposing transversal stresses of different magnitude.

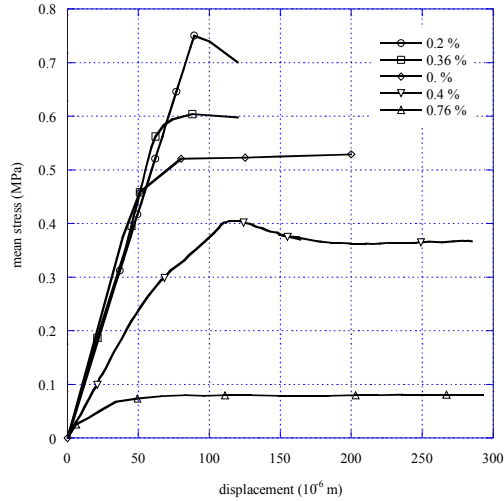


Figure 3: Influence of corrosion on the mechanical behaviour

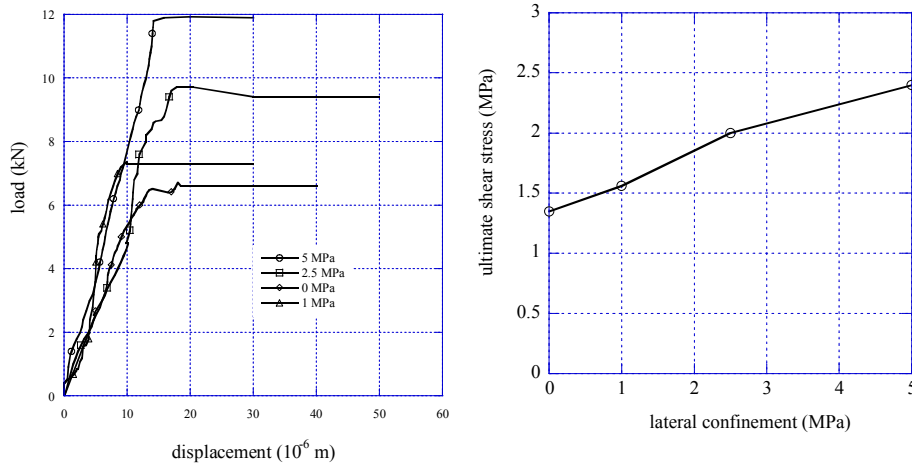


Figure 4: Influence of the lateral confinement on smooth bars

The identification of frictional Coulomb law can be achieved allowing to identify a cohesion of  $c = 1.35$  MPa for a frictional angle of  $\varphi = 12^\circ$ .

#### 4 Digital images correlation

In order to identify any constitutive equations based on plasticity or damage mechanics, one has to be able to measure the plastic flow of different direction to evaluate the threshold function as well as the plastic potential and the dilatancy angle for non associated plasticity. With regards to the specimen geometry, the digital images

correlation techniques allow such an approach of experimental measure. This section is devoted to the presentation of the possibility of such analysis. In figure 5 we present the results obtained by digital images correlation techniques on the ribbed bar without lateral stresses. One can observe the displacement field along the vertical and horizontal directions. The discontinuity between the two materials can be observed in accordance with the level of mechanical loading. For a better use of experimental results with regards to plasticity model identification, one can compute and plot the discontinuity evolution in the two directions. The figure 6 illustrates the capability to plot the discontinuity propagation along the interface function in the imposed loading.

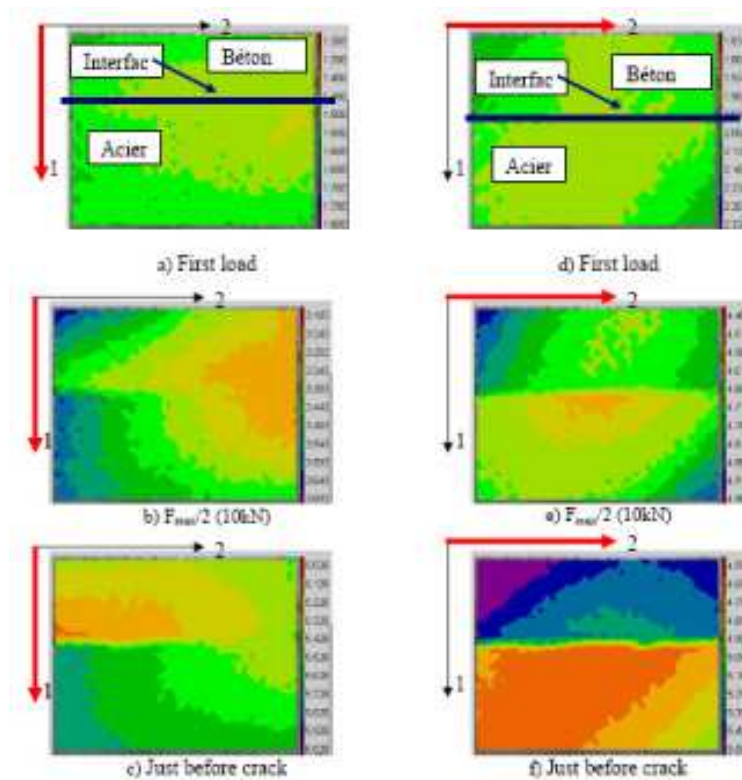


**Figure 5.** Digital images correlation applied on the ribbed bars for the “horizontal” and “vertical” direction.

## 5 Conclusions

The objective of this paper is to present a novel experimental technique allowing analyzing the mechanical behaviour of the steel-concrete interface in presence of corrosion. Due to the specimen geometry as well as the boundary condition, the state of stresses (shear and confinement) is controlled along the interface. The possibility to perform digital images correlation allows computing kinematics discontinuities along the interface to identify constitutive equations based on plasticity theory or continuum damage mechanics. The state of stresses (lateral and longitudinal) is measured and controlled.

More results are still needed and expected for different rebar diameter and geometry so as to obtain a complete experimental data base allowing constitutive equations model identification.

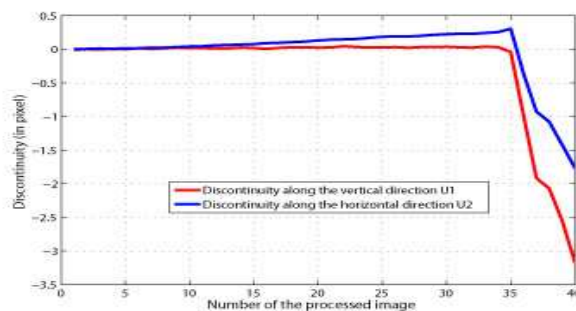


**Figure 6:** Discontinuity of the displacement across the interface for a ribbed bar

## References

- Auyeung Y., Balaguru P., Chung, L., 2000, «Bond Behaviour of Corroded Reinforcement Bars», *ACI Mat. Jour.*, 97, 2, 214-220.
- Bamonte, P., Coronelli, D. & Gambarova, P.G. (2002) Size Effect in high-bond bars. "Bond in Concrete: from research to standards" Proceedings of the 3<sup>rd</sup>. International Symposium at the Budapest University of Technology and Economics : 43-52.
- Cabrera J. G., 1996, « Deterioration of Concrete Due to Reinforcement Steel Corrosion », *Cem. & Conc. Comp.*, 18, 47-59.
- Eligehausen, R., Popov, E.P. & Bertero, V.V. (1983). Local bond stress-slip relationships of deformed bars under generalized excitations. University of California ; Report no. UCB/EERC-83/23 of the National Science Foundation.
- Hild F., 2002, « CORRELI<sup>LMT</sup>: a software for displacement field measurements by digital image correlation », Internal report N° 254 of LMT-Cachan.
- Lee H. S., Noguchi T., and Tomosawa F., 2002, « Evaluation of bond properties between concrete and reinforcement as a function of the degree of reinforcement corrosion », *Cem. & Conc. Res.*, 32, 1313-1318.
- Malvar, L.J. (1992) Bond reinforcement under radial confinement. *ACI Materials Journal*, 89(6): 593-601.
- Ouglova A., (2004) Etude du Comportement Mécanique des Structures en Béton Armé Atteintes par la Corrosion. Thèse de Doctorat. ENS-Cachan.
- Ouglova A., Berthaud Y., Foct F., François M., Ragueneau F., Petre-Lazar I. (200). Influence of corrosion on bond properties between concrete and reinforcement in concrete structures, *Mechanics & Materials*, RILEM, 41(5), pp. 969-980.
- Ragueneau F. Dominguez N. and Ibrahimbegovic A. (2006). Thermodynamic-Based Constitutive Model for Concrete-Steel Bond Modeling, *Computer Methods in Applied Mechanics in Engineering*, 195(52), pp.7249-7263.

## Risk-based design of reinforced concrete structures: uncertainties maximization related to corrosion process

Bruno Capra<sup>1</sup>, Christophe Descellier<sup>2</sup>, Christian Soize<sup>2</sup>

<sup>1</sup> Oxand S.A., France  
[bruno.capra@oxand.com](mailto:bruno.capra@oxand.com)

<sup>2</sup> Université Paris-Est, Laboratoire de Mécanique, 5 bd Descartes, 77454 Marne-la-Vallée, France  
[christophe.descelliers@univ-paris-est.fr](mailto:christophe.descelliers@univ-paris-est.fr); [christian.soize@univ-paris-est.fr](mailto:christian.soize@univ-paris-est.fr)

---

**Abstract.** In the case of structures with important stakes at the design level; or for existing structures for which the question of the extension of service life is a major concern, it is important to assess the risks related to the durability. Reliability approaches allow structure owner to have more information taking into account uncertainties compared to a deterministic approach. If these approaches become more and more usual, one key point is related to the available data and the way uncertainties are estimated. This article presents a methodology, based on the maximization of entropy theory, able to maximize uncertainties according to the level of knowledge related to the different parameters of the model. An application is presented for the chloride and carbonation-induced corrosion of reinforced concrete structures.

**Keywords:** chloride, carbonation, corrosion, reinforced concrete, reliability, maximum of entropy.

---

### 1 Introduction

The design of reinforced concrete structures with respect to durability is driven by standards and recommendations (EN 206-1, Eurocodes for example in Europe) that are mainly linked to global material parameters easily accessible (concrete compressive strength, minimum cement content, minimum concrete cover,...). These rules include important feedback and are applicable to a large range of structures and environment.

In the case of structures with important stakes at the design level; or for existing structures for which the question of the extension of service life is a major concern (nuclear power plant, bridges, dams,...), it is important to assess the risks related to the durability of the structure in a more detailed way. In the decision making process related to the service life of reinforced concrete structures, reliability approaches allow structure owner to have more information taking into account uncertainties compared to a deterministic approach.

Nevertheless, if probabilistic approaches are now used for risk-based design, or assessment of structures, one key point remains the available data or the way uncertainties are estimated. Generally, as it is expensive to collect real data on site, usual distribution laws are used to model parameters uncertainties without specific justification (normal, lognormal laws,...).

The aim of this article is to present a methodology, based on the maximization of entropy theory, able to maximize uncertainties according to the level of knowledge related to the different parameters of the model. An application is made to the assessment of a reinforced concrete structure subjected to chloride and carbonation-induced corrosion.

## 2 Corrosion process in reinforced concrete structures

Corrosion of steel rebars in concrete is the most frequent pathology which induced the most important costs of maintenance for concrete structures owners. A lot of models have been derived for assessing corrosion effects due to chloride ions ingress and carbonation. Chloride-induced corrosion is a difficult process to model because it implies a lot of factors: local electro-chemical reactions depending on humidity, temperature, water/cement ration (W/C) of concrete, surface state of steel, microstructure of concrete at the interface with steel... When pH in the pore solution of concrete decreases to a certain level, steel rebars are no longer protected from corrosion and local electro-chemical piles leads to rust formation which can lead to concrete cracking.

A key parameter to describe the beginning of the corrosion process is the critical content of chloride ions at the rebar level above which corrosion may occur. This critical content has been studied by many authors and there is a wide range of proposed values (0.35% to 3% of total chlorides by cement mass (Alonso *et al.*, 2000), (Glass et Buenfeld, 1997)). Generally, for structure design according to a prescribed service-life, a typical value of 0.4%/mass of cement is considered as the critical chloride threshold but this value can be adapted following environmental conditions (aerial or immersed zones in marine environment for example) (Izquierdo *et al.*, 2004). Besides this definition of a chloride threshold another criterion is also widely used which considers the influence of pH:  $[Cl^-]/[OH^-] \geq 0.6$  where  $[.]$  stands for the concentration of the ion (Hausman, 1967). The interest of such a criterion is the ability to couple the effects of carbonation (pH reduction) with chlorides. Carbonation induced corrosion is generally less difficult to assess because it is mainly driven by diffusion process of  $CO_2$  in concrete. The chloride threshold can vary in a wide range (typically between 0.6 and 1). Some tests have been carried out to estimate the distribution of the chloride threshold (fig. 1) (Izquierdo *et al.*, 2004). These experiments are very long, costly and generally not performed for a given structure. Nevertheless, it can be seen that the threshold range is important and that a log-normal has been fitted on the experimental results.

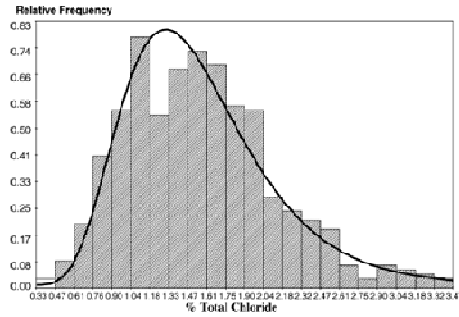


**Figure.1.** Distribution law of critical total chloride threshold for an immersed CEM I (W/C=0.5) (Izquierdo *et al.*, 2004).

The chloride ingress in concrete involves numerous physical phenomena: molecular (Fick’s law) and ionic diffusions (Nernst-Planck) in unsaturated material, chloride interaction with the cementitious matrix (chloride binding).

A summary of existing models for both chloride and carbonation-induced corrosion can be found in AFGC (2007).

### 3 Corrosion model for reinforced concrete structures

In this article, we consider a phenomenological model that accounts for both chloride and carbonation-induced corrosion and allows to predict steel section loss (Petre-Lazar, 2000). This mean model considers  $N$  parameters, two families are considered. The first one corresponds to the  $N_1$  “uncertain” parameters (after expert analysis) noted  $q_1, \dots, q_{N_1}$  with  $N_1=14$ . The second family corresponds to the  $N_2$  “certain” parameters noted  $a_1, \dots, a_{N_2}$  with  $N_2=19$ . The following table represents the uncertain parameters considered:

Table 1: Uncertain parameters of the corrosion model.

| Variable | Signification                          | Variable | Signification                 |
|----------|--|----------|-------------------------------|
| $q_1$    | Exposition coef. to carbonation        | $q_8$    | Chloride-matrix binding       |
| $q_2$    | Relative humidity                      | $q_9$    | Concrete cover                |
| $q_3$    | Compressive strength of concrete       | $q_{10}$ | Critical chloride threshold   |
| $q_4$    | Temperature                            | $q_{11}$ | Carbonation corrosion current |
| $q_5$    | Chloride diffusion coefficient at 20°C | $q_{12}$ | Chloride corrosion current    |
| $q_6$    | Chloride concentration at surface      | $q_{13}$ | Concrete porosity             |
| $q_7$    | Initial concentration of chloride      | $q_{14}$ | Volumetric mass of cement     |

$\mathbf{q} \in \mathbb{R}^{N_1}$  and  $\mathbf{a} \in \mathbb{R}^{N_2}$  are vectors of parameters  $q_i$  and  $a_i$  such as  $\mathbf{q}_j = \{q_j\}_j$  et  $\mathbf{a}_i = \{a_i\}_i$ .

### 3.1 Carbonation model

Let  $p(\mathbf{a}, \mathbf{q}; t)$  be the carbonation depth depending on the different variables  $\mathbf{a}$ ,  $\mathbf{q}$  and the time  $t$ :

$$p(\mathbf{a}, \mathbf{q}; t) = 10q_1 k(\mathbf{a}, \mathbf{q}) f(\mathbf{a}, \mathbf{q}) S t$$

Where  $k(\mathbf{a}, \mathbf{q})$  is a coefficient which stands for the influence of concrete compressive strength and  $f(\mathbf{a}, \mathbf{q})$  a coefficient related to the relative humidity:

$$k(\mathbf{a}, \mathbf{q}) = \begin{cases} \sqrt{\frac{a_1}{q_3}}(a_3 + a_4 \times (a_2 - a_1)) - a_3 & \text{si } q_3 \leq a_1 \\ a_4(a_2 - q_3) & \text{si } a_1 < q_3 < a_2 \\ 0 & \text{si } q_3 \geq a_2 \end{cases}$$

$$f(\mathbf{a}, \mathbf{q}) = -a_5 q_2^2 + a_6 q_2 + a_7 \quad .$$

### 3.2 Chloride penetration model

Let  $c_{Cl}(\mathbf{a}, \mathbf{q}; t)$  be the chloride concentration at concrete cover  $q_9$  depending on the different variables  $\mathbf{a}$ ,  $\mathbf{q}$  and the time  $t$ :

$$c_{Cl}(\mathbf{a}, \mathbf{q}; t) = \left[ q_7 + (q_6 - q_7) \left[ 1 - \operatorname{erf} \left( \frac{q_9}{2\sqrt{\alpha(\mathbf{q})\eta(\mathbf{q})d_{Cl}(\mathbf{q})t}} \right) \right] \right] \frac{1}{M_{Cl}}$$

Where  $\alpha(\mathbf{q})$  is a coefficient for ionic interaction between chloride and other ions,  $\eta(\mathbf{q})$  is the coefficient for chloride/matrix binding,  $d_{Cl}(\mathbf{q})$  is the chloride diffusion coefficient,  $M_{Cl}$  the molar mass of Chloride:

$$\alpha(\mathbf{q}) = 1 + \frac{M_{Cl}}{4q_6} \quad \eta(\mathbf{q}) = \frac{1}{1 + q_8} \quad d_{Cl}(\mathbf{q}) = q_5 e^{2500\left(\frac{1}{293.15} - \frac{1}{q_4 + 273.15}\right)}$$

### 3.3 Steel rebar section loss

The steel rebar section loss  $p_{dia}(\mathbf{a}, \mathbf{q}; t)$  due to corrosion is defined by the following equation where the corrosion current  $I(\mathbf{a}, \mathbf{q}; t)$  is due to the sum of carbonation and chloride-induced corrosion currents  $I_1(\mathbf{a}, \mathbf{q})$  and  $I_2(\mathbf{a}, \mathbf{q}; t)$  respectively

$$p_{dia}(\mathbf{a}, \mathbf{q}; t) = \int_0^t a_{17} I(\mathbf{a}, \mathbf{q}; \tau) d\tau$$

$$I_1(\mathbf{a}, \mathbf{q}) = q_{11} f_I(\mathbf{a}, \mathbf{q}) g(\mathbf{q})$$

$$I_2(\mathbf{a}, \mathbf{q}; t) = q_{12} f_I(\mathbf{a}, \mathbf{q}) g(\mathbf{q}) h(\mathbf{a}, \mathbf{q}; t) w(\mathbf{a}, \mathbf{q})$$

Where  $f_I(\mathbf{a}, \mathbf{q})$  represents the influence of humidity on the corrosion current,  $g(\mathbf{q})$  stands for temperature effects,  $h(\mathbf{a}, \mathbf{q}; t)$  is related to the chloride concentration,  $w(\mathbf{a}, \mathbf{q})$  the water content and  $s(\mathbf{a}, \mathbf{q})$  the saturation ratio:

$$f_I(\mathbf{a}, \mathbf{q}) = \begin{cases} a_8 e^{a_9 q_2} & \text{si } q_2 < a_{12} \quad , \\ a_{10} \frac{1 - q_2}{1 - a_{12}} & \text{si } a_{12} \leq q_2 < 0.99 \\ a_{11} & \text{si } q_2 \geq 0.99 \quad , \end{cases} \quad \begin{aligned} g(\mathbf{q}) &= e^{5000\left(\frac{1}{293.15} - \frac{1}{273.15 + q_4}\right)} \\ h(\mathbf{a}, \mathbf{q}; t) &= \frac{a_{13}}{q_{14}} c_{Cl}(\mathbf{a}, \mathbf{q}; t) \\ w(\mathbf{a}, \mathbf{q}) &= q_{13} s(\mathbf{a}, \mathbf{q}) \\ s(\mathbf{a}, \mathbf{q}) &= (1 + [-a_{14} \ln(q_2)]^{a_{15}})^{-a_{16}} \end{aligned}$$

### 4 Probabilistic model of uncertain parameters

Generally, it is difficult to have access to real statistical distribution of the previous uncertain parameters  $\mathbf{q}$ . The framework of this model is the use of the generalized probabilistic approach of uncertainties (Soize ,2009) based on the maximum of entropy principle (Shannon, 1948). This approach allows to derive the distribution laws of the uncertain parameters that maximize the uncertainty according to the available information. This information can take the form, for a given uncertain parameter, of mean value, standard deviation, support of the probabilistic density function (pdf),...

The use of the maximum of entropy principle leads to a problem of optimization under constraints to be solved according to the available information. The resulting pdf belongs to different classes with related parameters to be determined. The use of this theory leads to the following results for the problem of corrosion and the random variables  $Q_i$  associated to  $\mathbf{q}$ :

Table 2: Random variables and associated types of laws

| Random variable | Law type | Random variable | Law type |
|-----------------|----------|-----------------|----------|
| $Q_1$           | 1        | $Q_8$           | 1        |
| $Q_2$           | 2        | $Q_9$           | 1        |
| $Q_3$           | 3        | $Q_{10}$        | 3        |
| $Q_4$           | 3        | $Q_{11}$        | 3        |
| $Q_5$           | 1        | $Q_{12}$        | 3        |
| $Q_6$           | 4        | $Q_{13}$        | 6        |
| $Q_7$           | 5        | $Q_{14}$        | 3        |

type 1 :  $p_Q(q) = \mathbb{1}_{[0,+\infty[} e^{-\lambda_0 - \lambda_1 q - \lambda_2 q^2}$

type 2 :  $p_Q(q) = \mathbb{1}_{[0,1]} e^{-\lambda_0 - \lambda_1 q - \lambda_2 \ln(q)}$

type 3 :  $p_Q(q) = \mathbb{1}_{[a,+\infty[} e^{-\lambda_0 - \lambda_1 q - \lambda_2 \ln(q)}$

type 4 :  $p_Q(q) = \mathbb{1}_{[0,1,1]} e^{-\lambda_0 - \lambda_1 q - \lambda_2 q^2}$

type 5 :  $p_Q(q) dq = \delta_0(q - q_7)$

type 6 :  $p_Q(q) dq = \delta_0(q - q_{13})$

Then, the  $\lambda_i$  parameters are determined and the random generators of the  $Q_i$  variables build in order to perform Monte-Carlo simulation. The following figure presents the pdf of the steel section loss after 50 years:

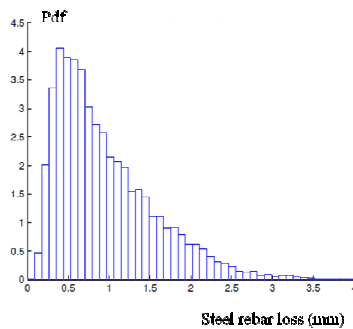
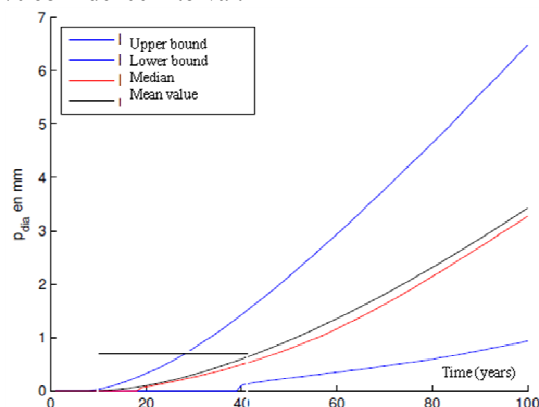


Figure.2. Probability density function of steel rebar loss after 50 years.

The following figure presents the evolution of the mean and median values of the rebar steel loss and the 90% confidence interval.



**Figure.3.** Steel rebar loss evolution versus time.

## 5 Conclusion

The prediction of service life of concrete structures is of major interest for structure owner to estimate their maintenance cost. To fulfil this requirement, accurate durability models are needed but not sufficient. Indeed, due to the uncertain nature of concrete and its environment, predictions must be performed in a probabilistic way. Moreover, it is not always easy to access real statistical data for all the uncertain parameters. The maximum of entropy approach gives a framework which allows to maximize uncertainties according to available information.

## References

- AFGC (2007) - *Concrete design for a given structure service life. Durability management with regard to reinforcement corrosion and alkali-silica reaction*, AFGC Editor, April 2007.
- Alonso, C., Andrade, C., Castellote, M. et Castro, P. (2000). Chloride threshold values to depassivate reinforcing bars embedded in a standardized opc mortar. *Cement and Concrete Research*, 30:1047-1055.
- Glass, G. K. et Buenfeld, N. R. (1997). The presentation of the chloride threshold level for corrosion of steel in concrete. *Corrosion Science*, 39:1001-1013.
- Hausman, D. A. (1967). Steel corrosion in concrete : how does it occur ? *Materials protection*.
- Izquierdo, D., Alonso, C., Andrade, C. et Castellote, M. (2004). Potentiostatic chloride threshold values for rebar depassivation: experimental and statistical study. *Electro. Acta*, 49:2731-2739.
- Petre-Lazar I., Heinfling G., Marchand J., Gerard B. (2000). Application of probabilistic methods to analysis of behavior of reinforced concrete structures affected by steel corrosion, *Proceedings of the 5th CANMET/ACI International Conference on Durability of Concrete*, June 4-9, 2000, Barcelona, Spain, SP-192 (Ed. by V.M. Malhotra, ACI, pp 557-572.
- Shannon C. E., (1948), A mathematical theory of communication, *Bell System Tech.J.*, **27**, 379-423 and 623-659.
- Soize C., Generalized Probabilistic approach of uncertainties in computational dynamics using random matrices and polynomial chaos decompositions, *International Journal for Numerical Methods in Engineering*, (Accepted: 12 June 2009), on line DOI 10.1002/nme.2712.

## Learning from experiences: forensic engineering and collapse databases

Breysse D.

Université Bordeaux 1, Ghymac, Avenue des Facultés, 33405 Talence cedex, France  
d.breysse@ghymac.u-bordeaux1.fr

---

**Abstract.** Collapses in civil engineering are not uncommon. Some cases have known a worldwide echo but, in many cases, the echo of collapses remains in a very limited area, that of the client and company directly involved, when useful information could be obtained after an in-depth analysis of what happened.

Collapses of structures can result of many factors (loadings, materials, organization, lack of maintenance...) but their analysis can always bring useful lessons for improving practice. Forensic engineering is the name of new science which consists in post-mortem analysis, such as to understand its reason and to draw useful lessons.

We try to show, based (a) on few examples and (b) on more general considerations, what can be gained in collecting “collapse experiences” under a more formal basis. The main difficulties of such a work are described. The new knowledge drawn from these databases would be useful for risk management in civil engineering projects, for teaching, and, more widely, for improving the quality of our works.

**Keywords:** database, failure, forensic engineering, risk management, safety

---

### 1 Introduction

The more common field in which construction engineers are learning from experience is that of seismic collapses. It is now common that, after each important earthquake, groups of experts try to understand what could have been improved (in building codes, in building practices...) such as to reduce the consequences of such hazards. The same approach has been used for understanding the collapse mechanisms of many bridges during the Katrina hurricane and retrofitting them (Padgett, 2008). It has also been used for building vulnerability curves for hurricanes (Li, 2005) or soil subsidence (Saeidi, 2010).

Earthquakes are thus not the only field in which analysis of collapses can provide useful informations. Collapses in civil engineering are not uncommon. Some cases have known a worldwide echo (like Tacoma or Palau bridge failures, Heathrow or Roissy airport collapses or Hyatt Regency disaster) while, in many cases, the echo of collapses remains in a very limited area, that of the client and company directly involved, even if useful information could be obtained after an in-depth analysis of what happened. Some efforts have recently been done, such as to gather and analyse collapses on a more formal basis.

Forensic engineering is the name of a new field of engineering which consists in *post-mortem* analysis, such as to understand its reason and to draw useful lessons (Delatte, 2009). We will try to show, based (a) on few examples and (b) on more general considerations, what can be gained in collecting “collapse experiences” on a more formal basis. The main difficulties of such a work will be described. The new knowledge drawn from these databases would be useful for risk management in civil engineering projects, for teaching, and, more widely, for improving the quality of our works.

## 2. Civil engineering structures failures : common events

### 2.1. Failure : what is normal and what is not ?

What is called « failure » is not only the catastrophic collapse. Failure means that the system (or one part of it) is unable to work as expected. In building safety regulations (like Eurocodes), fundamental requirements deal with structural capacity, deformability, additional functions like comfort, tightness, comfort, and durability. Regulations are written in such a way that the frequency of failure is “low enough” to be (in matter of frequency and consequences) socially acceptable (Breyse, 2009a). In construction, explanations for failure lie either in material properties or in loadings : failure happens when the effects of loading is more severe than what the material can bear (accounting also for possible deterioration with time). However, this “mechanical logic” cannot explain all, and human factors have an important influence, whatever the stage of life is: design, building or service. Human error can originate from bad decisions, insufficient knowledge, understanding or communication problems... Accidents can also be the result of risks which are consciously considered and accepted, either because their elimination is technically impossible, or economically not acceptable (Schneider, 1997).

### 2.2. Feedback and forensic engineering

When a failure occurs, one wonders about its (ab)normality : is it *normal* that building collapses frequently happen in Egypt (a partial data sampling lead to identify 18 such collapses between 2000 and 2009, having caused 154 victims...)? Is it *normal* that urban tunneling works induce so much damage in their neighbourhood ? Is it *normal* it was the same architect who designed the Transvaal Park which collapsed in 2004 in Moscow (28 victims) and the Yasenovo market failure which caused 60 victims in the same town two years later ? Answering these questions is, of course, not possible, if one does not considers the technical, economical and social contexts in which they are asked.

After a failure, the civil engineering expert is asked to understand and explain what happened, so as to draw some lessons and, perhaps to adapt the regulations or building principles (Breyse, 2009b). Case studies on past failures enable to identify their causes (or possible causes), to analyse them and to draw some lessons (Bordes, 2005). These lessons enrich the collective expertise. The failure could happen because the risk was underestimated or not correctly accounted for, because the technology was insufficiently experienced, because some warnings were not considered...

More generally, feedback qualifies the process and the lessons drawn from an unforeseen (and often dramatic) event. Regarding parasismic design, feedback is performed at first when a team of experts visits the site of an earthquake and tries to get information on how to improve the design rules and construction practices. This feedback can be: (a) qualitative

or quantitative, (b) based on case studies or on statistics. The detailed case study requires a high level of expertise and may imply sophisticated means (laboratory tests, numerical simulations...). It is mainly used when some juridical/legal dimensions appears, i.e. when the question of responsibility arises. The development of this dimension, mainly in anglo-saxon countries, gave birth to forensic engineering.

The word « *forensic* » originates in the latin word « *forum* », which was the open space where collective city matters were discussed. Forensic engineering can be seen as a medico-legal analysis on structures : it is a (*post-mortem*) retro-analysis after the failure, back to its root causes, such as to rebuild the logical chain of causes and consequences which finally resulted in the collapse... and such as to enable the allocation of responsibilities. The « forensic engineer » has now his academic journals and conferences (Rens et al, 2000) and, in the US, the American Society for Civil Engineering has created a Technical Council on Forensic Engineering – ASCE TCFE (Delatte, 2009).

### 3. Feedback enabling a continuous improvement process

#### 3.1. Improvement of the knowledge

Case studies have a long history in the anglo-saxon world and gave birth to a rich specific literature. They can be used by practitioners, since they enrich the technical expertise, but also because they draw attention on ethical or juridical matters. Many civil engineering students have seen the Tacoma collapse movie (USA, 1942). It remains the most famous case in which a new phenomena was discovered thanks to failure: the «Von Karman whirls» which made it fail because of an aero-elastic coupling had been understood only many years after the event.

But engineers have gained knowledge from various other failure cases:

- the buckling effect in metallic bridge was better accounted for in design and in the building provisional stages after severall bridge collapses (Akesson, 2008),
- the Millenium bridge in London (and its sister the Solferino bridge in Paris) experienced dangerous vibrations which revealed that some unprecedented mechanical coupling phenomena between the pedestrians and the structure existed,
- the sudden failure of a metallic bar in the Uster pool (Switzerland, 1985) initiated the consideration of stress corrosion when ambient air contains a large amount of chlorides.

#### 3.2. Improvement in the practices

The sudden failure, hopefully without dramatic consequences, of the Ynys-y-Gwas bridge, Wales, in 1985, revealed that the metallic cables of this prestressed structure were highly corroded, due to water penetration in joints. The failure had not been anticipated and many years were necessary before UK authorities accept again the use of prestressed concrete in bridges, with additional requirements regarding their design and building.

These last 20 years, urban tunnels have provoked many accidents with, in some cases, dramatic consequences at the ground surface, for people and existing structures (Heathrow and Munich in 1994, Taegu in South Korea in 2000, Meteor in Paris in 2003, Nicoll Highway in Singapour in 2004, Lane Cove in Sydney in 2005, Köln in 2009...), either



#### 4.2. Knowledge build-up and education

Learning from failure can be very efficient. Failures or accidents can be used at several levels:

- at a statistical level, since their repeated occurrence sometimes enables to build laws and to quantify occurrence probabilities,
- at a qualitative level, when a case is strong enough to draw lessons which cannot be forgotten,
- at an intermediate level, when apparently isolated cases reveal, after a thorough analysis, some genericity, which makes possible to go from the specific to the regular, and to draw practical lessons in a wider field.

A case studies database has been developed at Alabama Univ. (Delatte, 2000) with learning purposes. For each case, the (unique or multiple) cause(s) for failure have been identified and discussed. Thus the cases have been grouped in categories according to these causes. This idea could be developed in many fields like : roof collapse due to snow overloads, instability collapse (e.g. due to buckling), disorders induced by tunnel works, accidents in temporary works...

#### 4.3. Difficulties in getting and validating information : how to cope with them ?

Nowadays, Internet provides a continuous flow of information. The amount of information about civil engineering failures is only a small part of the whole, but it suffices to make realistic the project of a collective database on such facts. Several challenges have however to be faced with, mainly regarding organization and validation.

Each important accident is a source of information (news releases, open or professional forums, technical reports...). Being able to sort between all these data is not always easy, For instance, the WTC collapse has been the source of a huge amount of alternative and pseudo-scientific data where conspiracy theory has its part. We are entering here the field of sociology and psychology and the seriousness and quality of many works like those of FEMA can do nothing against the weight of rumors (Kausel, 2002).

In some countries, like France, another limiting factor is that professional are often reluctant for spreading data about events like failures, collapses or accidents, except when they are obliged to. Informations are said to be confidential, which is sometimes true because of juridic matters. However, one must look with optimism at what has been developed in UK, under the auspices of SCOSS (Standing committee for the structural safety), which has developed a reporting system, which combines the spreading of useful data and the care of confidentiality (Breyse, 2008). SCOSS ( <http://www.scoss.org.uk/> ) is an independent entity, born in 1976, with the purpose to maintain a watchfulness on structural safety matters. It serves as an intermediate organism between authorities, engineers and building industry. The CROSS process (« confidential report on structural safety » ) has been defined such as to reduce the number of accidents (or near-accidents) on structures, and to improve their reliability all along their service life. The method consists in getting feedback from professionals (through confidential reports) and in writing synthetic reports when needed, such as to influence practices. All reports are analysed by independent experts and, after having cancelled some information such as to make the report anonymous, are published. When some facts emerge because similarities appear between different reports, in-depth research programs can be developed.

A database has been developed in Japan by Pr. Hatamura (Hatamura, 2007 - (<http://www.shippai.jst.go.jp>) with the central question: « is it possible to develop useful and consistent models for failure, from the analysis of unique cases, since they can be many but also remain specific ? ». Case studies are analyzed by developing a three steps logical model, like in a fault-tree analysis : « causes – actions – consequences ». Each of these steps is further developed in a two-level classification and enables, for each individual case, the identification of a pattern, thus of a group of cases to which it belongs. For instance, the causes are divided into 10 classes at a first level and into 27 classes at a second level. These classes are defined according to the fact that the cause mainly comes from an individual, an organization, the societal context or that nobody can be considered as responsible (unknown or unpredictable events). This description probably remains too general to be efficient, but nothing prevents to go further, for instance by working into more details on some specific type of structures (dams, bridges, tunnels...). Thus, it will be possible to have a more detailed description and to obtain more practical conclusions, either for the statistical analysis of failure process or for practical risk management. Few other examples of failure databases can be cited: a Swiss study, focussing on bridge failures (Bailey et al, 2001), the analysis of accidents during the construction phase (Behm, 2008), a failure database on dams (Xu, 2009). In all these cases, the data were used with the idea of improving knowledge and, therefore, safety.

## 5. What is possible ?

Organizing feedback on a global scale faces many challenges : defining the kind of data to collect, the way to organize and validate them, the way to analyse them and draw conclusions. A first database is being developed by the author through various sources: technical reports on case studies, yet existing databases, information provided through the Internet. It has been chosen to exclude from the database failures induced by natural hazards like earthquakes and flooding, as well as fire disasters. The database presently contains more than 500 cases, with a bias due to the gathering process, which tends to highlight recent cases (from the last thirty years and, even more, from the last ten years).

However, some interesting information can yet be get, like that presented on Figure 3. This figure is a classical F-N diagram on which curves represent the annual probability of being affected (here to die because of a structural collapse, also named FAR for “fatal accident rate”) as a function of the magnitude of the event (number of victims N). The probability value for each N is calculated by dividing the cumulated number of victims due to events with at least N victims by the number of years (here 20 years) and the population at risk.

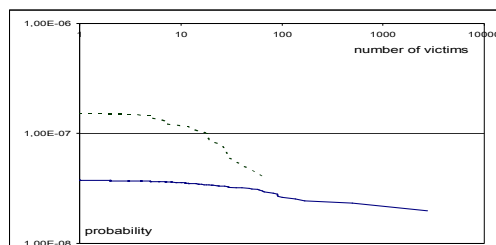


**Figure 2.** F-N curves (fatal annual rate vs fatalities) for building collapses

*(continuous curve: worldwide cases, dotted curve: Egyptian cases)*

Such F-N curves are known to provide data (and guidelines for decisions) regarding the allowability and acceptability of risk levels. The continuous curve (worldwide curve for 1990-2009) is drawn from a total number of 94 events (collapses of buildings with casualties). The dotted curve corresponds to 18 building collapses with victims from Egypt for the same period. Due to sampling biases, these curves cannot be considered as reliable, especially for the low N values, but it is yet possible to make some comments. First, the magnitude of the probability, between  $10^{-8}$  and  $10^{-6}$  is usual for such sources of risks [Breysse, 2009] a value of  $10^{-7}$  corresponding, for instance, to 10 victims each year for a reference at risk population of 100 millions inhabitants. Second, it can be seen that the risk level is much higher in Egypt (the same would probably be found in other developing countries like Nigeria and Kenya where these questions are a public matter) than worldwide.

Using the database under development, it would be possible to draw identical curves for any type of structures, like bridge or dam collapses, or cumulating all types of structural collapses. Such curves can help regulators if they have to compare the real “safety level” between different contexts (different countries or types of structures) or if they want to compare reality (feedback) to safety objectives. The main limit for the development of approaches based on feedback is the data gathering. It is important to ask (and answer) questions like: the gathering process (type of data to gather, validation process), organisation of the database, access for specialists and/or general public, property and confidentiality... What has been developed by SCOSS can serve as a possible model. We think that a common decision and collective efforts between all parties (authorities, professionals, universities) is possible and would be fruitful.

## 6. References

- Akesson B., 2008, Understanding bridge collapses, Taylor & Francis.
- Bailey S.F., Antille S., Béguin P., Imhof D., Brühwiller E., Niveau de sécurité requis pour l'évaluation de ponts-routes existants, Ecole Polytechnique Fédérale, Lausanne, 2001.
- Behm M., 2005, Linking construction fatalities to the design for construction safety concept, Safety science, 43, 589-611.
- Bordes J.L., 2005, A propos de l'histoire des barrages en France, quelles leçons du passé ?, Annales du BTP, avril 2005.
- Breysse D., Pourquoi et comment développer une ingénierie forensique à la française ?, Colloque Le Pont, Univ. Toulouse, 22-23 oct. 2008.
- Breysse D., Ingénierie forensique : la défaillance comme base de savoirs, Rencontres AUGC, Saint-Malo, 4-6 juin 2009. (2009a)
- Breysse D., Maîtrise des Risques en Génie Civil, Volume 1 : multiples dimensions des risques en génie civil, Hermes Lavoisier, 222 pages, 2009. (2009b)
- Delatte N.J., 2000, Using failure case studies in civil engineering education, in Forensic engineering, Proc. of the second ASCE congress on Forensic Engineering, San Juan, Porto-Rico, 21-23 mai 2000, pp. 430-440.
- Delatte N., 2009, Failure literacy in structural engineering, Engineering structures, ASCE, doi:10.1016/j.engstruct.2009.12.015.
- Ellingwood B.R., 1999, Probability-based structural design : prospects for acceptable risk bases, Conf. ICASP 8, Sydney, déc. 1999.

- Hatamura Y., Failure knowledge database to learn lessons from past experience, IAEA Regional Asian Workshop on Managing Nuclear Knowledge, Tokyo, 24 oct. 2007.
- ITIG, 2006, A code of practice for management of tunnel works, International Tunnelling Insurance Group.
- Kausel E., The towers lost and beyond, MIT, 2002, <http://web.mit.edu/civenv/wtc/> .
- Li Y., Ellingwood B.R., 2006, Hurricane damage to residential construction in the US: importance of uncertainty modeling in risk assessment, Eng. Str., 28, 1009-1018.
- Padgett J., DesRoches R., Nielson B., 2008, Performance of coastal bridges during hurricane Katrina, 1<sup>st</sup> Medachs conf., Lisbon, 28-30 jan. 2008.
- Rens K.L., Rendon-Herrero O., Bosela P.A., 2000, Forensic engineering, Proc. of the second ASCE congress, San Juan, Porto-Rico, 21-23 mai 2000.
- Saeidi A., 2010, La vulnérabilité des ouvrages soumis aux aléas mouvements de terrains ; développement d'un simulateur de dommages, Doct. INPL, Nancy, France.
- Schneider J., 1997, Introduction to Safety and Reliability of Structures, ed. International Association for Bridge and Structural Engineering.
- Wood J.G.M., L'ingénierie forensique – l'approche anglaise, Colloque Le Pont, Univ. Toulouse, 22-23 oct. 2008.
- Xu Y., Zhang L.M., Breaching parameters for earth and rockfill dams, J. Geotech. Geoenviron. Eng., ASCE, 12/2009, vol 135, 12, 1957-1970.

## *Author Index*



# Index

- Abbeche K., 343, 801  
Abdelkrim M., 151  
Abderahmane B., 579  
Abriak N., 587, 595, 601, 607, 653, 685  
Abriak N. E., 893  
Adam L., 251  
Ait Mokhtar K., 893  
Ait-Mokhtar A., 879  
Aloulou F., 129  
Amendola A., 83  
Amouri C., 701  
Angelillo M., 109  
Antonelli L., 551  
Arfaoui M., 123, 835  
Ascione F., 63  
Auricchio F., 135  
Averseng A., 435  
Ayadat T., 801
- Babilio E., 57  
Bagané M., 847  
Barboura S., 239  
Barrat J. T., 303  
Belhadj E., 775  
Ben Ayed H., 757  
Ben Jamaa N., 847  
Ben Mekki O., 129, 135, 769  
Ben Ouezdou M., 157, 203, 579  
Ben Salah H., 129  
Benboudjema F., 413  
Benhaissaine A., 617  
Benjeddou O., 157  
Benkechkeche G., 707  
Bennani A., 421  
Bensebti S. E., 707  
Bentchikou M., 679  
Benzerzour M., 587, 601, 607, 653  
Berga A., 45
- Berger F., 407  
Berthaud Y., 487  
Berthet-Rambaud P., 429  
Bertolo P., 269  
Bertrand D., 399, 407  
Bettiol G., 509  
Bichler A., 311  
Bigot C., 407  
Binda L., 523, 529  
Binetruy C., 607, 653  
Blesgen T., 83  
Bonavigo L., 623  
Bonelli S., 867  
Bonenfant J., 445  
Borio L., 323  
Bost M., 317  
Bouabid A., 741  
Boukhatem G., 245  
Boukria Z., 421  
Boumezerane D., 781  
Bourbatache K., 879  
Bourdin B., 17  
Bourgeois E., 163  
Bourrier F., 407  
Boutillier B., 393  
Breugnot A., 289  
Breyse D., 465, 499  
Briffaut M., 413  
Buonsanti M., 103
- Cabane N., 631  
Cacciola M., 217  
Calcagno S., 217  
Cantini L., 523  
Capra B., 493  
Cardani G., 523  
Caron J. F., 239  
Casarin F., 509, 535

- Ceraldi C., 109  
 Chabane A. H., 707  
 Chabbi H., 809  
 Chaki S., 653  
 Chateauneuf A. , 747  
 Chauvel R., 399  
 Chesi C., 529  
 Clastres P., 261  
 Coué R., 89  
 Croci G., 551, 559  
 Crosnier B., 435  
 Crouigneau S., 479  
 Cyr M., 261, 913
- Da Porto F., 509, 535  
 Dagrain F., 541  
 Daoud A., 203  
 Daoud D., 229  
 Daraio C., 83  
 Darve F., 873  
 Datoussaid S., 195  
 Daudeville L., 855  
 De Buhan P., 151, 163  
 De Canio G., 559  
 De Tommasi D., 51  
 Debieb F., 679  
 Deboffe C., 601  
 Del Piero G., 89  
 Del Regno R., 83  
 Delannay L., 187  
 Demagh L., 801  
 Denk M., 379  
 Derriche Z., 257  
 Descamps T., 181  
 Descellier C., 493  
 Desprez C., 459  
 Dheilly R., 647  
 Diliberto C. , 775  
 Djenatte M., 349  
 Doghri I., 187, 251  
 Donze F. V., 861  
 Dubé J. F., 435  
 Dubois L., 317  
 Dufour F., 379
- El Arem S., 459  
 El Ghezal L., 823
- Elachachi S. M., 465  
 Ertl Z., 567, 661
- Faddoul R., 747  
 Farah F., 787  
 Fatnassi C., 769  
 Feregotto M., 317  
 Ferraiolo P., 269  
 Filianoti P. F., 103  
 Foret G., 169  
 Fortin J., 893  
 Fortunato A., 57, 109  
 Foti P., 77  
 Fouletier M., 631  
 Frémond M., 63, 723  
 Fraddosio A., 77  
 Fraternali F., 83  
 Freddi F., 29
- Galusinski C., 867  
 Garcia-Diaz E., 617  
 Garcin P., 289  
 Gaudon P., 631  
 Gavaille S., 855  
 Gerard B., 479  
 Gerber W., 337  
 Ghavamian S., 445  
 Giacchetti G., 269  
 Giovine P., 209  
 Glover J., 379  
 Golay F., 867  
 Gonzalez-Gallego J., 303  
 Gotteland P., 289, 331  
 Goullieux A., 647  
 Grange S., 453  
 Guefrech A., 841  
 Guellouz L., 829  
 Guenfoud M., 905  
 Guerlement G., 181
- Hamberger M., 311  
 Hanini S., 679  
 Hanzlicek T., 567, 661  
 Hassen G., 151, 163, 175  
 Hassis H., 741, 763, 793  
 Hellmich C., 141  
 Helmericha R., 573

- Hemsas M., 465  
 Herzalla A., 551, 559  
 Heymann A., 331  
 Hicher P. Y., 815  
 Hicher P. Y. , 841  
 Hop T. B., 487  
 Houari H., 701, 707  
  
 Idir R., 913  
 Inoue S., 283  
  
 Jamei M., 713  
 Jamei M. , 823  
 Jason L., 445  
 Julien S., 913  
  
 Kacimi L., 257, 261  
 Kaid N., 913  
 Kallel A., 757, 769  
 Karoui A., 835  
 Karray M. A., 229  
 Khelafi H., 913  
 Khelidj A., 89  
 Kishi N., 355, 361, 367  
 Kohlmaier G., 297  
 Kon-No H., 367  
 Kon-no H., 355, 361  
 Kopp C., 573  
 Kotronis P., 453, 459  
 Krasraghy S. G., 367  
 Kurihashi Y., 355  
  
 La Borderie C., 413  
 Labiadh M. R., 579  
 Lachouette D., 867  
 Lambert S., 331, 407  
 Lancioni G., 23  
 Laouar M. S. , 343  
 Le Ngoc H., 653  
 Le Roy R., 733  
 Lecomte A., 775  
 Legeron F., 473  
 Leroy R., 169  
 Limam A., 385, 399, 421, 429  
 Limam O., 157, 757  
 Liu X., 815  
 Lominè F., 885  
  
 Lorentz J., 277  
 Lorrain M., 229  
 Ltifi M., 763, 787, 793  
 Lucchesi M., 115  
 Luis Fonseca R., 303  
  
 Machta K., 667  
 Magi J. , 529  
 Makni M., 229  
 Mansouri K., 123  
 Marigo J. J., 17  
 Marin F., 861  
 Marin M., 855  
 Marsili C., 529  
 Marzano S., 51, 77  
 Marzouk A., 393  
 Masmoudi A., 203  
 Masmoudi R., 203  
 Matallah M., 413  
 Maurini C., 17  
 Mazars J., 453, 459  
 Megali G., 217  
 Mekki F., 905  
 Meksaouine M., 809, 905  
 Mendjel D., 673  
 Mendjel D. , 245  
 Merlin M., 95  
 Merouane A., 257  
 Messaoud F., 343  
 Messast S., 245, 673  
 Miled B. , 187  
 Miled K., 733  
 Millet O., 879  
 Miraoui M., 595  
 Mitjana J. A., 303  
 Modena C., 509, 535  
 Mongelli M., 559  
 Montassar M., 129  
 Montassar S., 135  
 Morabito F. C., 217  
 Moriguchi S., 283  
 Munari M., 509  
 Munda S., 523  
 Muquet L., 277  
  
 Napoli G., 71  
 Nectoux D., 631

- Neji J., 685  
 Nguyen V. T., 175  
 Nicot F., 873  
 Nishi H., 355, 361  
 Nishida N., 283  
 Noel J., 181, 195
- Oggeri C., 269  
 Olivella S., 713  
 Omer A., 691
- Palle J. L., 373  
 Pampolini G., 89  
 Pandolfi A., 71  
 Parisi M., 529  
 Peila D., 323  
 Pelizza S., 323  
 Pellicano D., 217  
 Perna I., 661  
 Perna Y., 567  
 Perrotin P., 421  
 Pham K., 17  
 Piccioni M. D., 77  
 Pichler B., 141  
 Planes J. A., 303  
 Plassiard J. P., 277  
 Pontari A., 103  
 Potapov S., 855  
 Poullain P., 885  
 Puglisi G., 51
- Quéneudec M., 647  
 Qunitana C. R., 303
- R. Abdelmoula, 835  
 Rafrat S., 829  
 Ragueneau F., 487  
 Raous M., 45  
 Raphael W., 747  
 Remadnia A., 647  
 Rizzoni R., 95  
 Robit P., 385  
 Rocca E., 63  
 Rocher-Lacoste F., 317  
 Romero E., 713  
 Ronco C., 269, 323  
 Roselli I., 559
- Roth A., 303, 379  
 Rousseau J., 855  
 Royer-Carfagni G., 29
- Sab K., 239, 733  
 Saccomandi G., 51  
 Saiyouri N., 815, 841  
 Salah M., 349  
 Salem N., 763  
 Sawada K., 283  
 Sayed-Ahmed F., 169  
 Scheiner S., 141  
 Scholtès L., 885  
 Sebaibi N., 607  
 Selmi A., 251  
 Selmi M., 793  
 Seppecher P., 867  
 Sheikh M. N., 473  
 Sibille L., 885  
 Silhadi K., 679  
 Silhavy M., 115  
 Simon-Masseron A., 257  
 Simonato E., 509  
 Soize C., 493  
 Soltane S., 135  
 Soubra A. H., 747  
 Stelzer G., 311  
 Sung E., 283
- Terfaya N., 45  
 Tiraboschi C., 523  
 Tonello T., 373  
 Torrenti J. M., 413  
 Trabelsi H., 713  
 Trad A., 385, 399  
 Tran V. T., 861  
 Trifa M., 123, 835
- Ullah S., 141  
 Ushiwatari Y., 361
- Vairo G., 129  
 Valluzzi M. R., 535  
 Verbrugge L., 601  
 Versaci M., 217  
 Villard P., 289  
 Viskovic A., 551, 559

Volkwein A., 337, 379

Yaich S., 667

Yamaguchi S., 355, 361

Yashima A., 283

Zani N., 115

Zdiri M., 685

Zentar R., 595

Zenzri H. , 713

Zlender B. , 781

Zri A., 587

Zucchetti M., 623

Zurlo G., 51